The innate response to uropathogens: the urothelial defendome.

Carwyn Siôn Edwards

Doctor of Philosophy

University of York

Biology

September 2016

Abstract

Urinary tract infections (UTIs) will affect half of the female population within their lifetime. The urothelium, the epithelial lining which lines the urinary tract, plays an important role in mediating the defence against UTIs. Recent work has suggested that significant differences exist between normal human urothelial cell responses to uropathogenic stimuli and the responses observed in murine and cancer cell models. The work described in this thesis aimed to investigate the urothelial defendome: the soluble component of urothelial innate immunity, with a specific focus on antimicrobial peptides (AMPs), using i*n vitro* models of uropathogenic *E. coli* (UPEC) interaction with normal human urothelial (NHU) cells.

NHU cells expressed several antimicrobial peptide (AMP) genes constitutively and in response to UPEC. Beta-defensin 2 and 4 were upregulated in response to UPEC and isolated UPEC flagellin, but not in response to other isolated virulence factors. Despite expressing the flagellin receptor Toll-like receptor 5, barrier-presenting differentiated NHU cells did not exhibit an AMP response to UPEC or UPEC-derived flagellin. Damaging the urothelial barrier before flagellin exposure induced AMP expression, a response previously not shown *in vivo* or *in vitro*. Immunolocalisation studies revealed TLR5 to be expressed sub-apically, suggesting a possible novel mechanism of immunomodulation by the urothelium.

These results strongly support the concept of human urothelium as the crux of innate immune functionality in the urinary tract, The damage-dependent response exhibited by biomimetically differentiated NHU cells to uropathogenic stimuli suggests that the state of the urothelial barrier may play an important role in controlling urothelial immunity.

Table of Contents

Table of Figures

List of Tables

Acknowledgements

Firstly, thanks must go to my supervisors, Jennifer Southgate and Jane Thomas-Oates, and my TAP members, Marjan Van Der Woude and Ed Bergstrom, for their patience, supervision and advice over the past three and a half years.

A special thank you goes to all the members of the JBU past and present: for their advice, assistance and light-hearted (?) abuse. Particular mentions go to Ros Duke for all the cells, Simon & Jenny Baker for help, advice & RNA-seq data, Anna Radford and Rebecca Phillips for putting up with random medical questions and rants, Carl Fishwick for advice and pints, and Stefan Tran & Chloe Goodson for being exceptional summer and project students respectively.

Thanks in no particular order to Liz, Jason, Jake, Greg, Sam, Natasha, Richard, Joelle, Pasky, Katrina, Erin, JT, Megan… the list goes on, but thank you all for making PhD life bearable, especially Chris Sherrington and all at the Fulford Arms.

I am extremely grateful to the Wellcome Trust for funding my research, and to all the patients who donate their tissues for research, without whom the JBU would not exist.

Last, but not least:
Thank you Victoria, for being there.
Thank you, Mam & Dad for putting up with me for the past 26 years.

And to Nan, wherever you are, thank you for all those trips to the library:
I imagine you knew they'd pay off somewhere along the line.

Author's Declaration

The candidate confirms that the work submitted in this thesis is his own work, and that appropriate credit has been given where reference is made to the work of others, or for the efforts of collaborators. This thesis has not been submitted for any other award at this, or any other, institution.

Raw RNAseq data analysed and discussed in Chapter 3 and Chapter 5 was produced by Simon Baker.

1 Introduction

The overall aim of the project described in this thesis is to understand and profile the antimicrobial response of the urothelium to uropathogenic bacteria and their pathogen-associated molecular patterns (PAMPs). This brief introductory chapter outlines the background of the project: the basic biology of the urothelium and uropathogens, the epidemiology and clinical aspects of urinary tract infections and the advances made in the culture of urothelial cells which enabled this project to take place.

1.1 The urothelium

The mammalian urinary tract has evolved to excrete soluble, metabolic by-products from the body in a manner that conserves beneficial components and reduces the inherent loss of water during excretion. The primary function of the urothelium, the transitional epithelium that lines the bladder, ureters and renal pelvis, is as a protective physical barrier: confining toxic urine to the tract. The urinary bladder acts to store urine at a low pressure until it can be voided from the body: as such; the urothelium is required to be accommodating of increases in bladder volume, and the evolution of rapid and effective repair mechanisms to maintain barrier function.

The urothelium consists of a highly stratified epithelium, three to six cells thick (Figure 1.1). The epithelium comprises three zones of increasing cytodifferentiation: a single basal cell layer, multiple intermediate cells, (depending on the distension of the bladder), and a highly-differentiated superficial cell layer (also known as the umbrella cells) comprising large, sometimes binucleated cells. This arrangement of cells is conserved in mammals (Hicks, 1965). The apical surface of the urothelium is coated with a protective hydrophilic glycosaminoglycan layer, formed primarily of proteoglycan and glycoprotein structures, extended from the cell surface (reviewed by Hurst (2003).

In fitting with its protective barrier function, the urothelium is the least permeable epithelium in the body. Measurement of ionic permeability across epithelia can be measured as a function of the transepithelial electrical resistance (TER), calculated *via* Ohm's law. 'Tight' epithelia are characterised as having a TER > 500 $\Omega.cm^2$ (Frömter and Diamond, 1972). The TER of mammalian bladder is the highest of all epithelia, a characteristic which is conserved in mammals (Anderson and Van Itallie, 2009; Apodaca et al., 2003; Frömter and Diamond, 1972; Lavelle et al., 2000) .

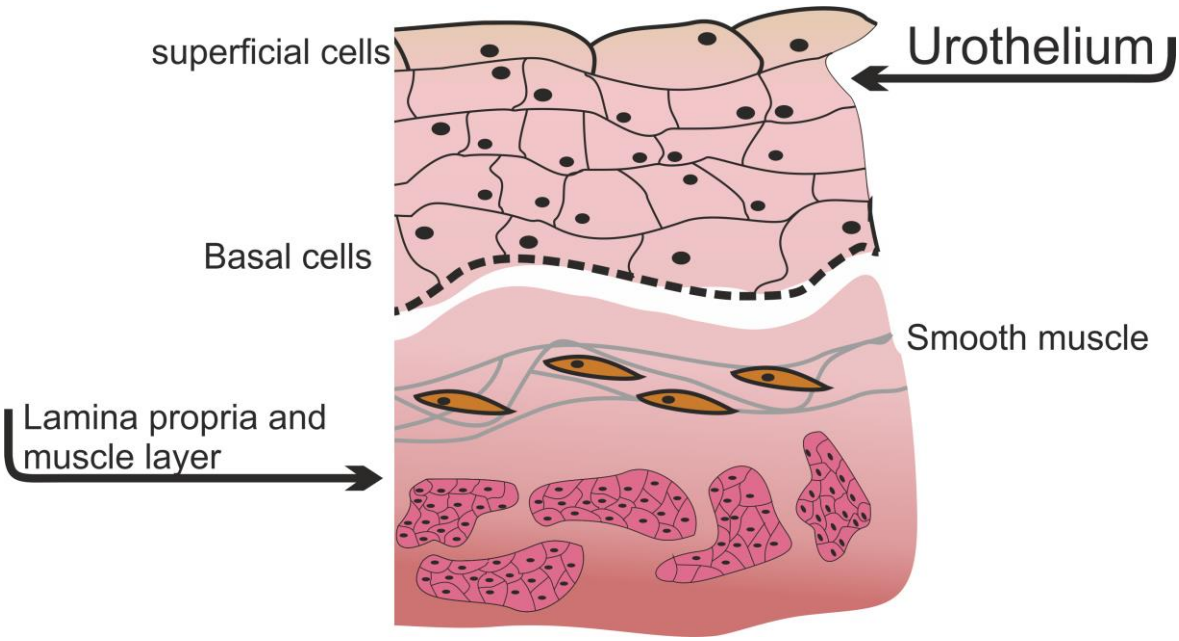

Figure 1.1 Pictorial representation of the bladder urothelium and underlying tissue. *Superficial cells cover several intermediate cells, hence the moniker of 'umbrella cells'. Superficial cells express AUM plaques, which maintain the protective barrier functionality. Basal cells are attached to the basal membrane (black dotted line). The bladder walls enable the contraction and distension of the bladder, and are formed of elastic connective tissue (grey) smooth muscle (orange) and detrusor muscle (pink).*

Urothelial barrier function is dependent on the expression of the asymmetrical unit membrane (AUM) plaques at the apical cell surface and expression of tight junction proteins and claudins at the paracellular junctions of superficial cells. AUM plaques cover up to 90% of the apical surface of the bladder, and are comprised of uroplakin multimers, limiting the exposure of the underlying urothelium to urinary toxins and enabling the change in surface area required for bladder distension (reviewed by Lewis (2000)). Urothelial tight junctions are formed from multiple proteins in complex, including occludins, claudins and zona occludens proteins, and are regulated by the complex transcriptional regulation of urothelial cytodifferentiation (Smith et al., 2015; Varley et al., 2006; Varley and Southgate, 2008).

In order to fulfil its function as a tight barrier, the urothelium has evolved rapid and effective mechanisms of repair. Under steady-state conditions, the urothelium is mitotically quiescent, with few cells expressing markers of proliferation and extremely slow turnover (Marceau, 1990). However, upon injury, and disruption of the urothelial barrier, the urothelium rapidly begins proliferation, re-epithelializing the wound and recovering a tight barrier within 48 hours in a rodent model (Kreft et al., 2005).

The regenerative and barrier function of the urothelium is supplemented by its sensory abilities, the disruption of which may be linked to pathologies such as interstitial cystitis (discussed by Birder, 2006). The urothelium is reported to detect chemical, mechanical and thermal stimuli *via* a broad range of ion channels and receptors, including TRP and sodium channels (discussed and reviewed in Birder, 2006 & Birder et al., 2010). The urothelium may also communicate with the underlying stromal and neuronal cells by release of neurotransmitters such as nitric oxide and acetylcholine, although the evidence of such mechanisms remains controversial (reviewed by Yu and Hill, 2011).

1.2 Urinary tract infection

Urinary tract infections are one of the most common infections worldwide, responsible for approximately 8 million visits per year to healthcare services in the United States, and over 640,000 hospital admissions in England in 2012. Women are significantly more at risk of UTI than men, with a third of women suffering from at least one episode of UTI by the age of 23 (Foxman, 2002; Laupland et al., 2007). UTIs are also prevalent in extremes of age and in immunocompromised individuals.

Escherichia coli is the primary causative agent of UTI, responsible for 64% to 80% of infections (Laupland et al., 2007; Ronald, 2002). Clinical presentation of UTI is often broadly divided into uncomplicated and complicated infections. Uncomplicated infections are acute onset, affecting the lower urinary tract in otherwise healthy women below the age of 65. Infections in otherwise healthy individuals are often self-limiting, and do not require treatment. Current UK clinical guidance (reviewed by Scottish Intercollegiate Guidelines Network, 2012) suggests empirical treatment with antibiotics only in severe cases.

Non-antibiotic treatments for UTI exist, however the evidence basis for their use in clinical practice is small. Cranberry juice has been suggested as a naturopathic prophylactic and treatment for UTI (Stothers, 2002). The evidence for cranberry juice or extracts having beneficial effects in treating or preventing UTI *in vitro* or in the clinic is positive, however study limitations have precluded 'official' recommendations (Vasileiou et al., 2013).

Recurrence of UTI is a common problem, particularly in the female and juvenile populations. The traditional definition of recurrent UTI is two or more infections within a

six month period, with up to 44% of women suffering from such an infection (Gupta and Trautner, 2013). The genotype of bacteria isolated from separate episodes of recurrence were often genotypically identical, and recurrence episodes with between 1 and 3 years separation were caused by the same species (Ejrnæs et al., 2011; Russo et al., 1995). Treatment of recurrent urinary tract infection (UTI) with low dose prophylactic antibiotics has been shown be highly effective compared to placebo, with a 85% reduction in the rate of recurrence with no favoured antibiotic class (Albert et al., 1996).

UTIs are a considerable healthcare burden and, despite the effectiveness of antibiotic treatment, can cause considerable morbidity in vulnerable populations. Much of clinical practice is based upon clinical observation for diagnosis and treatment with narrow spectrum antibiotics. The effectiveness of non-antibiotic options for the treatment and prevention of UTI is poor. Further understanding of the host-pathogen interactions with the urothelium and immune defences of the bladder would inform the development of new approaches for the treatment and prevention of UTI, helping to improve quality of life for patients, and reducing the burden of UTI on the healthcare system.

1.3 Normal human urothelial cells

Prior to the development of the normal human urothelial cell (NHU) culture system by Southgate and colleagues (1994), studies of urothelial biology were limited to 'scraped' cell samples from bladder (with poor viability in culture), bladder cancer cell models or murine models (the limitations of these approaches are discussed further in chapter 5). NHU cells are isolated from surgical specimens of bladder or ureter and can be reliably cultured as finite cell lines. Cells can be maintained in a proliferative state in a low-calcium (0.09mM), serum-free medium, forming a proliferative cell monolayer that express the cytokeratin markers of basal and intermediate urothelial cells. As *in vivo* urothelial cells are normally mitotically quiescent, it has been suggested that proliferative NHU cells adopt a 'wound healing' phenotype(Shabir and Southgate, 2008).

Proliferative NHU cells can be induced to form a biomimetic, differentiated phenotype, forming a high TER (>3000 $\Omega.cm^2$), recapitulating the structure and stratification of protein expression of urothelial cells *in vivo* (Cross et al., 2005). Differentiation was induced by seeding proliferating NHU cells upon porous TransWell™ inserts, and supplementing cultures with 5% (v/v) bovine serum and physiological (2.2mM) concentrations of calcium.

1.4 The urothelial role in innate defence

The urinary tract is traditionally considered to be a sterile environment. The urothelium, in a similar manner to other epithelial tissues such as the gut and the bronchi, acts as a interface and barrier against infectious organisms, and has evolved several layered defences, both physical and chemical, to prevent bacterial colonization. These defence mechanisms are largely successful: despite the prevalence of UTIs as the 2nd most common infection in man (Foxman, 2010), the majority of such infections are self-limiting and do not require treatment (Bent et al., 2002)

The concept of the urothelium as a sensor and effector of the innate immune system has gained significant traction in the scientific literature in the past decade (as discussed by Becknell et al., 2015; Birder et al., 2012; Birder, 2006; Lazzeri, 2006). Studies conducted *in vitro* and *in vivo* with human and murine models (discussed in chapter 5) have suggested that a complex mixture of compounds with antimicrobial activity are both constitutively expressed by the urogenital tract and are further induced by bacterial exposure (Becknell et al., 2015). The specialisation of uropathogenic bacteria to thrive within the urinary tract niche (discussed later in this chapter) has developed as a complex interplay during host and pathogen evolution.

In patients who are predisposed to infections, due to possible genetic factors (Hawn et al., 2009) or deficiencies in vitamin or hormonal signals (Lüthje et al., 2014), defences may be inhibited or incomplete, leading to poor bacterial clearance. Long-term and recurrent bacterial colonisation with uropathogens can cause serious clinical sequelae, including ascending infection, urosepsis and renal scarring (Park, 2012), associated with decreased quality of life. Recurrent infections present a significant challenge to clinicians due to the lack of treatment options beyond prophylactic antibiotic administration and the emerging resistance to antibiotics by uropathogenic bacterial strains (Blango and Mulvey, 2010). An increased understanding of the innate antimicrobial response *in vivo* may provide avenues for the adaptation or exploitation of non-antibiotic mechanisms for the treatment of recurrent UTIs.

1.4.1 Uropathogenic bacterial specialisation

The number of verified bacterial species that cause UTI is limited. The majority of acute infections are caused by Gram-negative species, in particular *E. coli,* which is responsible for 64-80% of community-acquired infections (Laupland et al., 2007; Ronald, 2002).

Significant heterogeneity in the causative species of UTI has been observed in different healthcare settings, with *E. coli* infection less prevalent in the hospital and nursing home settings compared to cases presenting to primary healthcare (Laupland et al., 2007). *Klebsiella pneumoniae*, *Enterococcus sp*. and *Proteus sp*. are also prevalent causative species of community-acquired UTI, although at a much lower incidence than *E. coli* UTI. An important differentiation must be made between community-acquired UTI and nosocomial infections. Nosocomial infections are typically associated with the use of urinary catheters, and as such, a different spectrum of bacterial colonisation is observed, with a reduction in the number of *E. coli* isolates and increased prevalence of other atypical uropathogenic species, such as *Pseudomonas sp.,* Candida, *Enterococcal* and *Staphylococcal* species (Nicolle, 2014; Ronald, 2002). This thesis considers only the 'acute' phase of infection by *E. coli* as the causative organism.

The urinary tract is a harsh environment for bacterial colonisation. The continuous production and one way flow of urine, containing high concentrations of urea, inorganic salts and low concentrations of proteins and carbon sources provides a poor substrate for bacterial growth. This, in addition to the physical and chemical defences evolved by the urinary tract has driven the evolution of highly specialised virulence factors, expressed by uropathogenic species of *E. coli*, in order to survive and colonise the urinary tract 'niche'.

UPEC display a high level of genetic variation, with many of the specialised uropathogenic virulence factors encoded on transferable pathogenicity islands, parts of which are specific to different uropathogenic strains (Brzuszkiewicz et al., 2006). UPEC can contain up to 13 horizontally transmitted pathogenicity islands, creating a 'mosaic' genome (Welch et al., 2002). UPEC virulence factors can be subdivided into three primary groups: initial colonisation factors that are important for gaining an initial foothold in the host; maintenance factors; required for the continued survival of the pathogen in the urinary tract, and immunomodulatory factors; which are responsible for reducing or subverting the host immune response to the uropathogen.

1.4.1.1 Initial colonisation factors:

In order to begin colonisation of any epithelium a pathogen first requires a method of attachment. Such a mechanism is essential in the context of the urinary tract, due to the continuous 'flushing' effect of urine exerting shear forces on the bacteria. Fimbriae are the most common mechanism of adhesion in gram-negative organisms (Edwards and

Puente, 1998). The fimbriae act as extracellular scaffolds upon the tip of which a subunit protein, the adhesin, acts at the bacterial receptor, conferring the specificity and tissue tropism of the pathogen. The expression of adhesins is a crucial determinant of pathogenic bacterial strains (Coutte et al., 2003), including uropathogens (Connell et al., 1996).

P fimbriae

P fimbriae, or pyelonephritis-associated pili (PAP) are *E. coli*-specific fimbriae that are highly associated with UPEC virulence (Johnson, 1998; Wullt et al., 2000). The PAP consists of a polymeric fibre, consisting of papA monomers, capped with three minor tip subunits: PapE, PapF and PapG. PapG is the adhesin subunit, conferring P-fimbriae's specificity to Galα(1-4)Gal (Gal-Gal) disaccharide motifs within surface glycolipids, however PapF is also required for receptor specificity(Lund et al., 1987).

Three classes of *papG* adhesin exist, with differing affinities to glycolipid structures containing the Gal-Gal moiety (Marklund et al., 1992). Human UPEC isolates express type II and III *papG*, which differ in their binding to cell membrane glycolipids. Type II PapG binds preferentially to globoside, a glycosphingolipid abundant in the upper urinary tract (Stapleton et al., 1998). Type III *PapG* displays preferential binding to the Fossman antigen and globoA, extended versions of globoside. As suggested by the specificities of the *PapG* isotypes, Type II *PapG* isolates dominate in pyelonephritis patients (Söderhäll et al., 1997), whilst Type III *PapG* is observed in cystitis isolates but rarely in pyelonephritis (Johanson et al., 1993).

The role of papG beyond simple adhesion in the human urinary tract is unclear. Human studies of experimental clinical colonisation utilising recombinant P-fimbriated asymptomatic bacteriuria strains of *E. coli* suggest that *PapG* expression establishes bacterial colonisation more rapidly than non-*Pap* expressing strains (Wullt et al., 2001, 2000). Similar studies also suggest that glycolipid-*PapG* interactions activate a mucosal inflammatory response
in vitro and *in vivo* in human cells, inducing the release of inflammatory cytokines(Hedlund et al., 1996; Svensson et al., 1994; Wullt et al., 2001). Such a response is counter intuitively hypothesised to enable further colonisation of the urothelium, and

to act as a differentiator between uropathogenic and asymptomatic E coli (Bergsten et al., 2004).

Type 1 fimbriae

Type 1 fimbriae (T1F) are the most common adhesion molecules expressed by UPEC (Bahrani-Mougeot et al., 2002; Marrs et al., 2005, p. 1). T1F consist of a helical rod-shaped scaffold, formed of *FimA* subunits, capped with a tip formed of multiple *fimH* adhesin molecules(Pak et al., 2001; Thumbikat et al., 2009; Wu et al., 1996; Zhou et al., 2001). T1F are prevalent in many pathogenic and saprophytic strains of *E. coli*, and were originally defined by their ability to haemagglutinate guinea pig erythrocytes in a mannose-sensitive manner (Duguid et al., 1979).

In vitro and *ex vivo* models of urinary tract infection have demonstrated the ability of UPEC *fimH* to bind specifically to mannose residues present on human uroplakin Ia and Ib (Pak et al., 2001; Thumbikat et al., 2009; Wu et al., 1996; Zhou et al., 2001). Uroplakins are integral elements of the urothelial plaques, which form 90% of the luminal surface of the urothelium and play an important role in urothelial barrier function (Wu et al., 2009). The role of *fimH* binding beyond its role in the initial adherence to the urothelium is unclear. Evidence from murine *in vivo* models of infection has suggested that *fimH* binding to uroplakin Ib may induce apoptotic signalling (Klumpp et al., 2006, 2001). Interactions between *fimH* and uroplakins may also play a role in intracellular colonisation of the urothelium by UPEC; this will be discussed further in Chapter 5.

Difficulties in the understanding of T1F as virulence factors in humans have also been raised by microbiological analyses of T1F expression. T1F are expressed in pathogenic, saprophytic and commensal strains of *E coli*, and *fim* gene frequency is not significantly different in high or low virulence strains of UPEC (Schwan, 2011; Wiles et al., 2008b). Clinically, small studies of T1F$^+$/*papG*$^+$ strains of *E. coli* isolated from acute pyelonephritis showed that *fim*$^+$ strains caused a rapid onset of symptoms with increased intensity compared to *fim* negative strains (Hull et al., 2002).

Flagella

Flagella are complex, multimeric organelles that mediate directed motility and chemotaxis in motile bacteria. Flagella are expressed by commensal and pathogenic

strains of *E. coli*, *Salmonella sp*. and others. Synthesis of flagellar components is ordered and highly regulated (Figure 1.2).

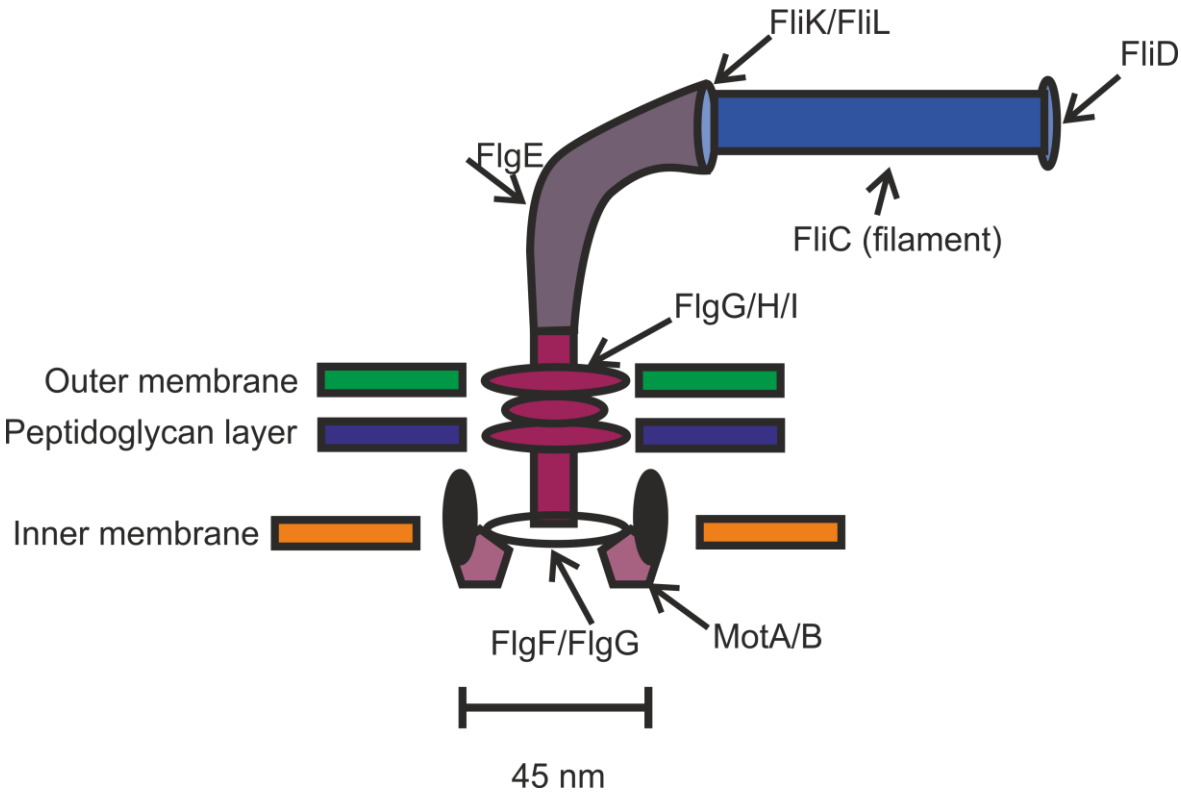

Figure 1.2 A simplified schematic of the flagellar machinery in motile bacteria.

The flagellum consists of the membrane-associated motor subunit (purple), the extracellular filament (blue) and the hook filament (grey). The filament and hook are polymeric in nature, consisting of repeating subunits of FliC and FlgE respectively. The flagellar filament consists of ~40,000 FliC (flagellin) subunits. Simplified and modified from Berg, 2003.

The importance of motility as a virulence factor in UPEC is an intuitive concept. UTIs are generally considered as ascending infections. Flagellum-mediated motility is hypothesised as an important mechanism for the dissemination of UPEC from the lower regions of the urinary tract, to the bladder and kidneys. Motility has been demonstrated as an important virulence factor in both cystitis and pyelonephritis in multiple *in vivo* models. Competitive co-infections in murine models of ascending UTI demonstrated that both aflagellar mutant pyelonephritis and cystitis UPEC isolates were at a fitness disadvantage to wild-type flagellated strains (Lane et al., 2005; Wright et al., 2005). In non-competitive colonisation studies, aflagellar UPEC remained able to colonise the

urinary tract, suggesting that expression of flagella may confer a subtle fitness advantage (Lane et al., 2005).

Temporospatial tracking of flagella filament expression has suggested that aflagellar UPEC were able to establish infection in the bladder 6 h following infection, but significantly attenuated in the kidney at the same time point in comparison with a wild type strain(Lane et al., 2005). The aflagellar mutant was also significantly attenuated in both the bladder and kidneys at 48 h post infection, suggesting motility may play a role in the maintenance of UPEC colonisation post initial infection.

1.4.1.2 UPEC Maintenance and immunomodulatory factors

As discussed above, the urinary tract is a harsh, nutrient-poor host environment for bacterial colonisation. Consequently, UPEC have evolved a range of mechanisms to protect against their environment and scavenge essential nutrients from the host cells and elsewhere. These processes can damage and lyse the host cells, releasing essential nutrients (e.g. iron). The nature of such mechanisms inherently exposes their components to the host immune system. As such, bacterial virulence factors involved in these processes have evolved to counteract the defensive mechanisms present in the urinary tract, and to adapt to growth in urine.

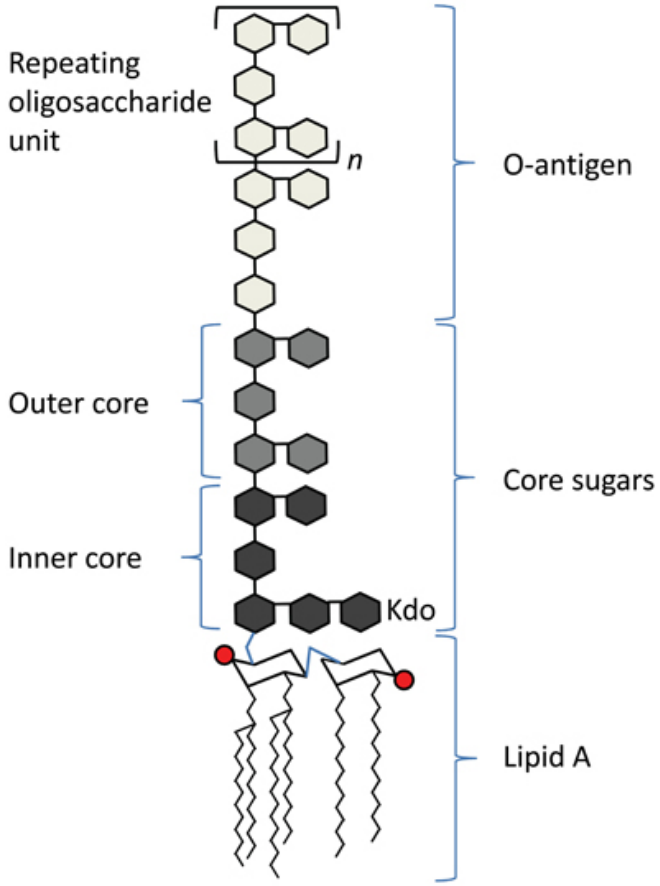

Figure 1.3 Structure of lipopolysaccharide.

The conserved lipid A 'tail' is embedded in the bacterial outer membrane, whilst the highly variable O antigen and core sugars project into the extracellular space. Schematic from Maeshima and Fernandez, 2013

Lipopolysaccharide

Lipopolysaccharide (LPS) is the dominant constituent of the outer membrane of Gram-negative bacteria. LPS consists of three primary sub-units: the hydrophobic glycolipid anchor (lipid A), a core oligosaccharide domain, and a repetitive polysaccharide chain, referred to as the O antigen (Figure 1.3). LPS confers permeability barrier integrity to the bacterial outer membrane (Alexander and Rietschel, 2001), and is hypothesised to protect against elements of the complement system.

As the primary outer membrane constituent, LPS is highly exposed to the host immune system. LPS has been demonstrated to activate a proinflammatory response *in vivo*, inducing nitric oxide and cytokine production (Bäckhed et al., 2001). The role of LPS in the urothelial response is unclear: studies utilising whole human biopsy samples suggest

that human urothelium is responsive to LPS (Samuelsson et al., 2004), whilst studies utilising normal human urothelial cells *in vitro* suggest that they are unresponsive to LPS, even in the presence of exogenous co-factors required for LPS sensing (Smith et al., 2011)

Peptidoglycan

Peptidoglycan (PG) is a simple cross-linked polymer, formed of a repeating glycopeptide subunit, which forms part of the cell wall in both Gram positive and negative bacteria. In *E. coli*, the glycopeptide comprises of a N-acetylglucosamine- N-acetylmuramic acid disaccharide linked to a 4-mer oligopeptide (Royet and Dziarski, 2007) (Figure 1.3a). PG is one of the primary constituents of the bacterial cell wall, forming a 3D mesh conferring structural strength and resistance to osmotic pressure (Figure 1.3b) (Young, 2011). Gram-negative bacteria (such as *E. coli*) have a much thinner peptidoglycan layer than Gram-positives, which is 'masked' from the external environment by the outer bacterial membrane.

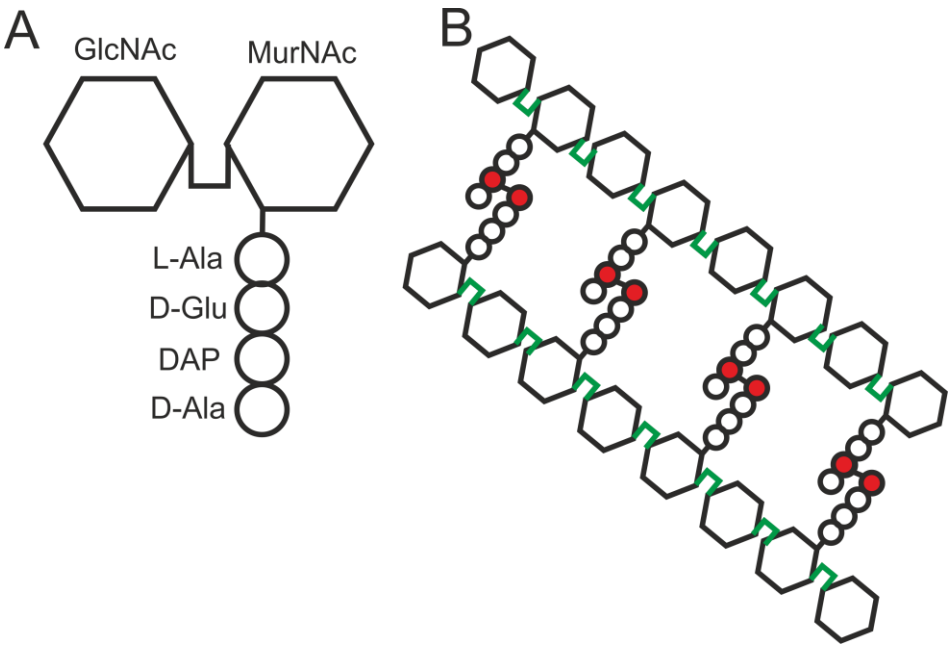

Figure 1.4 Peptidoglycan structure.

A: A peptidoglycan monomer from E. coli. The monomer is formed from an N-acetylmeramic acid-N-acetylglucosamine (MurNAc-GlcNAc) disaccharide. The N-acetylmuramic acid residue is modified with a 4-mer oligopeptide, formed of L-alanine (L-Ala), D-glutamic acid (D-Glu), Diaminopimelic acid (DAP) and D-Alanine (D-Ala). B: The basic polymeric structure of peptidoglycan. Each disaccharide unit is bound with a β(1-4) glycosidic bond (green) and each oligopeptide is bound by a peptide bond between DAP and D-Ala of opposite tetrapeptide (red).

Siderophores

Limitation of free iron concentration is a common strategy utilised by mammals in order to limit bacterial growth. Iron is an essential co-factor in prokaryotic biochemistry: bacteria require a cytoplasmic iron concentration of approximately 10^{-6} M for continued growth (Andrews et al., 2003). In pathogenic bacteria, this relatively high concentration must be scavenged from the host, where free iron concentrations are extremely low ($<10^{-25}$ M (Barasch and Mori, 2004).

Consequently, UPEC and other uropathogens express a complex and redundant set of iron acquisition systems that utilise siderophores to scavenge scarce free iron from the urine (Henderson et al., 2009). Siderophores are low molecular weight molecules with a high affinity to Fe^{3+} ions (Barasch and Mori, 2004). The siderophores are expressed into the environment, where they bind free iron, and are retrieved by siderophore receptors, increasing intracellular free iron concentration (reviewed in Andrews et al., 2003). Human urine contains a range of iron-chelating (Peters et al., 2013) and siderophore binding (Goetz et al., 2002) proteins which interfere with this process.

Secreted toxins

The host environment encountered by pathogenic *E. coli* in the urinary tract is nutrient-poor. A calcium-dependent, pore-forming toxin, α-hemolysin (HlyA) is encoded by 50% of UPEC strains, and is correlated with increased symptom severity in UTI patients (Marrs et al., 2005). High concentrations of HlyA, *via* its pore-forming activity, are hypothesized to lyse or damage host cells, releasing nutrients from the cytosol into the environment. However, at physiological conditions, HlyA is often present in sub-lytic concentrations (Dhakal and Mulvey, 2012).

Evidence from bladder cancer cell models has suggested that HlyA has pleiotropic effects on urothelial cell function *via* inactivation of Akt phosphorylation (Wiles et al., 2008a). Akt, or protein kinase B, plays important roles in the inhibition of apoptosis, the control of cell cycle and metabolic pathways, and perhaps most importantly, the regulation of NFkB activation, the 'master regulator' of inflammatory response (Fayard et al., 2005). HlyA is also hypothesised to induce proteolysis of the cytoskeletal scaffold

and regulatory mechanisms in bladder cancer cells by activation of host serine proteases (Dhakal and Mulvey, 2012).

HlyA is considered a prototypic UPEC toxin, however several other secreted toxins have been described with similar effects on host cell regulation. Expression of secreted autotransporter toxin (Sat) is associated with UPEC pyelonephritis isolates (Guyer et al., 2000), and acts *via* a similar mechanism of serine protease activation as HlyA, affecting cytoskeletal integrity (Maroncle et al., 2006).

1.4.2 The urothelial response to infection

Host defences against infectious organisms are multi-layered, consisting of physical barrier functions, the innate and adaptive immune systems. The innate immune system acts as the first line of immune defence, sensing and responding immediately to highly conserved pathogen-associated molecular patterns (PAMPs) expressed specifically by microbes. PAMPs are sensed by a limited number of germ-line encoded innate immune receptors expressed by the host.

The adaptive immune system is the second line of immune defence, which recognises and responds to specific 'non-self' antigens. These antigens are processed and recognised leading to a systemic recruitment and production of a response highly specific to that antigen, and the production of an immunological memory. The use of somatic mutations and recombination by the host allows for the generation of a vast number of different antigen receptors, allowing the adaptive immune system to respond to an almost unlimited set of antigens.

Compared to other epithelia, such as the intestine and respiratory tract, little is known about the steady-state professional immune cell population in the human bladder. Evidence exists for the presence of antigen presenting cells (Hjelm et al., 1982), antibody-producing plasma cells and T-cells (Christmas, 1994) in the human bladder at steady state, however little is known of the response of such tissue resident cells during infection. Limited evidence, primarily observations from murine models of infection, have suggested a modest role for adaptive immunity in the response to UPEC (reviewed in Ingersoll and Albert, 2013). Despite the lack of functional understanding of the adaptive immune response to uropathogens, several vaccine-based approaches to UTI prevention have been trialled, with limited success (discussed by Brumbaugh and

Mobley, 2012) further suggesting the modest role that adaptive immunity plays in uropathogen response.

1.4.3 Innate immunity at the urothelial barrier

The role of urothelial cells as important elements of innate immunity has been increasingly recognised, due to change from urothelium being considered as a simple, effective urinary barrier to an sensing/transducing tissue (Birder et al., 2010).

The physical characteristics of the urinary tract aid in its innate immune role. Urine is continuously produced by the kidneys and flows unidirectionally, preventing retrograde travel of microbial contamination from the lower tract to the bladder and kidneys. Constitutive expression of proteins such as uromodulin, lactoferrin and lipocalin inhibit bacterial colonisation in a bacteriostatic manner, binding bacterial adherins or limiting bacterial iron uptake (Goetz et al., 2002) (Åbrink et al., 2000; Goetz et al., 2002). Such mechanisms are however constitutive, and not induced by bacterial infection. In order for an inducible response to occur, bacteria or bacterial virulence factors must first be recognised by the host.

Human urothelial cells express several families of innate pathogen sensing receptors, including the toll-like receptor (TLR) family (Ayari et al., 2011; Smith et al., 2011), pentraxins (Jaillon et al., 2014) and NOD-like receptors (NLRs) (Kummer et al., 2007). This introduction will discuss primarily those expressed by the urothelium, and their role in the urogenital innate response.

1.4.3.1 Toll-like receptors

Originally identified as evolutionary-conserved homologues of the *Drosophila Toll* protein (Medzhitov et al., 1997; Rock et al., 1998), the discovery of Toll-like receptors (TLRs) heralded a deep change in understanding of the innate immune system from a basic, inelegant initiator of the adaptive immune system, to a complex and highly important 'stand-alone' element of the immune response (reviewed in O'Neill et al., 2013). Since the initial discovery of five human TLR homologues (Rock et al., 1998), a total of ten human TLR genes have been identified, and 12 in mice (reviewed in Kawai and Akira, 2009).

TLRs are omnipresent in immune cells, and are widely expressed by epithelial tissues. TLRs can drive the pleiotropic activation of both innate and adaptive immune reactions, including activation of T-cells (Komai-Koma et al., 2004; Sutmuller et al., 2006), B-cells (reviewed by Browne, 2012) and antigen presenting cells, (Rad et al., 2007) as well as the induction of a wide range of inflammatory signalling cascades (reviewed by Mogensen, 2009). As discussed previously, epithelial tissues act as barriers to microbes. As such, the evolution of innate immune sensors at these sites of host-microbial interactions, enabling rapid initial sensing of pathogens is favourable to the host.

TLR4

TLR4 was the first *Toll* receptor analogue identified in mammals (Medzhitov et al., 1997). LPS had been identified as the agent responsible for inducing Gram-negative sepsis, and as a non-specific inducer of immunity in mice since 1956 (Landy and Pillemer, 1956), however the TLR4 gene was not definitively identified as the cell-activating LPS receptor until 1998 (Poltorak et al., 1998). The mechanism of LPS sensing by TLR4 is complex, involving several accessory molecules (Figure 1.5). The lipid A core of LPS is believed to be the primary TLR4 agonist, however TLR4-dependent sensing of several other diverse compounds, including other bacterial components, has been described. Efficient LPS signalling requires the LPS co-receptor CD14, normally considered a macrophage-specific cellular marker (Haziot et al., 1988).

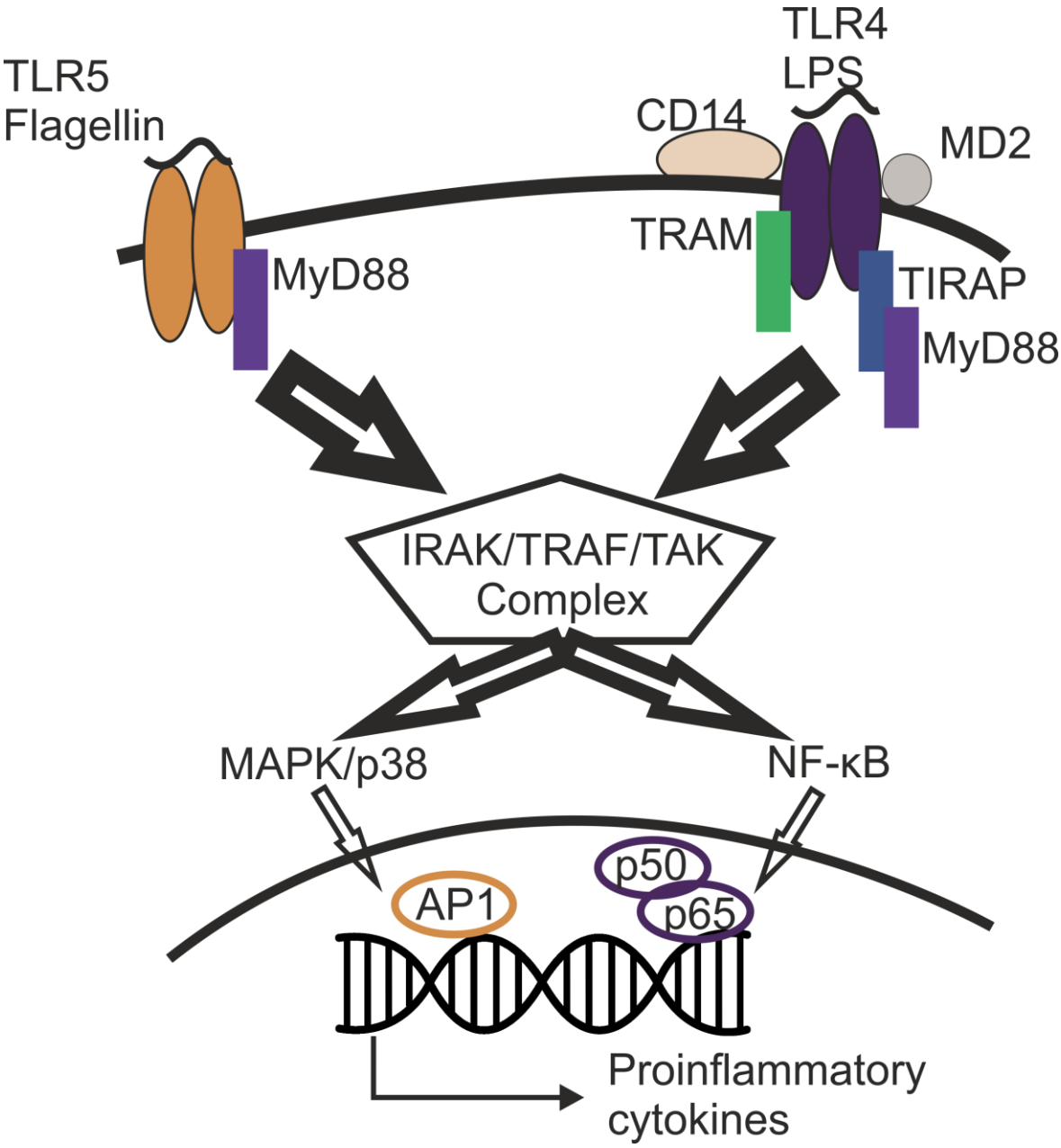

Figure 1.5 Overview of TLR4 and TLR5 signalling pathways.

Both TLR5 and TLR4 are activated by homodimerisation of two identical receptor subunits upon binding to the target PAMP.

The sensing of LPS by urothelial cells was first described by Bäckhed et al. (2001) in a T24 bladder cancer cell line. Prior to the identification of a TLR mediated sensing mechanism, bacterial interaction with the urothelium was thought to be primarily fimbriae and toxin-mediated (Hedlund et al., 1996). The role of LPS in UTI has been complicated by the use of several differing experimental systems, both *in vivo* and *in vitro*. This will be discussed further in Chapter 5.

TLR5:

TLR5 is the specific mammalian receptor for bacterial flagellin (Hayashi et al., 2001). TLR5 is highly conserved, and remains the sole TLR conserved in all vertebrates. Unlike TLR4, which is implicated in the binding and sensing of multiple molecules, TLR5 is the sole human TLR specific in sensing a single target, flagellin.

TLR5-flagellin sensing is dependent on the interaction of the horseshoe-shaped extracellular leucine-rich repeat (LRR) domain with a triple helix motif present in the D1 domain of flagellin (Yoon et al., 2012). Intracellular signalling occurs following the dimerization of two flagellin-bound TLR5 receptors. This dimerization juxtaposes the intracellular TIR domains, initiating a MyD88-initiated signalling cascade, shared by all human TLRs. Activation of the MyD88 signalling cascade leads to the activation of NF-kB and p38-MAPk signalling pathways, leading to cytokine synthesis and activation of other downstream targets.

Both professional immune cells, such as macrophages and dendritic cells, and epithelial cells express TLR5. Epithelial TLR5 function has primarily been studied in the intestinal epithelium, however functional expression of TLR5 has been noted in airway, gastric and caecal (Ortega-Cava et al., 2006; Wang et al., 2012) epithelial cells, and by the urothelium (Andersen-Nissen et al., 2007; Smith et al., 2011b).

TLR5 is expressed basolaterally in the intestinal epithelium, possibly as an evolved spatial mechanism of immunomodulation in the gut (Gewirtz et al., 2001). Both gut pathogens and commensals express flagellin. Pathogenic bacteria (e.g *Salmonella*) translocate flagellin across the epithelia, activating inflammatory cytokine production (Gewirtz et al., 2001). Polarised expression of TLR5 to the basolateral aspect of the epithelial may therefore play a role in preventing inflammatory responses to commensal bacteria.

1.4.3.2 Inflammosomes

Inflammosomes are multi-protein complexes activated by sensing of danger-associated or pathogen-associated molecular patterns (DAMPS/PAMPS), responsible for activation of caspase-1 and inflammatory cytokines IL1B and IL18 (Martinon et al., 2002). Functionally, inflammosome activation is similar to TLR activation, sensing a PAMP *via* interaction with a pattern recognition receptor, leading to downstream activation of signalling. Mechanistically, however, inflammosome activation is significantly different.

Inflammasomes are strictly cytosolic, whereas TLR activation is associated with a plasma membrane or vesicular membrane. Canonical inflammosomes act as a scaffold for recruitment of pro-caspase-1 proteins, inducing oligomerization and cleavage to active caspase-1 . Inflammosomes therefore act primarily *via* caspase-1 protease activity, generating biologically active cytokines and inducing pyroptosis, an inflammatory form of cell death(reviewed recently by Guo et al., 2015). Inflammosome assembly can be induced *via* several protein complexes in response to numerous exogenous and endogenous stimuli. Binding of a DAMP or PAMP to NLRP3, which initialises scaffold formation, induces the canonical inflammosome. A prior NFkB activating stimulus is required in order to 'kick-start' NLRP3 expression and post-translational modification before inflammosome activation can occur(Dziarski and Gupta, 2006). NLRP3 can bind a varied range of ligands, including ATP, toxins, nucleic acids, hyaluronan and bacterial flagellin (reviewed by Vanaja et al., 2015).

The role of inflammosomes in urothelial innate immunity is unclear. Few studies have been published discussing the role of inflammosome-mediated inflammation in the lower urinary tract, focusing upon LPS-mediated mouse models of cystitis (Hughes et al., 2016b, p. 3), bladder obstruction (Hughes et al., 2016a) and cyclophosphamide-induced cystitis (Hughes et al., 2014) providing evidence that NLRP3-mediated inflammation occurs in model systems of UTI.

1.4.3.3Peptidoglycan sensing

PG sensing is a highly conserved mechanism in insects and mammals, as part of the innate immune system. Peptidoglycan is an ideal target for innate immune sensing, due to its ubiquity and specificity to bacterial species. Several innate immune sensing mechanisms exist in mammalian cells for PG recognition. PG is sensed at the cell surface by membrane-bound CD14 in concert with TLR2 (Dziarski et al., 1998; Dziarski and Gupta, 2005; Iwaki et al., 2002), with evidence of this interaction existing in a bladder cancer cell model of UTI (Shimizu et al., 2004).

Intracellular sensing of PG is mediated by the NOD-like receptor family (NLR) with two human members, NOD1 and NOD2. NOD1 senses fragments of the PG tetrapeptide containing DAP, limiting NOD1's specificity to primarily Gram-Negative bacteria (Chamaillard et al., 2003; Girardin et al., 2003b), however NOD1 is also implicated in the intracellular sensing of other bacterial components such as LPS (Inohara et al., 2001). NOD2 is reported to sense the MurNAc-L-Ala-D-Glu (muramyl di-peptide) fragment of PG, suggesting that NOD2 can sense almost all PG variants (Girardin et al., 2003a, 2003b; Inohara et al., 2003).

Soluble PG sensing mechanisms also exist in humans. A family of four peptidoglycan recognition proteins (PGLYRP1-4) are expressed in humans, and interact with the muramyl tri-peptide or larger fragment of PG(Chang et al., 2004; Guan et al., 2006, 2005). PGLYRP3 and PGLYRP4 are expressed at epithelia which interact with the external environment, and all PGLYRPs act as bactericidal agents with differing specificities (Lu et al., 2006). PGLYRPs may also act synergistically with AMPs, increasing their bactericidal efficacy (Wang et al., 2007)

1.4.3.4 Other soluble response mechanisms to uropathogenic stimuli

In the broadest terms, cytokines are small (4- 20kDa) proteins which, when released, influence the movement and behaviour of cells around them, and are normally linked to immunomodulatory functions. Cytokines play a core role in innate and adaptive immunity, controlling almost all regulatory aspects of both systems: a full review of cytokine function is outside the scope of this thesis.

Previous studies have shown that the urothelium itself acts as a source of cytokines. NHU cells in culture produced both IL6 and IL8 constitutively, and production is further induced by TLR5 activation (Smith et al., 2011). IL6 and IL8 are both important elements of the acute phase of inflammatory response. IL8 (also known as CXCL8) acts a chemokine, attracting neutrophils and other granulocytes to the site of release, and inducing the activation and apoptosis of

neutrophils. IL6 is an important acute phase cytokine, inducing the production of acute phase proteins such as C reactive protein and factors of the complement system (reviewed in (Hunter and Jones, 2015)

1.5 Thesis aims and objectives:

This thesis aimed to develop the urothelial cell model to study the urothelial cell response to uropathogenic bacteria and uropathogen virulence factors, with a specific focus on antimicrobial peptide (AMP) production and detection of AMPs *via* mass spectrometry.

The main objectives of this thesis were:

- To determine the basal and inducible AMP responses to uropathogenic bacteria and uropathogenic virulence factors by normal human urothelial cells

- Develop a method to detect AMP release *via* mass spectrometry

- To assess the effect of urothelial differentiation upon the urothelial response to UPEC.

By increasing the understanding of NHU cell responses to UPEC and UPEC virulence factors, this thesis aimed to provide a better understanding of *in vivo* urothelial response to uropathogens, providing research questions for future investigation of UTI pathogenesis, and possible non-antibiotic treatments harnessing the host response to infection.

2 Materials and methods

2.1 Practical Work and Collaborations

Practical work was undertaken in the Jack Birch Unit (JBU), Centre of Excellence in Mass Spectrometry (CoEMS) and Centre for Immunology and Infection (CII), Department of Biology, University of York. The Genomics laboratory in the Department of Biology Technology Facility provided support and use of equipment. Dr David Ashford and Dr Ed Bergstrom maintained mass spectrometry instruments at CoEMS.

Lambda red recombination experiments were conducted in the lab of Dr Marjan Van der Woude (Centre of Immunology and infection, University of York), by Stefan Tran, a project student under my supervision. Purified UPEC flagellin was a gift from Professor Rob Pickard, University of Newcastle. K12-pKD46 and UTI89 *E. coli* and *Klebsiella pneumoniae* ATCC13883 were a gift from Dr Marjan Van Der Woude. FimH from RS218 *E. coli* was a gift from Professor Evgeni Sokurenko, (University of Washington, US). Raw RNAseq analyses and gene expression data in Chapter 3 and 5 were produced by Simon Baker at the Jack Birch Unit.

2.2 Water

All references to H_2O in this thesis refer to water treated with reverse osmosis in an ELGA water purifier to a resistivity of 18.2 MΩ. All water used for molecular biology experiments was treated with diethylpyrocarbonate (DEPC) to reduce nuclease contamination and associated nucleic acid degradation. ELGA treated H_2O was treated with 1mL DEPC per 1L of H_2O and autoclaved before use.

2.3 Suppliers

Suppliers and manufacturers are indicated at the first mention of a reagent or apparatus in the text.

2.4 Stock solutions

Recipes for all stock solutions are listed in Appendix 1. Chemical reagents were of analytical grade or higher unless noted.

2.5 Tissue Culture

2.5.1 Overview

All tissue culture was undertaken using aseptic technique in a class II biological safety hood. Externally vented hoods were used for any experiments using infectious organisms. All hoods were cleaned with 70% (v/v) ethanol before use. Cultures were maintained in Hera*Cell* 240 (Thermo Scientific) in humid 5% CO_2 in air, at 37°C. Waste cells and medium were aspirated by vacuum into a Buchner flask containing 10% (w/v) Virkon disinfectant (SLS) for decontamination before disposal. All cell centrifugation steps were performed in a Sigma bench-top swing-bucket centrifuge at 250 *g* for 5 min.

2.5.2 Urothelial sample collection

Human derived samples of ureter, bladder and renal pelvis were obtained from patients undergoing urological surgical procedures, with informed consent and relevant Research Ethics Committee approval. Each patient sample was allocated a unique identifying code (a 'Y number') on arrival to the JBU.

Surgical tissue samples were immediately collected in sterile 25 mL Universal containers containing sterile transport medium and stored at 4 °C until transported to the laboratory. Samples were processed immediately for NHU cell isolation, or stored at 4°C for a maximum of 24 h pre-processing. Aliquots of transport medium from patient samples thought to be at-risk of a recurrent urinary tract infection were cultivated in Luria-Bertani broth to assess the presence of bacteria. Isolates from positive cultures were cryopreserved and stored at -80 °C.

2.5.3 Normal Human Urothelial cell isolation

Primary, non-differentiated urothelial cell cultures were established from samples as described previously (Southgate et al., 1994). Samples were grossly dissected and stripped of excess fat and connective tissue using sterile forceps and scissors. The dissected samples was incubated in stripping buffer for 4 h at 37°C to aid disassociation

of the urothelium from the stroma. The disassociated urothelial cell sheets were gently detached from stroma using forceps and collected by centrifugation. The collected cell sheets were treated with 2 mL of collagenase solution (to disaggregate the cells, and incubated at 37°C for 20 min. Cells were collected *via* centrifugation, and seeded at a density of at least $4x10^4$ cells/cm^2.

2.5.4 Normal human urothelial cell culture and cryopreservation

Urothelial cells were maintained in supplemented keratinocyte serum-free medium (KSFM) (Life Technologies). KSFM was supplemented with 5 ng/mL recombinant epidermal growth factor (EGF), 50 µg/mL bovine pituitary extract (BPE) and 30 ng/mL cholera toxin (Sigma Aldrich). This supplemented media (referred to as KSFMc) was used for all NHU cell cultures. All NHU cells were cultured on Cell+^{TM} tissue culture plasticware (Becton Dickinson, UK).

NHU cells were sub-cultured at near-confluence by incubating cell monolayers in 0.1% (w/v) EDTA solution in PBS, to disassociate the cells. Cells were then incubated in trypsin versene solution for 1 min at 37°C. Cells were harvested in 5 mL KSFMc containing 1.5 mg/mL trypsin inhibitor (Sigma Aldrich), pelleted by centrifugation and the supernatant aspirated. Cells were resuspended in fresh KSFMc and split into fresh flasks or dishes. Cells were passaged at a ratio of 1:3. All experiments were conducted on cells of passage 3-5.

Cells required for long-term storage were preserved in liquid nitrogen dewars at -196°C. Cells were harvested as for passaging. Cells from one 75 cm^2 flask were resuspended in 6 mL of ice cold freeze mix. 1 mL of cell suspension was aliquoted into 1 mL polypropylene cryovials and transferred to an isopropanol-filled temperature-buffered freezing container. Cells were kept at -80°C overnight and transferred to liquid nitrogen. Cells were recovered from cryopreservation by quickly thawing with 5 mL warm KSFMc and centrifuged. Cell pellets were resuspended and plated at the required density.

2.5.5 Cell counting and imaging

Cells were observed during culture using an EVOS Core XL microscope (Life Technologies). Counts of single cell suspensions were undertaken using an 'Improved

Neubauer' haemocytometer. Cells were counted in 3 of the 4x4 grid cells, an average count calculated and multiplied by $1x10^4$ to obtain an average cell count per mL of medium.

Where cells were observed for extended periods of time, an Olympus IX71 differential interference contrast (DIC) microscope was used. The microscope was equipped with an environmental chamber with temperature and CO_2 control, and a mechanical stage to enable automated imaging of cultures. NHU cells were seeded in 24 well plates at least 24 hours before a time-lapse experiment. Individual images were captured every hour (unless noted) for 24 hours using a CoolSNAP-ProCF monochrome digital camera using a x10 objective.

2.5.6 In vitro differentiation of Normal Human Urothelium cells

Non-differentiated NHU cells were differentiated *in vitro* as described previously (Cross et al., 2005). NHU cells were cultured to near confluence, and the media replaced with KSFMc supplemented with 5% adult bovine serum (ABS) (SeraCell). Cells were maintained in 5% ABS for 5 days before the medium was changed to KSFMc supplemented with 5% ABS and 2 mM Ca^{2+}. Cells were maintained in ABS/Ca^{2+} supplemented KSFMc for 6-8 days, depending on the experimental protocol.

2.5.7 Biomimetic differentiation of NHU cells

NHU cell cultures preconditioned in KFSMc/5% ABS for 5 days were passaged as described above . Cells were suspended in KSFMc supplemented with 5% ABS and seeded onto 24mm, 0.4 µm pore size Transwell™ polyester membranes (Greiner Bio-One) at a concentration of $0.5x10^6$ cells/cm^2. Transwell™ inserts (Figure 2.1) required 500 µL and 1 mL of media in the apical and basal compartments respectively. The media was replaced 24 h post-seeding and the calcium concentration increased to physiological levels (2.2 mM). The cells were maintained in ABS-supplemented KSFMc for the remainder of the experiment, and the media replaced every 48-72 hours.

The differentiation status of the cultures was assessed *via* measurement of the trans epithelial electrical resistance (TEER) across the cell sheet. TER values were measured *in*

situ using an EVOM TEER meter (World Precision Instruments) using a 'chopstick' electrode. TEER values are expressed as $\Omega.cm^2$ using the surface area of the membrane as calculated to be 1.131 cm^2.

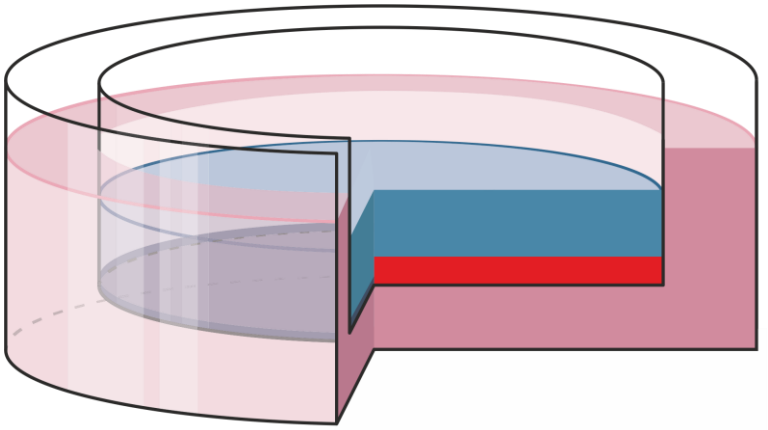

Figure 2.1. Schematic diagram of a TransWell® insert.

ABS treated NHU cells are seeded into the apical chamber and form a stratified layer upon the polyester semi-permeable membrane (red). Apical (blue) and basal (pink) chambers are separated. Based on a work at http://www.hhhoney.com/transwell-schematic/.

2.5.8 NHU: Bacterial cell co-culture

Experimental infection experiments were conducted using statically cultured bacteria in order to induce virulence factor expression (Old and Duguid, 1970). Overnight cultures of bacteria were collected *via* centrifugation and suspended at an OD^{600} of ~1 in sterile PBS, corresponding to $2.5x10^{10}$ CFU of UTI89 *E. coli* per mL. Bacterial suspensions were further diluted in sterile PBS before inoculation of cell cultures. An accurate count of the starting CFU/mL was performed by viable count methods (section 2.6.4.2)

2.6 Bacterial cell culture

2.6.1 Bacterial strains

Bacterial strains used are shown in Table 2.1.

Strains	Notes
***E. coli* UTI89**	Isolated from woman with uncomplicated cystitis
***E. coli* K-12**	wild type
***E. coli* K-12 pKD46**	amp^R, pKD46 for lambda Red recombination, grow at 30 °C (temperature-sensitive)
***E. coli* DH5-α**	cloning strain
***Klebsiella pneumoniae* ATCC13883**	amp^R
***E. coli* NU14**	'Archetypal' cystitis isolate
***E. coli* NU14-1**	fimH isogenic knockout (Johnson et al., 2001)

Table 2.1 Bacterial strains used in this thesis.

2.6.2 Bacterial culture conditions

Unless stated, bacteria were cultured in Luria-Bertani (LB) broth or on LB agar. LB broth and agar were sterilised by autoclaving at 121°C for 15 min. Antibiotic selection was undertaken on LB agar plates supplemented with 100 µg/mL ampicillin (LB-Amp), 12.5 µg/mL tetracycline (LB-Tet) or both ampicillin and tetracycline (LB-TA).

Experimental bacterial cultures were prepared by inoculation of 10 mL of LB with a single bacterial colony, picked from a LB agar plate streaked from a frozen glycerol stock. Unless noted, cultures were initially incubated overnight, with shaking, at 37°C prior to two passages in static culture at 37°C. Static culture induces the expression of bacterial adhesins (Hung et al., 2009; Old and Duguid, 1970)

2.6.3 Bacterial cryopreservation

Glycerol stocks of *E. coli* strains were prepared by inoculating 10 mL of LB broth with a single colony of bacteria and incubating overnight in a 37°C shaking (220RPM) incubator. 750 µL of overnight culture and 250 µL of sterile 80% glycerol (v/v) were added to a 1.5

mL polypropylene cryovial and stored at -80 °C. Experimental cultures were prepared by streaking ~1 µL of the glycerol stock onto an LB agar plate, culturing at 37 °C overnight, and preparing 10 mL overnight cultures from single colonies, picked using a sterile pipette tip.

2.6.4 Growth assays

2.6.4.1 Optical density measurements

Optical density measurements during preparative stages of experiments were undertaken using an Eppendorf BioPhotometer. Optical density was measured at 600nm in comparison to a blank measurement conducted on non-inoculated medium or buffer.

Comparative growth assays were conducted using a BMG FLUOstar Omega spectrophotometer measuring optical density at 650nm. Assays were conducted in 96 well plates. The external wells of the plate were filled with sterile water to minimise the effect of evaporation on the assay.

Overnight bacterial cultures were collected *via* centrifugation and resuspended in sterile PBS at a OD^{600} of 0.4, and diluted 1:100 in 200 µL of fresh, sterile medium per well. Plates were sealed with gas-permeable plate seals (4Media) to avoid accidental contamination of the plate reader. Blank samples were included in all experiments, and results reported as the blank-adjusted OD values. All experiments were set up with and results reported as the mean of 5 biological replicates (+/-SD).

2.6.4.2 Total viable counts

Total viable counts of bacterial cultures were conducted following the methods of Hung et al. (2009). Briefly, serial dilutions of bacterial cultures were prepared in a microtitre plate, and 5 µL of each dilution transferred to an LB agar plate. Both the serial dilution and transfer to the agar plate used a multi-channel pipette to reduce variability. Agar plates were incubated for 18 h and colonies counted. The number of bacteria per mL of starting inoculum was calculated using equation 1, where *n* is the number of colonies counted per 5 µL spot, *d* is the fold-dilution and *v* is the volume spotted. All counts were undertaken in triplicate.

$$CFU_{Inoculum} = \frac{n}{v} \times 1{,}000v$$

Equation 1.

2.6.5 Motility assays

The ability of bacterial strains to migrate was assessed using a chromogenic motility assay. The redox dye 2,3,5,-triphenyltetrazolium chloride (TCC) (Sigma Aldrich) was used as a marker for active cells. The colourless TTC reagent is reduced to red formazan in the presence of metabolically active bacteria. Stab cultures were prepared using soft motility medium and incubated overnight at 37 °C. Motile bacterial isolates produced turbid red cultures due to the movement of bacteria away from the stab mark (Figure 2.2, B) whilst non-motile isolates remain at the stab mark, creating a red track (Figure 2.2, A).

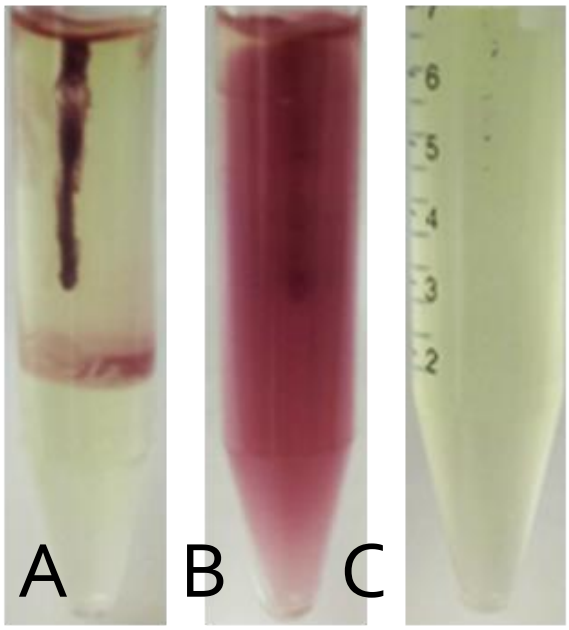

Figure 2.2 TCC motility assay.

A: Stab culture of a non-motile bacterial isolate. B: Motile bacterial isolate C: Negative control culture spiked with PBS

2.7 Molecular biology

2.7.1 RNA isolation and extraction

Culture medium was removed and 1 mL of TRIzol^{tm} (Life Technologies) added per ~15 cm^2 surface area of cultureware used. The cells were scraped from the culture with a cell scraper, passed several times through a pipette to further facilitate cell lysis before transfer to a RNAse-free 1.5 mL microcentrifuge tube. RNA samples in TRIzol^{TM} were stored at -80 °C until extraction.

The samples were thawed and incubated for 5 min at room temperature to ensure disassociation of nucleoprotein complexes. 200 µL of chloroform per 1 mL of TRIzol was added, mixed by vortexing and incubated at ambient temperature for 2-3 min. All centrifugation steps took place at 4°C. Samples were then centrifuged for 15 min at 12,000 *g*, and the aqueous phase collected in a fresh 1.5 mL microcentrifuge tube. 0.5 mL of isopropanol was added, mixed *via* inversion and incubated at ambient temperature for 10 min. The RNA was precipitated by centrifugation at 12,000 *g* for 20 min, and the supernatant removed. The RNA precipitate was washed twice in 1 mL of 75% ethanol and reprecipitated by centrifugation at 7,500 *g* for 5 min. The precipitated RNA pellet was air-dried and resuspended in 30 µL of nuclease-free H_2O.

RNA concentration and purity was assessed using a NanoDrop 1000 or 8000 UV-vis spectrophotometer (Thermo Scientific). The absorbance of each RNA extract was measured at 230 nm to calculate the concentration, using a conversion ratio of 40 µg per unit of optical density at 260 nm. The optical density at 230 and 280 nm were also measured to assess RNA purity, by assessing protein or phenol (ratio of 260/280 nm absorbance) or salt (230/260 nm ratio) contamination.

2.7.2 DNase treatment

All RNA samples were DNase treated using a DNA-*free*^{TM} DNA removal kit (Thermo Fisher) to remove genomic DNA contamination. 3.3 µ L of DNase I buffer and 1 µL recombinant DNase I was added to 30 µL of RNA solution, and mixed gently by pipetting

before incubation at 37°C for 30 min. 3.3 µL of DNase inactivation reagent was added to the solution. The mixture was incubated at room temperature for 2 mins with regular mixing, and the DNase inactivation reagent collected by centrifugation at 13,000 *g* for 90 s. The supernatant was collected and transferred to a new microcentrifuge tube.

2.7.3 Reverse transcription cDNA synthesis

Complimentary DNA (cDNA) was synthesised from total RNA samples using a SuperScript™ II second-strand synthesis kit (Thermo Fisher). 50 ng of random hexamer primers were added to 1 µg RNA diluted in 12 µL H_2O, and incubated at 65 °C for 10 mins to anneal the random primers to the RNA. 7 µL of First-Strand master mix (5x First-Strand buffer, 0.1M DTT and 10 mM dNTP mix, 4:2:1 ratio) was added and mixed by pipetting, before incubation at 25 °C for 2 min.

As a control for genomic DNA contamination, all synthesis reactions were conducted in duplicate, with no RT enzyme added to one set of samples as a RT- control. 50 U of SuperScript II reverse transcriptase was added to the positive synthesis reactions. Samples were incubated at 25°C for 10 mins, followed by 50 min at 42°C and 15 mins at 72°C to allow reverse transcription to occur and denature the reverse transcriptase enzyme, respectively. cDNA samples were used neat for RT-PCR reactions, or diluted to a total volume of 100 µL with nuclease-free H_2O for qPCR.

2.7.4 End-point Polymerase Chain Reaction

Polymerase chain reactions (PCR) were undertaken using the GoTaq reagent kit (Promega) utilising a BioRad T100 thermal cycler. PCR reactions were set up according to the manufacturer's recommendation, with 2 µM forward and reverse primer concentrations and 2.5 mM $MgCl_2$, in a final volume of 20 µL. Reactions were first heated to 95°C for 5 min to denature the DNA, followed by up to 35 cycles of denaturing for 30 s at 95°C, annealing at 50-65°C for 30 s and incubating for 1 min/kb at 72°C for extension of the PCR product.

2.7.5 High-fidelity PCR

PCR amplification of sequences where high accuracy was required were undertaken using the Q5® High-Fidelity DNA Polymerase reagent kit (New England Biosciences). Reactions were conducted at the 50 µL scale, utilising 200 µM dNTP, 0.5 µM forward and reverse primer concentrations and 0.02 U/µL polymerase per reaction. 1X High GC enhancer was added to enhance the effectiveness of the reaction. Reactions were heated for 3 min at 98°C for initial denaturation, followed by 34 cycles of 10 s denaturation at 98 °C, 30 s of annealing at a primer-dependent temperature, and 1 min of elongation at 72 °C, and a 2 min terminal elongation at 72 °C.

2.7.6 Primer design and optimisation

Primers were designed against target gene mRNA sequences using the online NCBI Primer-BLAST tool (http://www.ncbi.nlm.nih.gov/tools/primer-blast/) with default parameters. Gene sequences were obtained from the Ensembl database. Unless noted, all primers were designed against consensus sequences where multiple splice variants of a gene exist. Where possible, primers were designed to amplify both genomic and cDNA sequences in order to simplify testing of the primer pairs. Where noted, the Primer Express 1.5 software package was used to design primers for qPCR assays, using the default settings.

Primers were obtained from MWG Eurofins, diluted to a stock concentration of 100 µM upon receipt, and used at a working concentration of 10 µM unless noted. All primer sets, where possible, were tested using gradient PCR in the presence of human genomic DNA as template in order to optimise the annealing temperature. Primers are shown in Table 2.2.

Name	Target gene	Ascension	Amplicon (bp)	Annealing Temperature (°C)	Forward	Reverse
Chemerin	RARRES2	ENSG00000106538	161	64.1	GAGGAATTTCACAAGCACCCG	TTGCACTCGGGTTTCTTCCA
Cytokeratin 13	KRT13	ENSG00000171401	146	64	GAGCTCCTCTGCCAGCTATG	CACCAAAACCACAGCTCACG
Cytokeratin 14	KRT14	ENSG00000186847	107	60	CGGCCTGCTGAGATCAAAGA	ATCTGCAGAAGGACATTGGCA
Dermcidin	DCD	ENSG00000161634	116	62.3	TTTGGTGGCATACCCACTCC	CTTTGGTGCCTGTCTGGCTA
Elafin	PI3	ENSG00000124102	309	60.1	TGGCCTTAGCTCTTAGCCAAA	GCGGTTAGGGGGATTCAACA
GAPDH	GAPDH	ENST00000229239	90	N/A	CAAGGTCATCCATGACAACTTTG	GGGCCATCCACAGTCTTCTG
hBD-1	DEFb1	ENSG00000164825	116	62.3	GAGGTTGTGCAATCCACCAG	AGATCGGGCAGGCAGAATAG
hBD-2	DEFB4A	ENSG00000171711	117	63	ACCTGCCTTAAGAGTGGAGC	TTGGCCTCCTCATGGCTTTT
hBD-3	DEFB103	ENSG00000177243	335	57.2	TGAGTGGGTGTGTTCTGCAT	AGCACTTGCCGATCTGTTCC
hBD-4	DEFB104A	ENSG00000171711	151	60	TTGCCGGAAGAAATGTCGC	CCTACTTCCAGCGACTCTAGG
HNP1	DEFA1	ENSG00000206047	112	65	GCAAGAGCTGATGAGGTTGC	TTGAGCCTGGATGCTTTGGA
Psoriasin	S100A7	ENSG00000171195	116	62.3	AGACTACCACAAGCAGAGCC	CTGGTGGGAGAAGACATTTTATTG
Ribonuclease 7	RNASE7	ENSG00000143556	234	58.3	CAGGAGTCACAGCACGAAGA	GGCTGAGTTGCATGCTTGAG
TLR4	TLR4	ENSG00000136869	457	57	CAGATAAGCAGGGCATGCC	GATACCAGCACGACTGCTC
TLR5	TLR5	ENSG00000187554	476	54	CTTCTCCTCCTGTAGTGG	GAGAACGAGTCAGGGTAC

Table 2.2 Primers for end-point and qPCR.

2.7.7 Gel electrophoresis

Endpoint PCR products were separated using gel electrophoresis and visualised using UV light. Molecular biology grade agarose (2-4% w/v) was boiled in 1x Tris-Borate-EDTA (TBE) buffer, and the intercalating dsDNA dye SybrSafe GelRed ^{TM} added (1/10,000) to enable visualisation of the DNA product under UV light. Gels were cast and set for 30 min. PCR products were loaded directly onto the gels due to the inclusion of loading dye in the GoTaq reagent kit. Gels were electrophoresed submerged in 1x TBE for 30-60 min at 100V, before visualisation using a GeneGenius gel imaging system.

2.7.8 Quantitative polymerase chain reaction

Quantitative polymerase chain reaction (qPCR) was undertaken using the SybrGreen intercalating DNA dye-based system. Sybr Green I is an asymmetrical cyanine DNA-intercalating dye, and therefore binds to all double-stranded DNA (dsDNA) in a sample. During the PCR reaction, DNA polymerase will exponentially amplify the target sequence, each copy of which will bind more Sybr Green. As the PCR reaction progresses, Sybr Green will bind to the dsDNA in a concentration dependent manner.

The Sybr Green PCR Master Mix was used for all reactions, containing AmpliTaq Gold DNA polymerase, SybrGreen I dye, a passive ROX reference dye, dNTPs and buffer components. 5 µL of diluted cDNA was mixed with 10 µL of Sybr Green Master Mix and 300 nM of forward and reverse primers specific to the target gene or glyceraldehyde 3-phosphate dehydrogenase (GAPDH) as a housekeeping gene. All reactions took place in ABI FAST optical 96 well plate (Life Technologies) plates, and sealed to prevent evaporation. Plates were centrifuged briefly before running.

All reactions were run using a StepOnePlus qPCR instrument.. During each cycle, every well was excited with laser light and the fluorescence of the Sybr Green dye was detected. The fluorescence signal was normalised against the passive ROX dye to account for non-amplification related differences in fluorescence intensity, yielding the normalised reporter fluorescence values, which were plotted against cycle number to obtain the amplification curves. A melting curve analysis was also included to analyse the disassociation curves of the PCR products. Each cDNA sample was analysed in triplicate,

and negative control samples included. Negative control samples used no template, where H_2O was included instead of cDNA, or 'RT-' samples where reverse transcriptase was omitted during cDNA synthesis.

2.7.8.1 Data analysis and quality control

qPCR data was analysed using the StepOne V.2.3 software package. Baseline fluorescence values were calculated automatically based upon the fluorescence values detected in early PCR cycles prior to detectable amplification. Threshold values were set in the region of exponential amplification across all the amplification plots in an individual experiment: the threshold cycle (C_T) reported and used for downstream analysis is the cycle number at which the fluorescence signal rises above the threshold value. An example plot is shown in Figure 2.3 .

Data from melt curve analyses was automatically analysed by the StepOne software package and reported as a disassociation plot (an example is shown in Figure 2.4). Disassociation plots enable the differentiation between PCR products and primer dimers. Primer dimers form due to hybridisation of complimentary strings of nucleotides within each primer sequence (Li et al., 1990). The incomplete complementation of the sequences will however confer weaker binding between the primers that that of the PCR product, causing disassociation of the strands at a lower temperature. The presence of multiple PCR reaction products can also be ascertained using melt curve analysis due to the sequence-dependent differences in the melting point of dsDNA. The presence of primer dimers or multiple products can be observed as multiple peaks in the disassociation plot.

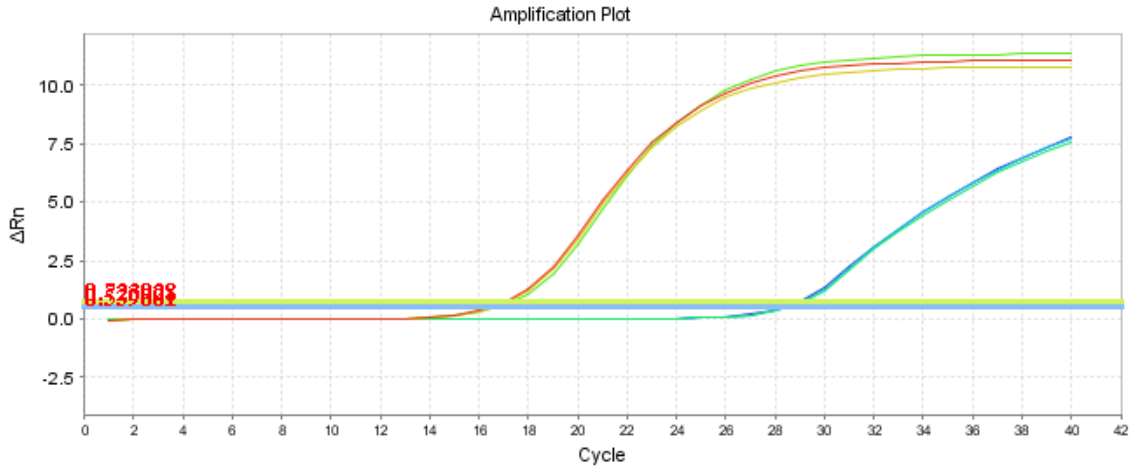

Figure 2.3 Linear amplification plot.

Amplification plot showing the normalised reporter value ΔRn (y axis) versus the number of cycles (x axis). A single triplicate cDNA sample is shown with amplification curved from GAPDH(yellow/red) and DEFB4A (blue) plotted. The threshold value is highlighted in green.

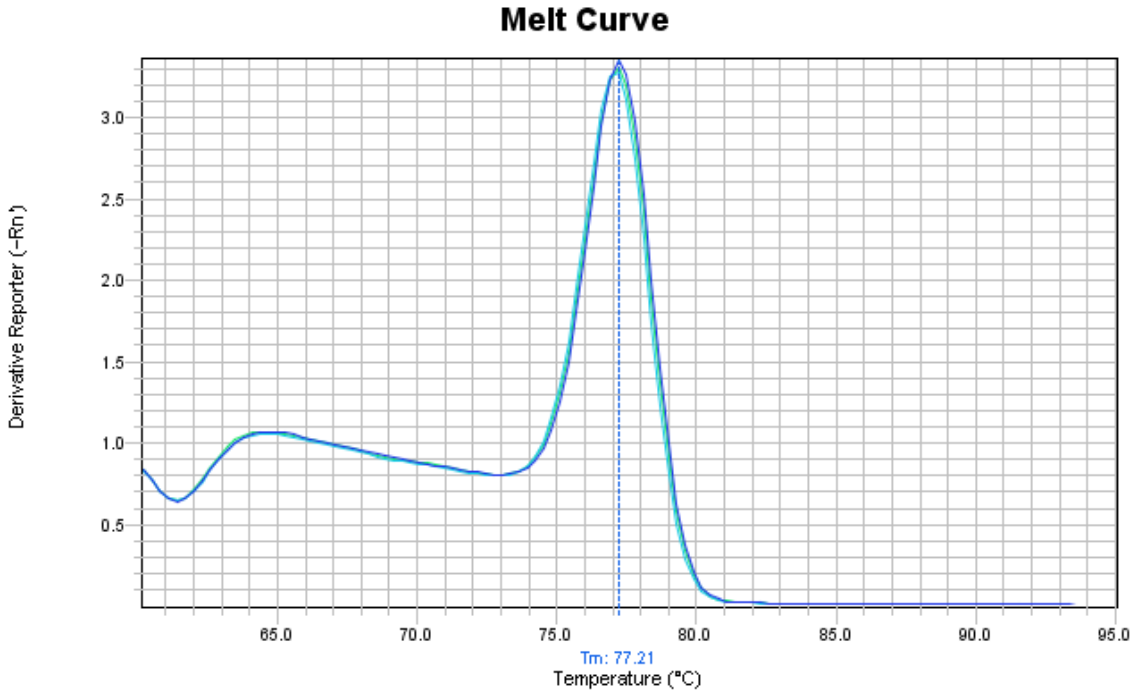

Figure 2.4 Example of a dissociation plot.

Dissociation plot showing the change in fluorescence (y axis) versus the change in temperature (x axis). Three replicate cDNA samples are shown. Note the presence of a single peak, representing the single specific product produced by the reaction.

All primer sets used for qPCR analysis were tested for efficiency prior to use. A standard curve of gDNA (for non-intron spanning primers) or cDNA from a sample known to contain the gene transcript of interest was prepared, and analysed in triplicate. Threshold cycle values, derived as described, were plotted versus the log DNA dilution

factor, and a linear regression analysis. Primers were considered efficient if the slope of the linear regression was between 3.6 and 3.3. 100% efficient primers would produce a 2-fold change in for each change in C_T. The linearity of the primer efficiency was assessed by calculating the coefficient of determination (R^2) of the linear regression.

Following quality control, relative quantitation was undertaken using the $\Delta\Delta C_T$ normalisation method (Livak and Schmittgen, 2001). For this, all samples were normalised against the housekeeping gene GAPDH and quantified using comparative CT analysis unless otherwise stated.

2.7.9 Lambda Red recombination

Lambda Red recombination enables the efficient and accurate recombination of linear DNA sequences into a bacterial chromosome (Datsenko and Wanner, 2000). A UTI89 *fliC* mutant was constructed in this study by disruption of the fliC gene by insertion of a tetracycline resistance cassette (tetRA) following the start codon of the *fliC* gene. The Lambda red recombination experiments described in this thesis were undertaken by Stefan Tran, a summer student under my supervision, with the help of Nick Smith and Marjan Van Der Woude, Centre for Immunology and Infection, University of York.

The plasmid vector pKD46 is a temperature sensitive plasmid, containing the Red operon expressed under the control of the L-arabinose inducible promoter *ParaB*. In the presence of L-arabinose, the expression of the genes *gam*, *exo* and *bet* is induced, which promote the insertion of the tetracycline resistance gene in the bacterial chromosome. The tetracycline resistance cassette serves as the selection of successfully transformed bacteria. Furthermore, the plasmid pKD46 contains the AmpR resistance gene for plasmid selection.

2.7.9.1 Transformation of *E. coli* UTI89 with pKD46

UTI89 *E. coli* were grown at 37°C under shaking conditions until they reached an OD^{600} ~ 0.4. The culture was collected *via* centrifugation at 4000 rpm for 15 min, and any residual medium removed by washing four times with H_2O. The cell pellet was resuspended in 400 µL H_2O. 100 ng of purified pKD46 was mixed with 50 µL of the resuspended culture, and the cells were electroporated at 1.8 kV. Recombinants were selected by plating on LB-Amp agar overnight at 30 °C to maintain the temperature selective pKD46 plasmid.

2.7.9.2 Preparation of linear DNA for recombination

The TetRA cassette was amplified from gDNA coding the Tn10 transposable element by high-fidelity PCR using the fliCKO_tetRA primer pair. fliCKO_tetRA consists of complimentary bases to the tetRA cassette, and a section within the UTI89 fliC gene, which determines the tetRA insertion site.

2.7.9.3 Electroporation of *E. coli UTI89* pKD46

50 ml of LB-broth was inoculated with 500 µL of overnight culture of *E. coli* UTI89 pKD46. The culture was incubated at 30 °C with shaking until OD_{600} reached ~ 0.4. To induce the expression of the lambda red genes (*gam, bet* and *exo*), L-arabinose was added to a final concentration of 0.2% (w/v) for 1 hour. 200 ng of fliCKO_tetRA PCR produce was added to 50 µL of the induced pKD46 UTI89 *E. coli,* and the mixture electroporated at 1.8 kV. Recombinant bacteria were selected by plating on LB-TA agar overnight at 30 °C.

2.7.9.4 Screening PCR of *fliC* mutants *via* colony PCR

The successful insertion of the tetRA cassette to the fliC gene was confirmed using colony PCR. Individual colonies were picked and resuspended in 50 µL H_2O, and incubated for 10 minutes at 95°C. 0.5 µL of the resuspended colony was used as template for high-fidelity PCR utilising the fliCKO_Control primer set. The fliCKO_Control primers are located approximately 200 bp up- and down-stream of the insertion site of tetRA cassette.

Successful insertion of the tetRA was further verified by Sanger sequencing of the insertion site. Two separate colonies were sequenced and compared with the wild-type UTI89 fliC sequence. The successful created mutants are hereafter termed as UTI89-ΔfliC.

2.7.9.5 Curing of pKD46 plasmid

After successful transformation, the pKD46 plasmid was removed. *E. coli* pKD46 fliC: tetRA strains were plated on LB-Tet agar and incubated at 42 °C overnight. Successful removal of the plasmid was confirmed by counter-selection by plating on LB-Amp agar.

Name	Amplicon (bp)	Annealing Temp(°C)	Fw	Rv
fliCKO_tetRA	n/a	61.4	TAGTGATAGTTTCACC GTCATTCGCACCAACCT GAATTTTTTAAGACCCA CTTTCACATT	CAGTTCAACGGCGTGAACGTACTG GCAAAAGACGGTTCGATGCTAAGC ACTTGTCTCCTG
fliCKO_Cont	401/2312	58	TGCAGCATCGGTAGTT AAC	ACAACAACTTACAGCGTATC

Table 2.3 Primers used for Lambda Red recombination

2.8 Protein isolation and western blotting

2.8.1 Protein harvesting

2.8.1.1 NHU cells:

Culture medium was aspirated and cells washed twice with ice-cold PBS. Cells were harvested by scraping in 50-100 µL SDS lysis buffer and transferred to a 1.5 mL micro centrifuge tube.

The collected cells were sonicated on ice for 20s at 25W, 40% amplitude using a Branson Sonifier. The lysates were chilled for 30 min on ice, and clarified by centrifugation at 18,000 *g* at 4°C. The supernatant was aliquoted to fresh micro centrifuge tubes and stored at -80°C.

2.8.1.2 Bacterial cells

Bacterial cells were cultured overnight, and collected by centrifugation at 5,000 *g* for 15 min at 4°C. The supernatant was discarded and cell pellets washed twice in cold PBS. Pellets were suspended in 50 µL SDS lysis buffer. The cell suspensions were sonicated as described above.

2.8.2 Coomassie assay

The protein content of lysates was determined using the Coomassie protein assay kit (Thermo Pierce). The Coomassie assay is a colorimetric protein assay based upon the absorbance shift of Coomassie Brilliant Blue G-250 dye at 575nm upon binding interactions between the sulfonic acid groups present on the dye and the positive amide residues of the protein backbone (Congdon et al., 1993).

Protein samples were diluted 1:12.5 in dH_2O and 10 µL of each dilution aliquoted in duplicate to a 96-well plate, and mixed with 200 µL of room temperature Coomassie reagent. Samples were plated alongside a dilution series of bovine serum albumin (from 0-1000 µg/µL in H_2O). Absorbance at 575 nm was measured using a Ascent spectrophotometer (Thermo Scientific. The Ascent Analysis software package was used

to fit the BSA standard curve, calculate R^2 goodness of fit and extrapolate the average protein concentration for each unknown sample.

2.8.3 SDS-PAGE

SDS-PAGE and western blotting experiments were conducted using the NuPAGE electrophoresis system. Proteins were resolved on 1 mm thick 10 well 4-12% Bis-Tris NuPAGE pre-cast polyacrylamide gels as required. 20 µg of protein was loaded per well (unless stated) following mixing with 4x lithium dodecyl sulphate (LDS) and 10x reducing agent to 1X concentrations in H_2O. Samples were heated at 70 °C for 10 min prior to loading. 5 µL of BioRad All-Blue protein ladder was loaded as a size marker in tandem with experimental samples.

Gels were electrophoresed at 200 V until the running buffer reached the foot of the gel in x1 MOPS or MES buffers, dependent on the size of the protein of interest.

2.8.4 Western blotting

Following electrophoresis, gels were removed from cassettes and the stacking gel and foot removed. Semi-dry transfer between fibre blotting pads at 30 V for 3 hours transferred proteins to pre-wetted PVDF membranes. PVDF membranes were washed in pH 7.4 TBS and blocked with Odyssey blocking buffer for 1 hour. Odyssey blocking buffer is optimised to reduce autofluorescence of the membrane during imaging using the LiCor scanning system.

Blots were labelled with primary antibodies (Table 2.4) diluted in Odyssey blocking buffer, incubated overnight at 4 °C. Membrane were washed in TBST (3 x 5 min) prior to incubation with fluorophore-conjugated secondary antibodies (diluted as above) for 1 hour. Membranes were washed in TBST (3 x 5 min) to remove excess antibody and once in H_2O to remove detergent prior to imaging.

Membranes were scanned using a LiCor scanner. The LiCor relies on secondary antibodies conjugated to near-infrared responsive fluorophores. Using two separate,

non-overlapping laser wavelengths to excite the fluorphores (700 and 800 nm) allows the dual labelling of blot membranes. Images were analysed using the Image Studio V.5.2 Software package, which was used to export images, measure band intensity and perform background subtraction.

If required, membranes were stripped for reprobing by incubation for 30 minutes in 1X Western Blot Recycling Kit reagent at room temperature. Membranes were washed in TBS and imaged before reprobing to ensure sufficient stripping. Anti-β-actin was used as a positive and loading control, whilst secondary antibody-only incubation was used as a negative control to ensure specificity of the secondary antibody.

Antigen	Clone/ Product code	Host	Supplier	Molecular weight	Dilution (WB)	Dilution (IHC)
β-actin	AC-15	Mouse	Sigma Aldrich	42 kDa	1:100,000	
Flagellin	ab93713	Rabbit	Abcam	55 kDa	1:10,000	
Flagellin	FLIC-1	Mouse	BioLegend	60 kDa	1:2,000	
DEFB4A	AF2758-SP	Rabbit	Novus Biologicals	10 kDa	0.1 µg/mL	
DEFB104A	L13-10-D1	Mouse	Abcam	8 kDa	1:1000	
Total Histone H3		Rabbit	Cell Signalling	10 kDa	1:10,000	N/A
TLR5	LS-B601	Rabbit	LifeSpan Biosciences	N/A		1/500
PIGR	APA012012	Rabbit	Sigma-Aldrich	N/A		1/500

Table 2.4 Details of primary antibodies used for western blotting and immunohistochemistry.

2.9 Histology and immunohistochemistry

2.9.1 Embedding of tissue samples

Tissue samples, grossly dissected of excess fat and stroma were fixed in 10% formalin (v/v) in PBS for 12-48 h, dependent on the size of the sample. Fixed samples were transferred and stored in 70% ethanol prior to processing. Samples were enclosed in an embedding cassette and dehydrated in 3 x 10 min washes of absolute ethanol and 1 x 10 min wash of isopropanol, followed by 4x 10 min washes of fresh xylene.

Specimens were embedded in paraffin wax by 4 x 15 min incubations in fresh paraffin wax at 60 °C. Sections were orientated in molten wax and left to solidify at -12 °C. 5 µm sections were cut using a Leica RM2135 microtome into a heated waterbath and collected onto SuperFrost Plus glass slides (Thermo Scientific). Dried sections were baked on a hot plate at 50 °C for 1 hour and stored at room temperature, pending analysis.

2.9.2 Embedding of cell sheets

Differentiated cell sheets grown on Transwell ™ inserts (section 2.5.7) were washed with pre-warmed PBS and lifted from the scaffold by replacing both the apical and basal media with 2 mg/mL dispase II (Roche Diagnostics) for ~30 mins at 37°C. Cell sheet were transferred in warm PBS using a Pasteur pipette to a CellSafe™ histology case and enclosed in an embedding cassette.

Cell sheets were fixed overnight in 10 % (v/v) formalin, and dehydrated in the same manner as tissue samples, with shorter wash times of 5 min. Cell sheets were embedded in paraffin wax by incubation for 4 x 10 minutes in fresh paraffin wax. Sections were prepared as for tissue samples.

2.9.3 Haematoxylin and Eosin staining

Haematoxylin and Eosin (H&E) staining of embedded samples was used to observe the general morphology and integrity of tissue and cell sheet samples, and as a counterstain for immunohistochemistry (IHC) analyses.

Paraffin wax embedded sections were dewaxed with 4 washes of fresh xylene (2 x 10 min and 2 x 1 min). Sections were rehydrated by incubation in graded alcohols (absolute to 70% ethanol) and running tap water. Sections were stained for 2 minutes in Meyer's Haematoxylin and washed in running tap water until the excess stain was cleared. Following a one minute incubation in Scott's tap water, sections were counterstained with 1% (w/v) aqueous eosin (Leica) for 1 minute and rinsed in running tap water until cleared. Sections were dehydrated through an alcohol gradient and 4 washes of xylene. Sections were immediately mounted in DPX (Fisher) and sealed under glass coverslips.

2.9.4 Immunohistochemistry

Immunolabelling of formalin fixed paraffin embedded sections was performed using an indirect streptavidin/biotin immunoperoxidase method (

Figure 2.5).

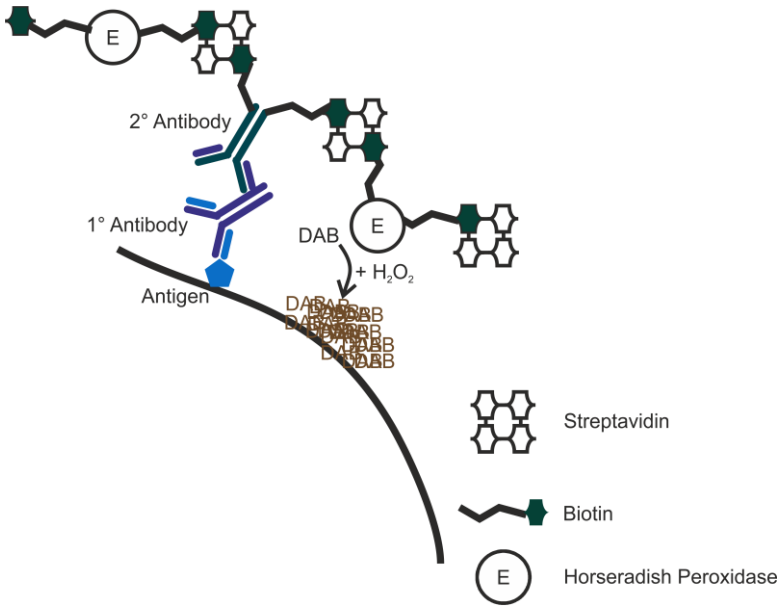

Figure 2.5 Indirect immunoperoxidase staining

Indirect immunohistochemistry utilises an antibody raised (in a mammalian host) against a specific antigen, targeted to the molecule of interest (the primary antibody, blue/purple). The primary antibody is recognised by a biotinylated secondary antibody (or 2° antibody) which is specific for antibodies produced by the primary antibody's 'host' species (purple/green). The primary-secondary antibody complexes are detected via binding of streptavidin-linked horseradish peroxidase to the biotinylated secondary antibody. Multiple complexes can bind to the same site, enabling the amplification of the detected 'signal'. The labelling is visualised by the addition of Diaminobenzidine (DAB), which is enzymatically converted by horseradish peroxidase to a dark brown precipitate.

Sections were dewaxed as for H&E staining. Native tissue sections were blocked with 3% (v/v) hydrogen peroxide for 10 minute to reduce background staining caused by endogenous tissue peroxidase activity, followed by a 10 minute wash in running tap water.

The nature of formalin fixation can reduce or block the immunoreactivity of the tissue due to the protein crosslinking caused by the fixation process (Zhang et al., 1998). Several enzymatic or chemical methods can be used to improve the immunoreactivity of the tissue by improving the access of antibodies to antigens, a process termed 'antigen retrieval' (Kiernan, 2008). Unless noted, antigen retrieval was conducted by incubation of sections in boiling 10 mM citric acid buffer (pH 6) for 13 minutes in a microwave. Following antigen retrieval, sections were cooled on ice and washed briefly in running tap water.

Sections were placed in a Shandon Sequenza ™ immunostaining system (Thermo Scientific) and 100 µL of Tris-buffered saline (TBS) added to each slide to check for leaks. Sections were blocked for endogenous avidin and biotin binding by incubation for 10 minutes at room temperature with 100 µL of avidin or biotin (Avidin/Biotin Blocking Kit, Vector Labs) followed by two 100 µL TBS washes.

Background labelling caused by non-specific binding of the secondary antibody was blocked by incubation with 10% (v/v) of the host species serum in TBS prior to incubation of the section with 100 µL of diluted primary antibody overnight at 4°C.

Unbound primary antibody (Table 2.4) was removed by washing with TBS, and sections incubated with biotinylated secondary antibodies and streptavidin/horseradish peroxidase (HRP) ABC complex (Vectastain Elite ABC kit, Vector Labs) for 1 hour and 30 minutes respectively, at room temperature. 200 µL of Fast DAB (Sigma Aldrich) was added to visualise the reaction, and sections incubated for 15 minutes before excess DAB was removed by washing with H_2O. Sections were counterstained for 15 s in Meyers haematoxylin, prior to dehydration and mounting as for H&E.

2.9.5 Photomicroscopy

Stained tissue sections were viewed and imaged using an Olympus BX60 bright-field microscope. Images were captured using an Olympus DP50 digital camera and Image-Pro® Plus software, using x20, x40 and x60 oil-immersion objectives.

2.10 Mass spectrometry

2.10.1 Peptide standards

Recombinant peptides for use as standards were obtained from a commercial supplier (Peprotech, New Jersey USA). Lyophilised standards were resuspended in 10 mM acetic acid at a concentration of 10 µM and stored at -80 °C until use.

2.10.1.1 Sample preparation & fractionation:

Samples of cell culture media for MS analysis were collected and stored in LoBind Protein microcentrifuge tubes (Eppenddorf, UK) at -80°C until use. Frozen samples were defrosted at room temperature and mixed by inversion before processing. 'Conditioned' medium refers to KFSMc medium that had been exposed to non-differentiated NHU cells for two days. Culture medium from three independent cell lines was mixed, aliquoted and frozen at -80°C.

2.10.1.2 Solid phase extraction (SPE):

Samples were fractionated by SPE, using C18 SPE cartridges (100mg, 1 mL, Phenomenex) or C18 ZipTip™ pipette tips (10 µL/0.2 µL bed volume, EMD Millipore).

Cartridge SPE:

SPE cartridges were conditioned with 1 mL of 0.1% formic acid (v/v) in acetonitrile, 1 mL of 50%:0.1% aqueous acetonitrile: formic acid and 1 mL 0.1% aqueous formic acid (v/v) prior to loading 0.5-1 mL of sample.

Following loading, the column was washed with 3x 1 mL of 0.1% aqueous formic acid (v/v), and serially eluted with increasing concentrations of aqueous acetonitrile: formic acid. Extracted fractions were dried using a SpeedVac vacuum concentrator (Thermo Scientific) without heating. Dried samples were resuspended in 10 µL of 50%:0.1% aqueous acetonitrile: formic acid (v/v).

ZipTip™ SPE:

Samples were acidified prior to extraction by addition of 1% tri-fluoroacetic acid (TFA) to a final concentration of 0.1% v/v.

Each tip was conditioned prior to analysis by wetting with 2x10 µL acetonitrile and washing with 2 x 10 µL of 0.1% aqueous TFA. The sample was drawn into the ZipTip™ and expelled 60 times to load the sample, and washed with 2x10 µL of 0.1% aqueous TFA. The sample was eluted by passing 3 µL of 50%:0.1% aqueous acetonitrile: TFA through the tip five times and expelling to a fresh 0.5 mL LoBind microcentrifuge tube.

2.10.1.3 MALDI-MS analysis:

A solution of α-Cyano-4-hydroxycinnamic acid (CHCA, 10 mg/mL, MALDI-grade, Sigma Aldrich) or 2,5-Dihydroxybenzoic acid (DHB, 10 mg/mL, MALDI-grade, Sigma Aldrich) was prepared in 50% aqueous acetonitrile. 1 µL of this solution was applied to the spots of a polished stainless steel Bruker MALDI target plate. 1 µL of sample solution was spotted upon the CHCA spot, and the solutions mixed with the pipette tip, without touching the plate. Samples were spotted in triplicate and dried at room temperature in air before analysis.

Spotted samples were analysed in positive mode using an ultraflex III MALDI-ToF-ToF MS with a smartbeam™ Nd-YAG 355nm laser or a solariX XR 9.4T FTICR MS with a smartbeam™ laser (Bruker Daltonics). Calibration was carried out using Bruker Peptide Calibration Standard II before each analysis session. Data processing was performed using the DataAnalysis 4.1 software package.

2.10.1.4 DI-ESI-MS

Samples were prepared for analysis by SPE fractionation or by dilution of recombinant standards from stock solutions. Samples were analysed in positive mode using a maXis oaTOF-MS, fitted with an electrospray ionisation source. Samples were injected at a flow rate of 3 µL min^{-1} using a syringe pump. Calibration was carried out using Bruker Peptide Calibration Standard II before each analysis session.

2.11 Statistical analysis

Data were analysed and represented graphically using Graphpad Prism version 6. Where appropriate, and unless noted, data are presented as the mean, with error bars representing +/- the standard deviation. Unless stated, statistical analysis assumed the

data were normally distributed. Analysis of variance (ANOVA) tests were used to compare two or more sample means, with the appropriate post-hoc test applied. Details of tests used, levels of significance, and number of replicates tested are cited in the text.

3 AMP expression by normal human urothelium

3.1 Introduction

As discussed in Chapter 1, the urothelium is an epithelial barrier that was, until recently, not thought to play an immunological role. However, in common with other epithelia, such as the intestine, the urothelium plays an important role in the defence against attack by pathogens. One such mechanism by the urothelium and other epithelia in the body is the expression of AMPs

Antimicrobial peptides are short, potent antibiotic peptides, expressed as an innate defensive mechanism by almost all classes of life, both prokaryote and eukaryote (Lehrer and Ganz, 1999). Originally discovered as an element of innate bacterial defence in insect hemolymph, AMPs are highly dissimilar in sequence, with a wide variety of primary structures, despite their highly conserved nature. AMPs have been studied extensively as elements of the innate response to infectious organisms and as possible sources of novel antimicrobial drugs.

Over 112 AMPs have been identified in humans, primarily members of the folded β-sheet and linear α-helical families (Wang et al., 2009). Human antimicrobial proteins were first identified as early as the 1920s, with the discovery of lysozyme in human saliva (Fleming, 1922). The isolation and characterisation of AMP*s* in humans however began in the 1980s (Selsted et al., 1985). The first family of peptides identified were the α-defensins (HNP1-3), identified in neutrophils isolated from whole blood (Selsted et al., 1985). Mouse orthologues of the α-defensin family were identified in the intestinal epithelia (Ouellette et al., 1989). Ouellette et. al. hypothesised that AMPs were expressed at epithelial surfaces, an hypothesis that was confirmed in humans with the discovery of two new α-defensin genes in human Paneth cells (Jones and Bevins, 1993, 1992) .

Two separate primary strategies have lead to the discovery of AMPs: fractionation and separation *via* chromatography based upon functional assays, and the use of bioinformatics techniques to 'mine' genome data for homologous and orthologous genes (reviewed in Smet and Contreras, 2005). These approaches have lead to the

discovery of three primary families of AMPs in humans: defensins, histatins and cathelicidin. The relevance of AMPS to urinary tract defence is the major focus of this thesis.

3.1.1 Mechanisms of action

The exact methods by which AMPs exert their antimicrobial effects are unclear. The knowledge base of how AMPs exert their bactericidal effects has stagnated in recent years, whilst the number of peptides discovered and the knowledge of their structure and genetics have expanded rapidly. The conservation of structural and cationic characteristics suggests that AMPs target a likewise highly conserved bacterial target: the bacterial membrane. Studies conducted in 'cell-free' biophysical models of lipid bi-layers utilising helical AMPs suggest that membranes can be compromised in a variety of mechanisms, including pore formation and direct disruption of the membrane by the formation of a peptide 'carpet' (Hancock and Rozek, 2002; Huang, 2000; Matsuzaki et al., 1996; Shai, 2002).

Such biophysical models of AMP function are inherently limited by their inability to model the effects of cellular interactions beyond those with the (artificial) lipid bilayer. Studies in whole organisms have suggested that pore formation may occur in tandem with changes in membrane phospholipid composition (Huang, 2000; Matsuzaki et al., 1996), alteration of cellular osmolarity, and de-stabilisation of extracellular structural moieties, such as LPS (Sahl et al., 2005).

The consensus view of AMP activity as being strictly membrane-focused and specific to microbes has remained since the original 'pioneering' studies of α-helical peptides of the past decade (Oren and Shai, 1998). Evidence has shown that several AMPs may have defined intracellular targets (Park et al., 1998). As such, the membrane damage observed has been suggested to act primarily as a mechanism to allow translocation of AMP molecules to the intracellular space (Takeshima et al., 2003). Evidence of AMP-mediated toxicity in mammalian cell (i.e. 'host' cells) has also suggested that the previous consideration of AMPs as selective antibiotics may be flawed (reviewed by (Matsuzaki, 2009).

3.1.2 AMPs in the urinary tract

As previously discussed in this chapter, the urothelium is an epithelial barrier that was until recently, not thought to play an immunological role. However, in common with other epithelia, such as the intestine, the urinary tract has constitutive expression of AMPs in the full length of the tract, from the kidney to the bladder. Six AMPs have been described in the human urinary tract: α-defensin 5 (Spencer et al., 2012), β-defensins 1 (Valore et al., 1998) and 2 (Lehmann et al., 2002) , cathelicidin , and ribonuclease 7 (Spencer et al., 2013).

Defensins

Defensins form the largest family of human AMPs, with 5 α-defensin peptides and over 40 β-defensin gene open reading frames identified in man (Schutte et al., 2002). Both defensin families are cationic peptides, approximately 25-45 AA long, with 6 conserved cysteine residues (Lehmann et al., 2002). Disulphide bonding between these residues confers a characteristic twisted anti-parallel β-sheet structure to the active peptide (Torres and Kuchel, 2004). α and β defensins share considerable similarity in structure, with subtle differences, such as the lack of a N-terminal α-helix and a different pattern of disulphide bonding (Hoover et al., 2001) (Figure 3.1) The conserved nature of the tertiary structure is at odds to the large variation in sequence, size, catholicity and residue distribution of the mammalian defensins (Sahl et al., 2005)). Such alterations are hypothesised as evolved modifications of the mode of action and targeting of the defensin family.

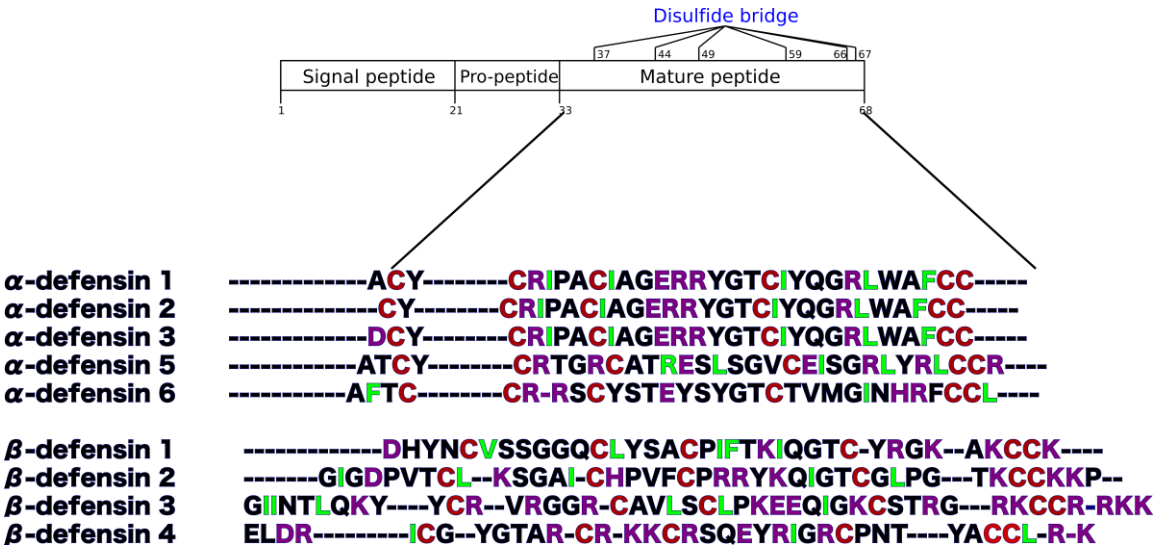

Figure 3.1 Alignment of human defensin sequences.

Amino acid sequences were derived from the Uniprot database (Uniprot Consortium, 2015). Charged amino acids are highlighted in purple and blue, and cysteine residues are highlighted in red.

Mammalian defensins display a broad spectrum of antimicrobial activity in experimental assays, killing or inactivating Gram negative and positive bacteria (Takemura et al., 1996), fungi (Feng et al., 2005; Joly et al., 2004), mycobacteria (Gupta et al., 2015) and viruses (Zhang et al., 2002). As discussed above, the mechanisms by which AMPs exert their antimicrobial effects is still unclear. Defensins are known to bind to bacterial membranes. Defensins have also been demonstrated to permeabilise the membranes of *E. coli* during the process of cell division, leading to the arrest of bacterial function (Lehrer et al., 1989). Suggestions of other antimicrobial mechanisms of action have been noted *via* study of bacterial defence mechanisms against defensins. Defensin resistant mutants of *P aeruginosa* express aminoarabinose-modified Lipid A, suggesting that defensin interactions with LPS is an important part of their antibacterial activity (Moskowitz et al., 2004).

LL-37/CAMP

CAMP (also known as LL-37 in humans) is the sole human member of the Cathelicidin family. Cathelicidin contains two functional domains: a conserved cathepsin L-like domain with high inter-species homology, and a highly variable (both inter and intra-species) antimicrobial C-terminal domain (reviewed by Zanetti et al., 1995). CAMP expression has been identified in neutrophils, skin, the GI and bronchial tracts, as well as

squamous epithelia of the mouth, tongue and oesophagus (reviewed in Kościuczuk et al., 2012).

Cathelicidins are members of the linear α-helical AMP family. Beyond the membrane damaging effects observed by such peptides (Oren and Shai, 1998), CAMP and other cathelicidins can also exert intracellular effects. Much of the evidence for such effects is derived from *in vitro* systems, however cathelicidin is implicated in the control of apoptosis, chemotaxis of professional immune cells to site of infection, induction of cytokine production *via* a range of hypothesised receptor interactions (reviewed in depth by Vandamme et al., 2012)

'Atypical' AMPs

Several human AMPs exert their inhibitory effects *via* mechanisms which do not bind the pathogen membrane or without direct interaction with the pathogen. Many of these AMPs exert an antimicrobial effect as a secondary or tertiary function, unlike the specialised AMPs described above.

Several AMPs with metal cation binding activity have been described *in vivo*, such as transferrin (Bezkorovainy, 1981) and hepcidin (Peters et al., 2013). Transferrin and hepcidin are strong iron binding agents, predominantly found in the serum, forming an important part of the iron homeostasis system in humans. Transferrins are thought to exert antimicrobial effects primarily *via* their affinity to iron, outcompeting bacterial scavenging mechanisms, therefore preventing bacterial survival.

3.2 Aims, hypothesis and experimental approach

3.2.1 Aims and hypothesis

It was the aim of the work included in this chapter to examine the expression of AMPs by the urothelium through interrogation of a normal human urothelial cell system. By exposing NHU cells to the prototypic cystitis isolate UTI89 and purified, isolated pathogenic *E. coli* virulence factors, the contribution of specific bacterial virulence factors to the induction of AMP synthesis can be assessed.

It was hypothesised that the release of a 'cocktail' of AMPs and other, unknown small molecule signalling mediators (the urothelial 'defendome') occurs as a sequelae of TLR5 activation by bacterial flagellin. A further hypothesis was that flagellin is the key mediator in the urothelial response to uropathogens, mediating expression of AMPs.

3.2.2 Experimental approach

Initial analyses of a existing RNA-seq transcriptomic data set were conducted to assess the constitutive, transcript-level expression of AMPs and previously described elements of urothelial interaction with bacterial virulence factors in non-differentiated, differentiated NHU cells and *in situ* urothelial cells. The data represented next-generation RNA sequencing of mRNA isolated from freshly isolated urothelial cells, or urothelial cells in both non-differentiated and differentiated states from three donors, and sequences were mapped to the Gencode 11 sequence dataset. Transcripts were normalised and relative abundance calculated. Genes previously described to interact with UPEC virulence factors were identified from literature searches.

A list of known anti-microbial peptides (AMPs) expressed by man was obtained from a search of the AMP Database (Wang et al., 2009). A 'longlist' (Table 3.1) of 29 peptides was produced from the 250 human-derived antibacterial peptides recorded in APD2. The shortlist was compiled based on literature searches for expression of the peptides at epithelial surfaces or the renal/urinary tracts. The basal gene expression of the 30 peptides shortlisted was assessed by analysis of the previously described transcriptomic dataset (Section 2.3.1).

Subsequently, non-differentiated and differentiated NHU cells were exposed to UTI89, the prototype UPEC cystitis isolate, to determine the induced antimicrobial response by NHU cells. Initial screening experiments to assess the expression profile of AMP production were conducted using RT-PCR. mRNA was isolated from non-differentiated and differentiated NHU cells treated for 6 h with between 10^3-10^6 colony-forming units per mL of medium. Induced AMPs genes were quantitated by quantitative RT-PCR, and protein expression *in vitro* was detected by western blotting. The effect of bacterial exposure on cell morphology was assessed by light microscopy.
Non-differentiated NHU cells have previously been shown to express the proinflammatory cytokines IL6 and IL8 in response to flagellin in a TLR5- and concentration-dependent manner (Smith et al., 2011). The effect of UPEC-derived flagellin, isolated from NCTC10418 *E. coli*, on AMP gene expression was assessed. Non-differentiated NHU cells were exposed to 10-1000 ng/mL of UPEC flagellin derived from type strain NCTC10418 for up to 24 h.

NHU cell cultures maintained in non-differentiated and differentiated conditions were also subsequently treated with purified virulence factors derived from pathogenic *E. coli*, and subsequent induction or changes in antimicrobial response were analysed. NHU cell cultures were exposed to varying concentrations of ultra-pure *E. coli* LPS (10-1000 ng/mL), *E. coli* peptidoglycan (10-1000 ng/mL), UPEC-derived type 1 fimbriae (10-10,000 ng/mL) and *E. coli* derived *papG* (10-1000 ng/mL) for 6 and 24 h to simulate the acute phase of infection. mRNA was extracted from cultures and expression compared to no treatment and flagellin treated cultures by RT-PCR to assess the effect of individual virulence factors on AMP gene expression.

To further determine the importance of UPEC virulence factors in the induction of AMP expression by NHU cells in response to UPEC, mutants of UPEC strains lacking virulence factors were used. Using the lambda red one-step PCR product recombination method (Datsenko and Wanner, 2000), a tetracycline resistance cassette was inserted to disrupt the start codon of the UTI89 *fliC* gene which encodes the flagellin subunit of the flagellar filament. PCR, functional motility assays and western blotting targeting the fliC protein product assessed the success of the *fliC* mutant. mRNA was extracted from non-differentiated cultures and gene expression compared to no treatment and flagellin

treated controls by RT-PCR to assess the effect of removing individual AMP-inducing virulence factors on AMP gene expression.

3.3 Results

3.3.1 Basal expression of virulence factor receptors in human urothelium

Of the ten known human Toll like receptors (TLR), freshly isolated urothelium expressed transcripts for TLRs 1 to 7 (Figure 3.2). *In vitro* non-differentiated and differentiated NHU cells expressed transcripts for TLRs 1 to 6. Non-differentiated and in situ NHU cells expressed TLR4 co-receptors CD14 and LY96 (MD2) transcripts, whilst differentiated NHU cells expressed increased amounts of CD14 transcript. Cytodifferentiation of NHU cells resulted in upregulation of the expression of TLR3 and TLR4 genes, with a log2 fold change of 2.94 and 1.09 respectively.

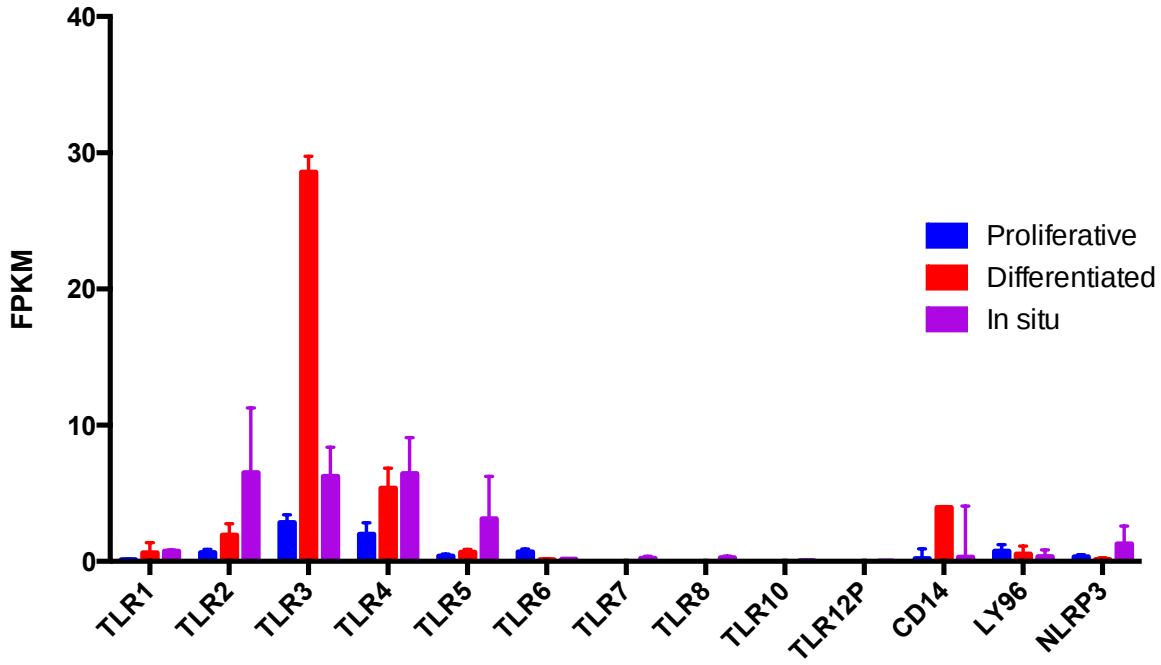

Figure 3.2: Normalised relative RNA-seq transcript abundance of TLR and co-receptor genes in normal human urothelium. mRNA extracted from freshly isolated NHU cells (in situ, purple, n=3) or NHU cells induced to differentiate (red) or maintained in non-differentiated culture (blue, matched donors, N=3) were analysed. Normalised abundance is reported as FPKM; fragments per kilobase of transcript per million mapped reads to correct for transcript length. Error bars represent standard deviation between donors.

Expression of peptidoglycan recognition proteins was also assessed from the same dataset (Figure 3.3). Of the four specialised peptidoglycan recognition proteins (PGLYRPs) described, urothelial cells *in situ* expressed low levels of PGLYRP1, 2 and 4 transcripts. Non-differentiated NHU cells expressed PGLYRP1, 3 and 4, whilst

cytodifferentiation of NHU cells induced the expression of all four PGLYRP transcripts. Constitutive transcript expression of the intracellular peptidoglycan recognition proteins NOD1 and NOD2 was observed both in situ and non-differentiated and differentiated NHU cells. NOD1 was more abundant across all three NHU cell types. Expression of both NOD transcripts was unaffected by cytodifferentiation.

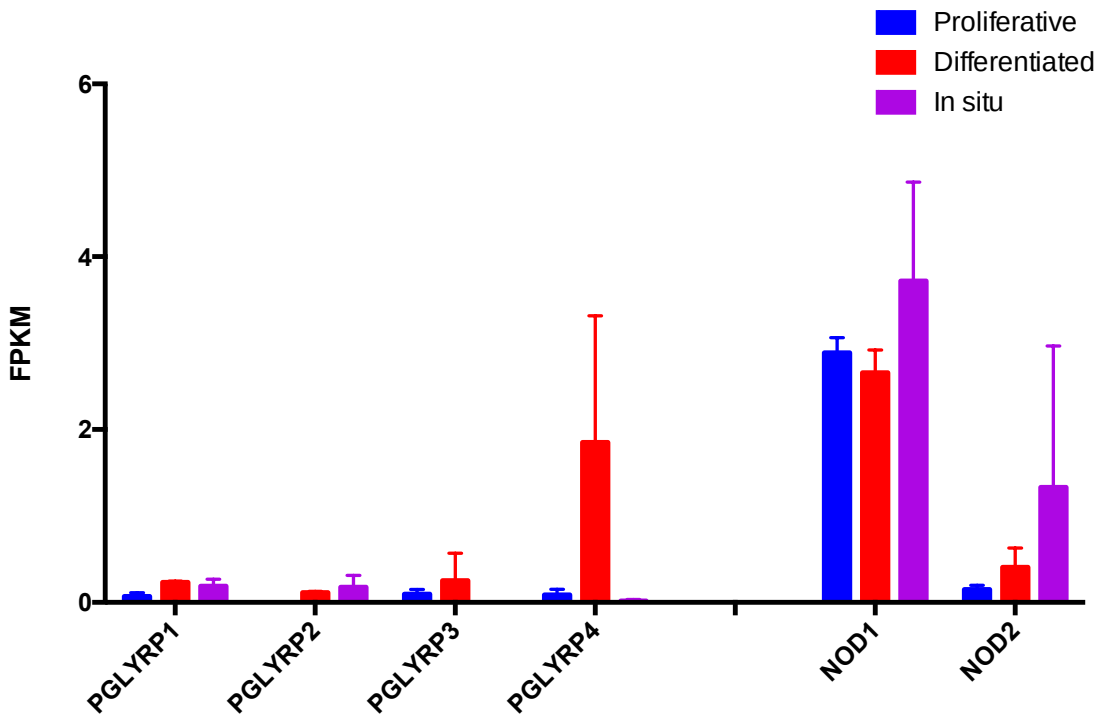

Figure 3.3: Normalised relative RNA-seq abundance of intracellular and extracellular peptidoglycan recognition genes.

mRNA from freshly isolated NHU cells (in situ, purple, n=3) or NHU cells induced to differentiated (red) or maintained in non-differentiated culture (blue, matched donors, N=3) were analysed. Normalised abundance is reported as FPKM; fragments per kilobase of transcript per million mapped reads to correct for transcript length. Error bars represent standard deviation between donors.

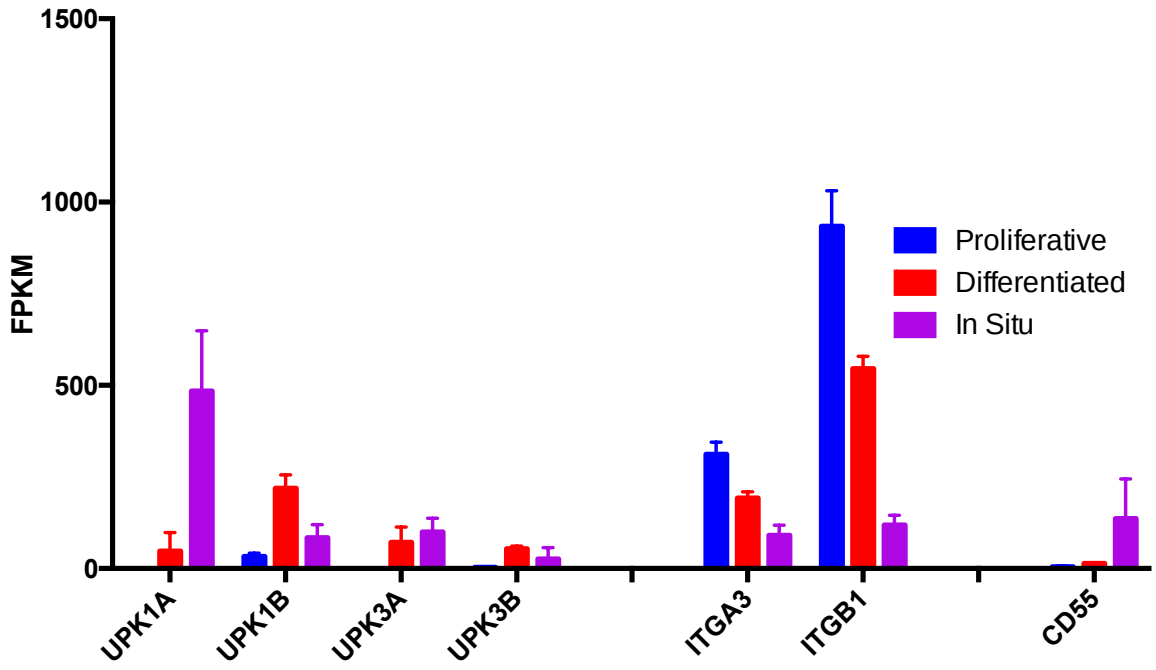

Figure 3.4: Normalised relative RNA-seq transcript abundance of urothelial receptors of bacterial adhesins.

mRNA from freshly isolated NHU cells (in situ, purple, n=3) or NHU cells induced to differentiate (red) or maintained in non-differentiated culture (blue, matched donors, N=3) were analysed. Normalised abundance is reported as FPKM; fragments per kilobase of transcript per million mapped reads to correct for transcript length. Error bars represent standard deviation between donors.

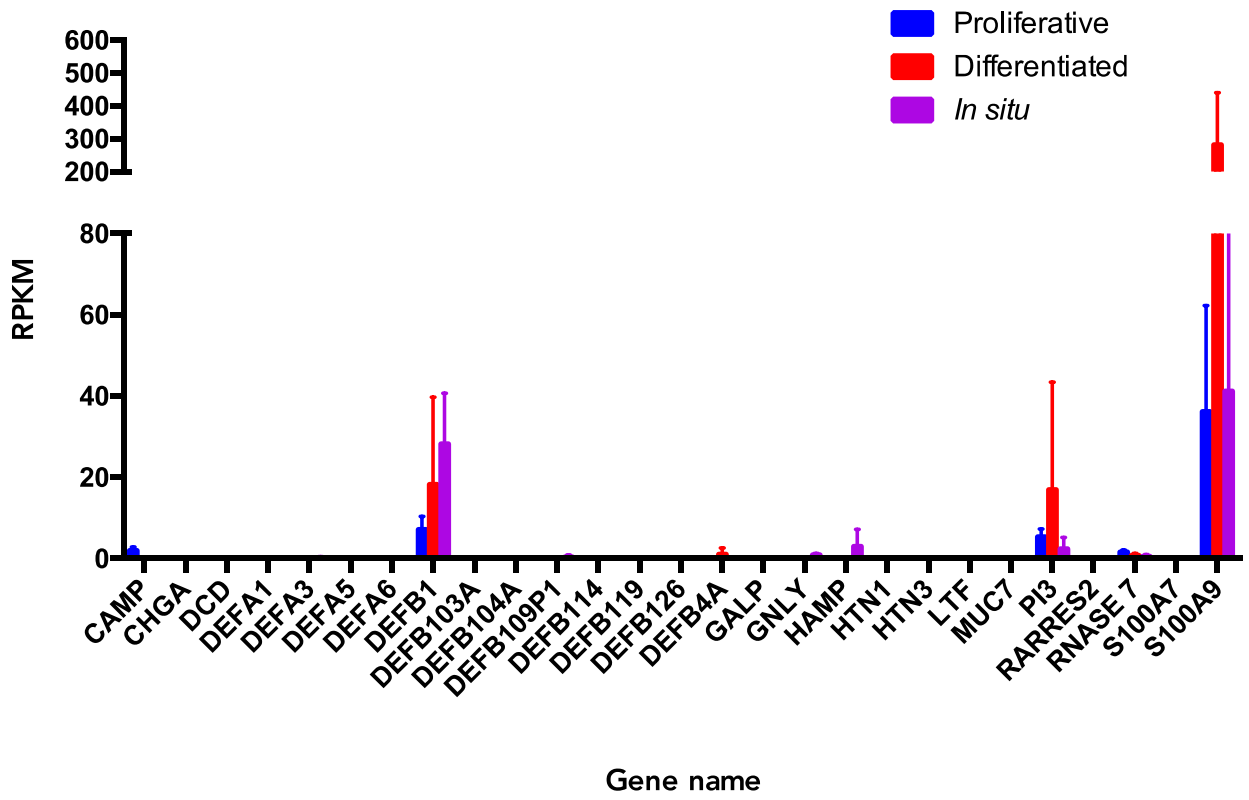

Figure 3.5 Normalised relative RNA-seq transcript abundance of AMP genes in normal human urothelium. mRNA from freshly isolated NHU cells (in situ, purple, n=3) or NHU cells induced to differentiate (red) or maintained in non-differentiated culture (blue, matched donors, N=3) were analysed. Normalised abundance is reported as FPKM; fragments per kilobase of transcript per million mapped reads. Error bars represent standard deviation between donors.

The transcript expression of targets used by UPEC adhesins was also assessed (Figure 3.4). Expression of differentiation-associated uroplakin 1b transcript was observed in *in situ*, non-differentiated and differentiated conditions. Induction of cytodifferentiation induced the expression of both UPK1A and UPK1B. Integrin subunit $\alpha 3$ and $\boldsymbol{\beta 1}$ transcripts were expressed in all three conditions, and were down regulated following cytodifferentiation. CD55 (decay accelerating factor) was expressed at a low level in both *in vitro* conditions, with increased expression in situ.

3.3.2 Constitutive expression of AMPs

Nine of the 30 shortlisted genes were expressed constitutively in all three conditions (Figure 3.5). A β-defensin gene, DEFB1 was expressed, alongside three specialised and four non-specialised AMP genes: RNAse7, lactotransferrin (LTF) and cathelicidin (CAMP), and the parent genes of psoriasin (S100A7), calcitermin (S100A9) elafin (PI3) and catestatin (CHGA). Four of the 30 shortlisted genes were expressed *in situ* alone: α-defensins 3, 5 and 6 (DEFA3-5) and hepcidin (HAMP). B-defensin 2 (DEFB4A) was expressed by differentiated NHU cells, whilst mucin 7 (MUC7) was expressed only in non-differentiated cells. Nine AMP genes were not expressed.

Based upon these results and the results of a literature search (as detailed in Section 3.2.2) a shortlist of AMP genes for further investigation was chosen (Table 3.1, highlighted in blue).

Name	Gene	Sequence Identifier	Reference
Cathelicidin	CAMP	ENSG00000164047	Chromek et al., 2006
Catestatin	CHGA	ENSG00000100604	
Dermcidin	DCD	ENSG00000161634	
hAD1	DEFA1	ENSG00000206047	Com et al., 2003
hAD3	DEFA3	ENSG00000239839	Com et al., 2003
HD5	DEFA5	ENSG00000164816	Com et al., 2003, Spencer et al., 2012
HD6	DEFA6	ENSG00000164822	Com et al., 2003
hBD-1	DEFB1	ENSG00000164825	Ali, 2013; Valore et al., 1998
hBD-3	DEFB103	ENSG00000177243	Ganz, 2003, Smet and Contreras, 2005
hBD9	DEFB109P	ENSG00000242296	Dua et al., 2014
hBD-114	DEFB114	ENSG00000177684	
hBD-120	DEFB119	ENSG00000180483	
hBD-26	DEFB126	ENSG00000125788	
hBD-27	DEFB127	ENSG00000088782	
hBD-28	DEFB28	ENSG00000185982	
hBD-2	DEFB4A	ENSG00000171711	Ali, 2013; Ali et al., 2009
hBD-4	DEFB104A	ENSG00000171711	García et al., 2001
Alarin	GALP	ENSG00000197487	
Granulysin	GNLY	ENSG00000115523	
Hepcidin 20	HAMP	ENSG00000105697	
Histatin 1	HTN1	ENSG00000126550	
Histatin 3	HTN3	ENSG00000205649	
Lactoferricin	LTF	ENSG00000012223	
Mucin-7	MUC7	ENSG00000171195	
Elafin	PI3	ENSG00000124102	Wehkamp et al., 2008
Chemerin	RARRES2	ENSG00000106538	Banas et al., 2013
Ribonuclease 7	RNASE 7	ENSG00000165799	Spencer et al., 2013
Psoriasin	S100A7	ENSG00000143556	Meyer et al.,

			2008
Calcitermin	S100A9	ENSG00000163221	

Table 3.1. Chosen longlist of candidate AMP genes for analysis. The 16 genes chosen for further analysis are highlighted in blue.

3.3.3 Exposure of normal human urothelial cells to uropathogenic bacteria

3.3.3.1 Cell morphology

The effect of bacterial exposure upon NHU cell morphology was assessed *via* time-lapse microscopy (Figure 3.6) Non-differentiated NHU cells maintained in KSFMc form a monolayer that demonstrates a cobblestone appearance as the culture approaches confluence. Partially confluent non-differentiated NHU cells were exposed to two clinically derived strains of *E. coli*, UTI89 and NU14, for up to 24 hours. Bacterial growth can be observed in the bacteria-exposed cultures after 6 hours as a grey 'haze' with increasing bacterial growth at later timepoints causing a gradual darkening of the image. Exposure of non-differentiated NHU cells to $1x10^9$ UTI89 or NU14 *E. coli* for 6 hours caused the cells to appear more condensed compared to control cells (Figure 3.6) UPEC exposed cells remained adherent after 6 h. Both NU14 and UTI89 exposed NHU cells appeared swollen, with condensed nuclei at 9 and 12 hours post exposure, with some cells lifting from the culture vessel. The control culture remained healthy at all time points.

Following the observation of cell lifting and nuclear condensation at later timepoints and previous experiments conducted in NHU cells (Smith et. al, 2001) it was decided to conduct future gene expression experiments with bacterial challenge for 6 hours.

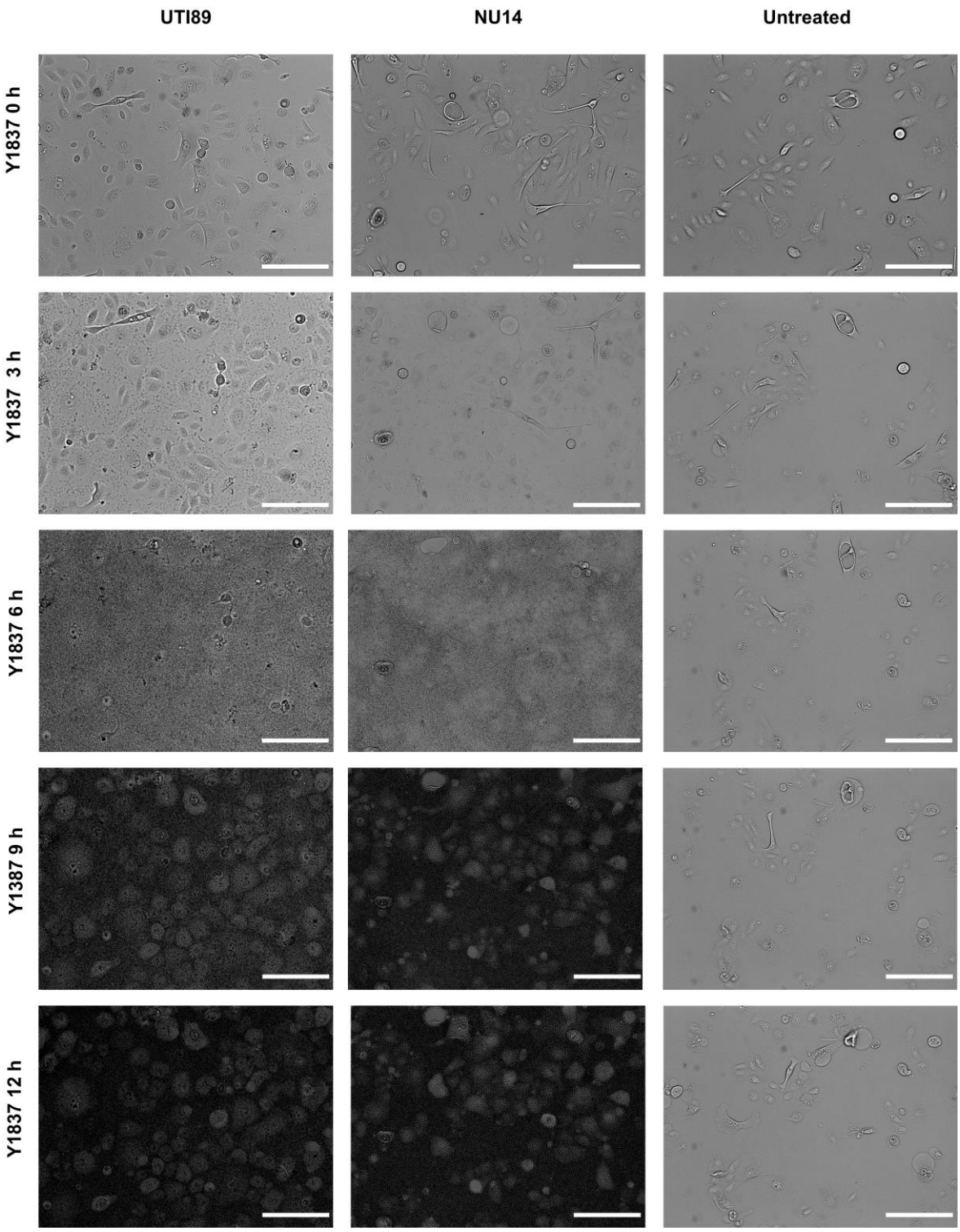

Figure 3.6 Morphological changes in non-differentiated NHU cells exposed to ~1x10^9 E. coli UTI89 or NU14 for 12 h.

Scale bars represent 100 µm.

3.3.4 AMP gene expression screening in response to uropathogenic E. coli

AMP gene expression by non-differentiated NHU cells was profiled using RT-PCR. Of the 16 shortlisted genes screened by RT-PCR, four were constitutively expressed by non-differentiated NHU cells (PI3, S100A7, RNASE7 and DEFB1). Three of the screened genes, DEFB4A, DEFA5 and DEFB104A, were induced by exposure to UTI89 (Figure 3.7). RT-PCR is a non-quantitative technique, however DEFB4A and DEFB104A expression appeared to be dose-related to bacterial challenge.

Differentiated NHU cells were also exposed to bacterial challenge (Figure 3.8). A similar pattern of gene expression was observed, however S100A7 appeared to not be expressed. PI3 expression appeared to be reduced in comparison to expression in non-differentiated cells.

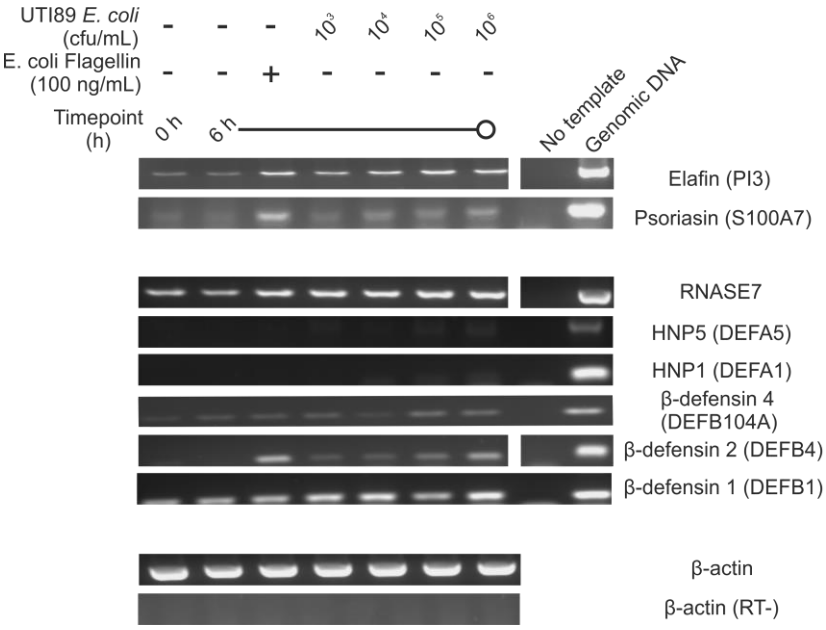

Figure 3.7 AMP gene expression by non-differentiated NHU cells in response to bacterial challenge.

NHU cultures were challenged with 100 ng/mL of UPEC flagellin or 10^3-10^6 cfu/mL of UTI89 E. coli for 6 hours. RT-PCR reaction products of AMP parent gene transcripts were resolved on a 2% agarose gel. 35 cycles of PCR were used, except for β-actin (25 cycles). Reverse transcriptase negative control (RT-) PCR for β-actin is shown at the bottom of the figure. Spaces between test and control samples are due to size differences between genomic control and cDNA products.

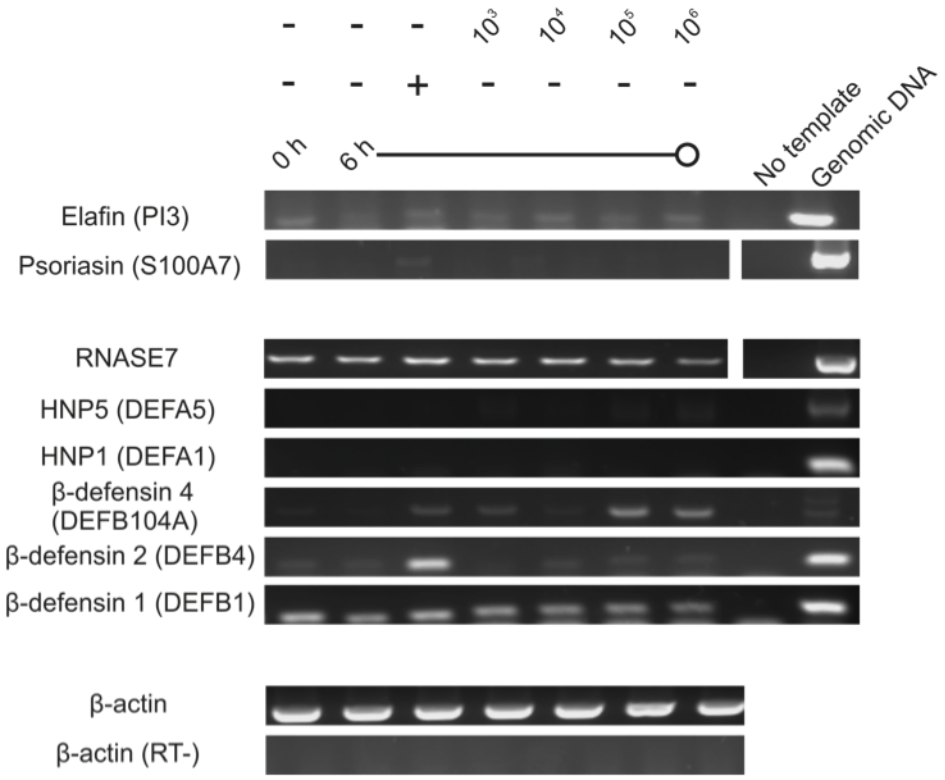

Figure 3.8 AMP gene expression by differentiated NHU cells in response to bacterial challenge.

NHU cultures were challenged with 100 ng/mL of UPEC flagellin or 10^3-10^6 cfu/mL of UTI89 E. coli for 6 hours. RT-PCR reaction products of AMP parent gene transcripts were resolved on a 2% agarose gel. 35 cycles of PCR were used, except for β-actin (25 cycles). Reverse transcriptase negative control (RT-) PCR for β-actin is shown at the bottom of the figure.

3.3.5 AMP gene expression by NHU cells in response to E. coli virulence factors

3.3.5.1*E. coli* flagellin

3.3.5.1.1 AMP gene expression

An AMP gene expression profile was determined for non-differentiated NHU cells exposed to UPEC flagellin (Figure 3.9). Four of the 14 genes screened in NHU cells were expressed constitutively: PI3, S100A7, RNASE7 and DEFB1. Two of the screened genes, DEFB4A and DEFB104A, were induced by flagellin exposure. RT-PCR is a non-quantitative technique, however PI3 expression appeared highly variable in both control and flagellin treated samples. Expression of DEFB4A and DEFB104A appeared to be induced from 0.5 h onwards, peaking at 6 h post exposure. These results were observed in three separate donor cell lines.

Differentiated NHU cells were also exposed to bacterial challenge (Figure 3.10). A similar pattern of gene expression was observed. PI3 expression appeared to be reduced in comparison to expression in non-differentiated cells.

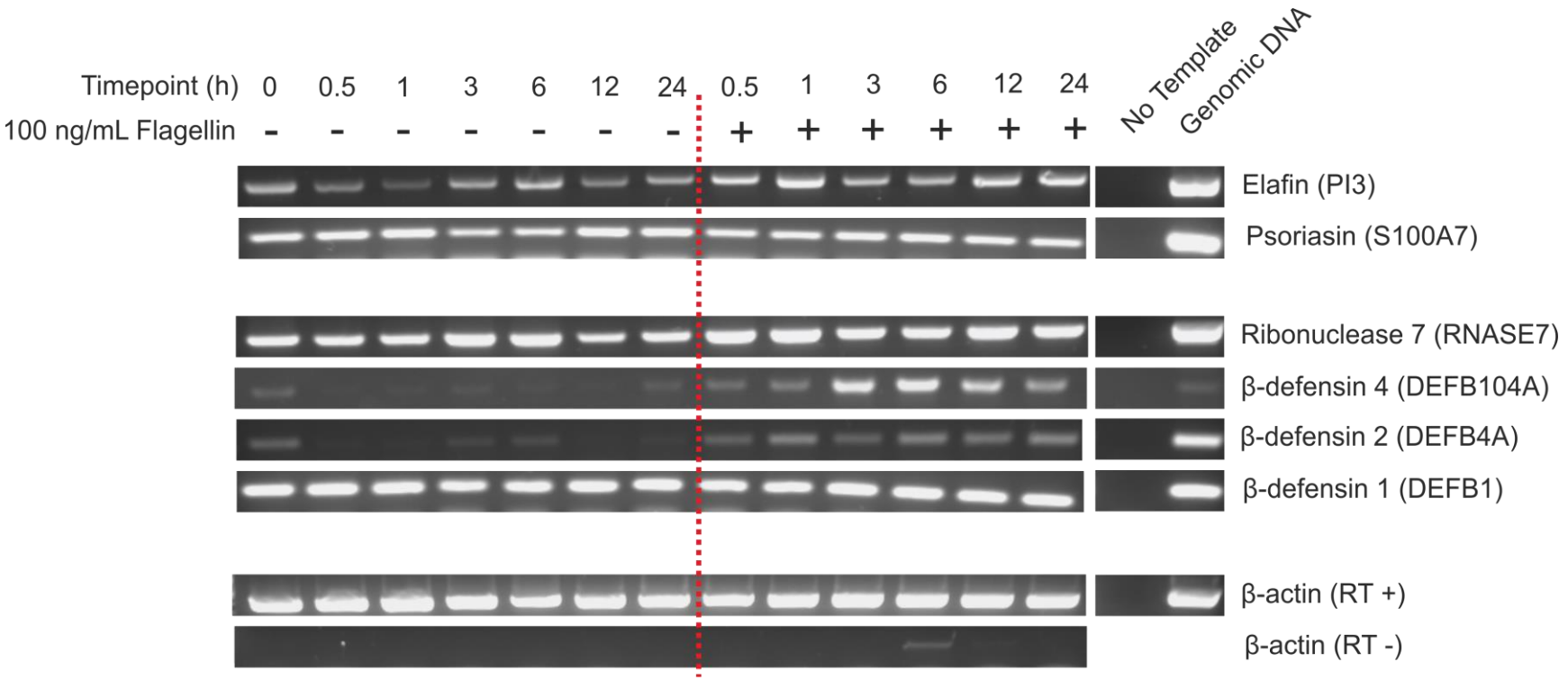

Figure 3.9. AMP gene expression by non-differentiated NHU cells in response to UPEC flagellin

NHU cultures were challenged with 100 ng/mL of UPEC flagellin for up to 24 h. RT-PCR reaction products of AMP parent gene transcripts were resolved on a 2% agarose gel. 35 cycles of PCR were used, except for β-actin (25 cycles). Reverse transcriptase negative control (RT-) PCR for β-actin is shown at the bottom of the figure

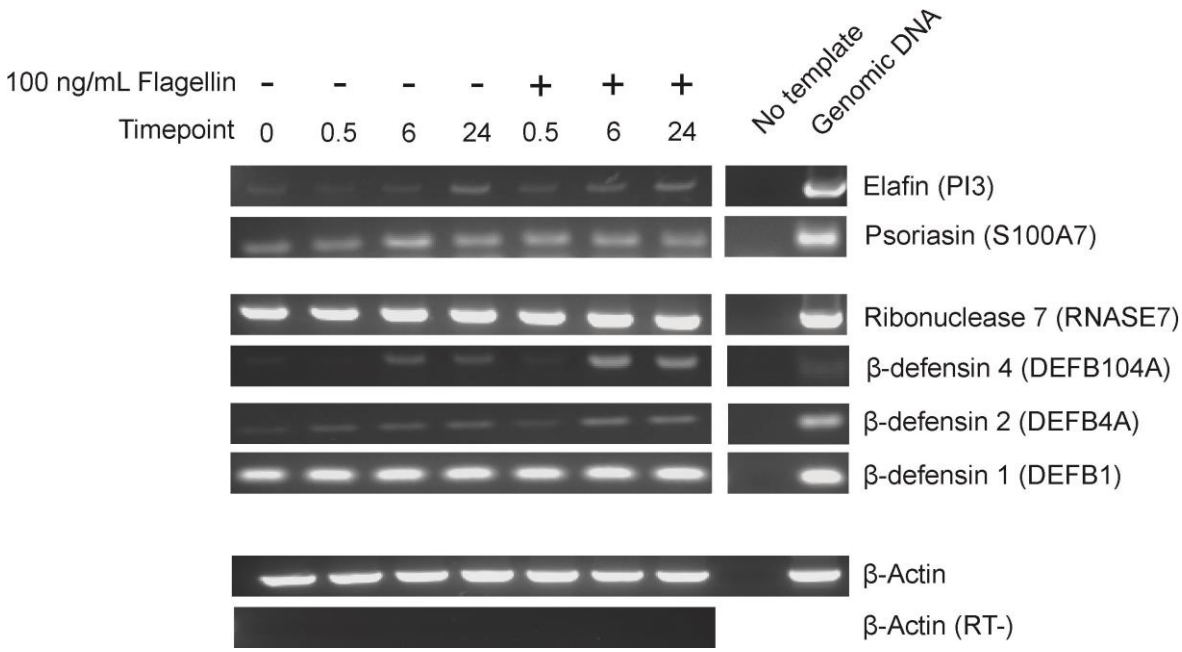

Figure 3.10. AMP gene expression by differentiated NHU cells in response to UPEC flagellin.

NHU cultures were induced to differentiate by serum and physiological levels of calcium, and subsequently challenged with 100 ng/mL of UPEC flagellin. RT-PCR reaction products of AMP parent gene transcripts were resolved on a 2% agarose gel. Reverse transcriptase negative control (RT-) PCR for β-actin is shown at the bottom of the figure.

3.3.5.1.2 Changes in cell morphology

The effect of UPEC flagellin upon NHU cell morphology was assessed by phase contrast microscopy of non-differentiated NHU cultures exposed to 100 ng/mL UPEC flagellin for up to 24 h (Figure 3.11). NHU cultures exposed to flagellin were morphologically indistinguishable from control cultures, with cells displaying phase-bright borders, characteristic of epithelial cell cultures. Both flagellin-exposed and control cultures were heterogeneous, with cultures a later time points approaching confluence.

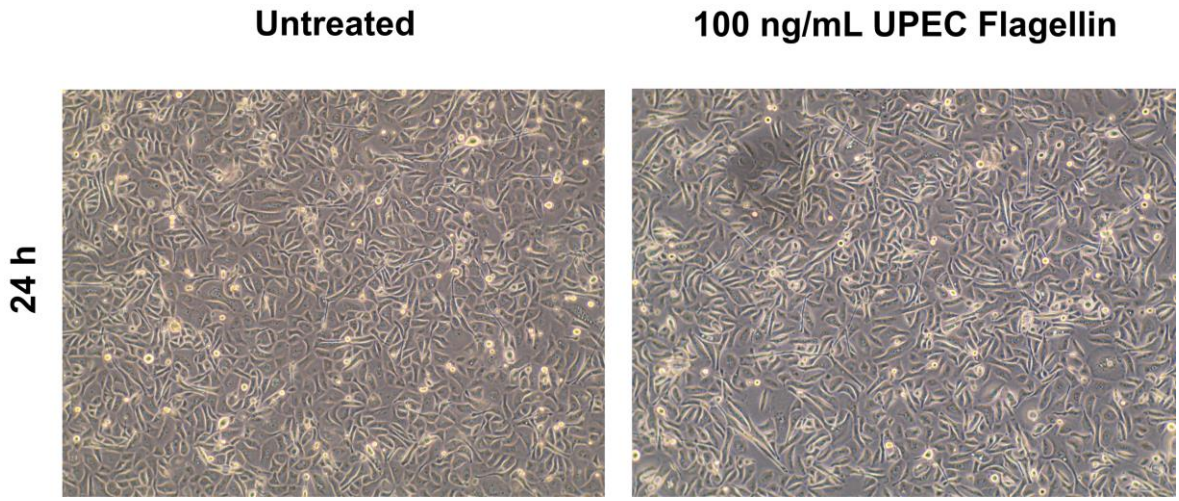

Figure 3.11. Effects of flagellin exposure upon non-differentiated NHU cell morphology. Proliferating NHU cells were exposed to 100 ng/mL flagellin for up to 24 hours.

3.3.5.1.3 Quantitative analysis of β-defensin 2 expression

Transcript and protein level expression of BD2 expression was assessed by qPCR and western blotting respectively. It was postulated that BD2 would be detectable in whole cells prior to extracellular release as the longer propeptide form in whole cell lysates. Exposing NHU cells to 100 ng/mL of UPEC flagellin induced the expression of β-defensin 2 transcript at the 6 hour time point (5.5-fold above unexposed NHU cells, Figure 3.12).

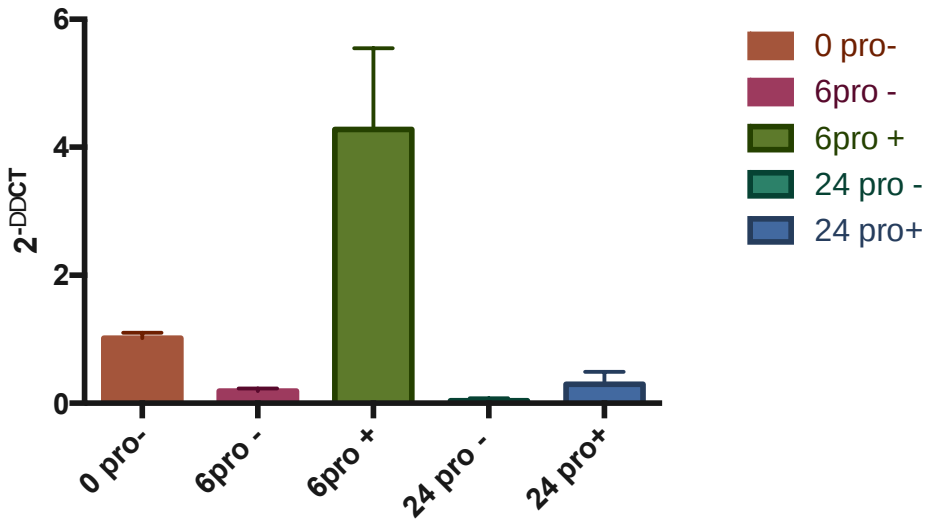

Figure 3.12. qRT-PCR analysis of AMP gene expression in response to UPEC flagellin exposure.

Mean fold change of BD2 transcript expression in 2 independent cell lines. Cells were exposed to 100 ng/mL of UPEC flagellin (+) or control (-) for 6 and 24 hours.

Immunoblotting of whole cell lysates prepared from non-differentiated NHU cells exposed to flagellin showed multiple non-specific bands in all samples, at a range of molecular weights (Figure 3.13). A strong positive band was observed in the recombinant BD2 lane, which suggested that the antibody used could detect isolated BD2. Despite the multiple bands observed in each sample, no band corresponding to the active (~4.3 kDa) or propeptide (~7 kDa) isoforms of BD2 was observed.

Following the advice of the antibody manufacturer, different blocking methods were tested to improve the antibody specificity (Figure 3.14). Both milk and bovine serum albumin methods of blocking were tested with whole cell lysates and recombinant antibody alone. Both methods showed a similar lack of specificity, with multiple bands present in both control and flagellin exposed whole cell lysate lanes, and a single band of the correct molecular weight in the recombinant BD2 lane.

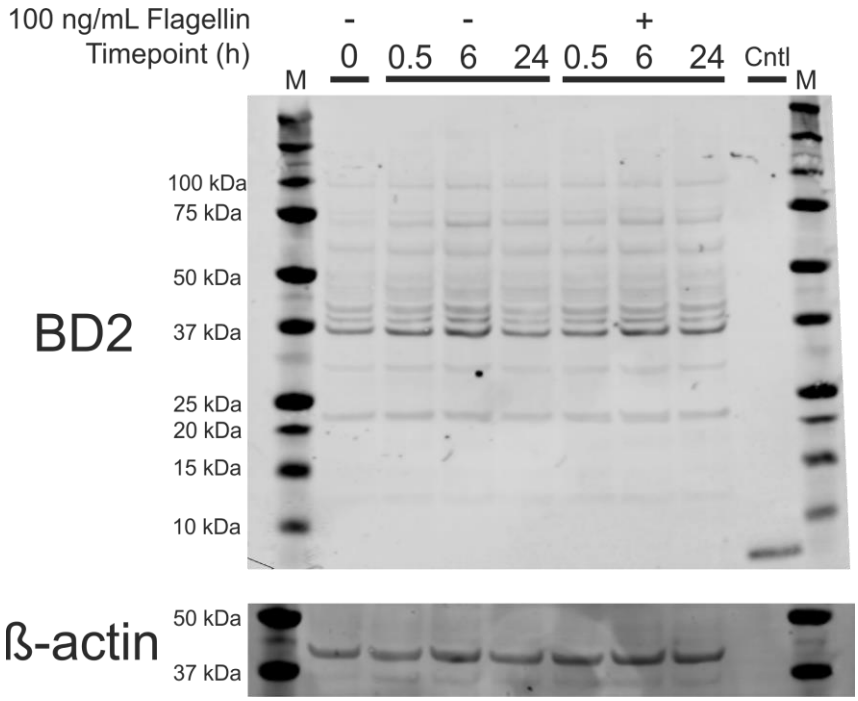

Figure 3.13. Western blot of flagellin-exposed non-differentiated NHU cells.

Protein lysates from non-differentiated NHU cells exposed to 100 ng/mL purified UPEC flagellin and 500 ng of recombinant BD2 (Cntl lane) were separated on a 4-12% Bis-tris gel and BD2 expression detected by western blot. Labelling of β actin was used as a loading control.

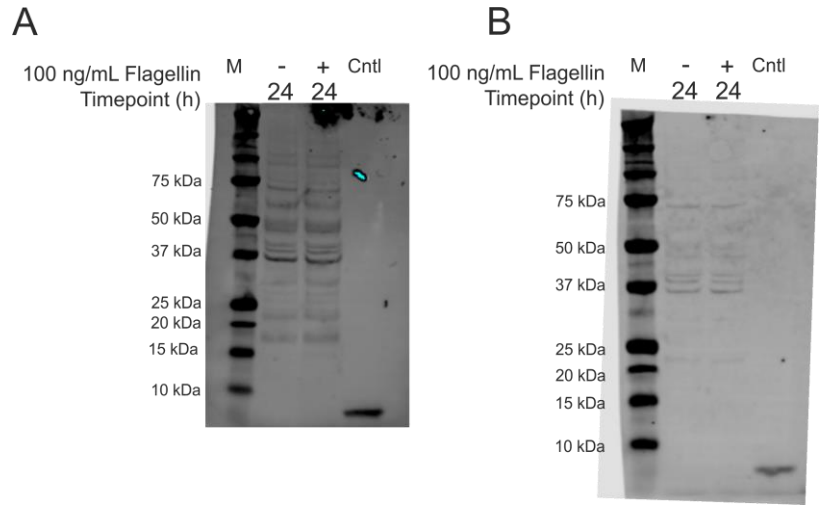

Figure 3.14. Western blot of flagellin-exposed non-differentiated NHU cells blocked with 5% milk solution (A) or 3% bovine serum albumin (B).

Protein lysates from non-differentiated NHU cells exposed to flagellin for 24 hours were separated on a 4-12% bis-tris gel and transferred to a PVDF membrane.

3.3.5.2 Ultra-pure *E. coli* LPS

Non-canonical mechanisms of LPS sensing, which utilise non-TLR4 sensing of LPS have been described (Inohara et al., 2001; Kayagaki et al., 2013). In order to assess the effect of LPS exposure on AMP expression by NHU cells, cultures were exposed to 10-1000 ng/mL ultra-pure 'smooth' LPS, derived from *E. coli* serotype O111 (Figure 3.15). Non-differentiated NHU cells were not induced to express DEFB4A or DEFB104A following 6 hours of exposure to all concentrations of LPS above that observed in control cultures without flagellin or LPS. Constitutive expression of RNASE7, DEFB1, PI3 and S100A7 was observed in all treatments, consistent with untreated controls. The expression profile was also observed following 24 h of LPS challenge (Figure 3.16).

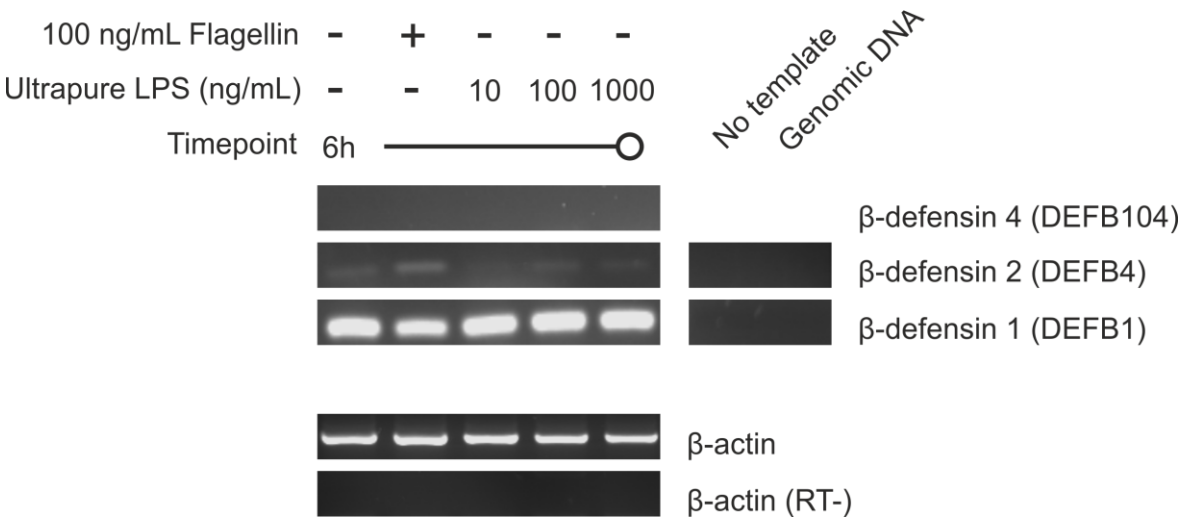

Figure 3.15 AMP gene expression by non-differentiated NHU cells in response to increasing concentrations of E. coli LPS.

Non-differentiated NHU cells were challenged with 100-1000 ng/mL of ultra pure E. coli LPS or 100 ng/mL UPEC flagellin as a positive control. PCR products were resolved on a 2% agarose gel.

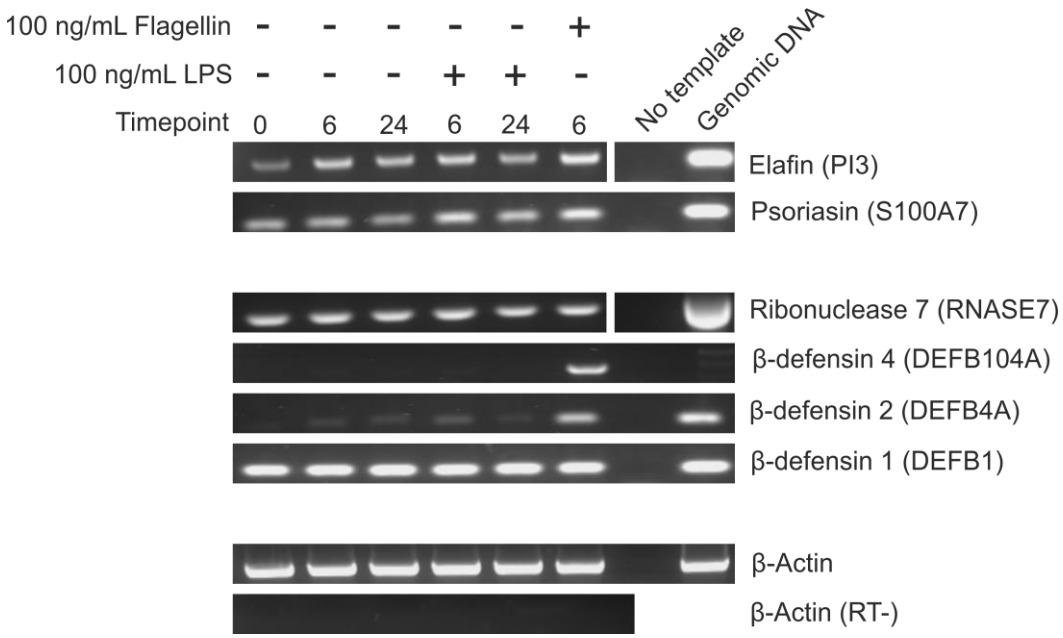

Figure 3.16 AMP gene expression by non-differentiated NHU cells in response to ultra-pure E. coli LPS for 6 and 24 h.

NHU cultures were challenged with 100 ng/mL of E. coli LPS, or 100 ng/mL UPEC flagellin as a positive control. RT-PCR reaction products of AMP parent gene transcripts were resolved on a 2% agarose gel. 35 cycles of PCR were used, except for β-actin (25 cycles).

3.3.5.3 *E. coli* peptidoglycan

Non-differentiated NHU cells bladder cancer cells were treated with purified peptidoglycan, a TLR2 and PGLYRP ligand expressed by Gram-negative bacteria. Cell cultures were challenged with increasing concentrations of peptidoglycan, and 100 ng/mL of UPEC flagellin as a positive control. Peptidoglycan did not induce expression of DEFB4A or DEFB104A, and expression of constitutive AMP genes remained similar to control conditions (Figure 3.17).

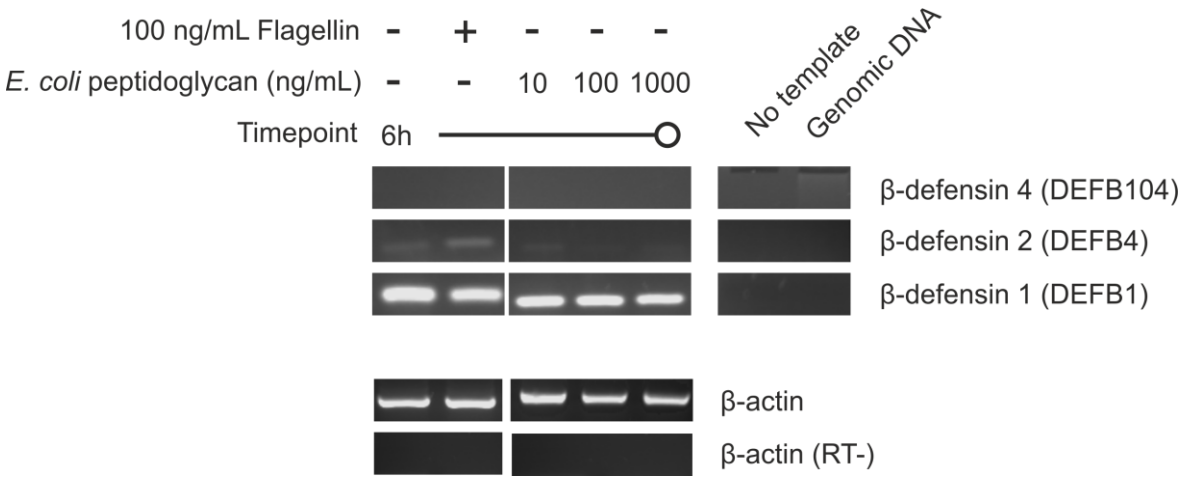

Figure 3.17 AMP gene expression profile of non-differentiated NHU cells following peptidoglycan challenge.

NHU cultures were challenged with 10-1000 ng/mL of E. coli peptidoglycan, or 100 ng/mL UPEC flagellin as a positive control for 6 h. RT-PCR reaction products of AMP parent gene transcripts were resolved on a 2% agarose gel. 35 cycles of PCR were used, except for β-actin (25 cycles). Reverse transcriptase negative control (RT-) PCR for β-actin is shown at the bottom of the figure. Peptidoglycan-negative and flagellin-positive control images are shared with Figures 3.13 and 3.16 as all reactions shown in these figures were conducted at the same timepoints and analysed on the same gel.

3.3.5.4UPEC type 1 fimbriae

Type 1 fimbriae are the hypothesised primary mechanism of UPEC attachment, and have been shown in cancer cell models of UTI to induce apoptosis following binding (Klumpp et al., 2006, 2001). The effect of type 1 fimbriae exposure on AMP expression was analysed in non-differentiated NHU *via* RT-PCR (Figure 3.18). Cell cultures were exposed to increasing concentrations of UPEC-derived *FimH* for 6 h. DEFB4A gene expression was induced in non-differentiated NHU cells challenged with 1000 ng/mL of UPEC *FimH*.

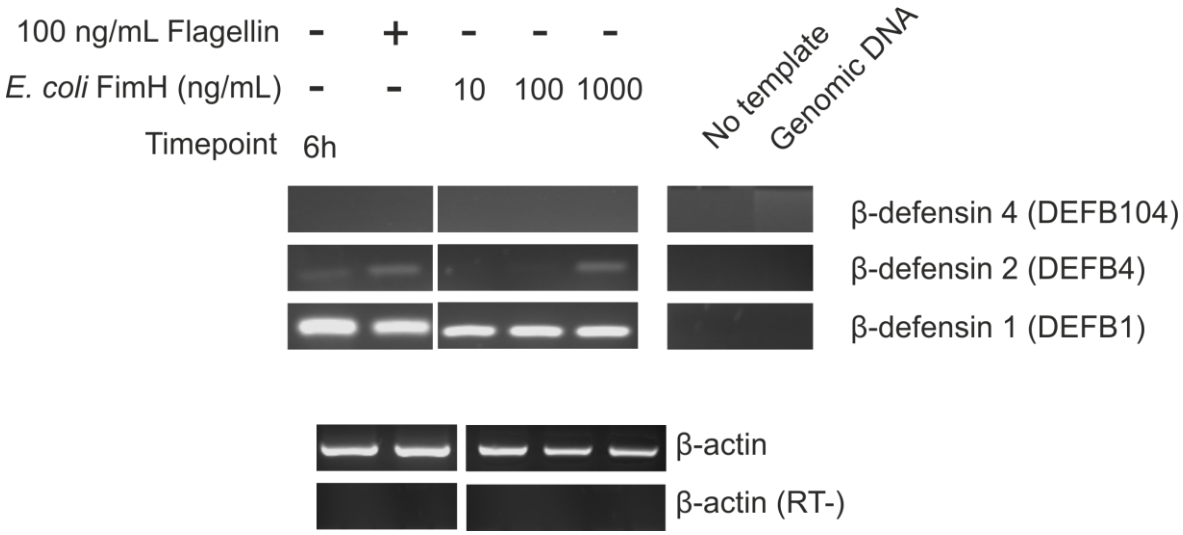

Figure 3.18 AMP gene expression profile of non-differentiated NHU cells in response to E. coli type 1 fimbriae.

NHU cultures were challenged with 10-1000 ng/mL of E. coli type 1 fimbriae, or 100 ng/mL UPEC flagellin as a positive control, for 6 h. RT-PCR reaction products of AMP parent gene transcripts were resolved on a 2% agarose gel. 35 cycles of PCR were used, except for β-actin (25 cycles). FimH-negative and flagellin-positive control images are shared with Figures 3.13 and 3.16 as all reactions shown in these figures were conducted at the same timepoints and analysed on the same gel.

It should be noted that the positive genomic control reactions included in Figures 3.15, 3.17 and 3.18 were not successful. All reactions analysed in these figures were conducted simultaneously, using the same PCR reagents: the presence of specific bands following reactions using DEFB1 and β-actin primers shown in all three figures suggest that the reaction was successful. Medium-only and flagellin-positive images lanes are shared across all three figures as all three experiments were conducted at the same time and were conducted in the same cell line with shared controls.

3.3.6 AMP response to a non-motile mutant uropathogenic E. coli strain

3.3.6.1 Construction of a UTI89 flagellin mutant

Lamba-red recombination was performed as described in Section 2.7.9, and successful recombinated clones were selected by growth on tetracycline-ampicillin LB agar. In order to verify the specific targeting of the *fliC* gene, PCR primers were designed flanking the insertion site (Figure 3.19). PCR amplification of isolated bacterial gDNA following successful recombination yielded a product of 2312bp, whilst wild-type gDNA yielded a product of 401 bp. PCR analysis of gDNA isolated from three tetracycline resistant colonies (ΔfliC17, ΔfliC18 and ΔfliC19) yielded positive verification of tetracycline resistance cassette insertion. Two clones were chosen for use in future experiments, clones ΔfliC18 and 19. Sanger sequencing of the inserted region in gDNA isolated from clones ΔfliC18 and ΔfliC19 confirmed successful recombination of the functional tetracycline cassette and disruption of the *fliC* start codon.

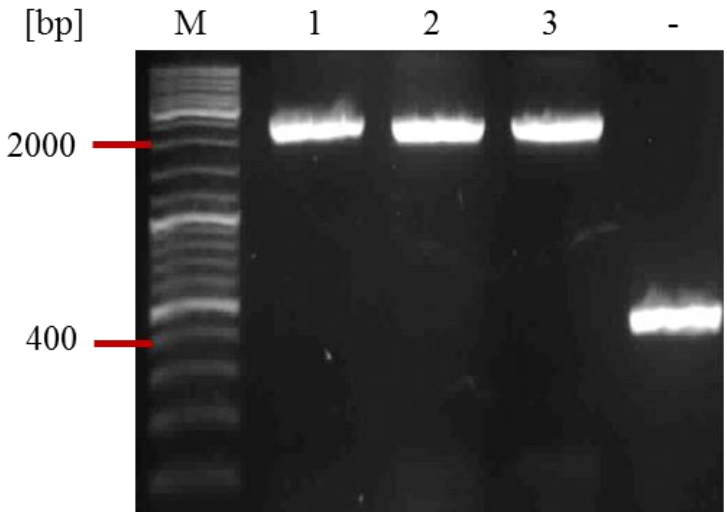

Figure 3.19. PCR verification of tetracycline resistance cassette insertion to UTI89.

PCR using insertion site flanking primers was performed on gDNA from ΔfliC17 (1), ΔfliC18 (2), ΔfliC19 (3) and wildtype UTI89 (-), and resolved on a 4% agarose gel.

3.3.6.2 Motility phenotypes of the UTI89 fliC mutant

A successful fliC disruption mutant was expected to be aflagellar and therefore non-motile. Motility of the recombinant strains was first assessed by stab culture of overnight cultures from wild-type, mutant (Δflic18 and ΔfliC19) and control strains of bacteria into motility test agar at 37 °C for 8 h (Figure 3.20).

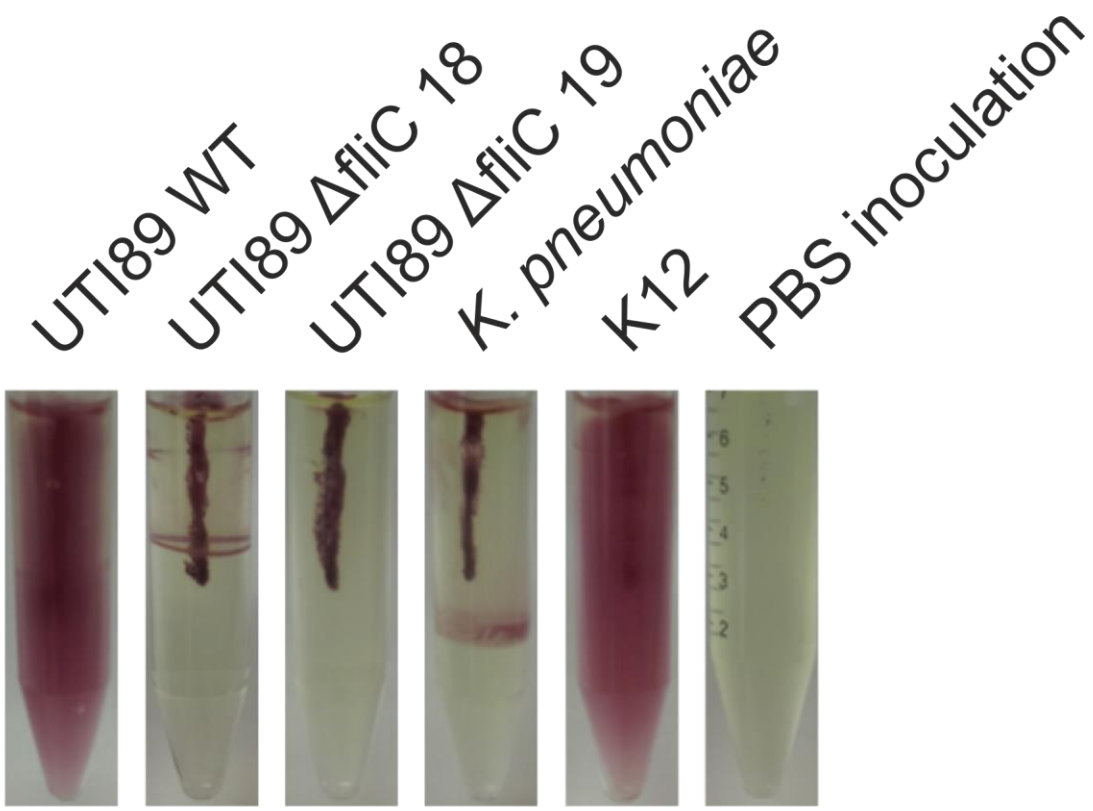

Figure 3.20: Motility assay of fliC mutants.

Overnight cultures of each strain were stab inoculated into motility agar with a sterile needle and incubated at 37 °C overnight.

As expected, wild-type UTI89 and positive control K-12 *E. coli* were motile in soft agar. In contrast, the negative control, *Klebsiella pneumoniae* ATCC13883 appeared non-motile in soft agar. All strains of *K. pneumoniae* are non-motile and non-flagellated. Both clones of *fliC*-disrupted UTI89 appeared to be non-motile; suggesting that lambda red mediated disruption of the *fliC* gene was successful.

The effect of fliC disruption upon bacterial growth was also assessed. The growth kinetics of wildtype UTI89 and strains 18 and 19 of the UTI89-ΔfliC in LB medium was assessed for 12 hours (Figure 3.21). The rate of exponential phase growth was

significantly reduced in UTI89-Δflic18 and UTI89-Δflic19 strains (slope of regression *k* = 6.6 x10^{-3} +/- 3.5 x10^{-4} min^{-1}and 6.5x10^{-3} +/- 2.4x10^{-4} min^{-1} respectively (+/- SD) in comparison with wild-type UTI89 (8.8x10^{-3} +/- 4.1x10^{-3} min^{1}).

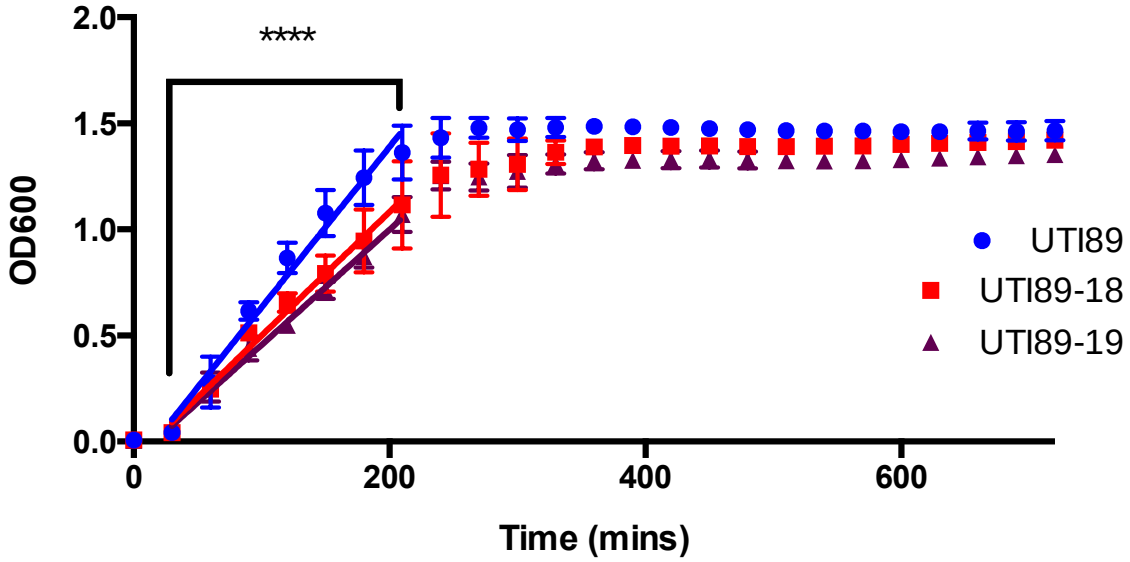

Figure 3.21 Effect of fliC disruption upon UTI89 growth kinetics.

*Each point represents mean (+/-SD) of 5 biological replicates. Differences in slope of exponential phases were measured by linear regression and F-test. **** denotes P<0.0001.*

3.3.6.3 Western blot detection of flagellin

To determine if a truncated or otherwise modified flagellin protein product was expressed following *fliC* start codon disruption, flagellin expression was assessed by western blot (Figure 3.22). Protein from overnight bacterial cultures were isolated, denatured, separated by SDS-PAGE and subjected to western blot analysis. Lysates from wild-type UTI89, ΔfliC UTI89 and *K. pneumoniae* were blotted using a commercial polyclonal antibody to flagellin. Multiple bands were observed in each sample, many shared between lysates from *K. pneumoniae* and *E. coli*. The manufacturer estimated flagellin to blot at approximately 66 kDa, however previous studies report *E. coli* flagellin ranging in molecular mass from ~37-67 kDa. An intense band was present at approximately 66-67 kDa, however the band was present in both the positive and negative control samples.

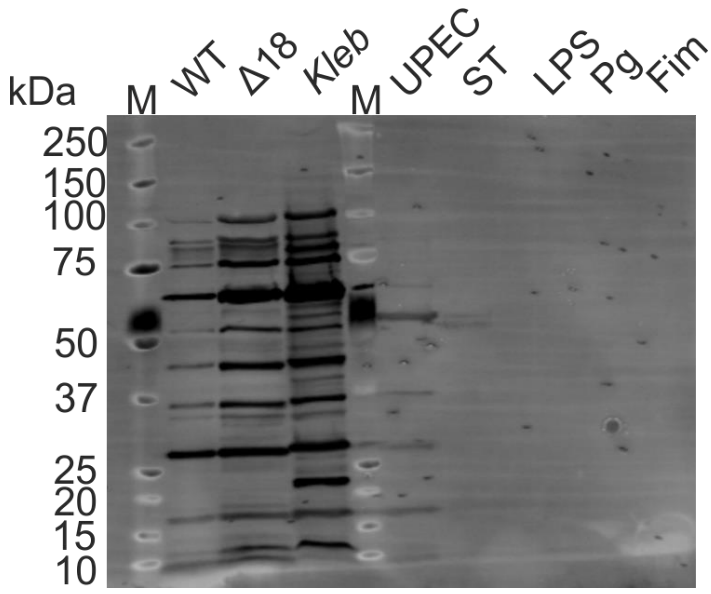

Figure 3.22 Western blot of bacterial proteins lysates and purified bacterial components for flagellin.

WT, wild-type UTI89 E. coli; Δ18, clone 18 of ΔfliC mutant; Kleb, Klebsiella pneumoniae; UPEC, NCTC10418 flagellin; ST, ultra-pure S. typhi flagellin; LPS, ultra-pure E. coli LPS; Pg, E. coli peptidoglycan; Fim, purified type 1 fimbriae from E. coli J96. 20 µg of protein lysate or 500 ng of purified protein loaded per lane, resolved on a 10-12% Bis-tris SDS-polyacrylamide gel and transferred to PVDF membrane, blotted for Flagellin with ab93713.

Denatured samples of purified flagellin, ultra-pure smooth LPS, *E. coli* peptidoglycan and UPEC type 1 fimbriae were run in parallel on the same gel in order to assess nonspecific binding of the antibody to other membrane components expressed by *E. coli*. Several weak bands were observed in the purified NCTC10418 flagellin sample, whilst all other samples were negative for flagellin.

*3.3.6.4*AMP gene expression in response to non-motile uropathogenic *E. coli*

Non-differentiated NHU cells were exposed to wildtype or fliC-disrupted UTI89 for 6 hours to assess the effect of flagellin disruption upon induction of DEFB4A transcript (Figure 3.23). AMP gene expression was profiled using RT-PCR. No expression of DEFB4A was observed in control or cultures at 35 cycles of RT-PCR. Extremely faint bands were observed upon increasing the number of cycles to 40.

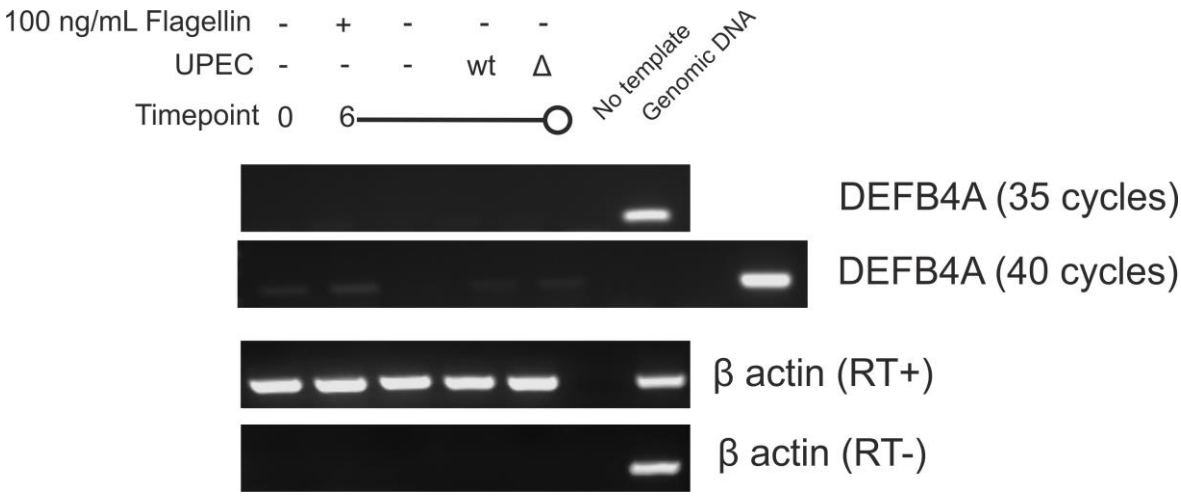

Figure 3.23: β-defensin 2 (DEFB4) gene expression by non-differentiated NHU cells following challenge with wild-type or fliC disrupted UTI89 UPEC.

NHU cultures were challenged with ~10^8 cfu of statically cultured UTI89 or clone 18 of UTI89-ΔfliC UPEC or 100 ng/mL UPEC flagellin as a positive control for 6 h. RT-PCR reaction products of AMP parent gene transcripts were resolved on a 2% agarose gel. 35 or 40 cycles of PCR were used, except for β-actin (25 cycles). Reverse transcriptase negative control (RT-) PCR for β-actin is shown at the bottom of the figure.

3.4 Discussion

In tandem with continuous release of antimicrobial factors, the urothelium releases a complex cocktail of protein and small molecule inflammatory factors when activated by pathogen-associated molecules. We have termed this the urothelial 'defendome'**: the sum of soluble biological molecules with innate immune function, which are released by the urothelium in response to a pathogenic stimulus**. These host components act to prime urothelial defensive mechanisms such as apoptosis and cell exfoliation (Klumpp et al., 2006), recruit neutrophils and other immune cells (Frendéus et al., 2000), and exert direct antimicrobial effects on the uropathogens themselves (Ali et al., 2009).

Targeted analysis of RNA-seq data from NHU cells and freshly isolated urothelium suggests that elements of the urothelial defendome and pathogen sensing mechanisms are expressed at steady-state. TLR2-5 gene expression was observed in all cell types, as were PGLYRP1-4 and NOD1/2 transcripts.

Biomimetic differentiation of NHU cells highly upregulated TLR3 transcript expression compared to non-differentiated NHU cells or *in situ* urothelium. TLR3 plays a core role in the innate response to viral infection, binding double-stranded RNA, a replication intermediary for many viruses. TLR3 dimerization causes activation of an interferon regulatory factor 3 (IRF3) mediated signalling cascade, potently inhibiting viral replication (Doyle et al., 2002). Endosomal TLR3 expression is considered almost ubiquitous in humans (Zarember and Godowski, 2002). Intriguingly, evidence from murine pyelonephritis models has suggested that IRF3 plays an important role in the response to uropathogenic bacteria through interactions with TLR4 (Fischer et al., 2010, p. 3). IRF1, an IRF3 homologue, has been implicated as an important intermediary TF in PPARγ-mediated differentiation of urothelial cells (Varley et al., 2008).

Low levels of PGLYRP1-3 were expressed in all three urothelial states, however PGLYRP4 was significantly upregulated upon differentiation. PGLYRP4 is expressed by a range of epithelial cells, including the epidermis, the tongue and oesophagus, in addition to the cornea, salivary glands and columnar absorptive cells of the small intestine (reviewed in Dziarski and Gupta, 2006). PGLYRPs have reported bactericidal activity, exerting reactive oxygen, thiol and metal stresses upon bacteria (Kashyap et al., 2014), and activate bacterial 'suicide' mechanisms (Kashyap et al., 2011). There is evidence to suggest that PGLYRPs can act as cytokine-like molecules to amplify the intracellular signalling cascade activated by NOD2-PG interactions, and directly cleave PG at the bacterial cell surface (Boneca, 2009).

Both NOD1 and NOD2 were expressed constitutively. The nucleotide-binding oligomerization domain-like receptors (NODs) are highly-conserved intracellular PAMP sensing receptors, similar to TLRs in function (Franchi et al., 2009). Both NOD1 and NOD2 are active as sensors of peptidoglycan, with differing specificities (Girardin et al., 2003a, 2003b) . Activation of NODs induces inflammatory gene expression *via* NFkB and MAPK pathway activation *via* a different mechanism to TLR activation (Franchi et al., 2009)

The RNA-seq dataset analysed in this chapter was focused on the comparative analysis of non-differentiated, biomimetically differentiated and *in situ* urothelial cell gene expression. As such, the dataset represents the 'steady-state' gene expression, and

would not reveal genes upregulated during infection, such as antimicrobials and signalling components required following infection.

Despite this, the RNA-seq data set revealed several AMP genes, which were constitutively expressed in all three cell types, including DEFB1, PI3, S100A9 and RNASE7. These results correlated with previous findings, as DEFB1 expression ahs been reported in the bladder previously (Com et al., 2003; Pazgier et al., 2006) . DEFB1 transcript expression was also detected in non-differentiated and differentiated NHU cells as part of this study. RNASe7 was detected in the RNA-seq dataset at low levels of expression, and constitutive transcript expression observed in non-differentiated and differentiated cells as part of this study. RNASE7 expression has previously been noted in both the urothelium and kidney (Spencer et al., 2013).

Expression of BD2 and BD4 was observed in response to treatment with UTI89 UPEC and isolated UPEC flagellin, and were not expressed constitutively. BD2 and BD4 expression were not induced by *E. coli* peptidoglycan or LPS. The insensitivity of NHU cells to LPS has been noted previously (Smith et al., 2011). The lack of response to PG was unexpected, considering the (albeit transcript-level) expression of a range of PG sensing mechanisms in urothelial cells. Evidence from Protein Atlas, an online proteomic atlas (Uhlén et al., 2005) also suggests that NOD2 is expressed at the protein level. Evidence from other model systems suggest that both NOD and PGLYRP act in concert with TLR and other signalling pathways, suggesting that multiple PAMP stimuli may be required in order to activate a downstream antimicrobial response.

BD2 is a member of the defensin family, originally discovered in psioratic skin lesions. It is inducible, produced at several epithelial surfaces in response to NFkB activation (Liu et al., 1998). BD2 is a highly effective anti-Gram negative and anti-yeast bactericidal peptide, with a LD_{90} does of approximately 10 μg/mL. BD2 is less effective against Gram-positive, acting only as a bacteriostatic agent versus *S. aureus* (Bals et al., 1998). Recent preliminary literature has reported the expression of BD2 in urothelial and vaginal epithelial cells in response to bacterial stimuli, however peer-reviewed publication are forthcoming (Ali et al., 2012).

hBD4 is a more recently discovered defensin, identified *via* bioinformatic analysis (García et al., 2001). hBD4 is expressed less widely that hBD2, with highest expression noted in the testis, uterus, kidney and lung, hBD4 induction may be specific to pathogens, as unlike BD2, expression was not induced by IL1 or TNF (Bals et al., 1998; García et al., 2001). Interestingly, hBD4 has poor antimicrobial efficacy versus *E. coli*, yet is high efficient versus *P. aeruginosa* (García et al., 2001). To our knowledge, this is the first description of BD4 expression in urothelial cells.

Previous work in this chapter has noted the flagellin-mediated induction of an AMP response in NHU cells. The TLR5 response is not dependent on the functional motility of the pathogen: TLR5 interacts specifically with the flagellin subunit, which forms the flagellar filament. It was hypothesised that disrupting the fliC gene using lambda-red recombination would prevent TLR5 activation and abrogate AMP induction. Lambda-red recombination was originally developed for use with lab strains of *E. coli*, enabling the large-scale insertion or deletion of chromosomal genes (Datsenko and Wanner, 2000; Murphy et al., 2000). However, large-scale recombinations in pathogenic *E. coli* have been unsuccessful (Murphy and Campellone, 2003), possibly due to evolved mechanisms to prevent genetic recombination (Tibayrenc and Ayala, 2012). Due to these complication, a tetracycline resistance cassette to disrupt the fliC start codon, avoiding a larger recombination of the whole fliC gene.

PCR, Sanger sequencing and antibiotic selection confirmed the successful insertion of the tetracycline resistance cassette to UTI89. UTI89-ΔfliC were functionally non-motile, however it was possible that a truncated fliC protein could be expressed and activate TLR5. Several techniques were attempted; including Western blotting, however the antibody tested exhibited a high degree of non-specific binding, even in bacterial strains, which did not express flagellin. Exposure of non-differentiated NHU cells to the wildtype and UTI89-fliC strains resulted in BD2 transcript expression, albeit at very low levels. Further work is required in order to assess if the knockout was successful, however the multiple virulence factors (other than flagellin) that are expressed by *E. coli* may be able to synergistically activate urothelial cells.

Many of the defensins have salt-sensitive antimicrobial activity: antimicrobial activity against a range of pathogens is significantly reduced in the presence of increased NaCl

concentration. The antimicrobial effect of human BD2 against *E. coli* was reduced 8-fold by increasing the NaCl concentration to 150mM (Bals et al., 1998). Accurate estimation of urinary salt concentration is difficult, however estimates suggest a normal physiological concentration of 110-250 mmol/L of Na+ or Cl- ions released per 24 h period. *In vitro* experiments using purified BD2 and lab strains of pathogens suggest that these concentrations may slightly inhibit the efficacy of hBD2 in urine, the environment where they will exert their antimicrobial effects.

Previous studies have quantified AMP expression in urine in both healthy and symptomatic UTI patients. Between 5-190 pg/mL of BD2 has been detected in symptomatic patient urine (Ali, 2013; Nienhouse et al., 2014): this is two orders of magnitude lower than the recorded LD90 of BD2 versus *E. coli*. BD4 levels have not been measured in urine. This may suggest that, in combination with high urinary salt levels, that BD2 may be less effective in the urinary tract than at other sites, such as the skin.

However, BD2 may play an important signalling role. In addition to their direct antimicrobial effects, AMPs can also act as signalling and chemotactic stimuli for a wide range of specialised immune cells and epithelia: hBD1 and hBD2 are chemotactic for immature dendritic cells and memory T cells; binding to the CCR6 chemokine receptor. BD2 can also activate mast cells to degranulate, causing histamine release and prostaglandin release (Subramanian et al., 2013). Less is known regarding the signalling effects of hBD4, however evidence exists for hBD4-mediated monocyte chemotaxis (García et al., 2001).

3.5 Conclusions

- A range of bacterial virulence factor receptors and AMPs are expressed by human urothelium at the transcript level
- The defensins BD2 and BD4 are expressed in response to UPEC and UPEC derived flagellin by non-differentiated and differentiated urothelium.
- A non-motile UTI89 strain was produced, however it is unclear if flagellin production is completely abolished.

4 Detection of AMPs by mass spectrometry

4.1 Introduction

Mass spectrometry (MS) is an enormously powerful technique for the analysis of an almost limitless range of analytes. The development of 'soft' ionisation techniques such as matrix-assisted laser desorption/ionisation (MALDI) and electrospray ionisation (ESI) has greatly facilitated the use of MS for analysis of biomolecules, particularly peptides, proteins and carbohydrates.

The past few decades have seen rapid progress in the sensitivity and scope of MS analysis of biomolecules, allowing for highly sensitive and massively multiplexed analyses on an 'omic' scale. This chapter discusses the development of mass spectrometric analyses of AMPs released *in vitro*, in response to bacterial challenge. This introduction will discuss the previous uses of analytical chemistry and mass spectrometry in the analysis of AMPs, and present a discussion of the operational principles of mass spectrometry in the context of peptide analysis.

4.2 Mass spectrometric methods and the analysis of AMPs

AMPs are expressed by almost all orders of life, including bacteria and plants, and exhibit broad antibiotic activity against a wide range of pathogens. The broad activity of AMPs has made them attractive targets and candidates for antibiotic drug development and so many of the studies using MS for AMP analysis have focused on the identification of novel AMPs from plant or animal sources.

Analyses of AMPs from such sources have largely used methods broadly similar to those used in traditional small molecule natural product discovery, wherein isolated organs/tissues or whole organisms are homogenised, fractionated and tested for 'activity' using an *in vitro* assay system (e.g. inhibition of bacterial growth). Active fractions are further fractionated and their compositions analysed. MS analysis during this process has focused on aiding in identification of the active factor following bioassays, after significant pre-concentration of the active factor (e.g. measuring the

mass of a novel peptide (James et al., 1994), identifying peptide homologues (Kannan et al., 2013) or helping to assign structural characteristics (Kannan et al., 2013; Storici et al., 1996)

Literature reports of applications of such methods to analyse *in situ* expression of AMPs are limited. The AMP-containing source material is often plentiful, therefore the efficacy of the extraction process is often not a priority (e.g the concentration of peptides from 24 whole frog skins for a single analysis (Yang et al., 2013) . These fractionation steps also aid in simplifying the analytical process by removing interfering matrix components and reducing the method sensitivity required to detect the analyte, compared to the complex matrices (such as urine, serum or saliva) that may be collected.

A more recent approach to AMP analysis has focused on 'genome mining', using bioinformatics techniques to identify novel AMPs based upon sequences of peptides with confirmed protein-level expression (Jia et al., 2001; Linzmeier et al., 1999). This approach has led to the identification of two novel AMPs from the β-defensin family, β-defensin 9 (Dua et al., 2014) and β-defensin 4 (García et al., 2001). Evidence of expression of these novel AMPs has been limited to the transcript level, and the production of recombinant peptides based upon the candidate transcripts to demonstrate antimicrobial activity.

Bioinformatic and transcriptional approaches have been hampered by contradictory evidence suggesting that several novel defensin genes may be truncated or non-functional *in vivo (Yang et al., 1999)*. Computational identification of novel AMP genes is also hampered by the poor sequence homology observed between peptides of the same family, which may nonetheless share significant higher-order structural homology.

The range of post-translational modifications and isotypes of AMPs also offers a considerable challenge to the use of 'traditional' biological techniques (e.g transcriptomic or antibody-based analysis) to detect AMPs. Most AMPs are translated into a propeptide or prepropeptide form, (e.g. β-defensin 2 and cathelicidin, shown in Figure 4.1, including a signalling peptide to initiate extracellular expression. Post-translational processing of the AMP cleaves the peptide to its active, biologically relevant form. Certain AMPs are differentially cleaved, forming different active peptides.

Cathelicidin can be differentially cleaved to form two active products: FALL-39 and LL-37, which differ in length by two amino acid residues.

Traditional biological techniques are poorly suited to analysing such subtle differences. Antibody specificity is dependent upon the antigen used to raise the antibody: an antibody raised against a full-length AMP may display affinity to any propeptide, active peptide or differentially cleaved products (Figure 4.1). Commercial availability of antibodies to defensins and other AMPs is limited, and non-existent in species beyond humans and rodents Transcriptomic analyses are limited to quantifying the production of AMP transcript, which encodes the full-length propeptide or prepropeptide, and cannot reveal details of the post-translational modification of the translated peptide itself.

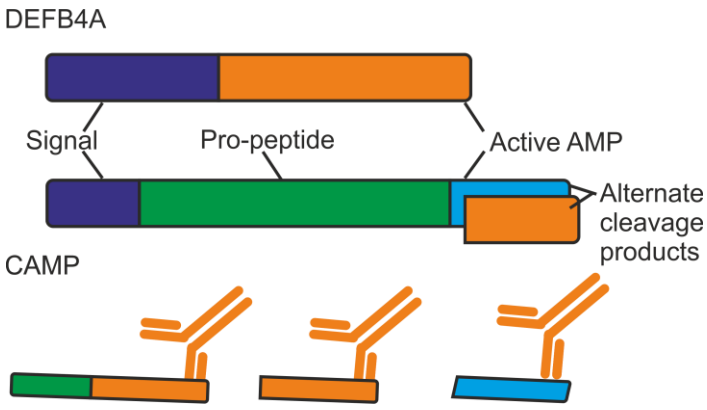

Figure 4.1. Examples of poor antibody specificity to post-translational modification of AMPs. Both DEFB41 and CAMP are cleaved from pro- or pre-pro- peptides to their active forms. Antibodies which are raised against the active AMP or differentially cleaved products may therefore detect the full pro-peptide or pre-pro-peptide sequence in addition to the cleaved peptide.

DEFB4A; β-defensin 2, CAMP; Cathelicidin.

4.2.1 Operational principles of sample preparation and MS analysis

4.2.1.1 Chromatographic separation

Chromatography is the primary separation method used in the analysis of complex biological mixtures, therefore the basic theory of the method is described in this section.

Chromatography is used to prepare samples for MS analysis by separating the components of complex mixtures in order for the individual components to be analysed with minimal interference from other components of the mixture. In basic terms, a chromatographic system consists of a mobile phase, in which the analyte mixture is dissolved, and an immiscible stationary phase (immobilised onto a substrate) over which the mobile phase is forced. Chromatographic separation of an analyte mixture depends on the relative affinity of each analyte for the mobile and stationary phases. The strength of this analyte-phase interaction can be described using the partition coefficient *K* (Equation 2.).

$$K = \frac{[Analyte_{stationary}]}{[Analyte_{mobile}]}$$

Equation 2.

Analytes with a low partition coefficient interact strongly with the mobile phase, so taking a shorter time to flow through the stationary phase compared with an analyte with a high *K*. Therefore, analytes are separated based upon their relative affinities for the stationary and mobile phases.

The time between the introduction of an analyte to the system and its elution from the system is termed the retention time (t_R). In chromatography, it is important that analytes are separated sufficiently to collect them in their 'purest' form, minimising interfering effects. An 'efficient' chromatographic system has the capacity to separate a greater number of analytes in a given time period than an 'inefficient' system. The separating power, or chromatographic efficiency of a system is described in terms of theoretical plates. The height equivalent to a theoretical plate is the column length required for the equilibration of analyte between the mobile and stationary phase; the more 'plates' in the system, the more efficient the separation.

Chromatography & sample preparation

Solid phase extraction (SPE) is a selective form of sample fractionation based upon chromatographic principles. High-performance liquid chromatography and other liquid chromatography techniques are optimised to give chromatographically efficient and

finely resolved peaks. SPE is however optimised to provide a coarse separation of, frequently, analyte(s) from matrix components, which is still dependent on the interaction between the stationary phase and the analyte (Figure 4.2).

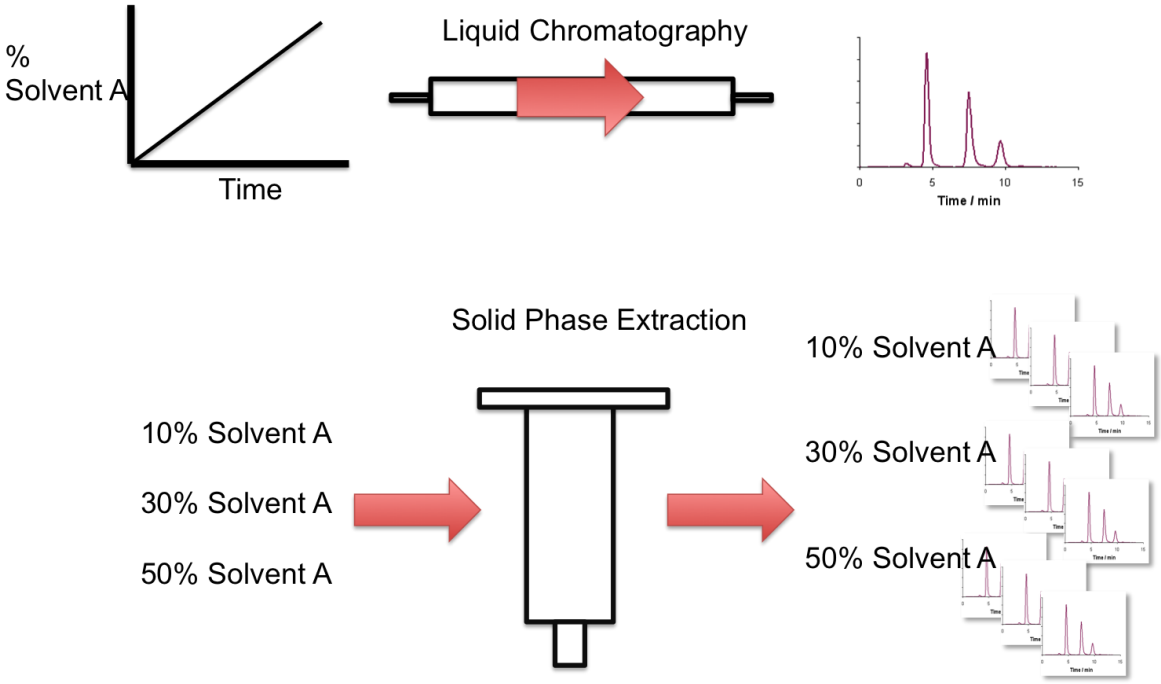

Figure 4.2. Solid phase extraction versus liquid chromatography.

During liquid chromatography, analytes are eluted by a constant flow through the chromatographic medium of solvent the composition of which can be changed over time. This results in the elution of defined analyte peaks from the column. In contrast, analytes are eluted during SPE using discrete batches of differing concentrations of solvent, resulting in each eluent fraction potentially containing more than one analyte.

4.2.2 Overview of mass spectrometry

MS is the primary analytical technique used in the work described in this chapter, therefore a general description of MS and the MS techniques used are included in this introduction. MS is an extensively used analytical method, which in the broadest terms measures the mass of ions and their ionic fragments to gain information about their structure.

A mass spectrometer comprises three main systems: an ion source, a mass analyser and a detector, coupled to a computer for instrument control, data collection and analysis. The ion source is required to produce gas-phase ions from neutral analytes; all mass

analysers use magnetic or electric fields to control and separate ions, therefore an ion source is required to create charged species. The analyte ions are then separated by their mass-to-charge ratio (*m/z)* in the mass analyser and detected at the detector.

The performance of a mass spectrometer is measured based upon five main characteristics: the detectable *m/z* range, scan speed, transmission efficacy, mass accuracy and resolution. The *m/z* range denotes the limits of *m/z* that the MS can measure, whilst the scan speed denotes the rate at which the MS can measure over the *m/z* range (measured in *m/z* units per second).

Transmission efficiency is the ratio of ions reaching the detector versus the number of ions that enter the mass analyser. This measurement includes ion losses in other parts of the MS, such as the process of ion transfer. This is not to be confused with the duty cycle, which denotes the proportion of time which a device or machine is operating usefully. In the context of MS, the duty cycle denotes the percentage of ions of a particular *m/z* that are effectively analysed and detected as a fraction of all the ions introduced into the instrument. The ion transmission efficiency depends upon the characteristics of the whole instrument, whilst the duty cycle is dependent both upon instrument design *and* the mode of operation used. Both duty cycle and transmission efficiency are closely associated with the limit of detection of a mass spectrometer (e.g. if a MS has a duty cycle of 0.1%, only 1/100th of the ions introduced to the MS are successfully detected, lowering the limit of detection of the instrument).

Mass accuracy indicates the accuracy of the *m/z* values reported by the MS: the difference observed between the theoretical *m/z* value of the ion versus the measured *m/z* . Mass accuracy is highly correlated to the resolution of an instrument. Resolution is the ability of an MS to yield distinct *m/z* values for ions with a small *m/z* difference. Two peaks are considered to be resolved if the valley between the two observed peaks is equal to 10% (if an ICR or magnetic sector instrument is used) or 50% (if a TOF or quadrupole instrument is used) of the peak intensity of the weaker peak. As the precision of the *m/z* measurement depends upon the centroid of a peak, an instrument with low resolution (i.e. that is unable to differentiated between peaks of similar *m/z)* will give less accurate results, and *vice versa*.

4.2.2.1 Ion sources

Electrospray ionisation

Electrospray ionisation (ESI) is a 'soft' ionisation technique, developed for MS by J. B. Fenn in 1984 (for which he was awarded a share of the 2002 Chemistry Nobel Prize). ESI was a great advance over previous soft ionisation techniques used in MS due to the efficiency of ionisation, minimal in-source fragmentation, its ability to ionise high molecular weight analytes *via* multiple charging, and the simplicity of coupling to liquid chromatography separation methods.

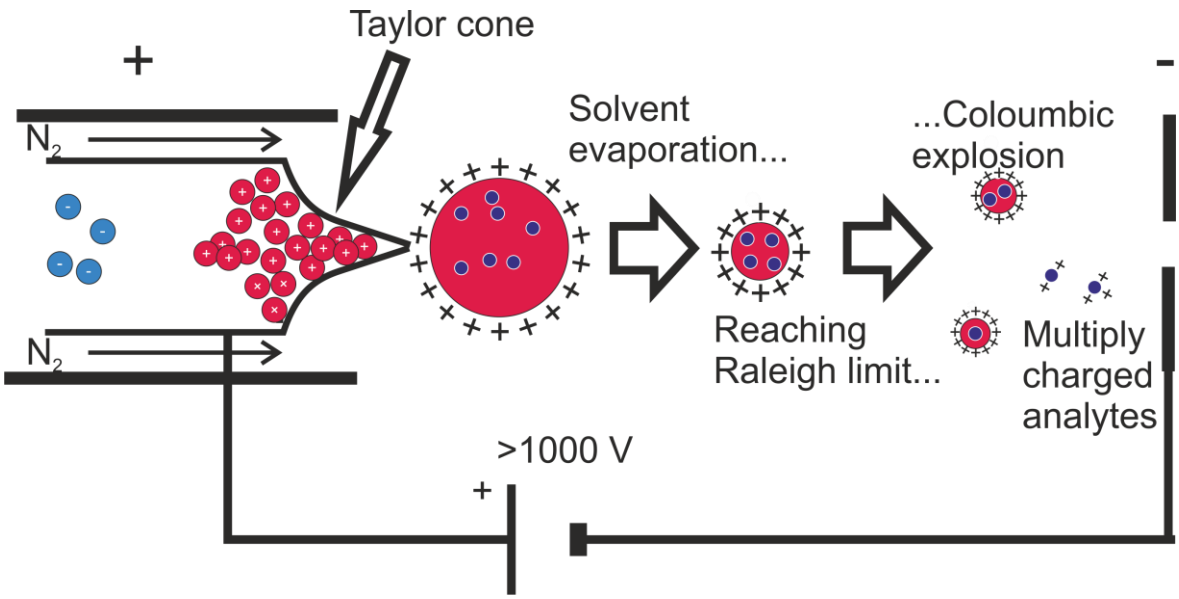

Figure 4.3. Magnified schematic of an ESI source, describing the main stages of gas-phase ion production.

ESI is based upon the principle of electrospray (Figure 4.3). The analyte solution is introduced into the source *via* a thin conductive capillary, which is maintained at a kV-level potential difference with respect to an endplate. The high potential difference leads to the formation of a droplet at the capillary tip due to the equilibrium between the surface tension of the liquid and the electrostatic repulsion of the ions. The ions consequently move to the surface of the liquid. Above a threshold voltage, a Taylor cone is formed at the tip, which emits a constant stream of droplets from the capillary towards the end-plate due to the potential difference between the capillary and the end plate.

The droplets derived from the Taylor cone form the basis of the 'spray'. Inert gas may be sprayed counter to the electrospray direction, facilitating the constant desolvation of the droplet until the analyte charge overcomes the surface tension of the liquid droplet. This

causes the droplet to explode, forming several smaller, more stable droplets. Two theories exist to explain the formation of gas-phase analyte ions from the smallest droplets: the charge residue model (CRM) and the ion evaporation model (IEM). The CRM suggests that the process of ESI droplet formation occurs until a single analyte molecule is present per droplet. As this droplet evaporates, the analyte molecule gains the charge of the droplet surface and moves into the gas phase. The IEM suggests that individual ions are created as analyte ions are 'pushed' from the droplet as the droplet reaches the limit of its charge carrying capacity (the Rayleigh limit).
The ions produced are accelerated through a hole in the end plate, and advance through the source. A pressure differential is created *via* sequential pumping stages until the mass analyser and sufficient vacuum is reached.

MALDI

Matrix-assisted laser desorption/ionisation mass spectrometry (MALDI) was developed principally by Karas and Hillenkamp (1988). MALDI is used as a powerful method for soft ionisation of large, non-volatile and thermally labile compounds and biological molecules including proteins, oligonucleotides and oligosaccharides (reviewed by (Stuler and Meyer, 2004). MALDI differs from other desorption-based methods of ionisation by using a matrix, consisting of highly light-absorbent small organic molecules. The sample to be analysed is dissolved in a concentrated solution of matrix and dried prior to analysis, creating a solid crystalline matrix 'doped' with analyte molecules.
Sample desorption and ionisation is generally conducted under vacuum. The sample is ablated using intense short pulses of laser light. The analyte-doped matrix crystals are excited by the laser light pulses, causing the accumulation of a large amount of energy and rapid heating of the matrix. The rapid local increase in heat causes the sublimation of the matrix into the gas phase, entraining analyte molecules into the 'plume' of sublimated matrix (Figure 4.4)

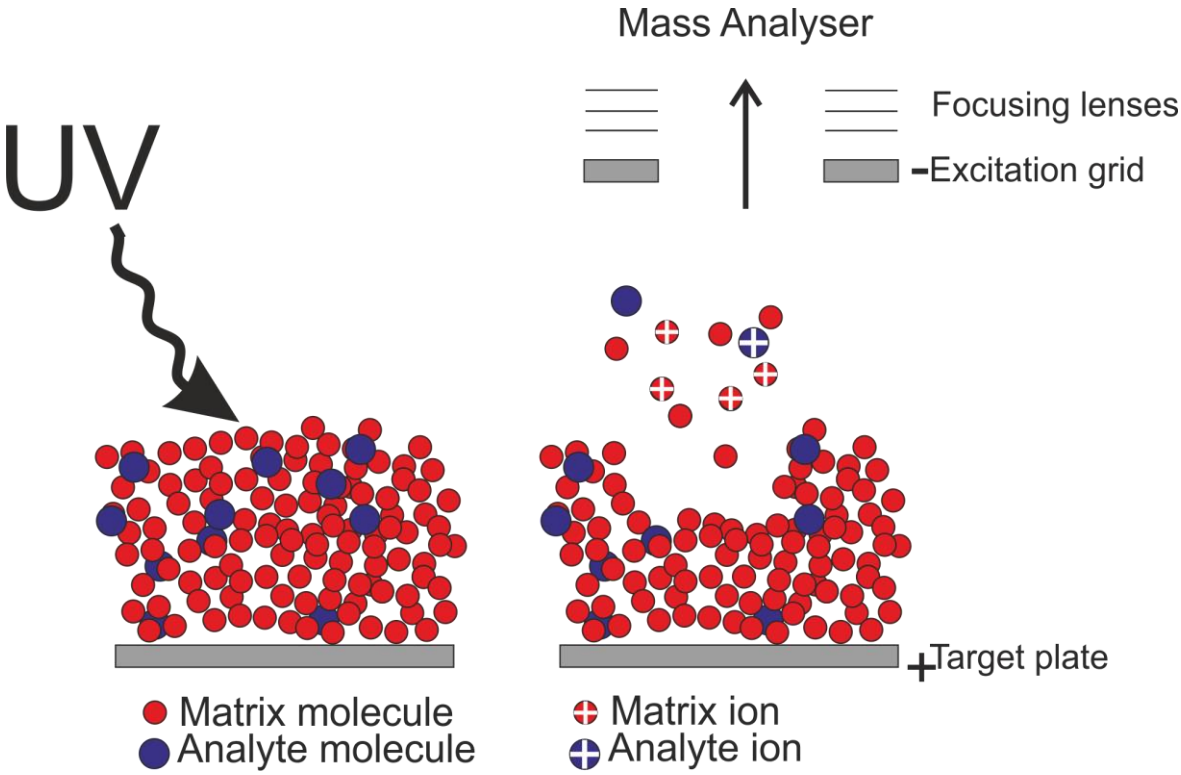

Figure 4.4 The principles of matrix-assisted laser desorption/ ionisation. A pulse of UV laser light excites the co-crystallised matrix and analyte molecules. The sudden increase in energy causes the desorption and ionisation of the co-crystal, forming ions which are attracted towards the negatively charged excitation grid and transported into the mass analyser.

The mechanism of ion formation in MALDI is not fully understood, although several theories have been described, including photoionisation of gas-phase molecules desorption of pre-formed ions and others (Hoffmann and Stroobant, 2013). The most widely accepted mechanisms of ion formation are proton transfer between matrix and analyte ions in the solid phase, prior to desorption into the gas-phase, or proton transfer in the gas phase prior to desolvation of the matrix molecules from the analyte.

MALDI is more sensitive and 'universal' than other laser-based ionisation techniques (Hoffmann and Stroobant, 2013). MALDI does not require the tuning of the laser wavelength to the absorption frequency of each analyte as the matrix molecule is the primary absorber of the laser energy. The suspension of analyte molecules in the matrix crystals minimises sample damage and inhibits the formation of sample clusters. These characteristics allow the analysis of high molecular mass analytes, up to the 1,000 kDa range and beyond (Müller et al., 2010).

The nature of MALDI ionisation produces spectra dominated by singly-charged ions, with few multiply-charged ions and generally very few fragments. MALDI is widely considered to be more tolerant of sample contamination (e.g by salts and buffers) than other ionisation techniques. The primary challenge of MALDI is however a high shot-to-shot variability, with choice of matrix, spotting method and pH of matrix and analyte solutions dramatically altering the reproducibility and ability to detect analytes(Szájli et al., 2008). Local variations in reproducibility and ion intensity can exist within each spot. Different analytes can also be localised in different areas of the spot. Data acquisition is therefore normally conducted at random points across the spot, and the resulting spectra summed to produce an average spectrum. For these reasons, MALDI is typically not defined as a fully quantitative analytical technique.

4.2.2.2 Mass analysers

Quadrupoles

The quadrupole mass analyser is composed of four metal rods with a hyperbolic or circular cross section, held parallel to each other and electrically connected in pairs. The paired rods form electrodes. Ions are injected into one end of the analyser, pass through the inner diameter between the rods, and exit to a detector, or another mass analyser (e.g. in the case of quadrupole-time of flight instruments). A schematic diagram of a quadrupole is shown in Figure 4.5.)

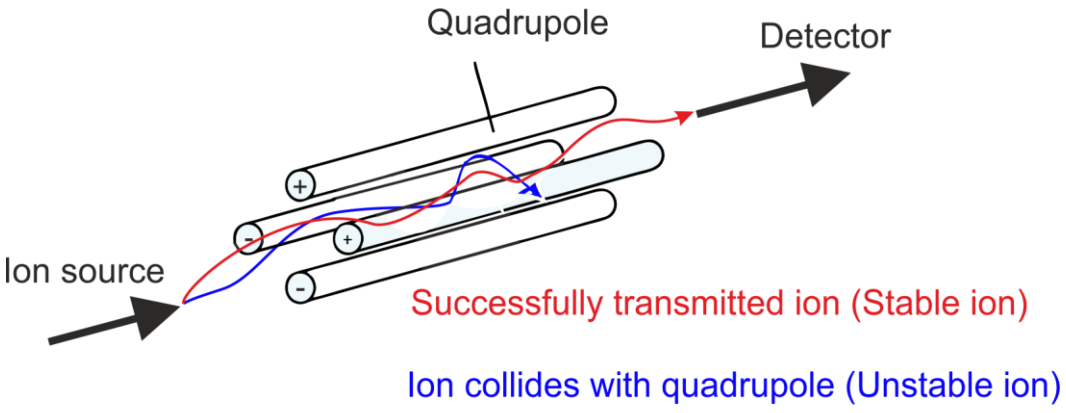

Figure 4.5. Cross-section of a quadrupole mass analyser.

The quadrupole mass analyser transmits ions of a specific *m/z* or a range of *m/z* values. The specificity of *m/z* values is conferred by the electric field induced between the rods of the quadrupole. D.C. and R.F potential differences are applied to the electrode pairs. As

demonstrated by the red and blue traces in Figure 4.5 ions travel along the *z*-axis of the quadrupole because of their injection velocity, and only successfully traverse the quadrupole if their trajectories in the *x* and *y* axes do not exceed the internal radius of the quadrupole. The applied electric field causes the ions to move along the *x* and *y* axes, in a constantly changing manner due to the R.F component of the applied potential difference.

The stability of the ions in the quadrupole is dependent upon the RF and DC voltages, and the *m/z* ratio of the ion. Only ions of a certain *m/z* ratio successfully traverse the quadrupole for a given range of voltages, causing other ions to collide with the electrodes due to their unstable trajectories. The quadrupole thus can act as a mass filter, by selecting voltages that stably transmit ions of a limited *m/z* range, or in a scanning mode, altering the applied voltages to scan across a *m/z* range. Quadrupoles and their derivatives (such as octopoles) are often used as ion guides or collision cells in hybrid mass spectrometers, such as quadrupole-time of flight or FT-ICR instruments.

4.2.2.3 Time-of-flight mass analysers

Time-of-flight (TOF) mass analysers differentiate *m/z* values of ions based upon the time taken for ions to travel a fixed distance along a flight tube, free of an electric or magnetic field. TOF mass analysers consist of an acceleration region and a field free region, with ions reaching a detector at the far end of the field-free region. Ions are accelerated to a constant velocity by the acceleration region, conferring the same kinetic energy on all ions, independent of *m/z.* The time taken for the ion to travel the length of the field-free region is proportional to the square root of the *m/z* value of the ion, multiplied by a constant dependent on the length of the field-free region (L^2), the velocity of the ion (V) (equation 3).

$$t^2 = \frac{m}{z}\left(\frac{L^2}{2eV}\right)$$

Equation 3

The *m/z* of each ion can therefore be directly related to the time taken to transit the flight tube, allowing the flight tube to act as a mass analyser. The theoretical basis of TOF analysis is simple, although technical limitations exist in practice. Despite the acceleration before the field-free region, small differences in kinetic energy and spatial distribution of the ions exist, causing the ions to reach the detector at slightly different times, introducing flight time variability to ions of the same *m/z* and decreasing the resolution of the instrument. Modifications of the original TOF design have evolved to address these issues and provide better resolution and sensitivity, and to enable the use of continuous ion sources with TOF instruments.

One such modification is the orthogonal acceleration time-of-flight (oa-TOF) instrument. The oa-TOF-MS differs from a 'pure' TOF instrument by directing the ion stream into the instrument at an angle to the incoming ion path. The ions are focused into an orthogonal accelerator, placed before the TOF tube (Figure 4.6, right). As ions fill the accelerator, they maintain their original direction of movement orthogonal to the flight tube. A voltage pulse is applied to the back plate and sequentially to each of the grids, causing the ions to be accelerated towards the flight tube. Once the ions leave the orthogonal accelerator, the voltages applied to the plate and grids returns to zero, allowing more ions to fill the accelerator. This cycle is repeated to continuously sample ions from the continuous ion source. The formation of ion 'packets', with minimal dispersion of ions in the direction of the flight tube is favourable for increased mass resolution, accuracy and stability of calibration. However, due to the orthogonal acceleration process, the duty cycle of oa-TOF instruments is lower than that of a true TOF instrument. The flight tube distance can also be increased through the use of a reflectron, an 'ion mirror' which reverses the direction of ion travel, increasing the length of the free field area in comparison with a simple linear TOF tube.

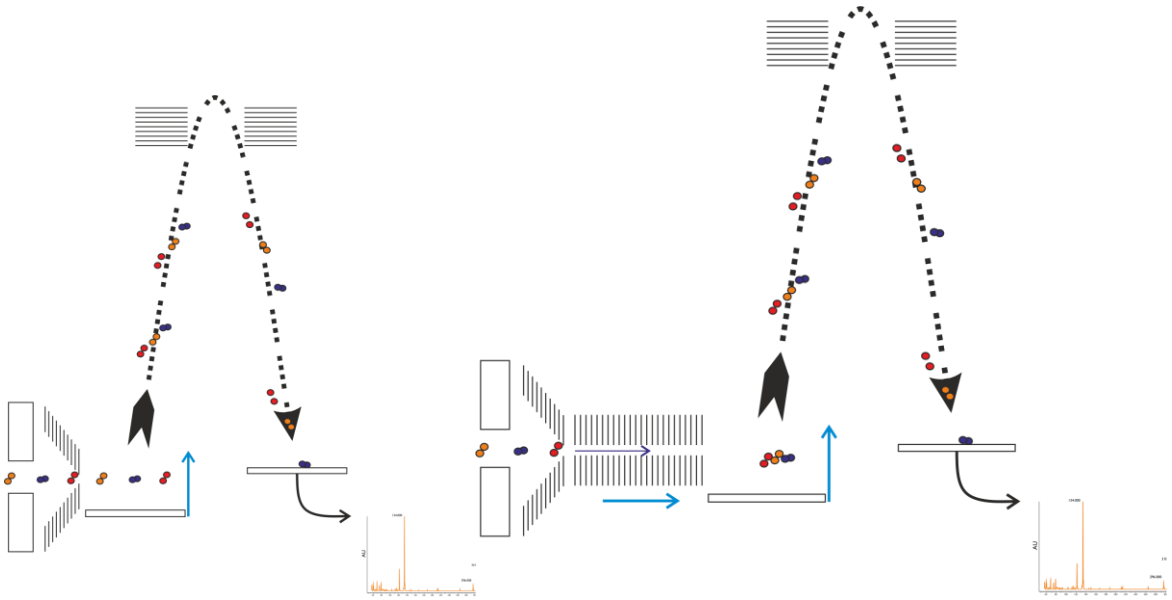

Figure 4.6. Comparison of TOF and oa-TOF instruments.

Left; TOF-MS. Ions are introduced to the acceleration region and accelerated into the field-free region (direction of blue arrow). Right; oaTOF-MS. Ions are accelerated by the orthogonal accelerator into the acceleration region prior to the 'packet' of ions being accelerated into the flight tube.

4.2.2.4 Fourier-transform ion cyclotron resonance mass spectrometry

Ion cyclotron resonance MS (ICR-MS) uses the motion of trapped ions in order to create a mass spectrum with very high mass accuracy and resolution. ICR-MS relies on the behaviour of ions in a magnetic field. Following the Lorentz force law, moving ions in a magnetic field are subjected to a force perpendicular to the direction of velocity, causing the ion to travel in a curved trajectory. If the original velocity of the ion is low, and the magnetic field is intense, the ion will travel in a stable circular trajectory due to the balance between centripetal and centrifugal forces acting upon the ion. The angular velocity and frequency of the ions' circular trajectory is determined by the ratio of mass to charge, if the magnetic field is stable. (Amster, 1996)

In practice, FT-ICR-MS involves trapping a 'packet' of ions within the ICR cell (also known as a Penning trap) formed of three sets of plates: trapping, excitation and detector plates, shown in Figure 4.7. A strong magnetic field is produced using a superconducting

magnet around the trap. A small voltage is applied across the trapping plates in order to prevent the ions escaping the trap along the magnetic field axis.

The FT-ICR method depends upon the excitation of the ion 'packet' introduced to the cell with a short, wide frequency scan transmitted *via* the excitation plates. This signal induces the ions to come into phase with one another, and pushes the trajectory of the ions close to the detector plates. The movement of an ion past the detector plate induces an AC image current which enables the calculation of *m/z* from the frequency of the ion movement (the ion's cyclotron frequency). Longer measurements of the image current allow for better resolution of the mass spectra. The amplitude of the image current reduces over time due to collisions between the ions and neutral molecules within the trap, so that the trap is maintained at an ultra-low vacuum to maximise the coherence of the signal(Amster, 1996).

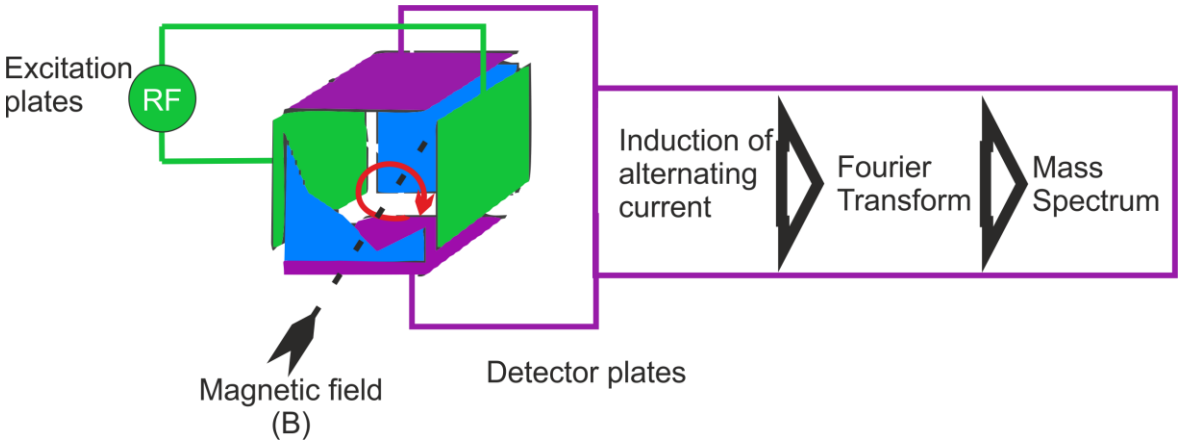

Figure 4.7 Schematic of an ion cyclotron resonance 'cell'.

Trapping plates,: blue, detector plates: purple, excitation plates: green.

The presence of many ions with differing *m/z* (and therefore different cyclotron frequencies) produces a highly complex composite image current, consisting of the multiple image current frequencies super-imposed upon one another. Fourier transform analysis of the composite image current allows the individual frequencies and intensities to be dissected, and following comparison with a calibration standard, converted to a *m/z to* intensity relationship.

FT-ICR-MS is a technique with high resolution and mass accuracy (>~1 ppm), however with some limitations. The number of ions in each analysed 'packet' is limited to ~10^6 due to ion repulsion, limiting the dynamic range.

4.2.3 Mass detection

After the mass analyser separates the ions, they must be sensed and the information transformed into a useful format. Mass spectrometry detectors do this by using the charge of the ions to generate a current proportional to the ion abundance. Two primary methods are used to detect ions: the 'direct' measurement of current produced as ions hit a surface and are neutralised (e.g Faraday cups or electron multiplier detectors) or the measurement of currents induced by ion movement in an ion trap (i.e. FT-ICR detection).

The primary difficulty in detecting ions leaving a mass analyser is the extremely small currents involved. The current produced by 100 singly-protonated ions per second corresponds to only $1.6x10^{-17}$ amps. Consequently, amplification of the signal is required in order to detect the ions.

The most common 'direct' detection method used is the electron multiplier. This method utilises a series of high-voltage electrodes (known as conversion dynodes) held at the opposite charge to the ions being measured. Analyte ions are accelerated to a high velocity and hit the charged electrode, causing the emission of secondary particles including positive and negative ions, electrons and neutral particles. As the secondary particles hit the second electrode, electrons are released. This process occurs repeatedly from electrode to electrode causing a cascade effect and the amplification of the current.

This process can occur at physically separate electrodes or the electrodes are formed as a continuous tube or cone. The sensitivity and dynamic range of continuous electron multipliers has been improved by the multiplexing of miniaturised electron multiplier tubes or spheres in parallel, increasing the amplification gain and reducing response time to ions.

FT-ICR-MS is unique in that the mass analyser also acts as the detector. The FT-ICR instrument is built around a Penning trap, constructed from flat electrodes contained within a strong magnetic field. Ions that are injected into the trap will travel in a consistent circular trajectory, with ions of a particular mass circulating in tight 'packets' within the wider circular trajectory.

The frequency that an ion travels at in the FT-ICR cell is equal to

$$v = 2\pi \frac{qB}{m}$$

Equation 4

B is the strength of the magnetic field, *q* is the charge of the ion, and *m* is the mass of the ion. Each separate ion therefore has its own specific cyclotron frequency. The FT-ICR method is based upon exciting all the ions within the trap with a pulse of AC potential scanning a wide frequency range. Excitation of all ions at their own specific frequency (using a short, broad-spectrum voltage pulse) with the same energy, will increase the radius of their orbit equally, and all the ion packets will therefore pass within a close distance to the detection plate within the trap, an effect independent of the *m/z* ratio, and therefore the frequency, of the ions.

The travel of charged ions past the detection plate leads to the induction of a complex image current, reflecting the passage of each ion or ion packet past the detection plate. This creates a complex frequency signal, the intensity of which is the sum of many frequencies superimposed over one another, each with their own intensity. This complex signal can be de-convoluted to find the individual frequencies and their intensities (and hence the *m/z* and intensity of each ion), using a mathematical technique termed a Fourier transform.

4.3 Aims and hypothesis

The aim of the work described in this chapter was to assess the feasibility of mass spectrometric detection of AMP release by NHU cell cultures. The primary experimental objective of this chapter was to develop a sufficiently sensitive analysis for the detection of AMPs in cell culture medium from flagellin-treated NHU cells.

AMPs are expressed as propeptides, which are cleaved as part of the mechanism of extracellular transport. Differences in cleavage patterns can confer differing characteristics on the active peptides. Existing mechanisms of detection rely on transcript-level detection or the use of antibodies, which cannot differentiate between the propeptide and cleaved 'active' forms of AMPs. It was hypothesised that a MS-based analysis would allow for the differentiation of propeptide and active AMPs.

4.4 Experimental approach

Targeted analyses of AMP transcript expression (described in chapter 3) suggested that NHU cells are induced to express BD2 and BD4 in response to flagellin and UPEC stimuli. Due to their potential role in the urothelial response to uropathogens, BD2 and BD4 (Table 4.1) were chosen as candidate AMPs for method development and proof of concept analyses. Both peptides were commercially available as purified recombinant products, and did not possess any known sites for post-translational modifications (e.g. glycosylation) removing a potential source of unpredictable changes in mass.

Initial proof-of-concept analyses were conducted using recombinant peptides, dissolved in MS-compatible buffers. A comparison of responses using known amounts of authentic standards of the two analytes was conducted MALDI and ESI sources on oaTOF, TOF/TOF and FT-ICR instruments in order to assess the most appropriate technique for detection of BD2 and BD4 in the biological system. Methods for separation of AMPs from cell culture media were also investigated using recombinant BD2 as a model peptide. SPE based techniques were investigated, in both cartridge and ZipTip™ formats. The ability of both formats to isolate BD2 from cell culture medium and the efficiency of isolation was tested.

Peptide	Amino acid sequence	Calculated mass (average/monoisotopic)
BD2	GIGDPVTCLK SGAICHPVFC PRRYKQIGTC GLPGTKCCKK P	4334.235/4331.171
BD4	EFELDRICGY GTARCRKKCR SQEYRIGRCP NTYACCLRKW DESLLNRTKP	5988.909/5984.906

Table 4.1. Amino acid sequences of analyte peptides.

4.5 Results

4.5.1 Comparison of MALDI-TOF, MALDI-FT-ICR and ESI-oaTOF methods for mass spectrometric detection of β-defensins

Previous reports of a*via*n defensin analysis suggested that defensin peptides were ionised well by MALDI (Kannan et al., 2013, 2009). Therefore, a proof-of-concept analysis of BD2 was undertaken using a Bruker Daltonics ultraflex III MALDI-TOF/TOF MS. 1 µL (10 nmol) of recombinant BD2 solution prepared in 50% (v/v) aqueous acetonitrile was deposited on a ground steel MALDI target plate, pre-spotted with 1 µL CHCA matrix (10 mg/mL) prepared in 1:1 acetonitrile/water. The sample was analysed in positive ionisation mode with the reflectron enabled.

The MALDI-TOF/TOF spectrum of pure BD2 is shown in Figure 4.8. Seven isotopic clusters of varying intensity were observed. The most intense cluster (monoisotopic peak *m/z* 4326.026) differed from the calculated monoisotopic mass of a singly-protonated BD2 peptide (*m/z* 4332.1) by 6 atomic mass units. As discussed in chapter 3, β-defensins exhibit conserved intra-peptide disulphide bridging between the six cysteine residues present in the molecule, therefore this signal can be assigned to the fully disulfide bridged species. The second most intense isotopic cluster (monoisotopic peak *m/z* 2614.081) unusually in MALDI, corresponded to the $(M+2H)^{2+}$ ion of the fully-bridged BD2 peptide.

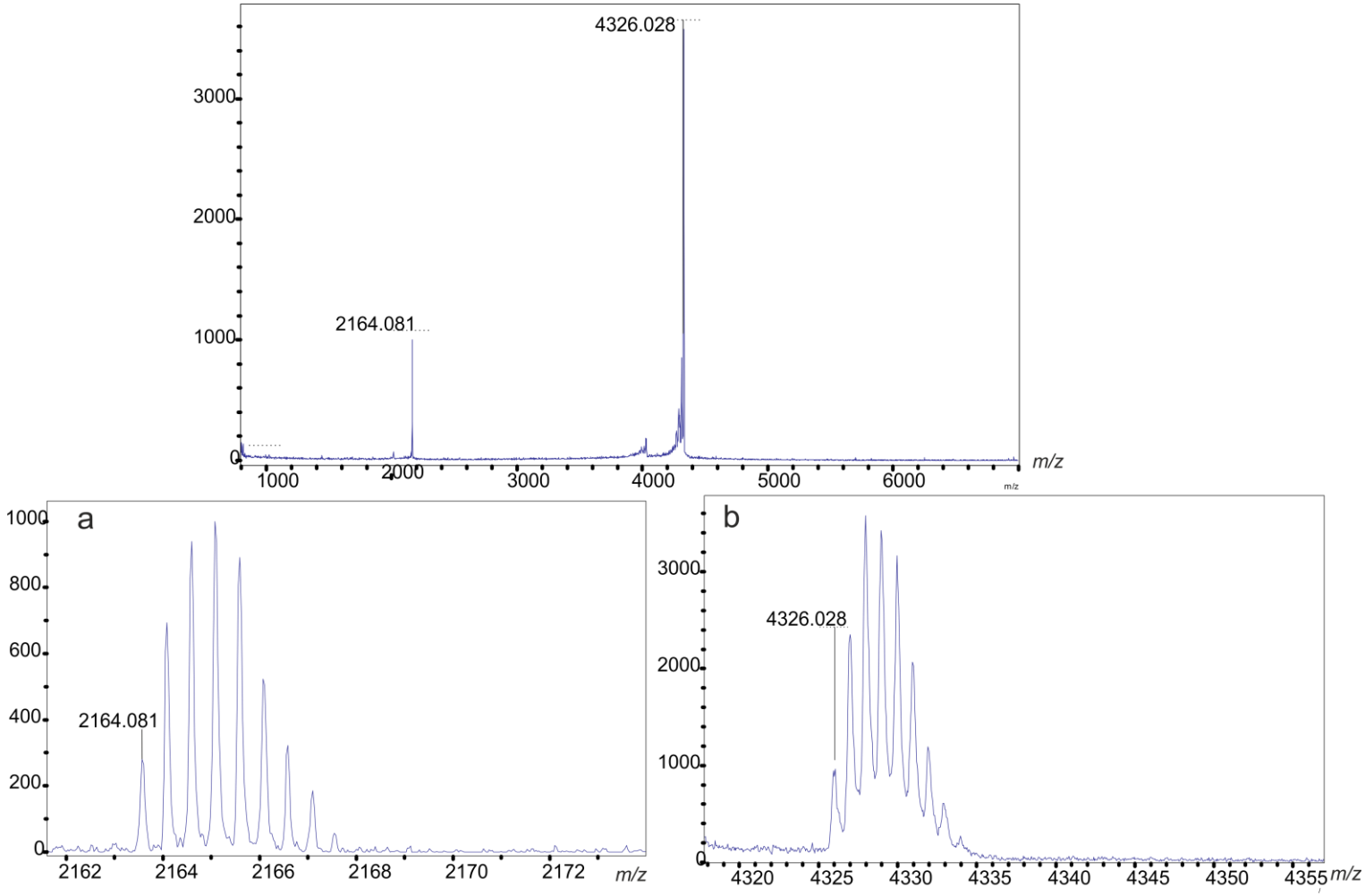

Figure 4.8. MALDI-TOF-TOF spectrum of pure recombinant BD2. A) Expanded image of spectrum corresponding to $[M+2H]^{2+}$ BD2 ion. B) Expanded image of spectrum corresponding to $[M+1H]^{1+}$ BD2 ion. X axis: m/z, Y axis: intensity.

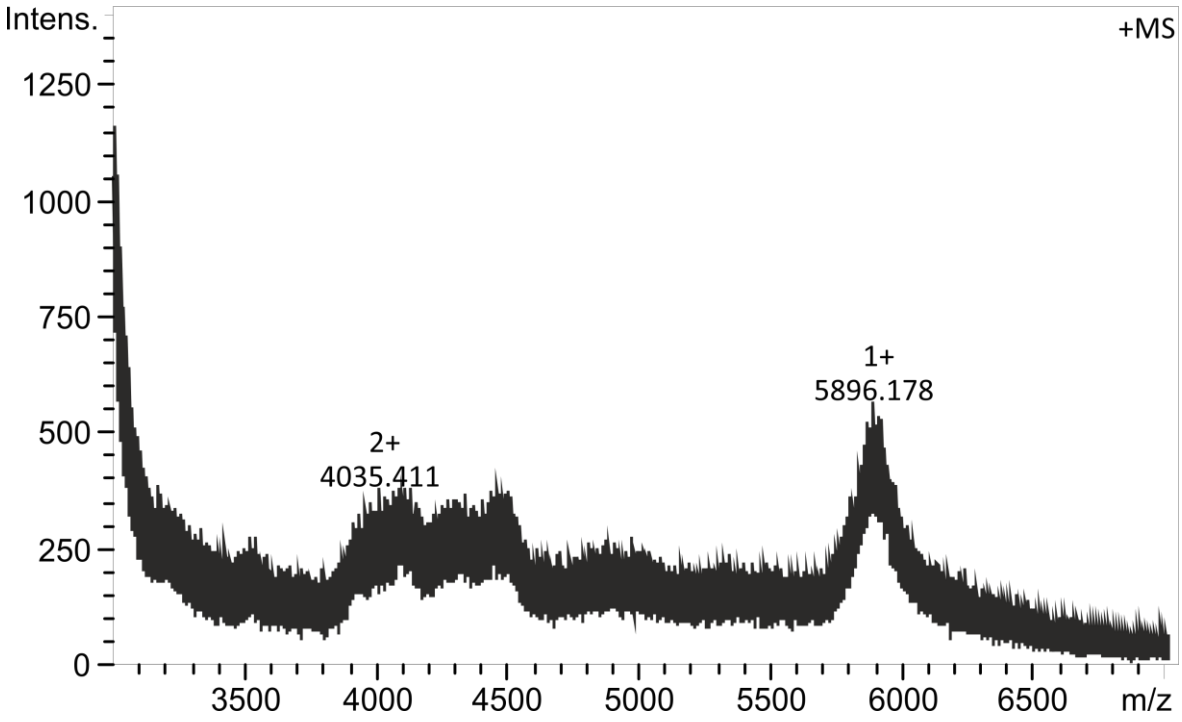

Figure 4.9 MALDI-TOF spectrum of purified BD4.

The MALDI-TOF spectrum of pure BD4 analysed using the same approach is shown in Figure 4.9. Several broad ill-defined peaks were observed, the most intense of which corresponded with the approximate calculated average *m/z* of the $(M+H)^{1+}$ ion of BD4 (nominal m/z 5896). The spectrum obtained from analysis of the BD4 sample with the reflectron disabled is shown in Figure 4.10. A single poorly resolved peak is observed at *m/z* 5981.4 (c.f. the calculated average mass of ~5988).

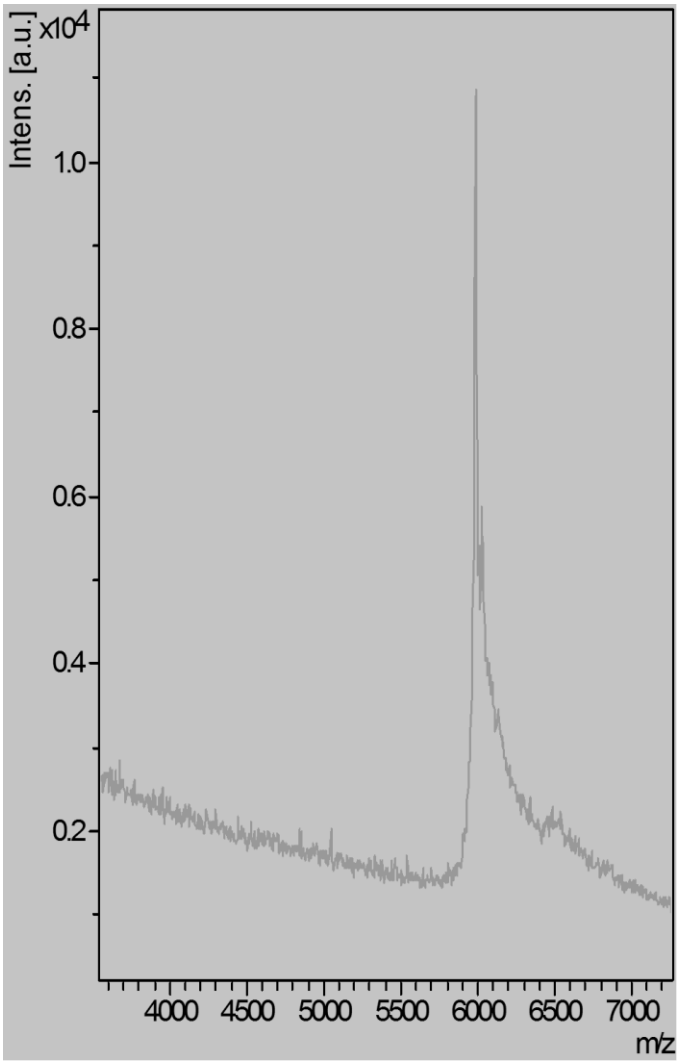

Figure 4.10 MALDI-TOF-TOF spectrum of pure BD_4 obtained with reflectron disabled.

4.5.2 Direct injection (DI)-ESI-oaTOF analysis of BD2 and BD4

The suitability of DI-ESI-oaTOF-MS to detect BD2 and BD4 was assessed. Recombinant BD2 and BD4 standard solutions were prepared in 50% aqueous acetonitrile supplemented with 0.1% formic acid. Each solution was prepared as such that the desired amount of recombinant peptide was injected in a 5 µL volume. Figure 4.11a shows the mass spectrum from direct injection of 1 pmol of recombinant BD2. Isotopic clusters corresponding to the $[M+4H]^{4+}$ (nominal mass *m/z* 866 , *Figure 4.11b)*) and $[M+5H]^{5+}$ (nominal mass *m/z* 722, *Figure 4.11a*) ions were observed. Several additional peaks were observed, including those of nominal mass *m/z* 1222 and *m/z* 1521. These corresponded to compounds included in the Bruker Peptide Calibrant II mix used to calibrate the instrument prior to each analytical run, and are likely present due to sample crossover.

Analysis of BD4 prepared in the same manner was unsuccessful, despite attempts to identify ionisation and MS conditions that would allow detection of this peptide

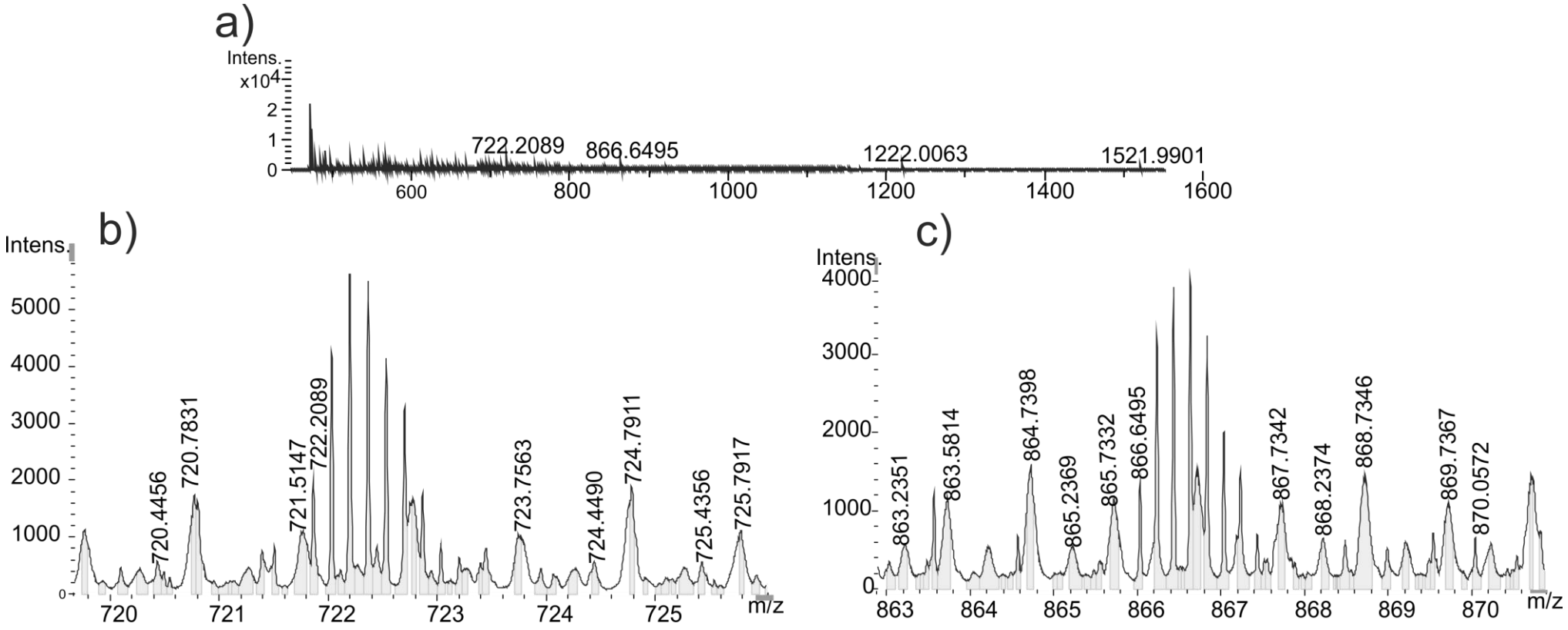

Figure 4.11 DI-ESI-oaTOF mass spectra of 1 pmol of BD2. a) Mass spectrum. b) Expanded of $(M+5H)^{5+}$ ion cluster (monoisotopic mass m/z *722.2089) c) expanded of $(M+4H)^{4+}$ ion cluster (monoisotopic mass* m/z *866.6495).*

4.5.3 FT-ICR analysis of BD2 and BD4

The instrument used for all of the experiments reported below was a Bruker Daltonics solariX XR FTMS 9.4T, operated using its MALDI ion source. Experiments reported in this section used a published method developed for high resolution peptidomic profiling of human serum focused on 'high-mass' peptides (3.5 kDa to 10 kDa) (Nicolardi et al., 2014), modified to increase the number of laser shots used to 1000 and the averaged number of spectra collected to 20, in order to increase the number of ions collected.

The MALDI-FT-ICR mass spectra of purified recombinant human BD2 and BD4 are shown in Figure 4.12 and 4.13. 1 µL (10 nmol) of recombinant BD2 or BD4, prepared in 50% (v/v) aqueous acetonitrile was deposited on a ground steel MALDI target plate, pre-spotted with 1 µL CHCA matrix (10 mg/mL) prepared in 1:1 acetonitrile/water. The sample was analysed in positive ionisation mode.

The spectrum of recombinant BD2 is shown in Figure 4.12. Several isotopic clusters were observed. The most intense isotopic cluster corresponded to the $[M+1H]^{1+}$ BD2 ion (*m/z* 4326.21092). Multiple CHCA-BD2 adducts were observed,, including $[M+CHCA+H]^{1+}$, $M+2CHCA+H]^{1+}$ (*m/z 4515.28 and 4704.38). The* $M+2H]^{2+}$ and $M+3H]^{3+}$ ions were also observed (m/z 2164.5636 and 1442.8599).

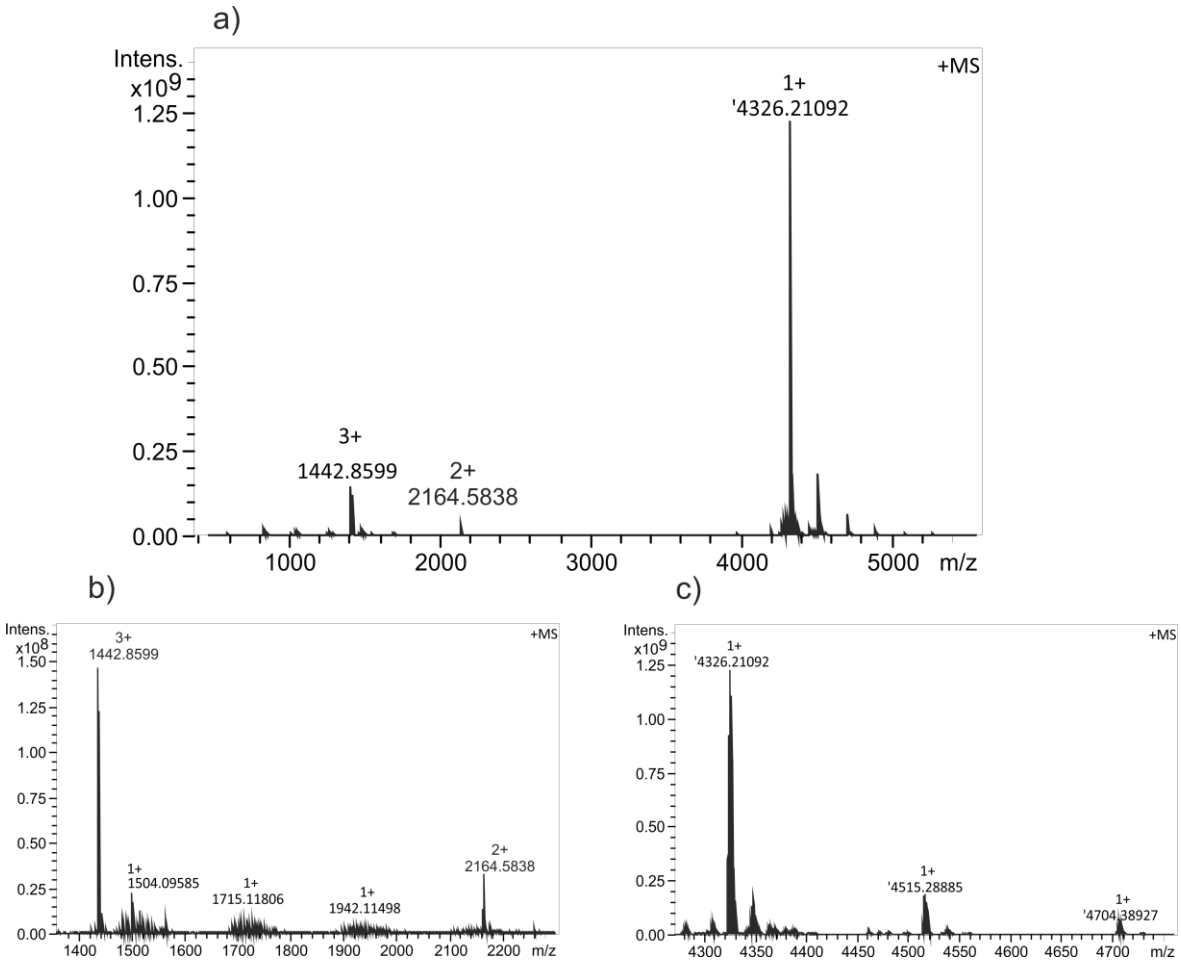

Figure 4.12 MALDI-FT-ICR-MS spectrum of recombinant BD2.

A) Whole spectrum. B) Expanded spectrum of m/z 1400-2200 C) Expanded spectrum of m/z 4300-4800

The mass spectrum of pure BD4 is shown in Figure 4.13 4.14 and 4.15. Several isotopic clusters are observed. The most intense cluster (*m/z* = 5980.309) differed to the calculated monoisotopic *m/z* of a singly-protonated BD4 molecule by 6 u. This suggests, as with BD2, that the recombinant molecule retained all three disulfide bonds. Multiple CHCA matrix adducts were also observed, including $[M+CHCA+H]^{1+}$, $M+2CHCA+H]^{1+}$, $[M+3CHCA+H]^{1+}$ and $[M+4CHCA+H]^{1+}$ (m/z 6169.355, 6358.36, 6547.459). The second most intense ion cluster (*m/z* 2991.049) corresponds to the $[M+3H]^{3+}$ ion of BD4 with full disulfide bonding. The $[M+2H]^{2+}$ ion of BD4 was also observed (*m/z* 2164.58) Several other low-intensity ion clusters were observed between *m/z* 1000-2000 that were non-specific and could not be assigned to BD4-derived species.

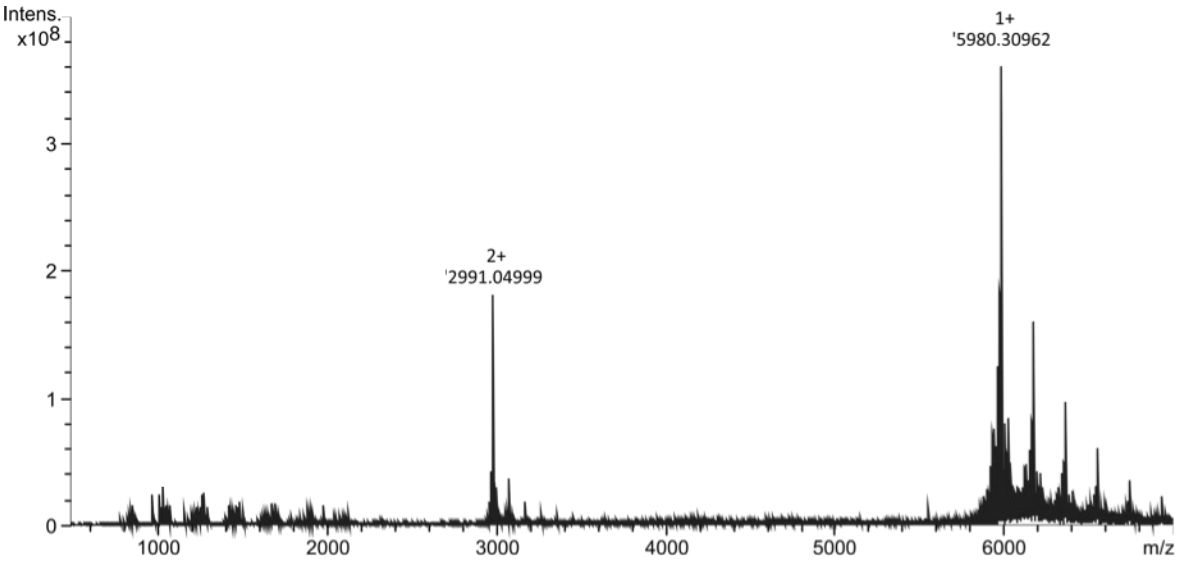

Figure 4.13 MALDI-FTICR spectra of 10 nmol BD_4 peptide.

The two ion clusters corresponding to the $(M+1H)^{1+}$ and $(M+2H)^{2+}$ ions of BD_4 are labelled A and B respectively.

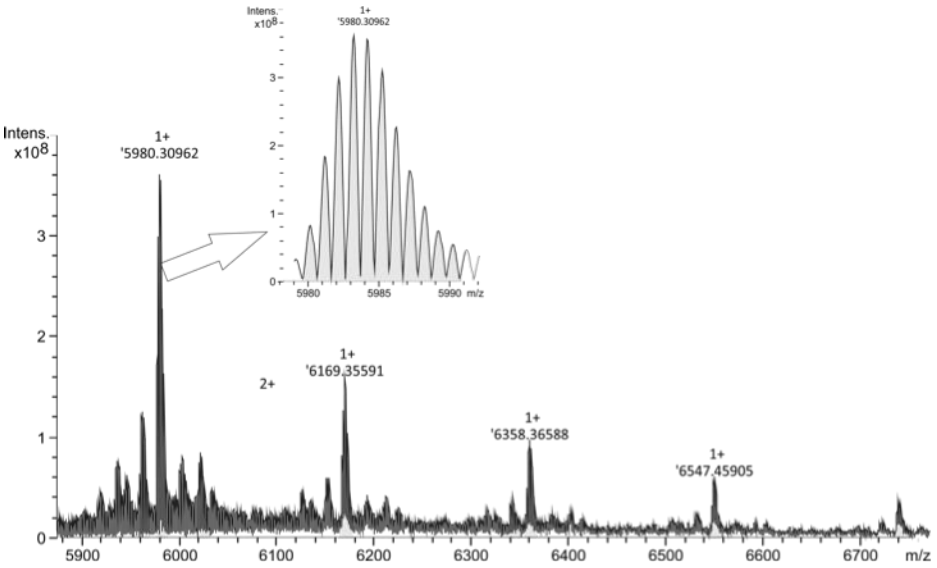

Figure 4.14 Expanded MALDI-FTICR spectra of the $(M+1H)^{1+}$ ion of BD_4 and associated CHCA adducts.

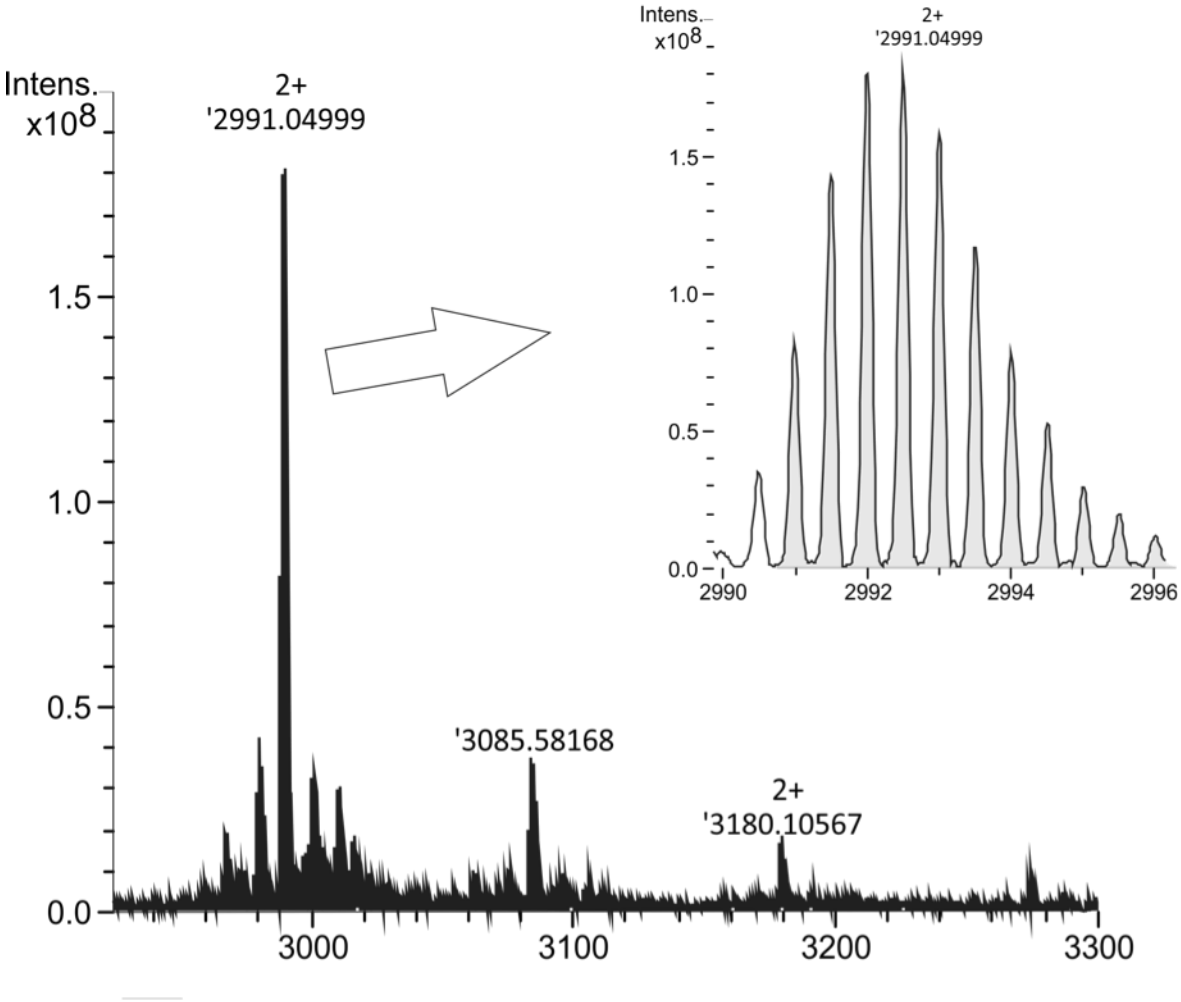

Figure 4.15 Expanded MALDI-FTICR spectra of the $(M+2H)^{2+}$ ion of BD4 and associated CHCA adducts.

4.5.3.1Effect of MALDI matrix choice upon AMP detection

Several matrices have been reported for the MALDI analysis of peptides, including 2,5-dihydroxybenzoic acid (DHB), α-cyano-4-hydroxycinnamic acid (CHCA) (Zhang et al., 2010), nicotinic acid (NA) (Karas and Hillenkamp, 1988) and succinic acid (SA)(Strupat et al., 1997). CHCA is the most common matrix used for the analysis of peptides, and is the standard matrix used for peptide analysis in reported in the previous experiments, however successful analyses of peptides has been reported with NA and SA (Zhang et al., 2010), and AMPs have been successfully analysed using DHB as the matrix (Kannan et al., 2009) with excellent reproducibility and sensitivity.

10 nmol of BD2 or BD4 were prepared in solution in 50% aqueous (v/v) acetonitrile and spotted upon a ground steel MALDI target plate pre-spotted with 10mg/mL CHCA, DHB, nicotinic acid or succininic acid, prepared in 1:1 acetonitrile: water (Figure 4.16 and 4.17). Samples were analysed in positive ionisation mode. The isotopic cluster corresponding

to the doubly-protonated $(M+2H)^{2+}$ (*m/z* 2991.49217 or 2163.620) ion was observed for 10 nM concentrations of BD4 and BD2 prepared with CHCA matrix. No singly-charged peak was observed for BD2 or BD4 samples prepared with CHCA. No signal was observed above baseline for samples of BD2 or BD4 prepared with the other matrices assessed.

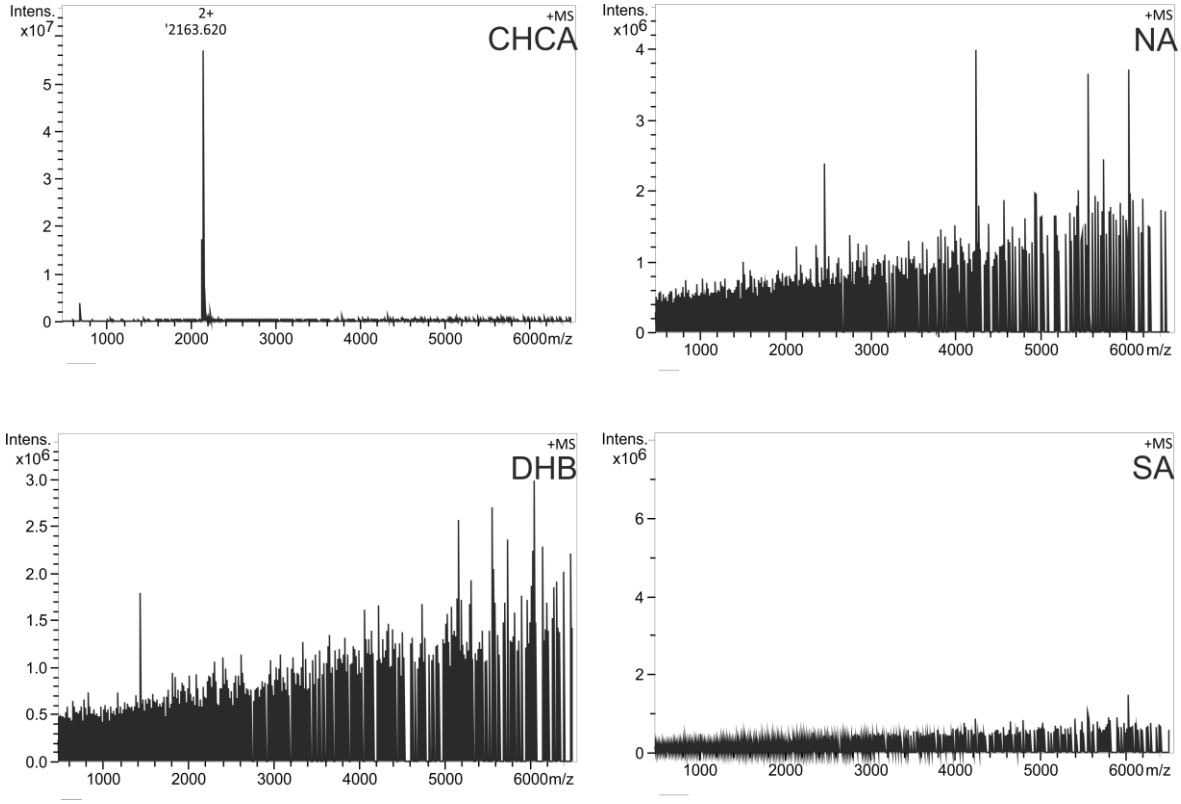

Figure 4.16. Comparison of alternate MALDI matrices to optimise detection of BD2.

CHCA: α-cyano-4-hydroxycinnamic acid; DHB: 2,5-dihydroxybenzoic acid; NA: nicotinic acid; SA: succinic acid.

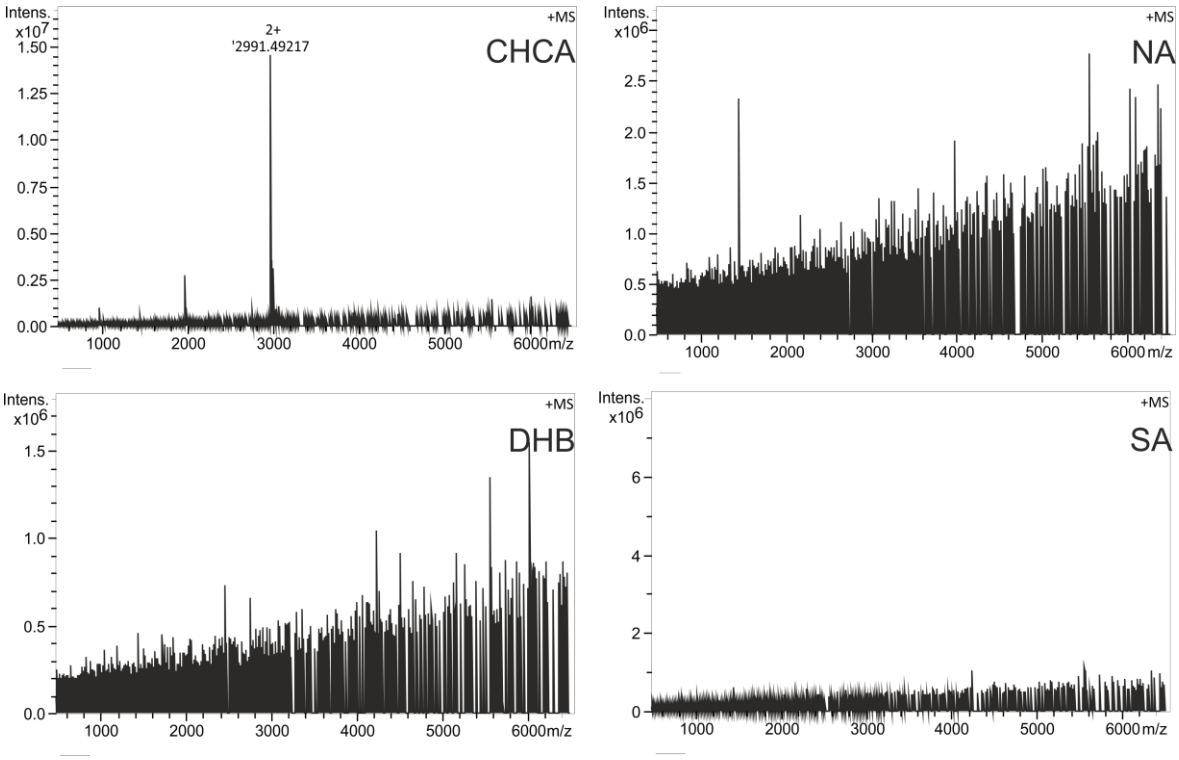

Figure 4.17. Comparison of alternate MALDI matrices to optimise detection of BD4.

CHCA: α-cyano-4-hydroxycinnamic acid; DHB: 2,5-dihydroxybenzoic acid; NA: nicotinic acid; SA: succinic acid.

4.5.3.2 Limit of detection

Recombinant BD2 standard in 50% (v/v) aqueous acetonitrile supplemented with 0.1% (v/v) formic acid was analysed by MALDI-FTICR-MS at a range of amounts, corresponding to 10, 1, 0.1 or 0.001 pmol per MALDI spot. Samples were spotted in triplicate. The intensity of the most intense peak from the isotopic cluster corresponding to the singly-charged ($[M+1H]^{1+}$) species was derived from the mass spectrum obtained from each spot, and the $\log_{10}$ mean intensity of these signals calculated and plotted versus the amount of BD2 per spot, as shown in Figure 4.18. BD2 was clearly and reproducibly detected at levels of 10 to 0.01 pmol per spot. No BD2 ions were detected following analysis of the 0.001 pmol spot, suggesting that the limit of detection of the FT-ICR-MS method lies between 0.01 and 0.001 pmol.

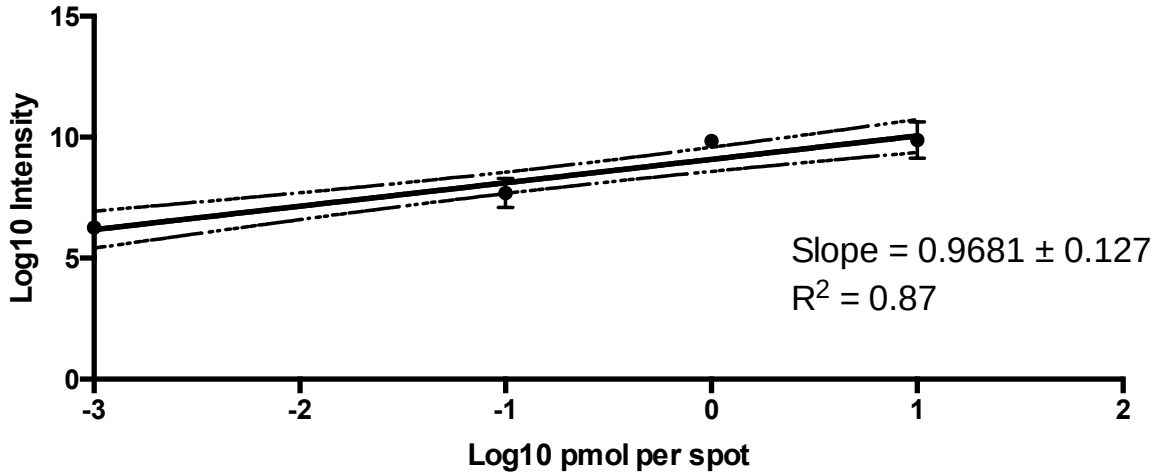

Figure 4.18 Linear regression analysis of BD2 standard curve.

Each point represents log_{10} mean intensity values from three individual MALDI spots (+/- SD). The dashed lines represents the 95% confidence interval of the linear regression line (solid line).

The limits of detection (LoD) and quantitation (LoQ) can also be assessed based upon the standard deviation of the response and slope of the standard curve, using the below equations.

$$LoD = \frac{3.3\sigma}{S}$$

Equation 5

$$LoQ = \frac{10\sigma}{S}$$

Equation 6

Where σ equals the standard deviation of the response, which can be derived from the residual standard deviation of a regression line (Sy.x). S is the slope of the standard curve. The methods used by the GraphPad Prism software package to calculate the residual standard deviation of the regression are not compatible with log-transformed data, therefore the calculation of LOD and LOQ was undertaken following linear regression of the raw dataset (Slope: $1.311x10^{21}$, $R^2 = 0.83$, $Sy.x = 3.57x10^9$). The calculated LOD and LOQ for the MALDI-FT-ICR method were 9.9 pmol and 27.2 pmol per spot respectively.

4.5.4 Detection of spiked and endogenous AMPs from cell culture medium

4.5.4.1 Solid phase extraction of spiked AMPs

Cell culture medium contains physiological levels of salts and other MS-incompatible contaminants. Solid phase extraction is a commonly used method to extract analytes from complex matrices based upon their interactions with the stationary phase of the extraction cartridge. Increasing the amount of sample preparation undertaken can result in sample loss, although SPE fractionation can concentrate the analyte as well as removing potentially interfering components of the matrix, improving the efficiency of analysis.

An initial 'proof of concept' experiment was conducted using Phenomenex C18 SPE columns (1 mL capacity, 100 mg stationary phase). Cartridges were preconditioned prior to use following the manufactures instructions. Conditioned KSFMc was spiked with 1 pmol of recombinant BD2 per mL of medium, and 1 mL of medium loaded onto the cartridge. Following sample loading, bound material was sequentially eluted with 0.5 mL of increasing concentrations of aqueous acetonitrile. 5 µL of each sample was analysed *via* direct injection upon the maXis oa-TOF instrument.

BD2 was detected in 30%, 50% and 70% acetonitrile elutions from spiked KSFMc samples, and was not detected in the unspiked controls (a representative spectrum is shown in Figure 4.19 and 4.20). The $[M+4H]^{4+}$, $[M+5H]^{5+}$ and $[M+6H]^{6+}$ BD2 ions were detected (highlighted in grey in Figure 4.20 and 4.21). A range of other multiply charged ion clusters was observed in both spiked and unspiked samples, with isotopic distributions which suggested the parent ions were peptides. Manual analysis suggested that none of the peptides detected corresponded with the likely masses of AMPs shortlisted in chapter 3, and similar peaks were present in both spiked and unspiked samples. Further analysis is on-going.

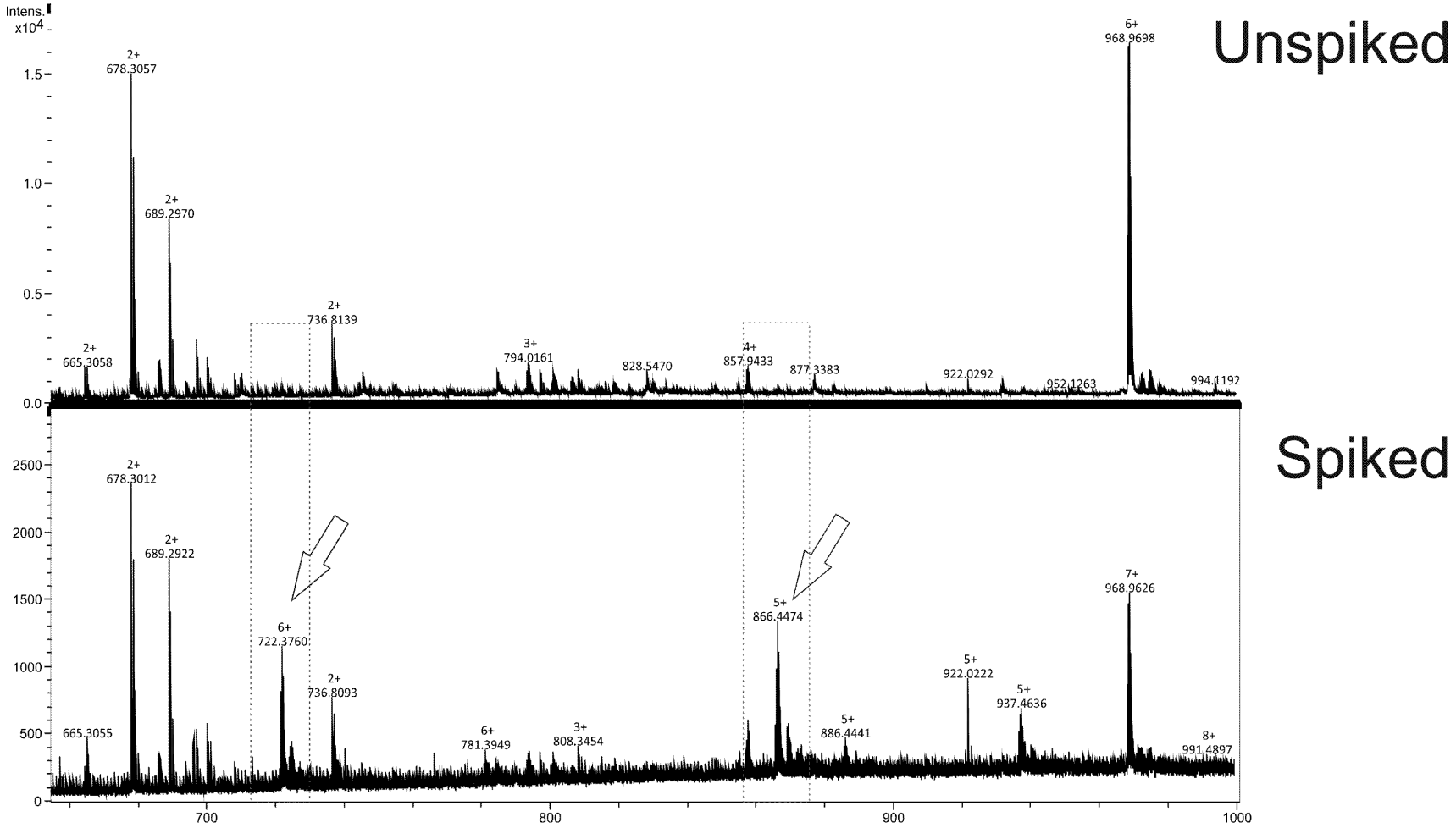

Figure 4.19 Comparison of spiked and unspiked conditioned KSFMc samples extracted by C18 SPE and analysed by DI-ESI-oaTOF-MS. Mass range 600-1000 m/z

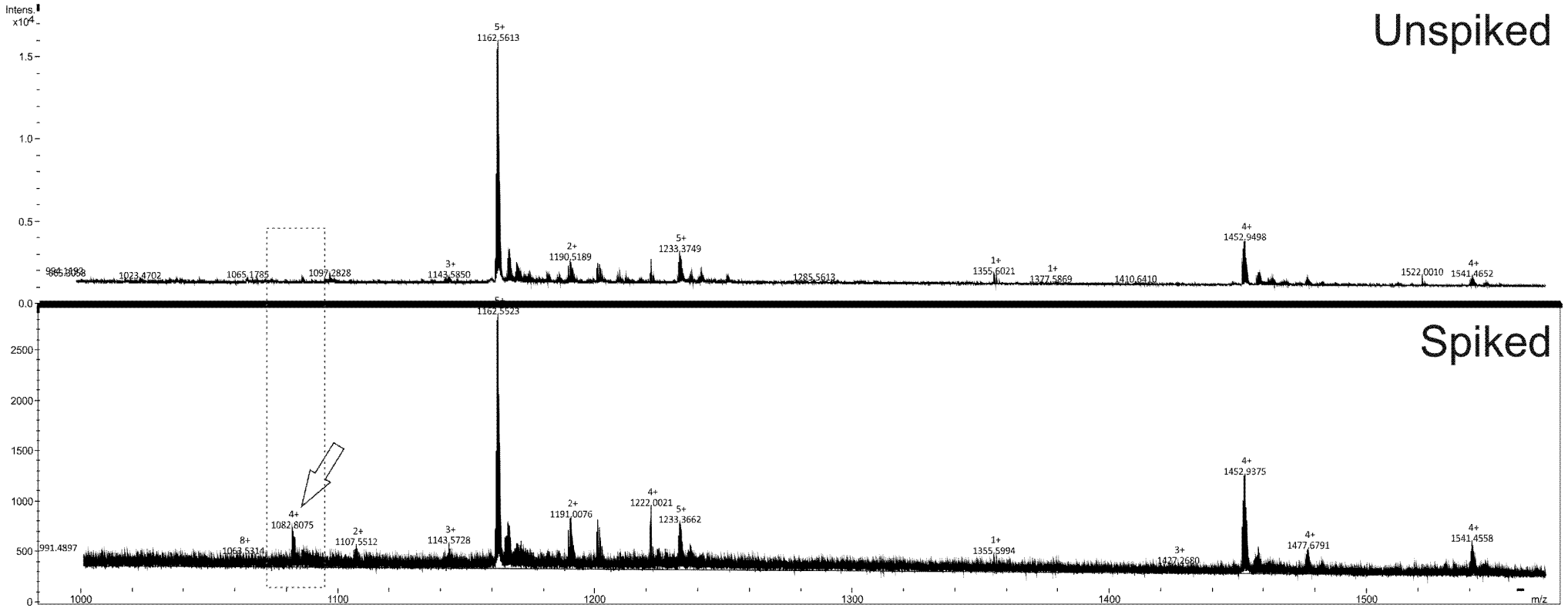

Figure 4.20 Comparison of spiked and unspiked conditioned KSFMc samples extracted by C18 SPE and analysed by DI-ESI-oaTOF-MS. Mass range 1000-1600

m/

The C18 SPE method was also examined in more detail using the MALDI-FTICR-MS technique and the authentic AMP standards. The SPE method was modified to elute the bound analyte in 0.5 mL of 70% (v/v) aqueous acetonitrile to maximise elution of BD2 from the column, and to facilitate drying the samples in a SpeedVac centrifugal evaporator. A dilution series of recombinant BD2 solutions containing 100, 80, 60, 30 and 10 fmol amounts of the AMP was prepared in 0.5 mL of 50% (v/v) aqueous acetonitrile supplemented with 0.1% formic acid (v/v). The dilution series was prepared in duplicate. One set of samples was dried immediately following preparation, whilst the remaining set was subjected to the modified C18 SPE protocol. The dried samples were resuspended in 3 μL of 50% (v/v) aqueous acetonitrile, spotted onto a ground steel MALDI plate (1 μL per spot) and analysed in triplicate.

Analysis of the 80 and 60 fmol - samples that had not been subjected to SPE was successful in detecting BD2, and reproducible (data not shown). In contrast, BD2 was not detected in two of the three MALDI spots produced from the 100, 30 and 10 fmol unfractionated samples. Unfortunately, FT-ICR-MS analysis failed to detect BD2 ions in those samples extracted using SPE, suggesting that cartridge SPE fractionation and the associated sample manipulation results in sample loss sufficient to compromise BD2 detection.

4.5.4.2 Miniaturised solid phase extraction of BD2 using ZipTip™s

Recombinant BD2 was solubilised in water, and the ZipTips were conditioned and extraction conducted following the manufacturer's method. Bound material was eluted with 50% aqueous acetonitrile acidified with 0.1% trifluoroacetic acid (v/v).

Duplicate solutions containing 1 pmol of BD2 were prepared. One was dried and resuspended in 3 μL of 50% (v/v) aqueous acetonitrile. The other was subjected to ZipTip extraction. Both the ZipTip eluate and the unZipTipped sample were dried and resuspended in 3 μL of 50% (v/v) aqueous acetonitrile. Each sample was analysed in triplicate, spotting 1 μL of sample solution in each of three spots. An example of a typical

spectrum of recombinant BD2 extracted from water using a Zip Tip is shown in Figure 4.21. The $[M+1H]^{1+}$ BD2 ion (*m/z* 4326.21092) was observed, together with multiple CHCA-BD2 adducts, including $[M+CHCA+H]^{1+}$, $M+2CHCA+H]^{1+}$ (*m/z* 4515.28 and 4704.38). The $[M+2H]^{2+}$ and $[M+3H]^{3+}$ ions were also observed (*m/z* 1442.8599 and 2164.5636). The mean base-peak intensity was used to estimate BD2 recovery (Figure 4.22). ZipTip extraction recovered between 99.66% and 88.6% of BD2 from aqueous buffers (based upon comparison of mean base peak intensity.)

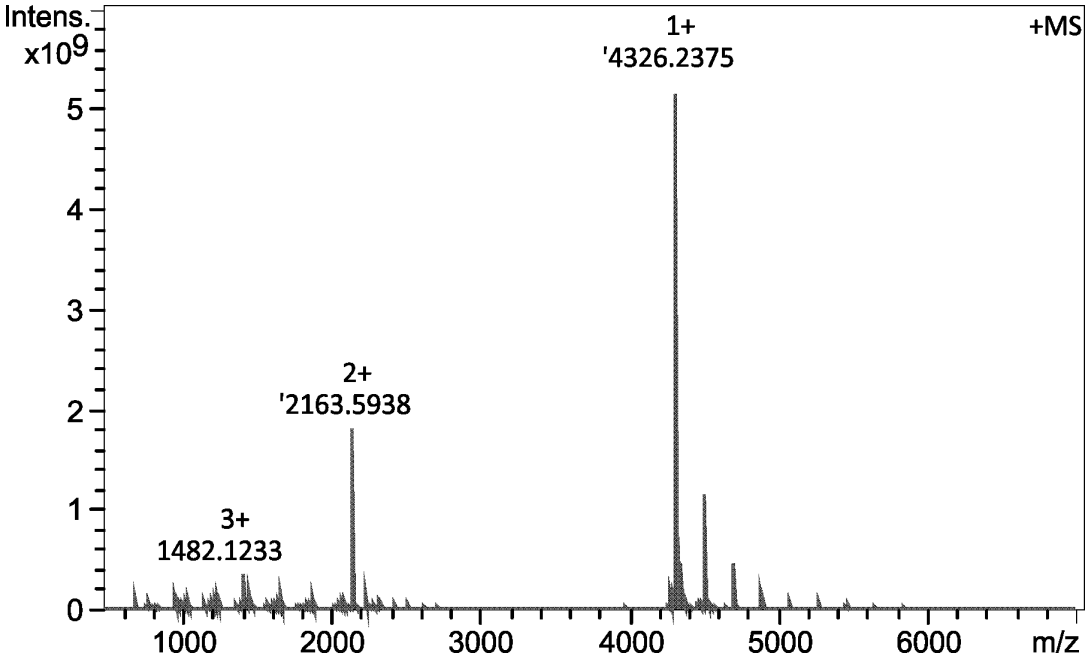

Figure 4.21 Example spectrum of ZipTip-extracted BD2 analysed by MALDI-FT-ICR-MS.

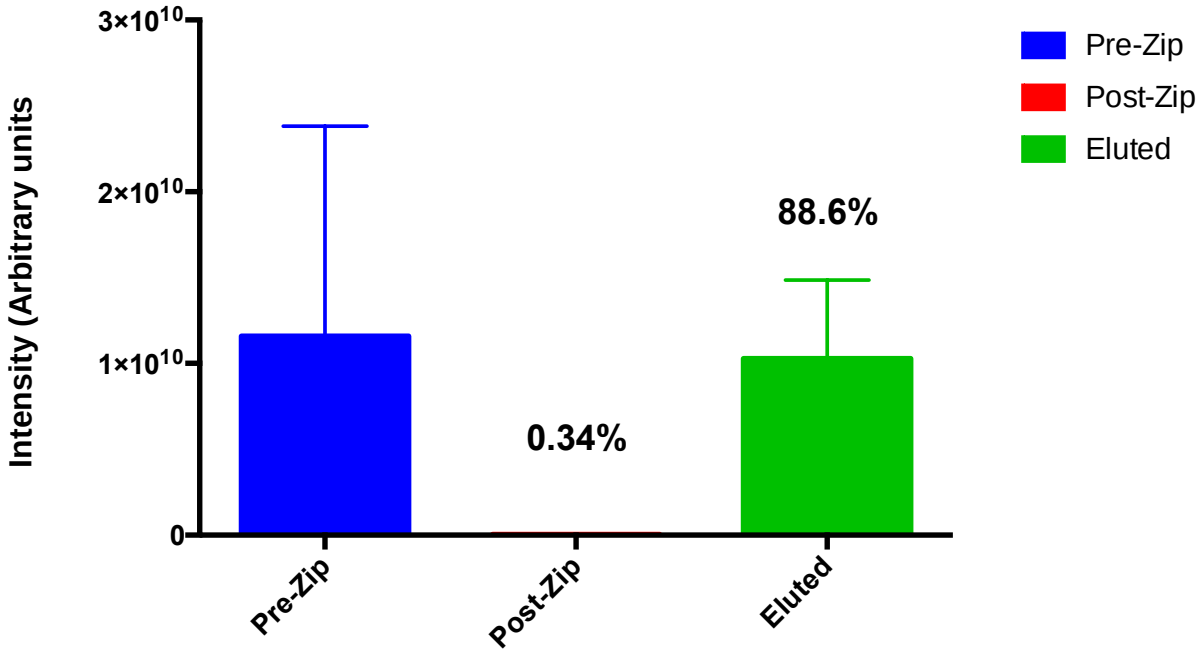

Figure 4.22. Recovery of BD2 from 10 pmol of aqueous solution, using a ZipTip.

The ZipTip SPE extraction method was then tested on samples of conditioned cell culture medium from proliferating NHU cells exposed to 100 ng/mL of UPEC flagellin for 24 hours, conditions that induced transcript expression of BD2 in multiple cell lines (chapter 3). A modified ZipTip extraction protocol (passing the sample through the tip approximately 100 times rather than 10 times in the recovery experiment) was performed on 0.5 mL aliquots of conditioned medium from flagellin-treated or control cultures, and analysed *via* MALDI-FT-ICR-MS (Figure 4.23). BD2 was not detected in the ZipTip eluate of either the flagellin-exposed or control samples. Few ions were observed in the control medium samples. Several non-isotopically clustered peaks were observed above baseline in the spectrum of the flagellin-treated medium sample, but did not correlate with any known AMP ion *m/z.* Given more time, product ion spectra of these signals would have been obtained and interpreted to determine whether these signals derive from peptides with amino acid sequences consistent with being related to the β-defensins.

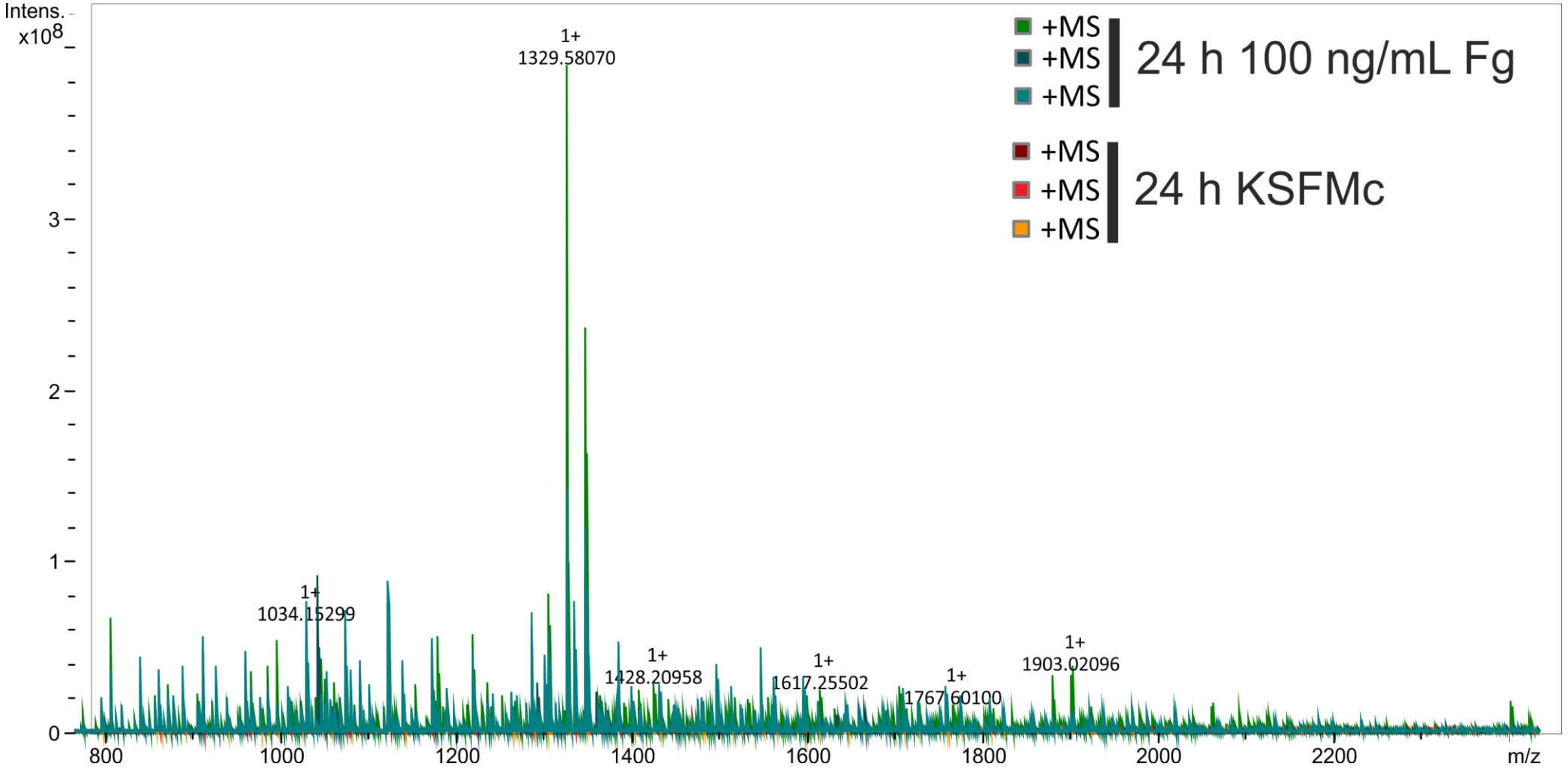

Figure 4.23 Comparison of spectra from cell culture medium samples obtained from NHU cells exposed to flagellin. The spectrum from each of the triplicate spots are shown.

4.6 Discussion

The aim of this work was to develop mass spectrometric methods to detect AMP release from an *in vitro* NHU cell model. Biological analyses of transcript-level AMP responses to bacteria (described in chapter 3) suggested that NHU cells expressed three beta-defensins. BD1 was expressed constitutively, whilst BD2 and BD4 were expressed in response to bacterial exposure or treatment with flagellin.

Using recombinant sources of BD2 and BD4, 'proof of concept' analyses of peptide standards prepared in MS-compatible buffers showed that both BD2 and BD4 were amenable to ionisation by MALDI-based techniques. Analyses used the ultraflex III instrument, a MALDI-TOF/TOF instrument with comparatively low resolution and mass accuracy compared with other, state-of-the-art instruments available in the CoEMS. Whilst BD4 was detectable using the ultraflex instrument, the spectra obtained were of low resolution. MALDI-FT-ICR analysis of the standard peptides produced high resolution spectra with very good mass accuracies for both BD2 and BD4. Only BD2 was detectable *via* ESI-MS using the maXis instrument, despite attempts to optimise the MS conditions. It was therefore decided to focus on the development of a MALDI based analysis that had the potential to be able to detect both AMPs in the same analysis.

Characteristically, MALDI preferentially produces singly charged ions. Whilst rare, MALDI can produce multiply charged ions. In this study, multiply charged BD2 and BD4 ions were observed consistently, and were the sole ions observed in some analyses. Recent studies attempting to elucidate the mechanisms of MALDI ion formation have postulate a combined theory of MALDI ion formation, in which analyte characteristics such as size, proton affinity and pre-existing charge increase the likelihood of protonation (Jaskolla and Karas, 2011). The cationic nature of BD2 and BD4 may therefore mean that these species are preferentially multiply protonated, leading to an increased incidence of multiply charged ions.

Methods for assaying defensins in saliva and other bodily fluids using both MS and antibody based techniques have been described previously; however the detection of human BD4 *via* MS has not been described previously. Limits of detection for these assays fell between 1-10 ng/L (approx. 1-10 pM), which are significantly lower than those obtained in this study. Previous studies have utilised matrix additives (e.g. n-

octylglucoside) to increase sensitivity and reduce spectrum to spectrum variability (Jørgensen et al., 2006).

There are limited data from which to establish a likely range of BD2 and BD4 concentrations *in vivo* in order to better assess the required sensitivity for an MS assay. BD2 was discovered first, and therefore more data is available. Evidence of BD2 expression exists for several epithelia, including airway, gut and the ocular surface (Oppenheim et al., 2003). Several defensins, including BD2 and BD1, have been detected in human urine. The extrapolation of these data to an isolated urothelial cell culture model is difficult; concentrations of defensins in urine are expected to fluctuate due to physical variables such as the volume of urine and time elapsed since voiding, in addition to up- or down-regulation of AMP production in the tract due to pathogen sensing or other inflammatory stimuli.

Evidence of *in vivo* BD1 peptide expression has been noted in human and mouse urinary tracts, localised to the urothelium (Lehmann et al., 2002; Valore et al., 1998). However, whilst BD1 was detected constitutively at the transcript level in NHU cells, no BD1 was detected in conditioned cell culture media using the MS methods developed for BD2. Whilst method development was focused on detection of BD2 and BD4, defensin peptides share core structural characteristics, suggesting that a method that detects BD2 may detect other defensins.

4.7 Conclusions

The work presented here attempted to develop methods with minimal sample preparation to analyse cell culture medium for AMPs, with a specific focus upon the β-defensin family of peptides. Both MALDI and ESI-based methods were tested, due to previous reports of successful MS-based detection with these methods, albeit following chemical modification of the peptides and significant sample fractionation and preparation.

Under controlled conditions, using MS-compatible buffers and relatively high concentrations of recombinant peptide standards, detection of both BD2 and BD4 was achieved using MALDI-FT-ICR-MS. Recombinant BD2 standards were successfully detected using DI-ESI-oaTOF-MS, although BD4 was not. SPE sample preparation was

successful in isolating spiked recombinant BD2 from conditioned cell culture medium; however attempts at detecting endogenous BD2 failed. Miniaturisation of the SPE approach using ZipTips successfully improved recoveries, but ultimately, the sole attempt in the time permitted to detect endogenous BD2 from challenged urothelial cells was unsuccessful.

The work presented here provides 'proof of concept' for the feasibility of detecting β-defensins with minimal sample preparation from cell culture medium. The estimated LOD of ~10 pmol and variability of the MALDI-FT-ICR method developed in this chapter suggest that further attempts to detect endogenous BD2 release are certainly warranted.

5 Biomimetic modelling of bacterial interactions with normal human urothelium

5.1 Introduction

> **"Since *all models are wrong* the scientist cannot obtain a "correct" one by excessive elaboration. On the contrary, following William of Occam he should seek an economical description of natural phenomena."**
>
> **George E. P Box, 1976**

The use of model organisms and systems is a cornerstone of biomedical science. The scientific community are unlikely to ever know every detail of a living organism: Ideally, biological model systems allow for the development of an in-depth body of knowledge of a convenient, ethical and appropriate representative organism or mechanism. This body of knowledge can be used to design appropriate studies of the non-model organism in an ethical, timely and cost-effective manner.

The poor predictive value of results from animal models has become a 'hot-topic' in the field of biology, in particular regarding drug discovery and toxicology. A broad, cross-discipline industrial consensus has developed that many preclinical animal models do not 'take us any closer to understanding human disease' (Horrobin, 2003) and that data from animal testing of toxicity was 'of little or no use' (Chapman and Robinson, 2007).

Despite these widely publicised flaws, i*n vivo* animal models remain widely used in industrial and academic research for the simple reason that animal models the sole ethical method to observe and test hypotheses in a whole living organism. Such studies are often considered the 'gold standard', compared to those studies conducted on isolated primary cells or *ex vivo* tissue. However, if the system under investigation (or to be exact, the specific functions of the system) is sufficiently self-contained to a specific cell or tissue type, data with direct *in vivo* relevance may be obtained without the use of a

whole animal model. . This approach has already been validated for use in toxicity studies of cosmetics using a reconstructed skin system based on cultured human keratinocytes (EURL ECVAM, 2014.)

5.1.1 Modelling urinary tract infections in vivo and in vitro

Model systems can provide an extraordinarily powerful way to analyse the function of complex organisms. All model systems are however based upon two major assumptions: that the observations from the model system can be extrapolated to the 'real' system of interest, and that the model system displays a similar diversity of response to a specific stimulus as the 'real' system. Without suitable controls to demonstrate that these assumptions are true, the data derived from such systems can be significantly flawed. A model system in the context of this thesis is a *physical* experimental system, as opposed to a computational representation of experimental system.

The majority of research conducted on the mechanisms of urinary tract infection has taken place in two main experimental systems: *in vivo* murine infections, and *in vitro* infection experiments using immortalised or bladder cancer cell culture models. Both systems have utilised type strains of uropathogenic bacteria and clinical isolates.

Many different murine infection models have been described in the literature (Bokil et al., 2011; Hung et al., 2009; Lanne et al., 1995; Rouschop et al., 2006; Yamamoto et al., 1991), however the laboratories of Matthew Mulvey and Scott Hultgren have dominated the field of murine UTI studies in the past decade, and the majority of reports utilise the protocol published the Mulvey group (Hung et al., 2009).

The core of the technique is the instillation of a concentrated titre of bacteria, suspended in PBS, into the rodent bladder *via* a urethral catheter. Titres above 10^7 CFU/mL are generally used, compared to the generally accepted clinical definition of bacturia at 10^3-10^5 CFU/mL (Kass, 2002). Models of lower tract UTI and pyelonephritis are almost identical, differing only in the number of bacterial instillations or non-quantitative estimates of instillation pressure (Hung et al., 2009). Indeed, little differentiation between pyelonephritis and lower tract infection is made in murine models, with common UTI models causing severe upper tract infections and sequelae (such as

induction of vesicoureteric reflux) that are serious and rarely, if ever, observed in humans suffering uncomplicated UTI (Hopkins et al., 1995).

Several bladder cancer cell lines (BCCs) have been used to study UPEC interactions with urothelial cells *in vitro*, with a majority of studies using T24 and 5637 cell lines. Both cell lines are derived from high-grade invasive urothelial carcinomas, and are immortal. Immortalised cell lines are widely used in biomedical research as model organisms for *in vivo* tissues, both normal and cancerous. Immortalised cell lines are readily available, do not require ethical approval for use, and are genetically identical: these characteristics avoid many of the issues surrounding experimental systems incorporating primary cells or *ex vivo* tissue.

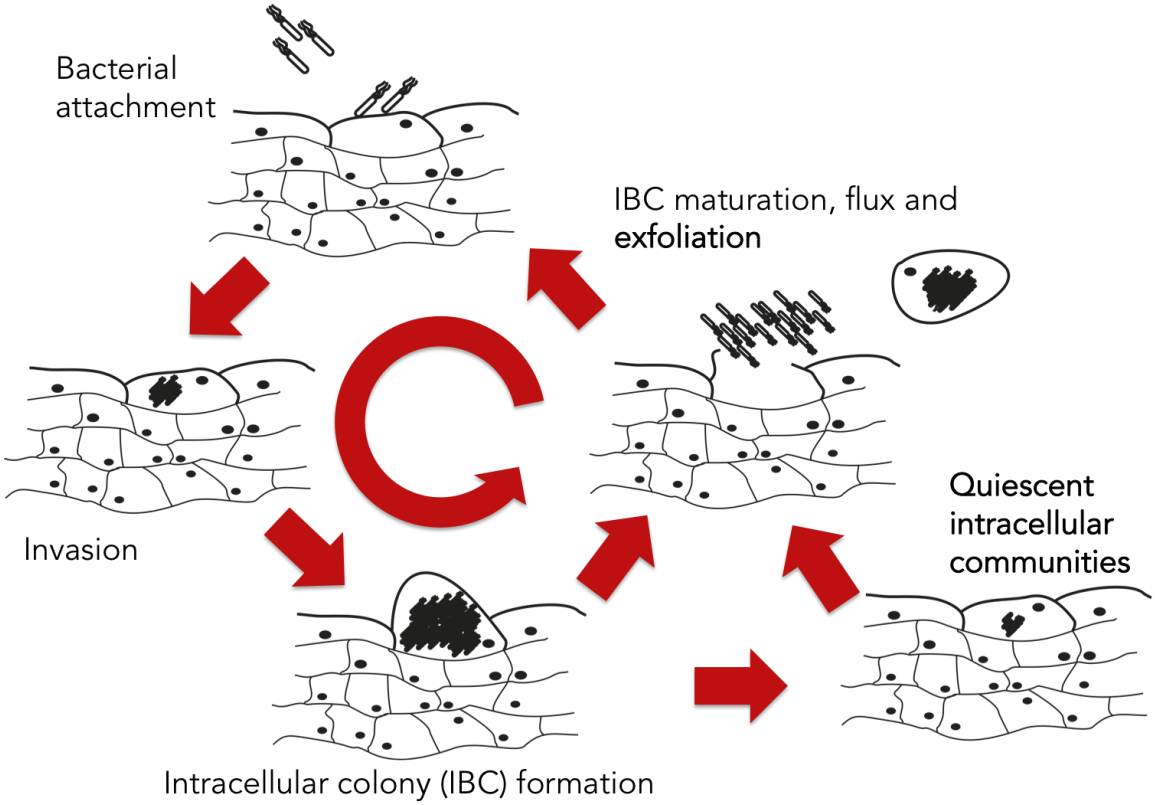

Figure 5.1. Summary of the intracellular bacterial lifecycle of UPEC as hypothesised by Hultgren, Mulvey and colleagues (Barber et al., 2016).

The primary breakthrough attributed to the models developed by Hultgren and Mulvey is the intracellular bacterial community (IBC) hypothesis of chronic recurrent urinary tract infections. Mulvey, Hultgren and colleagues describe a complex bacterial lifecycle (summarised in Figure 5.1) wherein UPEC can bind, internalise and replicate within urothelial cells, forming biofilm-like intracellular 'pods', which are protected (hidden)

from the immune system. Following maturation of the 'pod', reaching extremely high bacterial loads, the bacteria 'flux', bursting out into the bladder lumen and re-infecting other urothelial cells. Formation of small, quiescent IBCs, (also known as QICs) have been observed in otherwise asymptomatic hosts for months following an active infection.

Evidence of intracellular bacterial communities has also been noted in immortalised bladder cell models.*in vitro* infection of T24 cells with 40 clinical cystitis isolates lead to binding and invasion of cells by all isolates, even by isolates expressing no known adhesin molecules (Miyazaki et al., 2002). Cellular invasion by UPEC is suggested to both augment and downregulate the inflammatory response of BCC models. Schilling and colleagues noted an LPS-dependent, fimH independent upregulation of IL-6 production, potentiated by bacterial invasion, (Schilling et al., 2001).

The IBC hypothesis is, however, poorly supported by *in vivo* human evidence. Evidence of only one lifecycle stage, (where IBC-containing differentiated urothelial cells are exfoliated into the urine) has been observed in humans (Kelley et al., 2014; Robino et al., 2014, 2013).

Much of the evidence obtained from murine models suggests that TLR4 plays a crucial role in the urothelial response to UPEC. Mice with mutations affecting TLR4 signalling do not produce cytokines or chemokines in response to UPEC (Patole et al., 2005; Samuelsson et al., 2004; Shahin et al., 1987; Svanborg-Edén and Svennerholm, 1978), preventing neutrophil recruitment. Bone marrow transplantation studies suggested that reintroduction of wildtype TLR4-expression in both hematopoietic and stromal (i.e. neutrophil and epithelial) precursor cells was required to mount a strong antibacterial response in the urinary tract (Schilling et al., 2003a).

Canonical TLR4 activation requires the presence of CD14 and MD2, co-receptors for LPS which aid the induction of cell signalling (Akashi et al., 2000; da Silva Correia et al., 2001). TLR4 and CD14 are both expressed in the murine urinary tract, including the renal epithelia (El-Achkar et al., 2007) whilst only TLR4 is present in the human tract. Evidence exists for the presence of soluble CD14 (sCD14) in human urine, however it is unclear if sufficient sCD14 is present to influence cell signalling *in vivo (Carey et al., 2015)*. Evidence from bladder cancer cell models has suggested that CD14 expression is dependent on the

cell line used, with significant variation in protein level expression of TLR4, CD14 and MD-2 noted in T24 and 5637 bladder cancer cell lines (Shimizu et al., 2004) .

Studies using T24 and 5637 BCCs have supported findings from murine models that LPS acts as the primary PAMP activating the urothelial response to UPEC, activating NFkB translocation and induction of IL6 and IL8 cytokine responses (Schilling et al., 2003b).

Several investigators have noted increased levels of UPEC invasion of host urothelium following abrogation or knockout of TLR4 (Ashkar et al., 2008; Schilling et al., 2001; Song et al., 2007) These studies suggested that abrogation of TLR4 caused an increase in bacterial invasion at time points prior to recruitment of neutrophils and induction of an inflammatory response. It was therefore hypothesised that the inability of TLR4 mutant mice to clear infection was due to the initial UPEC colonisation overwhelming the innate defences during the initial stages of infection (Song et al., 2007).

Interactions between other UPEC virulence factors and TLR4 have been described, suggesting that multiple stimuli may activate responses to UPEC *in vivo*. Type 1 fimbriae, tipped with FimH, the prototypical UPEC adhesin, are important uropathogenic virulence factors. Type 1 fimbriae-expressing uropathogens have been shown to induce a fimH/LPS co-dependent response in murine and cell culture models of infection, even in models where the CD14 LPS co-receptor was absent (Hedlund et al., 2001; Liu et al., 2015). In addition, interactions between UPEC FimH and uroplakin 1a (the canonical urothelial binding partner of the type 1 fimbrus) is suggested to mediate cytoskeletal and membrane reorganisation to enable bacterial invasion of urothelial cells in murine models of infection (Hannan et al., 2012; Martinez et al., 2000; Mulvey et al., 2000).

Similar responses have been observed with P-type fimbriae (Frendéus et al., 2001; Godaly et al., 2007) in response to binding to urothelial glycosphingolipid targets (Wullt et al., 2000). However, some investigators suggest that invasion of urothelial cells and the induction of an inflammatory response can be induced in the absence of most fimbiral virulence factors (Miyazaki et al., 2002).

Wider studies of murine inflammatory responses have suggested that systemic responses to inflammatory stimuli differ significantly to those observed in humans, with

poor correlation of human gene expression to their murine orthologues. Specific differences in the murine innate immune sensing have also been described, such as the absence of TLR11 in humans. TLR11 was first described by Zhang et. al, following its discovery by bioinformatics analysis of putative TLR genes in mice (Zhang et al., 2004). A close relative of TLR5, TLR11 is expressed in mouse liver, kidney and bladder, activating NFκB signalling *via* the classical TLR signalling cascade. *In vitro* and *in vivo* murine analyses suggested that UPEC induced the activation of TLR11 signalling, and that such activity was specific to UPEC.

TLR11 knockout mice were extremely susceptible to ascending UPEC infection, with 10,000 times more bacteria present in the kidneys of TLR11-null mice than wild-type controls (Zhang et al., 2004). The TLR11 gene is however non-functional in humans due to three premature stop codons (Gazzinelli et al., 2014). The relevance of the findings in humans were argued by Zhang and colleagues, who suggested that non-functional TLR11 expression in humans may confer a susceptibility to UTI, in a similar manner to that of premature stop codons in TLR5 in *Legionella* infection.

Further sequencing analysis of the human genome has however confirmed that TLR11 is non-functional in humans, and that expression of TLR12, a mouse-specific TLR receptor is required for TLR11 function in mouse (Koblansky et al., 2013). Authors using murine models of UTI rarely discuss the role a mouse-specific UPEC-targeting TLR despite the evident implications upon the validity of the model.

Few studies have focused on the use of human urothelial cells to model interactions with bacterial stimuli. Previous studies of TLR function with NHU cells has shown, despite the expression of TLR4 transcript, NHU cells do not bind or respond to LPS, responding instead to flagellin (Smith et al., 2011). Few murine-model based investigations have discussed flagellin as a mediator of uropathogen sensing (Andersen-Nissen et al., 2007; reviewed by Song and Abraham, 2008.), with most focused upon the utility of motility in colonising the urinary tract.

As discussed at the beginning of this chapter, poorly validated models can provide flawed, and at worst, spurious data. Several hypotheses have been developed using mouse models, which despite limited supporting evidence from human studies, have

garnered much clinical discussion. The limitations of mouse and cancer cell models of UTI are diverse, yet rarely discussed in the scientific literature. The development of biomimetic models of normal human urothelium may offer the best of both worlds: the ethical and cost efficiency benefits of an *in vitro* model system, with direct applicability towards human biology.

5.2 Aims

Current murine and cancer cell models of UPEC interaction with the urothelium correlate poorly to the observed phenotype in normal human urothelium *in vivo* and *in vitro.* The NHU cytodifferentiation model previously developed by Cross et al. provides a biomimetic *in vitro* model of normal human urothelium, which replicates the function of the urothelial barrier *in vivo.* The aim of this chapter was to develop the *in vitro* biomimetic NHU cytodifferentiation system to model the function of the urothelial barrier *in vivo* for investigating interactions between UPEC and human urothelium. Towards this aim, the experimental objectives of the work described in this chapter were to:

1. Assess the effects of artificial urine medium (hereafter referred to as FakePee or FP) upon the differentiation state of biomimetically differentiated NHU cells and the effect of FP upon UPEC growth kinetics

2. Characterise the AMP response of biomimetically differentiated urothelium to uropathogenic *E. coli*

5.3 Experimental approach

Monitoring of TER values and (immuno)histochemical analysis of cell sheets was used to assess the response of barrier-forming differentiated NHU cells to artificial urine medium.. Cultures seeded on Trans-Well™ inserts were maintained in differentiation-inducing conditions as described in Materials and Methods 2.3.9.

Biomimetic cell cultures were maintained under normal differentiation conditions until TEER values reached >1000 $\Omega.cm^2$ or until the TER stabilised for 24 hours. Following differentiation, the medium in the apical chamber of the Trans Well™ device was changed to FakePee. FakePee was prepared as described by Brooks and Keevil (1997) . Cultures were harvested for RT-PCR, protein or immunohistochemical analysis.

The morphology of the differentiated cell sheets was assessed *via* H&E staining. The constitutive innate immune transcriptome of NHU cells was assessed by gene ontology analysis of a RNA-seq dataset. The effect of FakePee treatment upon expression of

innate immune pathways was assessed *via* IHC staining for TLR5 and PIGR. To assess differences in cellular response to uropathogenic bacteria and bacterial virulence factors, the apical medium chamber of biomimetically differentiated NHU cultures were inoculated with UTI89 E coli or spiked with UPEC-derived flagellin for 6 hours. RNA and cell sheets were harvested and AMP expression assessed by RT-PCR.

5.4 Results

5.4.1 Effect of urinary biomimetic culture conditions on NHU cells

5.4.1.1 Barrier function

Biomimetically differentiated NHU cells were maintained until TER values stabilised at day 9 post differentiation. Following media change to FP or control differentiation medium, an initial decrease in barrier function was observed in both control and FP-treated cells, below that of the mean pre-treatment TER values Figure 5.2. Barrier function of the control group increased above mean pre-treatment values one hour post treatment. Following an initial increase one hour post treatment, the FP treated cultures decreased to below the pre-treatment mean and remained significantly reduced in comparison to control cultures. However, the TER values of the FP treatment group remained stable for 24 hours, and above the 500 $\Omega.cm^2$ tight barrier limit.

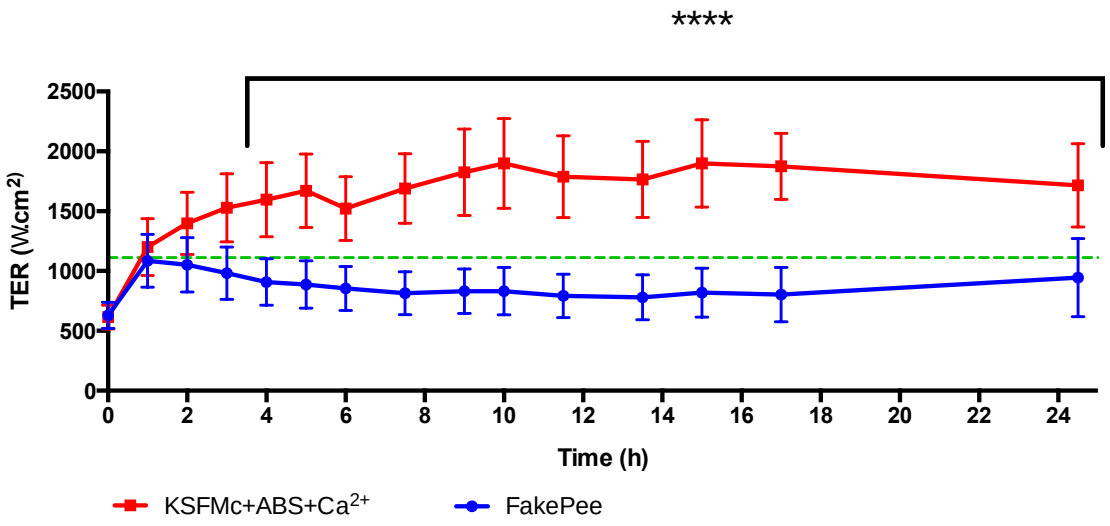

Figure 5.2 Effect of FakePee treatment upon transepithelial resistance of differentiated NHU cell sheets.

*Four replicate cultures of a single cell line were differentiated and maintained until barrier function stabilised, then exposed to FakePee (blue) or KSFMc (control, red) medium in the apical chamber and TER measured hourly (mean +/- SD). The green dashed line represents the mean TER value of cultures pre-treatment. **** denotes p <0.0001, two-way ANOVA with Bonferroni's correction for multiple comparisons. FP significantly reduced barrier function in comparison with control, however TER of FP treated cells remained above the tight barrier value of 500 ohm.cm^2*

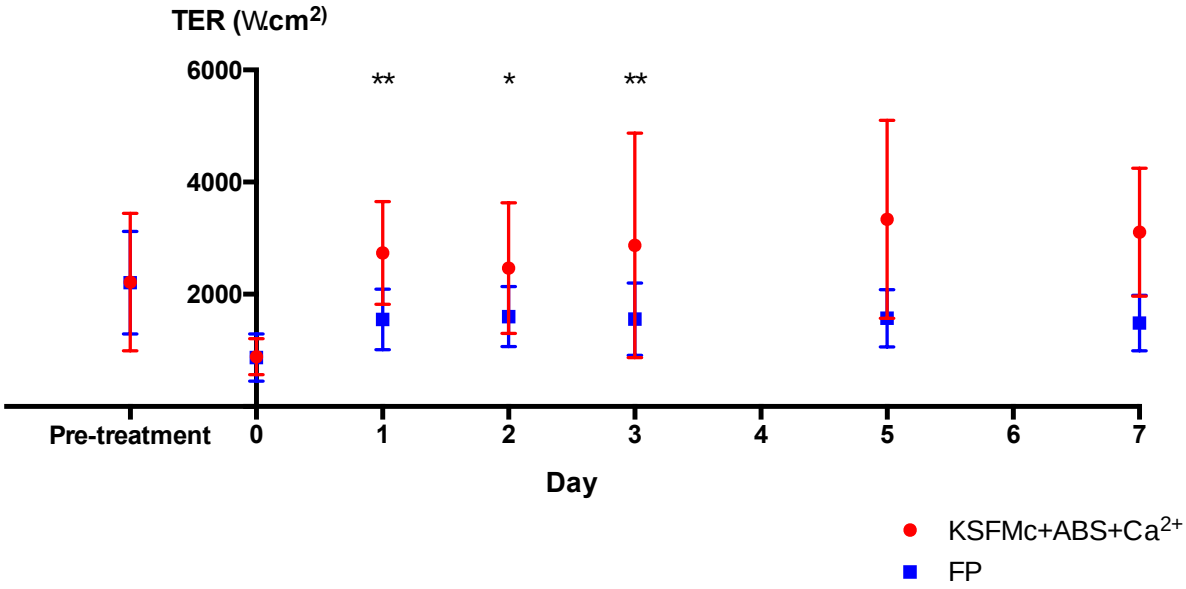

Figure 5.3. Effect of FakePee treatment upon transepithelial resistance of fully differentiated NHU cell sheets.

*Each point represents four replicate cultures of three independent cell lines were exposed to FakePee (blue) or control (red) medium in the apical chamber and TER measured each hour (mean +/- SD). * denotes p< 0.05, ** P<0.01, two-way ANOVA with Bonferroni's correction for multiple comparisons.*

The longer-term effect of FP treatment upon differentiated NHU barrier function was also assessed. As above, differentiated NHU cells were maintained until TER values stabilised and apical medium changed for FP or control. TER values were measured for seven days. An initial decrease in TER values was observed following media change in both treatment groups Figure 5.3. The TER values of the control sheets recovered and remained above the mean pre-treatment values at all time points; however TER values were highly variable after 24 h. The mean TER values of the FP-treated group remained reduced in comparison to control throughout the time course, however with high levels of variability in the control group.

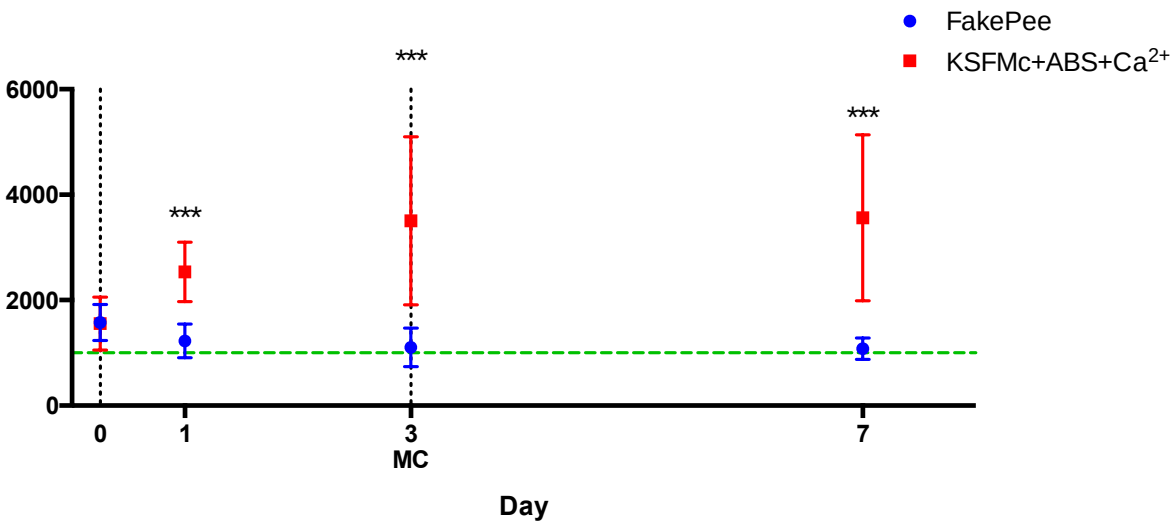

Figure 5.4. Effect of FakePee treatment upon transepithelial resistance of differentiated NHU cell sheets.

*Four replicate cultures of two independent cell lines were exposed to FakePee (blue) or control (red) medium in the apical chamber and TER measured. NHU cell lines were maintained in differentiation medium until a barrier of approximately 1000 ohm.cm² were achieved, and the apical medium changed to FP or control medium. TER values were measured one, three and seven days post treatment. **** denotes statistical significance (p <0.0001) by two-way ANOVA with Sidak's post test correction for multiple comparisons. MC; media change, green line denotes pre-treatment mean.*

The effect of FP treatment on NHU cell sheets prior to terminal differentiation was assessed (Figure 5.4). The barrier function of all FP cultures was significantly reduced compared to controls, however a 'strong' barrier (> 500 ohm.cm²) was constant and maintained for seven days following FP exposure. Barrier function in the control group continued to rise until day three of the experiment, following which the TER values stabilised. TER values in the control group remained more variable than those observed in the FP group, as was observed in the 'fully' differentiated cell sheet experiment.

5.4.1.2 Wound response

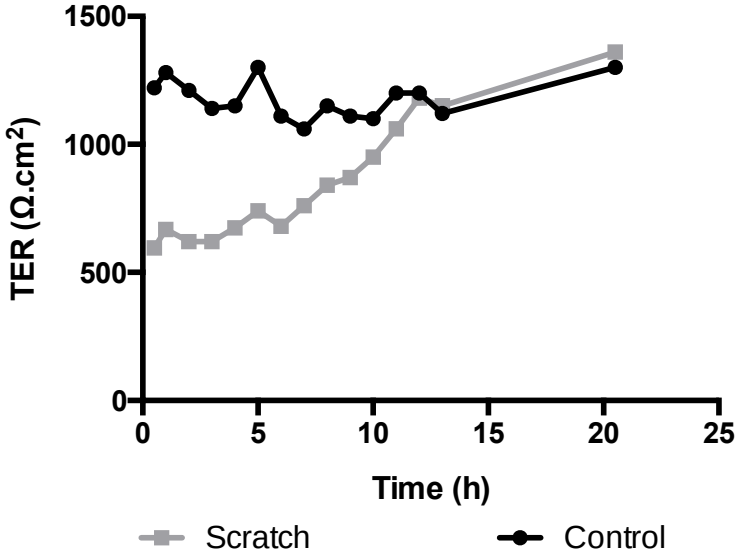

Figure 5.5. Barrier repair in response to scratch wounding of FakePee-exposed cell sheet.

A differentiated cell sheet maintained in FakePee for seven days was wounded with a sterile micropipette tip ('Scratch') and TER barrier function observed for 24 hours in comparison with an unwounded control cell sheet (Control)

The barrier repair response of differentiated NHU cells exposed to FakePee was assessed using a scratch wound assay (Figure 5.5). The cell sheet was wounded using a sterile micropipette tip and the apical medium replaced to remove cell debris. The TER values were monitored in comparison with an unwounded control cell sheet for 24h. The barrier function of the wounded single culture recovered within 15 hours of wounding, suggesting that the repair response to wounding was maintained in FakePee medium.

5.4.1.3Morphology

The effect of FakePee culture upon NHU cell sheet morphology was assessed by histological analysis. Micrographs are displayed in Figure 5.6. Cell sheets maintained in FakePee post-differentiation appeared to maintain the stratified structure of normal biomimetically differentiated NHU cell sheets. The presence of vacuoles was noted in both FakePee and control cell sheets, and a pronounced eosinophillic staining pattern was observed at the basal aspect of the 24h control cell sheet. Both FakePee and control cell sheets remained intact following 7 days culture post-differentiation, however cell sheets from both treatment groups appeared to lose stratification, with many patches of

the sheets consisting of a single layer of cells. Conversely, cell sheets from cultures exposed to FakePee pre-differentiation maintained their stratified structure.

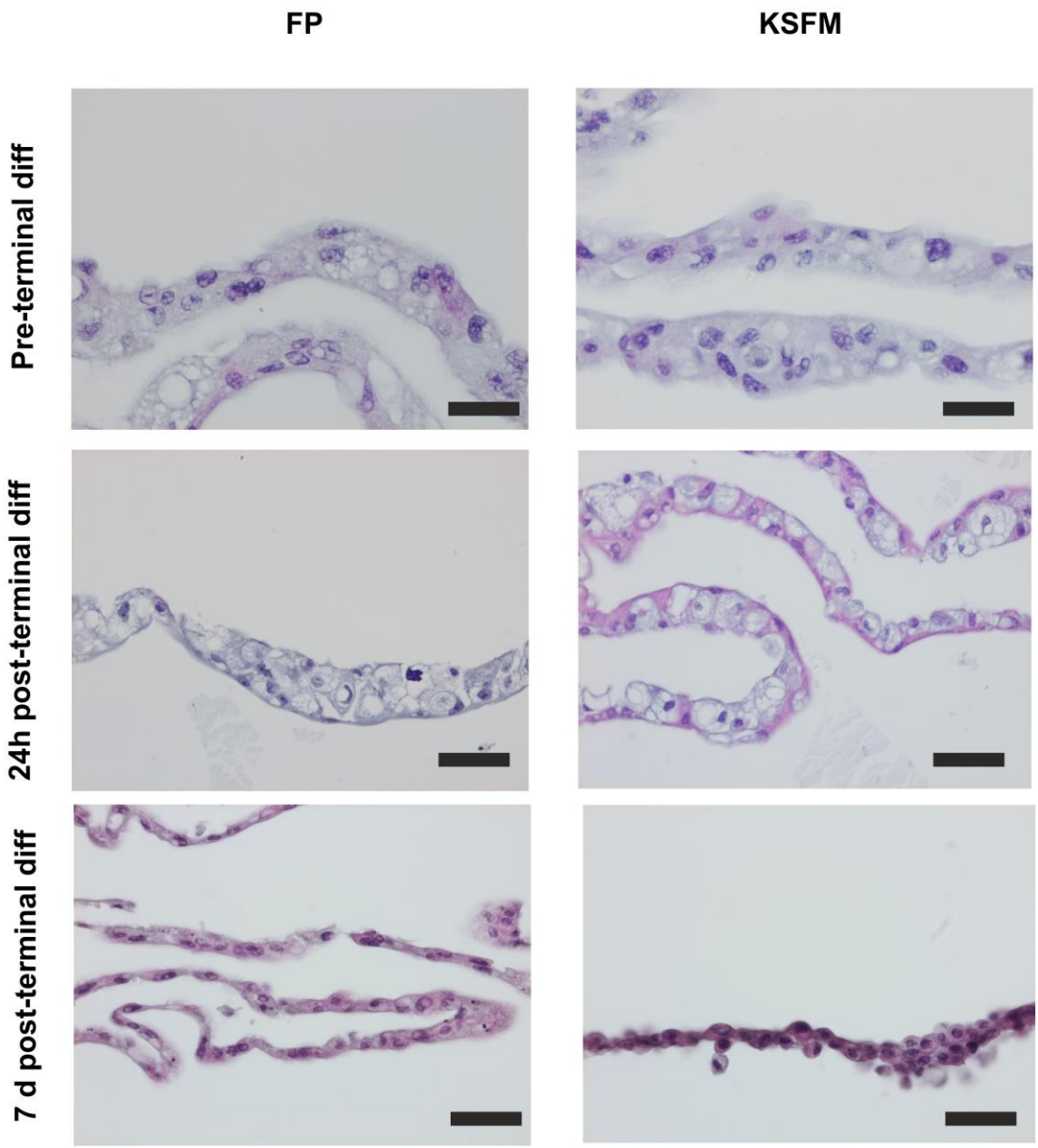

Figure 5.6. H&E staining of differentiated NHU cell sheets maintained in FakePee (FP) or control KSFM differentiation medium (KSFM).

Cell sheets were harvested following 24 h or 7 days culture in FakePee or control medium. Formalin-fixed paraffin-embedded cell sheet sections from cultures maintained in FakePee or control medium, pre- and post-differentiation were H&E stained. Black bars denote 100 µm.

5.4.2 *Effect of biomimetic culture conditions on UPEC growth*

In order to assess the effect of altering growth medium on the growth kinetics of the uropathogenic isolates used in this study, the growth of UPEC cystitis isolates UTI89 and NU14, the flagellin knockout UTI89-ΔfliC and the fimH deficient NU14-1 were assessed in standard Luria-Bertani broth and FakePee medium. Bacterial culture in FakePee caused a significant reduction in the static phase OD (Figure 5.7) and the slope of the exponential phase of growth (Figure 5.8) for all four isolates. Culture in FakePee increased the variability between biological replicates in both NU14 isolates and in the UTI89-ΔfliC knockout compared to control LB cultures.

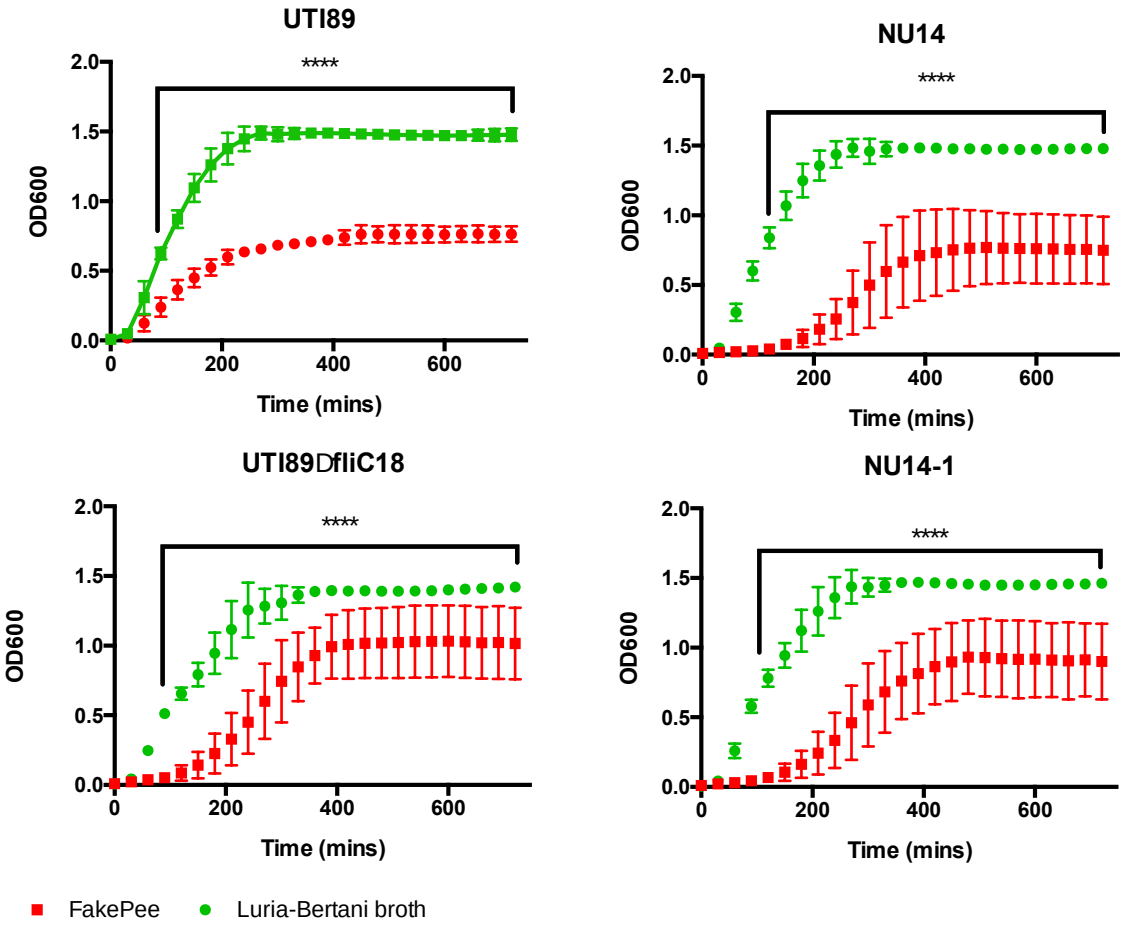

*Figure 5.7. Growth curves of UPEC isolates in LB and FakePee culture media. Optical density at 600 nm (OD600) was measured at 30 minute intervals for 24 hours. 5 biological replicates from separate starting cultures were prepared. two-way ANOVA with multiple comparisons was conducted with Bonferroni's test for multiple comparisons. **** denotes P < 0.0001. Significant differences were observed at all time points 2h post-incubation.*

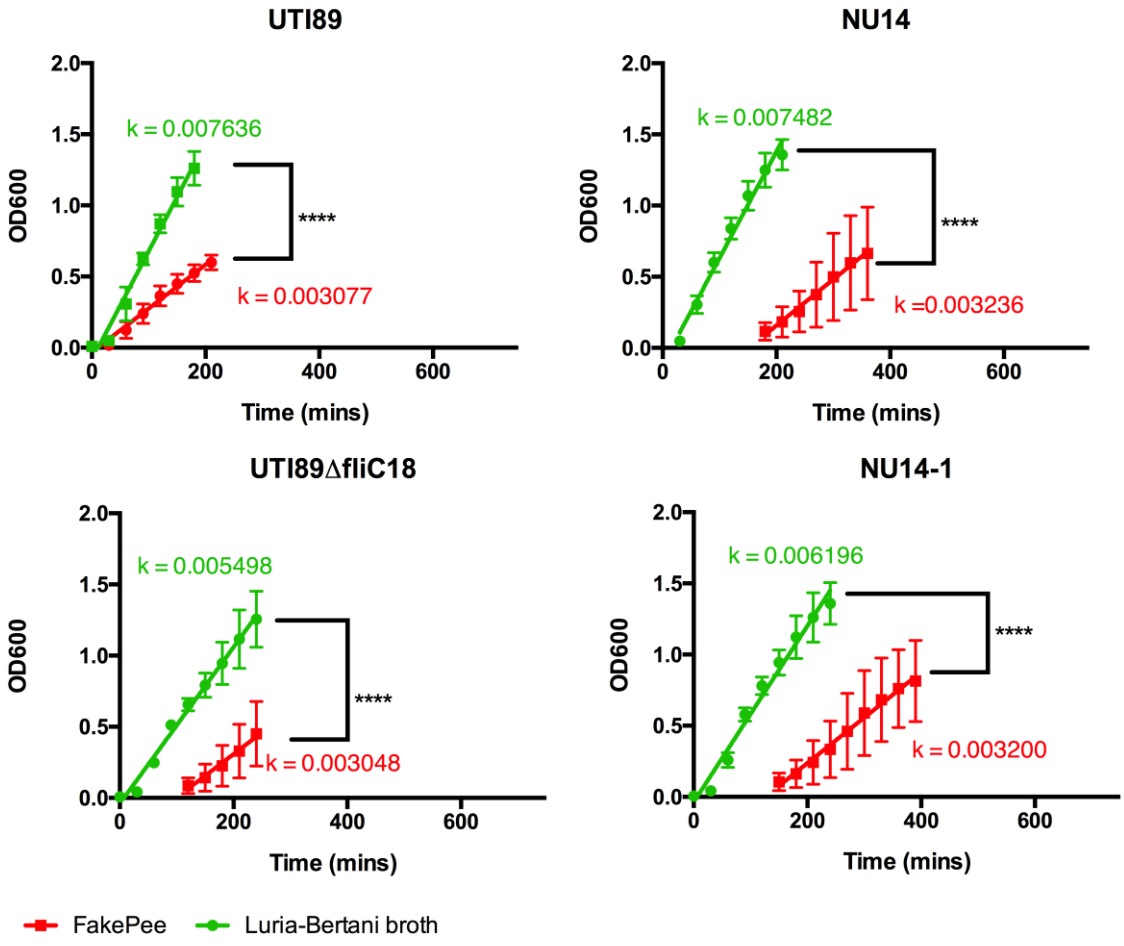

Figure 5.8. Comparison of exponential growth phase of UPEC isolates in LB and FakePee culture media. k denotes growth rate for each isolate.

*The OD600 values from the exponential phase of growth for each isolate were analysed by linear regression. The slope of the linear regression was compared by a two-tailed F-test. **** denotes P >0.0001. Each point denotes mean +/- SD from 5 biological replicate cultures.*

5.4.2.1 AMP response of biomimetic culture to UTI89 UPEC

Fully-differentiated barrier-forming NHU cells were exposed to statically-cultured UTI89 *E. coli* for 6 h, based upon the incubation time required for maximal expression of BD2 in proliferating and non-barrier forming differentiated NHU cells. NHU cells were exposed to a multiplicity of infection of approximately 20 or 2 bacteria per cell and barrier function measured prior to cell harvesting for RNA. A significant drop in barrier function was observed at 15 and 60 minute time points in the control and flagellin-exposed cultures, whilst UPEC89 exposure increased the barrier function slightly (Figure 5.9). The barrier function of the control cultures recovered two hours post-exposure. The mean barrier function of both bacteria exposed cultures temporarily increased significantly four hours following exposure before recovering to baseline levels at the five and six hour time points.

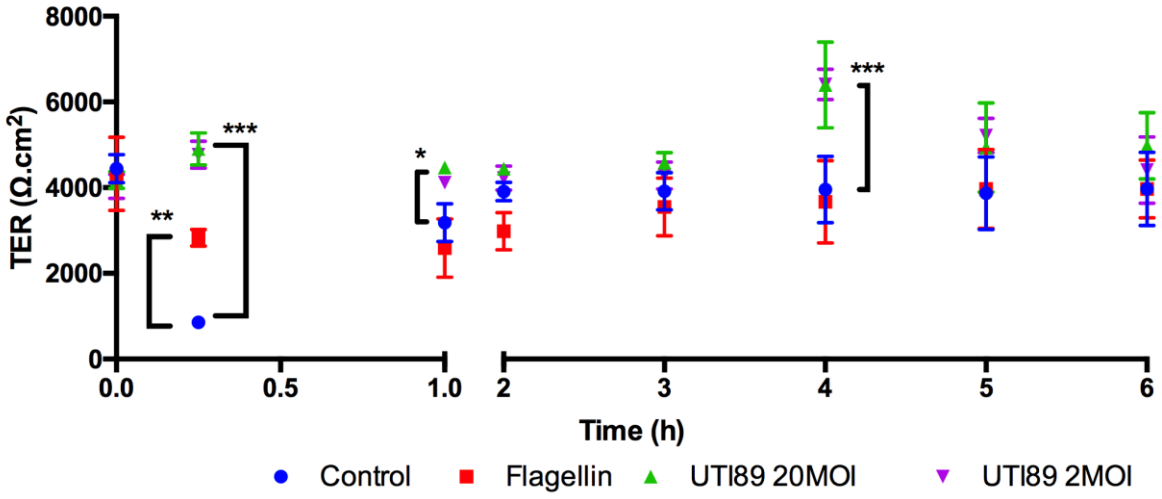

Figure 5.9. Effect of UPEC and UPEC flagellin exposure upon differentiated NHU cell barrier function.

*Fully differentiated NHU cells were exposed to an MOI of 2 or 20 bacteria:NHU cell or 100 ng/mL UPEC flagellin and the TER measured until cell sheets were harvested for RNA. Each point denotes mean +/- SD of 3 replicate cultures of a single cell line. Each timepoint was analysed for significant differences using two-way ANOVA with Tukey's correction for multiple comparisons. *** denotes P< 0.001, ** denotes P<0.01, * P<0.05.*

AMP gene expression was profiled using RT-PCR (Figure 5.10). Neither DEFB4A nor DEFB104A were induced by exposure to UTI89 *E. coli* or purified UPEC flagellin at the 6 h time-point. Constitutive expression of DEFB1 and RNASE7 was observed, coinciding with previous results observed in proliferating and non-barrier forming differentiated NHU

cells Expression of PI3 and S100A7 was not observed in barrier-forming differentiated cells.

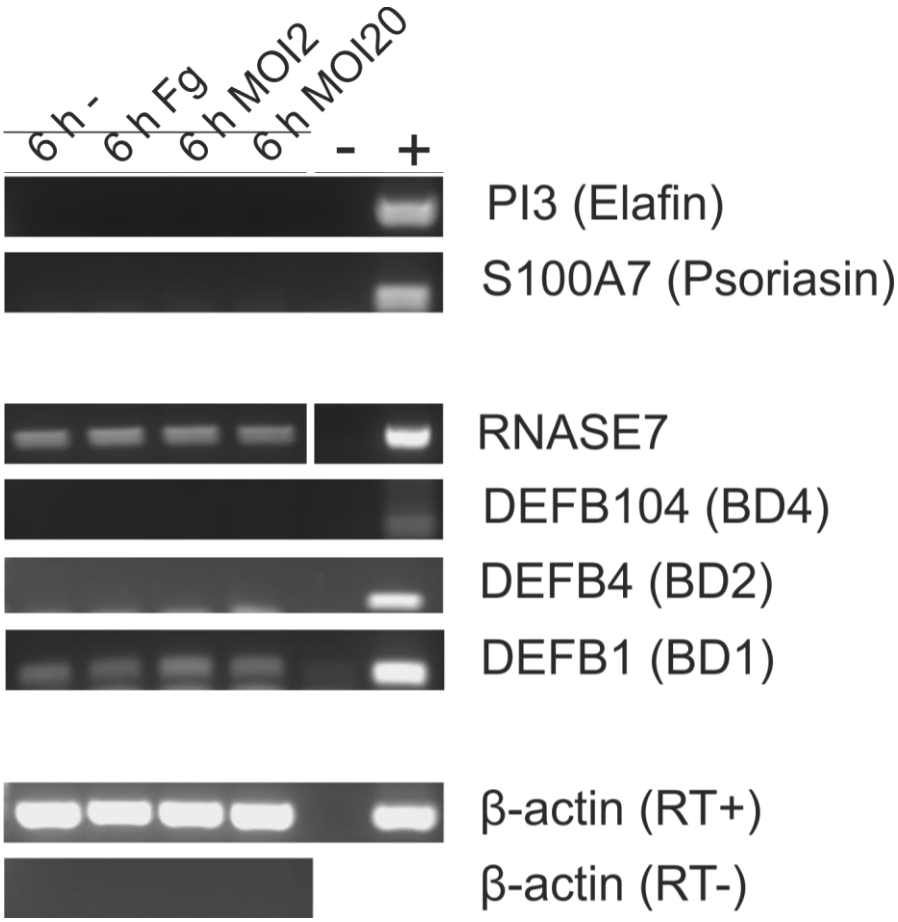

Figure 5.10. RTPCR analysis of AMP gene expression by biomimetically differentiated NHU cells in response to uropathogenic bacteria.

NHU cell sheets were challenged with a multiplicity of infection (MOI) of 2 or 20 bacteria per NHU cell or 100 ng/mL UPEC flagellin as a control for 6 hours. PCR reactions were run for 35 cycles and products were resolved on a 4% agarose gel. + denotes genomic DNA positive control, - denotes negative control.

The lack of AMP induction in barrier forming differentiated NHU cells by both UPEC and UPEC flagellin exposure did not correlate with the results obtained from proliferating and non-barrier forming differentiated cells (Chapter 3).

Immunohistochemical analysis of differentiated NHU cell sheets and *ex vivo* ureteric urothelium was undertaken to assess the protein-level expression and localisation of TLR5, the flagellin receptor hypothesised to drive AMP production by human urothelium

in response to UPEC (Smith et al., 2011). TLR5 expression in *ex vivo* tissue was primarily focused to intracellular membranes with some cytoplasmic staining, and highly donor-dependent (Figure 5.11). Expression patterns varied from a basolaterally-focused expression to full-thickness urothelial expression. Closer inspection of the apical urothelial cells revealed that the apical surface did not express TLR5, even in those cells that were positive for TLR5 expression.

TLR5 expression in differentiated cell sheets was similar to that observed *ex vivo* (Figure 5.11). TLR5 was expressed with varying donor-dependent intensity. TLR5 staining was particularly intense in areas of cell-cell contact in cultures from two donors (B and C). As in the *ex vivo* samples, the apical surface of the cell sheet was negative for TLR5 staining in all cultures.

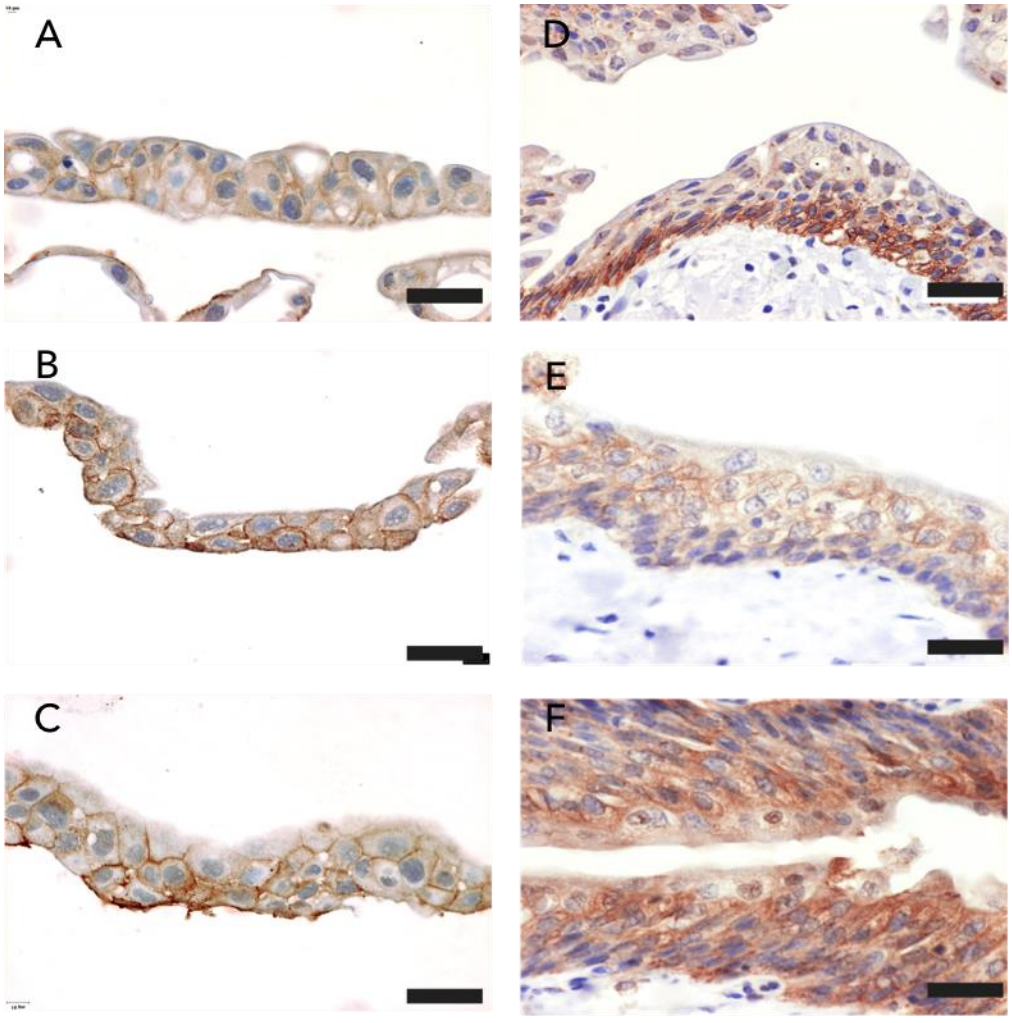

Figure 5.11. Immunohistochemical labelling of differentiated NHU cell sheets (A-C) and human ureteric urothelium (D-F) for TLR5.

Brown staining denotes positive expression of TLR5, blue staining denotes cell nuclei. Black bars denote 100 μm.

In order to test the hypothesis that damage of the apical cell surface was required to expose apical flagellin to TLR5 positive cells, NHU cell sheets were damaged *via* scratch wounding with a pipette tip prior to flagellin exposure for 6 hours. TER values were monitored throughout the experiment at bi-hourly intervals, and RNA was harvested at the terminal six-hour time point. A significant difference was observed between the terminal TER values in the Scratch and Scratch+Fg treatment groups. Linear regression analysis of each time course suggested that the difference in slopes was significant, indicating that flagellin exposure reduced the rate of wound repair compared to non-flagellin exposed control (Figure 5.12, Figure 5.13).

RT-PCR analysis suggested that BD2 induction was dependent upon scratch wounding of the cell sheet combined with flagellin exposure, as BD2 was not induced in control, scratch-alone or flagellin-alone treatment groups (Figure 5.14).

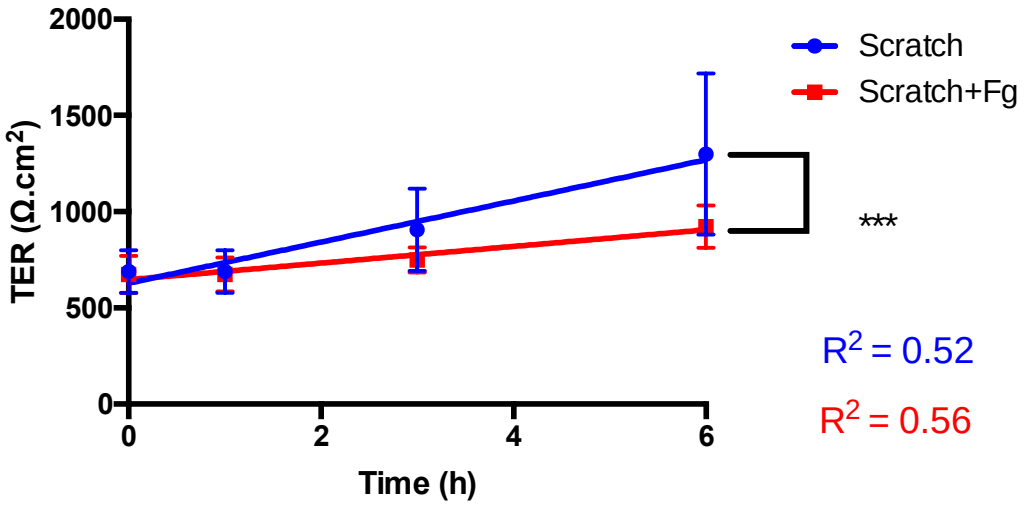

Figure 5.12. Effect of flagellin exposure upon barrier repair post-scratch wound. Differentiated biomimetic NHU cells were scratch wounded in the presence or absence of 100 ng/mL of UPEC flagellin and the TER values measured for 6 h post wounding. Each point denotes mean +/- SD of 3 replicate cultures of a single cell line. A significant difference (P<0.05) was observed between TER of flagellin-treated or control cultures at the 6 h terminal time point, as measured by two-way ANOVA with multiple comparisons with Bonferroni's correction. A significant difference was also observed (P<0.001) between the slopes of each linear regression, as assessed by F-test, suggesting that the rate of barrier repair differed significantly.

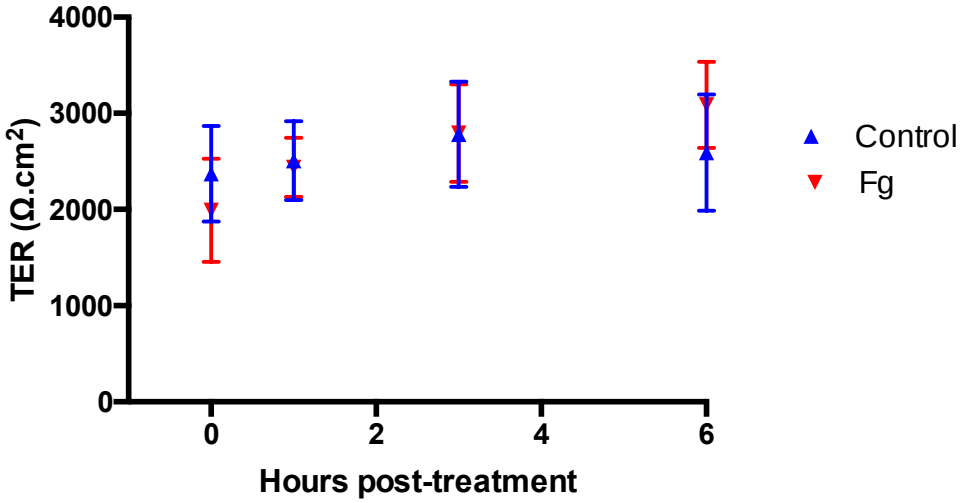

Figure 5.13. Effect of flagellin exposure without scratch wounding upon differentiated NHU barrier function.

Differentiated NHU cells were exposed to 100 ng/mL UPEC flagellin (red) or control medium (blue) for six hours, and TER values measured for 6 hours. Each point represents the mean (+/- SD) of 3 replicate cultures of 2 independent cell lines. No significant difference was observed between control and flagellin-exposed cultures at any timepoint, as assessed by two-way ANOVA with Bonferroni's correction for multiple comparisons.

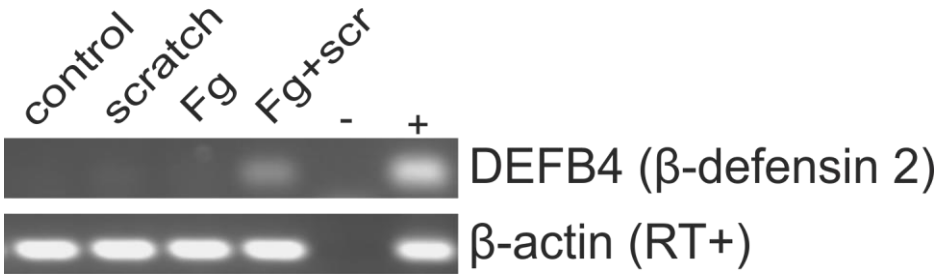

Figure 5.14 AMP gene expression by biomimetically differentiated NHU cells in response to 100 ng/mL UPEC flagellin for 6 hours.

Biomimetically differentiated cell sheets were scratch wounded in the presence (Fg+scr) or absence (scratch) of UPEC flagellin, or exposed to UPEC flagellin at the apical surface without damage (Fg). PCR reactions were run for 35 cycles and products were resolved on a 4% agarose gel.

5.4.3 Differentiation-associated expression of innate immune components

5.4.3.1 Bioinformatic analysis of differentiation-associated genes

The lack of response observed in response to flagellin exhibited by biomimetically differentiated NHU cells suggested that cytodifferentiation might play an important role in the regulation of innate immune sensing and function by the urothelium. Analysis of a pre-existing RNAseq dataset identified 8,943 genes with significantly altered expression upon biomimetic differentiation, 1,910 of which were upregulated by 2-fold or more.

The Gene Ontology (GO) aims to assign attributes and 'functionality' to groups of genes and proteins *in vivo*, enabling the rapid comparison of large gene lists. The list of identified gene transcripts, ranked by $\log_2$ fold change were submitted to the PANTHER Gene Ontology Statistical Enrichment Tool (Mi et al., 2005). GO analysis of the dataset revealed that both the immune response and immune system process gene sets were positively enriched upon biomimetic differentiation.

PANTHER-GO Slim biological process	Enrichment	P-value
developmental process (GO:0032502)	+	5.44E-04
transcription from RNA polymerase II promoter (GO:0006366)	+	2.09E-02
immune response (GO:0006955)	+	2.23E-02
immune system process (GO:0002376)	+	2.44E-02
regulation of transcription from RNA polymerase II promoter (GO:0006357)	+	8.93E-04
transcription, DNA-dependent (GO:0006351)	+	6.75E-06
biological regulation (GO:0065007)	+	3.25E-02
signal transduction (GO:0007165)	+	2.97E-02
exocytosis (GO:0006887)	+	1.18E-02
cell communication (GO:0007154)	+	4.73E-05
response to external stimulus (GO:0009605)	+	1.85E-02

Table 5.1 Biological processes positively enriched upon NHU cytodifferentiation, ranked by fold enrichment.

Ranking of differentially expressed genes by fold change (Table 5.2) revealed that full length PIGR transcript was the 5th most upregulated gene upon differentiation, and the most upregulated immune system-related gene. PIGR encodes the polymeric immunoglobulin receptor. PIGR is responsible for expression of dimeric Immunoglobulin A and multimeric immunoglobulin M across mucosal surfaces (Kaetzel et al., 1991) playing an important role in the innate immune response at mucosal epithelia. Lipocalin-2, an iron-sequestering protein though to play a role in innate immunity by preventing iron uptake by pathogens (Goetz et al., 2002), Complement protein 3, which plays a central role in the activation of the classical and alternative Complement pathways (Sarma and Ward, 2011) and C-X-C motif chemokines 5 and 6, responsible for chemoattraction of neutrophils (Koltsova and Ley, 2010) and neutrophilic granulocytes ((Proost et al., 1993) respectively were also highly upregulated upon differentiation.

Ensembl ID	Log2 fold change	Symbol	Gene name
ENSG00000146674	9.919489	IGFBP3	Insulin-like growth factor binding protein 3
ENSG00000118849	8.374303	RARRES1	Retinoic acid receptor responder 1
ENSG00000184012	8.110767	TMPRSS2	Transmembrane protease, serine 2
ENSG00000164266	7.658639	SPINK1	Pancreatic secretory trypsin inhibitor 1
ENSG00000162896	*7.4706*	*PIGR*	*Polymeric immunoglobulin receptor*
ENSG00000148346	*6.672693*	*LCN2*	*Lipocalin-2*
ENSG00000164120	*6.399751*	*HPGD*	*Hydroxyprostaglandin Dehydrogenase 15-(NAD))*
ENSG00000100373	6.081675	UPK3A	Uroplakin 3A
ENSG00000173432	6.076487	SAA1	Serum Amyloid A1
ENSG00000107742	6.035945	SPOCK2	Sparc/Osteonectin, Cwcv And
ENSG00000167653	5.934064	PSCA	Kazal-Like Domains Proteoglycan (Testican) 2)
ENSG00000163435	5.790844	ELF3	E74 like ETS transcription factor 3
ENSG00000125730	*5.783196*	*C3*	*Complement protein 3*
ENSG00000064042	5.778424	LIMCH1	LIM And Calponin Homology Domains 1)
ENSG00000134339	5.618962	SAA2	Serum Amyloid A2
ENSG00000163735	*5.610329*	*CXCL5*	*C-X-C motif chemokine 5*
ENSG00000180861	5.482775	LINC01559	Long Intergenic Non-Protein Coding RNA 1559
ENSG00000139055	5.424663	ERP27	Endoplasmic Reticulum protein 27.
ENSG00000162366	5.413827	PDZK1IP1	PDZK1 Interacting Protein 1
ENSG00000105668	5.368314	UPK1A	Uroplakin 1A
ENSG00000185215	*5.346709*	*TNFAIP2*	TNF Alpha Induced Protein 2
ENSG00000137868	5.250448	STRA6	Stimulated by retinoic acid 6
ENSG00000130822	5.219718	PNCK	Pregnancy Up-Regulated Non-Ubiquitously Expressed CaM Kinase
ENSG00000158816	5.182148	VWA5B1	Von Willebrand Factor A Domain Containing 5B1
ENSG00000064787	5.180932	BCAS1	Breast Carcinoma Amplified Sequence 1
ENSG00000110375	5.135952	UPK2	Uroplakin 2
ENSG00000140279	5.097875	DUOX2	Dual oxidase 2
ENSG00000124875	*5.082124*	*CXCL6*	*Chemokine (C-X-C motif) ligand 6*
ENSG00000140274	4.846318	DUOXA2	Dual Oxidase Maturation Factor 2
ENSG00000005001	4.843813	PRSS22	Protease, Serine 22

Table 5.2. The thirty most upregulated genes upon urothelial cytodifferentiation.

Immune system-related genes highlighted in italics.

PIGR and IgA protein expression by human urothelium was assessed by IHC analysis of sequential formalin-fixed paraffin wax embedded specimens of bladder urothelium (*Figure 5.15*), and *in vitro* biomimetically differentiated NHU cells (Figure 5.16). Bladder specimens from all four donors were positive for both IgA and PIGR, however expression patterns were highly variable, with little correlation between IgA and PIGR in each donor. Donor A, for example, expressed PIGR through the full thickness of the urothelium, with IgA expression focused on punctate areas of the apical portion of the urothelium.

Conversely, donor B expressed IgA diffusely through the full thickness of the urothelium, whilst only the apical cells and punctate areas of the stroma expressed PIGR. All *in vitro* differentiated cell sheets expressed PIGR, however IgA expression was not observed. As with the *ex vivo* urothelium, PIGR expression was highly variable between donor cell lines. Expression varied from highly intense full-thickness expression with foci at the basal aspect of the cell sheet to sparse, weak labelling of individual cells within the cell sheet.

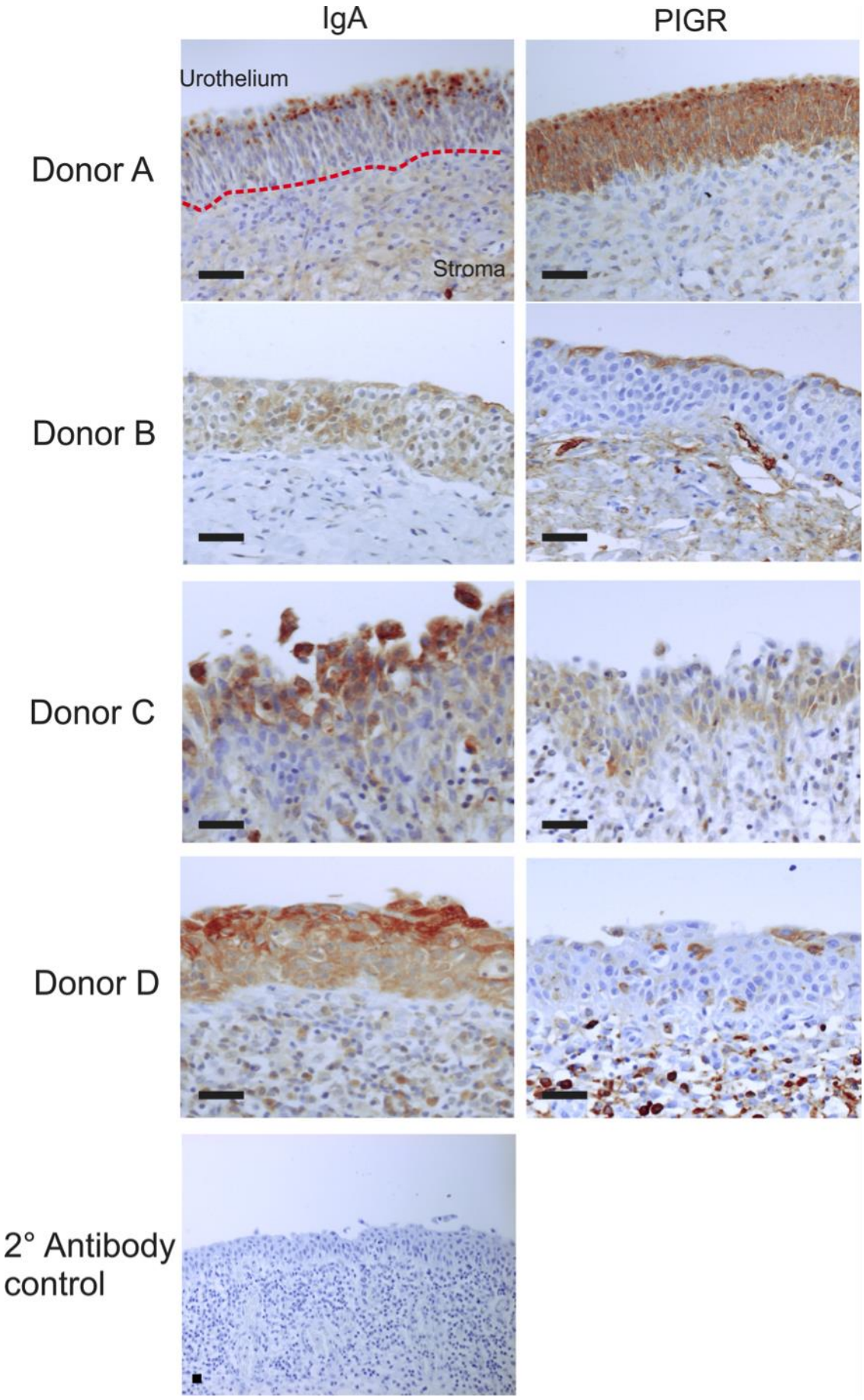

Figure 5.15 Immunohistochemical staining of donor bladder sections for PIGR and IgA. Scale bar denotes 100 µm.

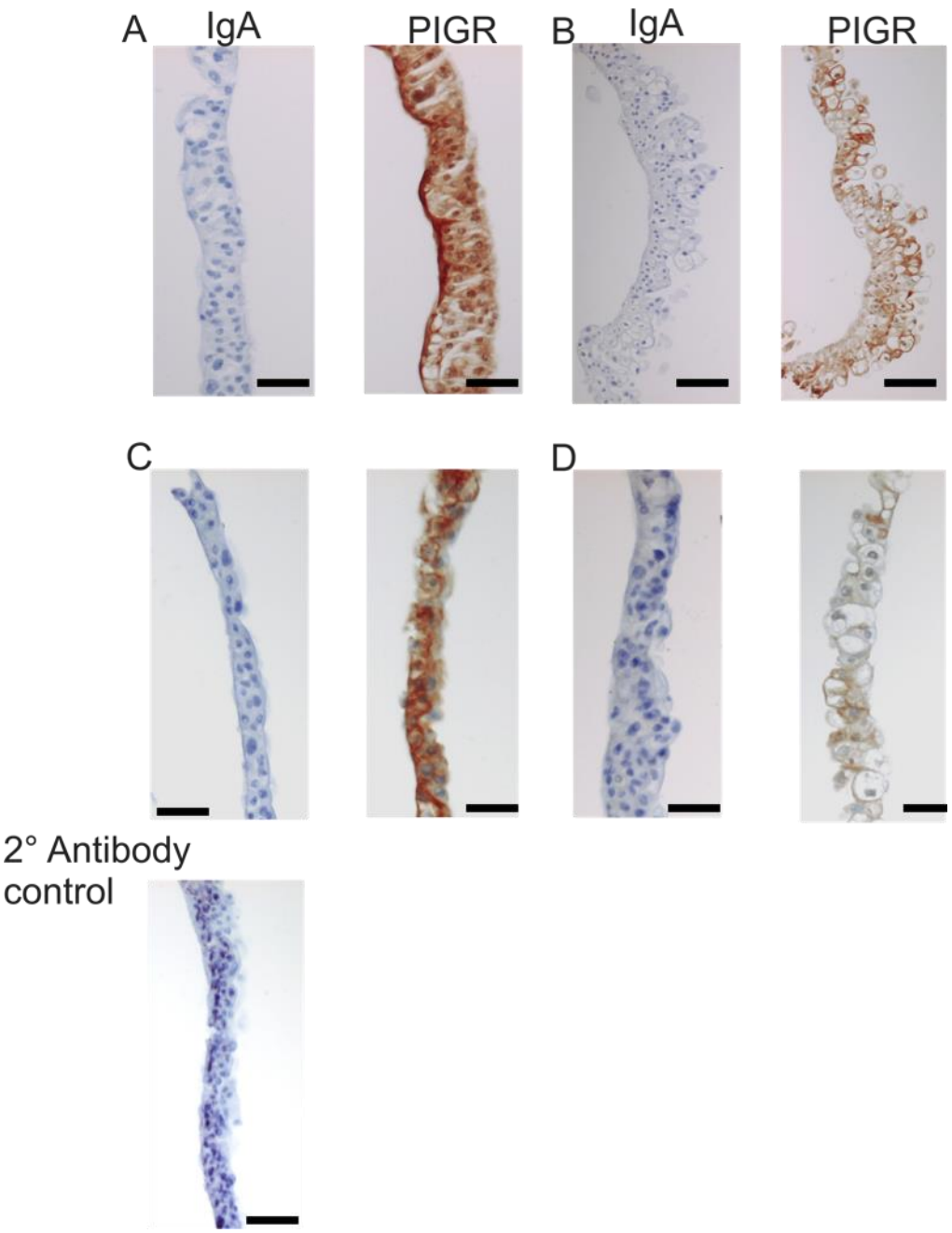

Figure 5.16 Immunohistochemical labelling of differentiated NHU cell sheets for PIGR and IgA. A-D denote different cell donors. Sequential sections were stained from IgA and PIGR. Black bars denote 50 µm

5.5 Discussion

This chapter aimed to examine the suitability of an artificial urine substitute, (developed by Brooks and Keevil (1997) as a replacement for human urine in uropathogen culture) to replace the apical medium with a substance approximating human urine. The initial aims of this chapter were to assess the effect of artificial urine upon a biomimetic urothelial differentiation model, and on the growth dynamics of uropathogenic type strains of *E. coli*. The biomimetic differentiation model developed by Cross et al., whilst modelling urothelial function, lacks a crucial feature of *in vivo* urothelium: both the apical and basal aspects of the differentiated cell sheet are maintained in cell culture medium, whilst the *in vivo* apical urothelium maintains continuous contact with urine.

Biomimetically differentiated NHU cell cultures remained viable and functional for up to seven days following replacement of the apical cell culture medium with FakePee. Cultures that were fully differentiated prior to altering the apical medium displayed considerable variability of TER in both control and FakePee treatment groups, suggesting that long-term maintenance of differentiated cultures may introduce additional variables.

Introducing FakePee prior to barrier stabilisation reduced the observed variability in both control and FakePee culture TER values. Barrier function remained significantly reduced in FakePee compared to control cultures. Barrier function was however maintained above the 500 ohm.cm^2 value considered as a 'tight' epithelial barrier. Interestingly, cultures exposed to FakePee displayed less variation than those maintained in control medium. Results from a single culture suggested that a repair response to wounding remained following FakePee culture. FakePee culture appeared to have little effect upon cell morphology in the small number of cell lines assessed.

Culture in FakePee had significant effects upon uropathogen growth kinetics, significantly reducing the rate of growth in the exponential phase and the density of culture in the stationary phase compared to cultures maintained in LB broth. The original studies conducted by Brooks and Keevil focused strictly upon the feasibility of FakePee to support uropathogen growth, however the authors suggested that FakePee acts as a minimal medium due to the absence of glucose and low concentrations of amino acids.

The limited availability of nutrients (compared to nutrient-rich LB agar) would limit the cell density of the stationary phase as observed in the growth kinetics experiments conducted in this chapter.

The original artificial urine recipe developed by Brooks and Keevil has been widely used to model the effects of urine upon uropathogen adaptation and survival in the urinary tract, however this study is the first to attempt to combine this approach with mammalian cell culture. Reducing the bacterial growth rate in culture would be beneficial in the context of a static cell culture scenario due to the lack of a mechanism to reduce or void the bacterial load (e.g urination and urothelial shedding *in vivo).*

Artificial urine substitutes exhibit several advantages over the use of donated urine: The 'urinary' composition is defined, removing 'inter-batch' variability between experiments and allowing for controlled experimentation. The metabolite and protein composition of urine however includes many biologically active compounds which can influence uropathogen growth, gene expression and virulence, some of which (such as cyclic AMP) are derived from the urothelium (Donovan et al., 2013), whilst others (such as Thamm-Horsfall protein (M D Säemann, 2005)) are derived from the kidney itself, or are excreted into the urine. Such compounds may have significant effects upon bacteria and the host immune response, and their removal may significantly change *in vitro* responses Previous studies of urothelial response to uropathogens or uropathogenic virulence factors have utilised non-human models of infection, or bladder cancer cell lines, which by their nature are deficient or abnormal in their differentiation capacity. The results reported in this chapter suggest that TLR5 activation (leading to BD2 expression) by UPEC flagellin does not occur in biomimetic urothelial cell cultures in the absence of damage to the urothelial barrier. The lack of a response to damage alone suggests that this effect is specifically due to TLR5 activation, not due to a generalised damage or stress response.

Previous studies of normal human urothelial cell interactions have utilised proliferating NHU cells, and the experiments discussed in chapter 3 utilised non-biomimetically differentiated NHU cells. Experiments in chapter 3 suggested that both proliferating and differentiated NHU cells exhibited an inflammatory response to uropathogenic bacteria, and a specific response to flagellin. However, the experiments described in this chapter

indicate that barrier-forming differentiated NHU cells are non-responsive to UPEC and UPEC flagellin unless the barrier is damaged, and that flagellin may slow the rate of barrier repair.

Previous studies conducted in intestinal and airway epithelia suggest that TLR5 is expressed basolaterally, an observation that has been noted in urothelium for the first time in this thesis. Basolaterally restricted epithelial expression of TLR5 in gut has been hypothesised to act as an immunomodulatory mechanism to prevent harmful innate immune activation. The gut has a large population of flagellated commensal bacteria that, without an immunomodulatory mechanism, would cause chronic activation of the innate immune system and associated pathogenic inflammation. Gastrointestinal pathogens (e.g. *Salmonella sp*.) express type 3 secretion systems, which can translocate bacterial virulence factors (including flagellin) across the epithelial barrier, activating TLR5 in the basolateral cells (A. T. Gewirtz et al., 2001).

The utility of such an immunomodulatory system in the urothelium is unclear: canonically, the urinary tract is considered sterile, and the presence of any bacterial colonisation is considered pathogenic. This dogma is currently being challenged by studies suggesting that a urinary microbiome exists (Hilt et al., 2014; Lewis et al., 2013; Nelson et al., 2010), and can be perturbed in a variety of different benign conditions. Existing analyses of the urinary microbiome have been limited to species-level analyses based upon next-generation DNA sequencing data: only limited evidence of the 'live' bacterial load and the motility characteristics of any such commensal bacteria exist (Hilt et al., 2014).

The virulence factors expressed by uropathogens also differ compared to those in the gut: UPEC do not express type 3 secretion systems, and therefore lack the ability to actively translocate virulence factors (Wiles et al., 2008b). The activation of a basolaterally-expressed sensing mechanism by a factor located in the bladder lumen would therefore require a deficiency or damage to the urothelial barrier or an active mechanism of transport across the urothelium. Evidence from mouse models supported by patient samples suggest that apical urothelial cells are shed into the urine during cystitis (Robino et al., 2014, 2013; Thumbikat et al., 2009), and that bacterial invasion can

occur to initiate this process, which may provide a route by which this activation can occur.

The possible role of urothelial differentiation in modifying the immune function of NHU cells was further investigated by analyses of a pre-existing RNAseq dataset comparing proliferating and biomimetically differentiated NHU cells *via* analysis of upregulated genes using a gene ontology (GO) over-representation analysis approach. Over-representation analyses are based upon statistically analysing the 'upregulated' genes (divided into GO classifications) from an experiment, versus a reference list of all genes (divided into the same GO classifications) (Mi et al., 2013). If the percentage of genes from the experimental data set involved in an individual GO classification (e.g a biological process such as 'the regulation of apoptosis') is higher than the control dataset, the GO term is said to be over-represented, and vice versa (Mi et al., 2013). Several immune-defence related pathways were enriched following differentiation, in the absence of any immune stimulation.

Ranking of the most upregulated genes upon differentiation revealed that a range of immune effector related genes were highly induced. These included several elements of the innate immune defence, such as C3 and the CXCL chemokines 5 and 6, and a core element of the 'mucosal immune system' : PIGR (Mantis et al., 2011).

The observation of C3 gene expression by human urothelium is novel, however evidence of protein-level local synthesis of complement components has been well established at several epithelial sites, including the bronchi, kidney and intestine in both animal and *in vitro* systems (Ahrenstedt et al., 1990; Andoh et al., 1993; Andrews et al., 1995; Colten et al., 1968). *In vitro* evidence has also suggested that the local cytokine environment can influence complement production (Andoh et al., 1993; Varsano et al., 2000). C3 is the fulcrum of both the classical and alternative complement pathways, acting as the signal amplification step in both processes (Sarma and Ward, 2011). C3 breakdown leads to production of the membrane attack complex, opsonisation of pathogens and the production of signalling molecules which augment the immune response (Sarma and Ward, 2011)

PIGR is responsible for the trans-epithelial transport of polymeric immunoglobulin (both IgA and IgM) at mucosal (and glandular) epithelial surfaces. Dimeric IgA (dIgA) is produced by plasma B cells, which infiltrate the lamina propria of the epithelium. dIgA is covalently bound by PIGR at the basal surface of the epithelium and transported *via* a series of vesicular compartments to the apical plasma membrane, where the GPI membrane anchor of PIGR is cleaved. The proteolytically-cleaved PIGR fragment remains bound to the dIgA, and the resulting complex is termed secretory IgA (sIgA).

The results observed in urothelial donor tissue and differentiated cells suggest that PIGR is expressed *in vivo and in vitro, as expected*. Positive immunodetection of IgA was only observed *in vivo*. The absence of *in situ* production of IgA by differentiated NHU cells is to be expected, as IgA production *in vitro* would require the presence and continued survival of IgA^+ plasma B-cells in differentiated NHU cultures, or the unlikely scenario of NHU cells producing native IgA. NHU cell isolation protocol is specific for urothelial cells, with the basement membrane (where plasma cells congregate in mucosal epithelia (Brandtzaeg et al., 1999)) and underlying stroma remaining histologically intact following isolation (Scriven et al., 1997). The medium used is also selective for adherent epithelial cell growth.

The role of PIGR and IgA in epithelial defence is most studied in the intestinal tract, where 3-5 g of IgA is expressed each day (Fagarasan and Honjo, 2003). A highly complex and multifactorial system of immune defences exists in the intestine, due in part to the high commensal bacterial load. Specialisations of secondary lymphoid follicles within specific regions of the intestinal wall, known as Peyer's patches, cause the preferential activation and production of IgA-positive B-cells (Goodrich and McGee, 1999; Kunisawa et al., 2013). An extensive body of literature exists describing the regulatory mechanisms of IgA synthesis and transport in the intestine, based largely on murine models (reviewed in Fagarasan and Honjo, 2003).

Detection of secretory IgA and PIGR in the healthy and diseased bladder has been described previously, in the context of bladder cancer histology (Kirkham et al., 1983; Sirigu et al., 1995; Vaidyanathan et al., 2000) These studies, as with the results reported in this thesis, noted the detection of IgA and PIGR in normal urothelium with a high degree of variability. Early studies of urinary tract immunology have noted the effective

anti-adhesive effects of sIgA isolated from the urine of symptomatic UTI patients upon UPEC (Svanborg-Edén and Svennerholm, 1978). Links between recurrent UTI and low urinary sIgA levels (James-Ellison et al., 1997; Riedasch et al., 1983) have been suggested, however these studies did not postulate upon the source of urinary sIgA.

The urothelium lacks the complex lymphoid tissues and immune cell infiltration present at the intestinal mucosa: few immune cells are present in healthy tissue, with heavy immune cell recruitment and infiltration associated with acute infection or pathology (such as interstitial cystitis). The source of IgA in healthy urothelium remains unclear: some heavily labelled individual cells were observed at the basal lamina of donor bladder specimens, however further analysis would be required to confirm if these were IgA-producing plasma cells.

5.6 Conclusions

- Biomimetically differentiated urothelial constructs survive when exposed to artificial urine at the apical surface, and maintain barrier function
- Culture of UPEC in artificial urine significantly affects growth kinetics
- A defect in urothelial barrier function is required to activate an AMP response to flagellin, possibly due to the absence of TLR5 expression at the superficial urothelial surface
- Elements of the urothelial defendome and innate immune sensing mechanisms are induced/upregulated following NHU cytodifferentiation indicating an inherent evolved role.

6 Overview and future work

6.1 Key findings

- The urothelial differentiation state may play a crucial role in the urothelial response to infection: a role which is poorly modelled by current non-human and bladder cancer cell models

- Normal human urothelial cells express a range of AMPs, constitutively and in response to UPEC, in addition to a range of virulence factor sensors.

- MS detection of AMPs may provide a practical method to detect AMPs, which could be applied to analysis of peptides in cell culture media.

6.2 Final conclusions

The initial aims of the thesis were:

- To determine the basal and inducible AMP responses to uropathogenic bacteria and uropathogenic virulence factors by normal human urothelial cells
- Develop a method to detect AMP release *via* mass spectrometry
- To assess the effect of urothelial differentiation upon the urothelial response to UPEC.

The work presented in this thesis has partly fulfilled these aims, and broadly agrees with the current literature: The urothelium acts as a constitutive innate barrier, expressing constitutive and inducible actuators of the innate immune response, receptors of bacterial pathogen-associated molecular patterns and AMPs. AMP production is both constitutive and inducible, with evidence of constitutive expression of RNASE7 and BD1 and the inducible expression of BD2 and BD4 in response to stimulus of undifferentiated and differentiated NHU cells with UPEC. The induction of BD2 and BD4 appeared specific to stimulation with flagellin: stimulation with LPS or PG appeared to have little effect, however *E. coli* FimH may induce some response, although the specificity of this requires confirmation.

Initial attempts to repeat these observations in biomimetic urothelial cell constructs failed: exposure of barrer-forming cultures to UPEC did not induce AMP expression. Further investigation revealed evidence suggesting differentiation state plays an important role in urothelial innate defence: in order to induce a AMP response, the urothelial barrier needs to be disrupted. Investigation of TLR5 expression suggested that TLR5 is not expressed upon the apical-most surface of the urothelium. The cells forming the apical layer are the most differentiated, and are thought to contribute significantly to the tightness of the urothelial barrier (Smith et al., 2015). Further analysis has suggested that differentiation induces several other immune defence genes, such as PIGR, strengthening the hypothesis that the innate immune function of urothelium is an inherent evolved role.

The remaining arm of this thesis aimed to improve the biomimicry of the differentiated NHU cell system. Barrier-forming NHU cells were compatible with FakePee, an artificial urine substitute, and FP reduced uropathogen growth rate, enabling extended co-culture. The feasibility of SPE extraction and MS detection of AMPs from cell culture media were also assessed. Theses results are promising, however further work is required to verify these methods.

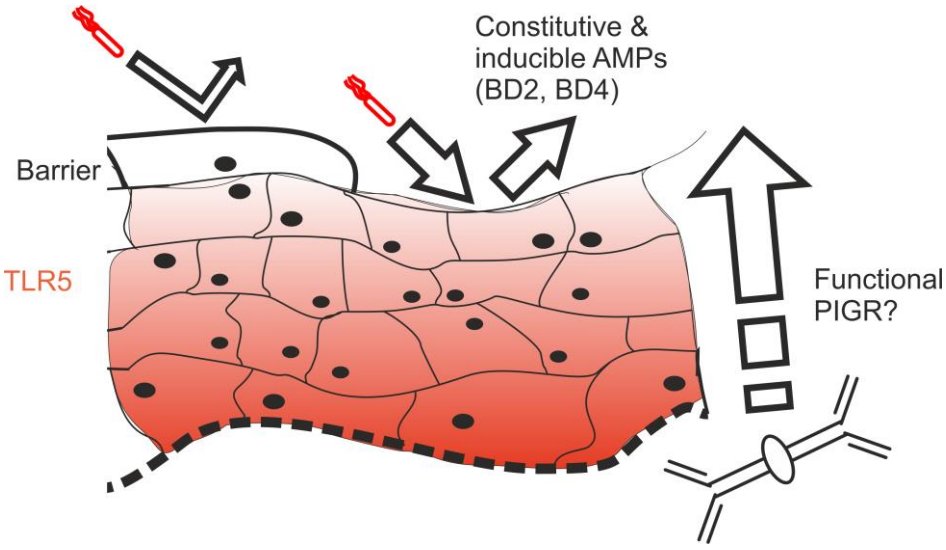

Figure 6.1 Schematic representation of novel results discussed in this thesis.

TLR5 expression was absent in the apical-most cells in the urothelium, and urothelial damage was required to enable a flagellin-mediated antimicrobial response. Both PIGR and IgA were present in the full thickness of urothelial biopsy specimens, suggesting that functional IgA transport may occur in vivo.

6.3 Future work

- RNA-seq/transcriptomic analysis of active infection:
  The RNA-seq data analysed in chapters 3 and 5 provided a powerful tool to analyse differences between the proliferating and differentiated urothelial states, and general urothelial biology. The data was, however, collected at steady state. The generation of RNA-seq datasets in NHU cells stimulated with UPEC or UPEC virulence factors would provide an immensely powerful tool to analyse the urothelial response to infection, and the role of differentiation upon this process.
- Further validation of the FP model
  Biomimetically differentiated NHU cells can survive in FP, however the barrier function is significantly reduced. The effect on FP upon paracellular tight junction protein constitution and other markers of barrier function (such as the claudin proteins) may play a role in the reduced barrier function of the FP model. The effect of FP upon expression of TLR5 and other elements of the innate defence would also need to be assessed in the FP model in order to ensure the relevance of the model to *in vivo* biology.
- What role does IgA and PIGR have in the urothelium?
  IgA transport by PIGR has been studied primarily in the context of the intestinal epithelium, using Caco-2 cell model (Sambuy et al., 2005). The intestinal epithelium is significantly different to the urothelium (Figure 6.2), with a high level of commensal bacterial load and high levels of interaction between the innate and adaptive immune systems. The urothelium does not exhibit the same interactions, and does not have a significant number of immune cells present in the urothelium or underlying stroma. Future work would include assessing if PIGR transport of IgA is functional in human urothelial cells, the source of dimeric IgA for transport across the urothelium, how PIGR transports IgA across multiple cell layers, and if IgA transport is affected by bacterial stimulation.

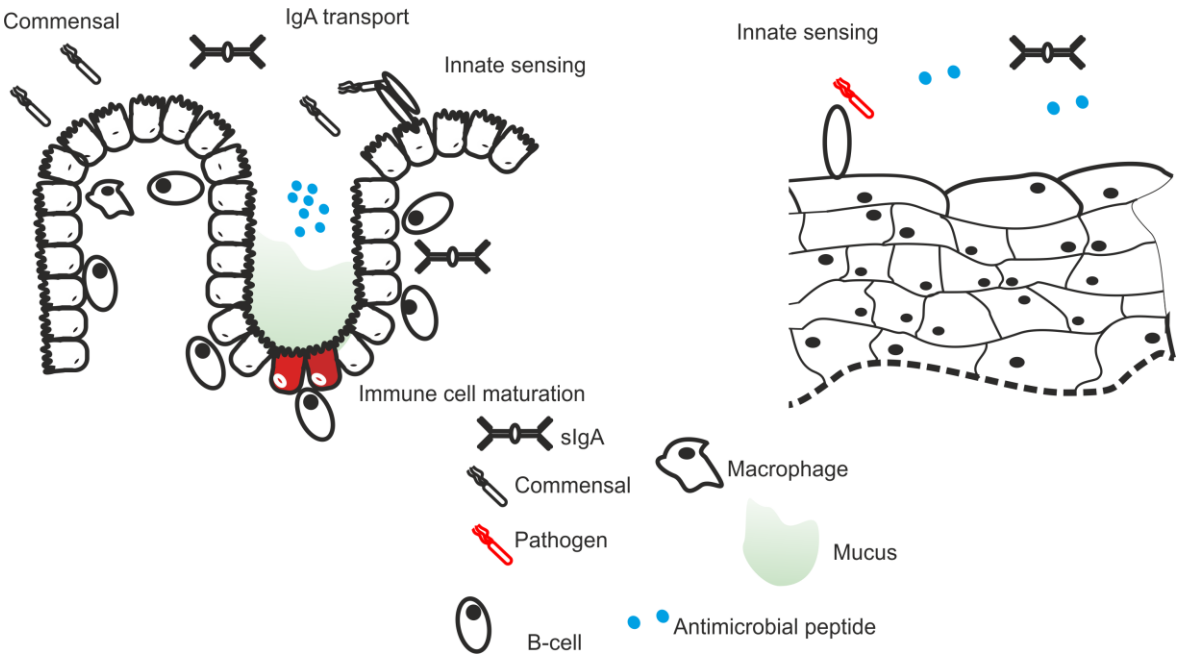

Figure 6.2 Comparison of intestinal epithelium and urothelium.

Intestinal epithelium (left) is a simple columnar epithelium, whilst the urothelium (right) is a transitional epithelium. Significant numbers of IgA$^+$ plasma cells infiltrate the basal lamina of the gut epithelium, providing the source of the 3-5g of secretory IgA produced in the gut. The intestinal epithelium is only 1 cell layer thick, unlike the urothelium, enabling the PIGR-mediated transfer of IgA.

7 Appendix 1: Buffers and solutions

General Buffers

Phosphate Buffered Saline (PBS):
137 mM NaCl, 2.7 mM KCl, 3.2 mM Na_2HPO_4 and 147 mM KH_2PO_4, pH 7.2 in dH_2O and autoclaved.

Tris Buffered Saline (TBS)
50 mM Tris-HCl and150 mM NaCl in dH_2O
+ 0.1% Tween-20 (TBST)

Tissue Culture

Collagenase IV
200 U collagenase IV/mL
10 mM 4-(2-hydroxyethyl)-1-piperazineethanesulfonic acid (HEPES)
pH 7.6 in Hanks Balanced Salt Solution (-Ca^{2+} -Mg^{2+})

Freeze mix:
10% (v/v) foetal bovine serum
10% (v/v) tissue-culture grade dimethyl sulfoxide (DMSO).
KSFMc, make under aseptic conditions

Stripper medium:
5,000 Kallikrein inactivating units/mL Trasylol (Bayer)
10 mM HEPES
0.1% EDTA
pH 7.6 in Hanks Balanced Salt Solution (-Ca^{2+} -Mg^{2+})

Transport medium
5,000 Kallikrein inactivating units/mL Trasylol (Bayer)
10 mM HEPES
0.1% ethylenediaminetetraacetic acid (EDTA)
pH 7.6 in Hanks Balanced Salt Solution (-Ca^{2+} -Mg^{2+})

Trypsin Versene (TV)
0.25% trypsin (w/v)
0.02% (w/v) EDTA in HBSS

Bacterial Cell Culture

Artificial urine (FakePee)
Per 1000 mL

1 g	Tryptone
0.005 g	Yeast extract
96,4 µL	Lactic acid
0.4 g	Citric acid

3.1 g	Sodium bicarbonate
10 g	Urea
0.07 g	Uric acid
0.8 g	Creatine
0.37 g	Calcium chloride · 2 H_2O
5.2 g	Sodium chloride
0.0012 g	Iron II sulphate · 7 H_2O
0.49 g	Magnesium sulphate · 7 H_2O
1.42 g	Sodium sulphate
0.95 g	Potassium dihydrogen phosphate
1.472 g	Di-potassium hydrogen phosphate · 2 H_2O
1.3 g	Ammonium chloride

adjust to pH 6,5

LB-Broth
1% (w/v) Tryptone,1% (w/v) NaCl, 0.5% (w/v) yeast extract in H_2O, pH 7. Sterilise by autoclaving.

LB-Agar
as LB broth with addition of 0.15% (w/v) bacto-agar

Motility medium
As LB-broth with 0.04% (w/v) Bacto-agar and 1% TTC. Aliquot to 15 mL centrifuge tubes.

Histology

Alcoholic Acetic acid
2% (v/v) acetic acid in ethanol.

Citric acid buffer
10 mM Citric acid
Adjust to pH6 with NaOH pellets

Crystal Violet
Solution 1: 10g crystal violet in 100ml industrial methylated spirit (10:1 ethanol: methanol)

Solution 2:
Dissolve 4g Ammonium Oxalate in 400ml distilled water.
Mix solutions 1 and 2, and filter.

Meyers Haematoxylin
50 g Chloral Hydrate
50 g Aluminium potassium sulphate
0.3 g NaI
1 g Citric Acid
850 mL H_2O
15% (w/v) Haematoxylin in ethanol
120 mL Glycerol
Filter before use.

Scott's tap water
2% (w/v) $MgSO_4$
0.35% (w/v) $NaHCO_3$
H_2O

Gram's Iodine:
2g Potassium Iodide
1g iodine
300 mL H_2O

Western Blotting

Odyssey Blocking Buffer
50% (v/v) Odyssey blocking buffer stock in TBST

SDS lysis buffer
10ml Glycerol (20% v/v)
1g SDS (2% w/v)
6.25ml Tris-HCl (pH 6.8) – 1M stock diluted 1:8 = 125mM
0.42g Sodium fluoride (NaF)
18.4mg Sodium orthovanadate (Na_3PO_4)
0.446g tetra-Sodium pyrophosphate
dH_2O to 50ml

Transfer Buffer
12mM Tris
96mM Glycine
20% (v/v) methanol in dH_2O

List of Abbreviations

AA	amino acid
ABS	adult bovine serum
AMP	antimicrobial peptide
ATP	adenosine triphosphate
AUM	asymmetrical unit membrane
BD	beta-defensin
BSA	bovine serum albumin
CAMP	cathelicidin
CFU	colony forming unit
CHCA	α-cyano-4-hydroxycinnamic acid
CII	Centre for immunology and infection
CoEMS	Centre of Excellence in Mass Spectrometry
DAMPS	danger associated molecular patterns
DAP	diaminopimelic acid
DEPC	Diethylpyrocarbonate
DHB	2,5-dihydroxybenzoic acid
DIC	differential interference contrast
DNA	Deoxyribonucleic acid
dNTP	deoxynucleotide triphosphate
DTT	Dithiothreitol
EDTA	Ethylenediaminetetraacetic acid
EGF	epithelial growth factor
ESI	electrospray ionisation
FT-ICR	Fourier-transform ion cyclotron resonance
H&E	hematoxylin & eosin
HRP	horseradish peroxidase
IBC	intracellular bacterial communities
IHC	immunohistochemistry
IL	interleukin
IRF3	interferon regulatory factor 3
JBU	Jack Birch Unit
KSFM	keratinocyte serum free medium
LB	Luria Bertani
LD90	lethal dose in 90% of population
LDS	lithium dodecyl sulphate
LOD	limit of detection
LOQ	limit of quantitation
LPS	lipopolysaccharide
LRR	leucine rich repeat
MALDI	matrix-assisted laser desorption ionisation
NA	nicotinic acid
oaTOF	Orthogonal acceleration time of flight
OD	optical density
PAMP	pathogen associated molecular pattern
PBS	phosphate buffered saline
PCR	polymerase chain reaction

PG	peptidoglycan
PG	peptidoglycan
PIGR	polymeric IgA receptor
PVDF	polyvinylidene difluoride
RF	Radio frequency
RNA	ribonucleic acid
RT	reverse transcriptase
RTPCR	reverse transcriptase polymerase chain reaction
SA	succinic acid
SD	standard deviation
SDS PAGE	sodium dodecyl sulphate-polyacrylamide gel electrophoresis
SPE	solid phase extraction
T1F	type 1 fimbriae
TAP	thesis advisory panel
TBE	tris buffered saline
TBST	tris buffered saline-tween
TCC	2,3,5,-triphenyltetrazolium chloride
TER/TEER	transepithelial resistance
TLR	toll-like receptor
TOF	time-of-flight
UPEC	uropathogenic *Escherichia coli*
UTI	urinary tract infection
UV	Ultraviolet

8 References

Åbrink, M., Larsson, E., Gobl, A., Hellman, L., 2000. Expression of lactoferrin in the kidney: Implications for innate immunity and iron metabolism. Kidney Int. 57, 2004–2010. doi:10.1046/j.1523-1755.2000.00050.x

Ahrenstedt, O., Knutson, L., Nilsson, B., Nilsson-Ekdahl, K., Odlind, B., Hällgren, R., 1990. Enhanced local production of complement components in the small intestines of patients with Crohn's disease. N. Engl. J. Med. 322, 1345–1349. doi:10.1056/NEJM199005103221903

Akashi, S., Ogata, H., Kirikae, F., Kirikae, T., Kawasaki, K., Nishijima, M., Shimazu, R., Nagai, Y., Fukudome, K., Kimoto, M., Miyake, K., 2000. Regulatory Roles for CD14 and Phosphatidylinositol in the Signaling via Toll-like Receptor 4-MD-2. Biochem. Biophys. Res. Commun. 268, 172–177. doi:10.1006/bbrc.2000.2089

Albert, X., Huertas, I., Pereiro, I., Sanfélix, J., Gosalbes, V., Perrotta, C., 1996. Antibiotics for preventing recurrent urinary tract infection in non-pregnant women, in: Cochrane Database of Systematic Reviews. John Wiley & Sons, Ltd.

Alexander, C., Rietschel, E.T., 2001. Invited review: Bacterial lipopolysaccharides and innate immunity. J. Endotoxin Res. 7, 167–202. doi:10.1177/09680519010070030101

Ali, A.S.M., 2013. Are Beta Defensin 1 and Beta Defensin 2 Key Innate Immune Effector Peptides against Urinary Tract Infection in Women? University of Newcastle.

Ali, A.S.M., Lanz, M., Townes, C.L., Varley, C.L., Suarez, M.-F.B., Robson, W.A., Southgate, J., Hall, J., Pickard, R.S., 2012. 183 Release of the anti-microbial peptide beta-defensin 2 protects against attack by flagellated Escherichia coli in human urothelium. Eur. Urol. Suppl. 11, e183–e183a. doi:10.1016/S1569-9056(12)60181-X

Ali, A.S.M., Townes, C.L., Hall, J., Pickard, R.S., 2009. Maintaining a Sterile Urinary Tract: The Role of Antimicrobial Peptides. J. Urol. 182, 21–28. doi:10.1016/j.juro.2009.02.124

Amster, I.J., 1996. Fourier Transform Mass Spectrometry. J. Mass Spectrom. 31, 1325–1337. doi:10.1002/(SICI)1096-9888(199612)31:12<1325::AID-JMS453>3.0.CO;2-W

Andersen-Nissen, E., Hawn, T.R., Smith, K.D., Nachman, A., Lampano, A.E., Uematsu, S., Akira, S., Aderem, A., 2007. Cutting Edge: Tlr5–/– Mice Are More Susceptible to Escherichia coli Urinary Tract Infection. J. Immunol. 178, 4717–4720.

Anderson, J.M., Van Itallie, C.M., 2009. Physiology and function of the tight junction. Cold Spring Harb. Perspect. Biol. 1, a002584. doi:10.1101/cshperspect.a002584

Andoh, A., Fujiyama, Y., Bamba, T., Hosoda, S., 1993. Differential cytokine regulation of complement C3, C4, and factor B synthesis in human intestinal epithelial cell line, Caco-2. J. Immunol. Baltim. Md 1950 151, 4239–4247.

Andrews, P.A., Finn, J.E., Lloyd, C.M., Zhou, W., Mathieson, P.W., Sacks, S.H., 1995. Expression and tissue localization of donor-specific complement C3 synthesized in human renal allografts. Eur. J. Immunol. 25, 1087–1093. doi:10.1002/eji.1830250434

Andrews, S.C., Robinson, A.K., Rodríguez-Quiñones, F., 2003. Bacterial iron homeostasis. FEMS Microbiol. Rev. 27, 215–237.

Apodaca, G., Kiss, S., Ruiz, W., Meyers, S., Zeidel, M., Birder, L., 2003. Disruption of bladder epithelium barrier function after spinal cord injury. Am. J. Physiol. Renal Physiol. 284, F966-976. doi:10.1152/ajprenal.00359.2002

Ashkar, A.A., Mossman, K.L., Coombes, B.K., Gyles, C.L., Mackenzie, R., 2008. FimH Adhesin of Type 1 Fimbriae Is a Potent Inducer of Innate Antimicrobial Responses

Which Requires TLR4 and Type 1 Interferon Signalling. PLoS Pathog. 4. doi:10.1371/journal.ppat.1000233
Ayari, C., Bergeron, A., LaRue, H., Ménard, C., Fradet, Y., 2011. Toll-Like Receptors in Normal and Malignant Human Bladders. J. Urol. 185, 1915–1921. doi:10.1016/j.juro.2010.12.097
Bäckhed, F., Söderhäll, M., Ekman, P., Normark, S., Richter-Dahlfors, A., 2001. Induction of innate immune responses by Escherichia coli and purified lipopolysaccharide correlate with organ- and cell-specific expression of Toll-like receptors within the human urinary tract. Cell. Microbiol. 3, 153–158. doi:10.1046/j.1462-5822.2001.00101.x
Bahrani-Mougeot, F.K., Buckles, E.L., Lockatell, C.V., Hebel, J.R., Johnson, D.E., Tang, C.M., Donnenberg, M.S., 2002. Type 1 fimbriae and extracellular polysaccharides are preeminent uropathogenic Escherichia coli virulence determinants in the murine urinary tract. Mol. Microbiol. 45, 1079–1093. doi:10.1046/j.1365-2958.2002.03078.x
Bals, R., Wang, X., Wu, Z., Freeman, T., Bafna, V., Zasloff, M., Wilson, J.M., 1998. Human beta-defensin 2 is a salt-sensitive peptide antibiotic expressed in human lung. J. Clin. Invest. 102, 874–880.
Banas, M., Zabieglo, K., Kasetty, G., Kapinska-Mrowiecka, M., Borowczyk, J., Drukala, J., Murzyn, K., Zabel, B.A., Butcher, E.C., Schroeder, J.M., Schmidtchen, A., Cichy, J., 2013. Chemerin Is an Antimicrobial Agent in Human Epidermis. PLOS ONE 8, e58709. doi:10.1371/journal.pone.0058709
Barasch, J., Mori, K., 2004. Cell biology: Iron thievery. Nature 432, 811–813. doi:10.1038/432811a
Barber, A.E., Norton, J.P., Wiles, T.J., Mulvey, M.A., 2016. Strengths and Limitations of Model Systems for the Study of Urinary Tract Infections and Related Pathologies. Microbiol. Mol. Biol. Rev. 80, 351–367. doi:10.1128/MMBR.00067-15
Becknell, B., Schwaderer, A., Hains, D.S., Spencer, J.D., 2015. Amplifying renal immunity: the role of antimicrobial peptides in pyelonephritis. Nat. Rev. Nephrol. 11, 642–655. doi:10.1038/nrneph.2015.105
Bent, S., Nallamothu, B.K., Simel, D.L., Fihn, S.D., Saint, S., 2002. Does this woman have an acute uncomplicated urinary tract infection? JAMA J. Am. Med. Assoc. 287, 2701–2710.
Berg, H.C., 2003. The Rotary Motor of Bacterial Flagella. Annu. Rev. Biochem. 72, 19–54. doi:10.1146/annurev.biochem.72.121801.161737
Bergsten, G., Samuelsson, M., Wult, B., Leijonhufvud, I., Fischer, H., Svanborg, C., 2004. PapG-Dependent Adherence Breaks Mucosal Inertia and Triggers the Innate Host Response. J. Infect. Dis. 189, 1734–1742. doi:10.1086/383278
Bezkorovainy, A., 1981. Antimicrobial properties of iron-binding proteins. Adv. Exp. Med. Biol. 135, 139–154.
Birder, L., Ruggieri, M., Takeda, M., van Koeveringe, G., Veltkamp, S., Korstanje, C., Parsons, B., Fry, C., 2012. How does the urothelium affect bladder function in health and disease?: ICI-RS 2011. Neurourol. Urodyn. 31, 293–299. doi:10.1002/nau.22195
Birder, L.A., 2006. Urinary bladder urothelium: Molecular sensors of chemical/thermal/mechanical stimuli. Vascul. Pharmacol. 45, 221–226. doi:10.1016/j.vph.2005.08.027
Birder, L.A., Kanai, A.J., Cruz, F., Moore, K., Fry, C.H., 2010. Is the Urothelium Intelligent? Neurourol. Urodyn. 29, 598–602. doi:10.1002/nau.20914

Blango, M.G., Mulvey, M.A., 2010. Persistence of Uropathogenic Escherichia coli in the Face of Multiple Antibiotics. Antimicrob. Agents Chemother. 54, 1855–1863. doi:10.1128/AAC.00014-10

Bokil, N.J., Totsika, M., Carey, A.J., Stacey, K.J., Hancock, V., Saunders, B.M., Ravasi, T., Ulett, G.C., Schembri, M.A., Sweet, M.J., 2011. Intramacrophage survival of uropathogenic Escherichia coli: Differences between diverse clinical isolates and between mouse and human macrophages. Immunobiology 216, 1164–1171. doi:10.1016/j.imbio.2011.05.011

Boneca, I.G., 2009. Mammalian PGRPs in the Spotlight. Cell Host Microbe 5, 109–111. doi:10.1016/j.chom.2009.01.007

Brandtzaeg, P., Baekkevold, E.S., Farstad, I.N., Jahnsen, F.L., Johansen, F.-E., Nilsen, E.M., Yamanaka, T., 1999. Regional specialization in the mucosal immune system: what happens in the microcompartments? Immunol. Today 20, 141–151. doi:10.1016/S0167-5699(98)01413-3

Brooks, T., Keevil, C.W., 1997. A simple artificial urine for the growth of urinary pathogens. Lett. Appl. Microbiol. 24, 203–206.

Browne, E.P., 2012. Regulation of B-cell responses by Toll-like receptors. Immunology 136, 370–379. doi:10.1111/j.1365-2567.2012.03587.x

Brumbaugh, A.R., Mobley, H.L., 2012. Preventing urinary tract infection: progress toward an effective Escherichia coli vaccine. Expert Rev. Vaccines 11, 663–676. doi:10.1586/erv.12.36

Brzuszkiewicz, E., Brüggemann, H., Liesegang, H., Emmerth, M., Olschläger, T., Nagy, G., Albermann, K., Wagner, C., Buchrieser, C., Emody, L., Gottschalk, G., Hacker, J., Dobrindt, U., 2006. How to become a uropathogen: comparative genomic analysis of extraintestinal pathogenic Escherichia coli strains. Proc. Natl. Acad. Sci. U. S. A. 103, 12879–12884. doi:10.1073/pnas.0603038103

Carey, A.J., Sullivan, M.J., Duell, B.L., Crossman, D.K., Chattopadhyay, D., Brooks, A.J., Tan, C.K., Crowley, M., Sweet, M.J., Schembri, M.A., Ulett, G.C., 2015. Uropathogenic Escherichia coli engages CD14-dependent signaling to enable bladder macrophage-dependent control of acute urinary tract infection. J. Infect. Dis. jiv424. doi:10.1093/infdis/jiv424

Chamaillard, M., Hashimoto, M., Horie, Y., Masumoto, J., Qiu, S., Saab, L., Ogura, Y., Kawasaki, A., Fukase, K., Kusumoto, S., Valvano, M.A., Foster, S.J., Mak, T.W., Nuñez, G., Inohara, N., 2003. An essential role for NOD1 in host recognition of bacterial peptidoglycan containing diaminopimelic acid. Nat. Immunol. 4, 702–707. doi:10.1038/ni945

Chang, C.-I., Pili-Floury, S., Hervé, M., Parquet, C., Chelliah, Y., Lemaitre, B., Mengin-Lecreulx, D., Deisenhofer, J., 2004. A Drosophila pattern recognition receptor contains a peptidoglycan docking groove and unusual L,D-carboxypeptidase activity. PLoS Biol. 2, E277. doi:10.1371/journal.pbio.0020277

Chapman, K., Robinson, F., 2007. Challenging the regulatory requirement for acute toxicity studies in the development of new medicines: Workshop Report. NC3Rs, London.

Christmas, T.J., 1994. Lymphocyte sub-populations in the bladder wall in normal bladder, bacterial cystitis and interstitial cystitis. Br. J. Urol. 73, 508–515. doi:10.1111/j.1464-410X.1994.tb07635.x

Chromek, M., Slamová, Z., Bergman, P., Kovács, L., Podracká, L. 'udmila, Ehrén, I., Hökfelt, T., Gudmundsson, G.H., Gallo, R.L., Agerberth, B., Brauner, A., 2006. The antimicrobial peptide cathelicidin protects the urinary tract against invasive bacterial infection. Nat. Med. 12, 636–641. doi:10.1038/nm1407

Colten, H.R., Gordon, J.M., Rapp, H.J., Borsos, T., 1968. Synthesis of the first component of guinea pig complement by columnar epithelial cells of the small intestine. J. Immunol. Baltim. Md 1950 100, 788–792.
Com, E., Bourgeon, F., Evrard, B., Ganz, T., Colleu, D., Jégou, B., Pineau, C., 2003. Expression of Antimicrobial Defensins in the Male Reproductive Tract of Rats, Mice, and Humans. Biol. Reprod. 68, 95–104. doi:10.1095/biolreprod.102.005389
Congdon, R.W., Muth, G.W., Splittgerber, A.G., 1993. The binding interaction of Coomassie blue with proteins. Anal. Biochem. 213, 407–413. doi:10.1006/abio.1993.1439
Connell, I., Agace, W., Klemm, P., Schembri, M., Mărild, S., Svanborg, C., 1996. Type 1 fimbrial expression enhances Escherichia coli virulence for the urinary tract. Proc. Natl. Acad. Sci. U. S. A. 93, 9827–9832.
Coutte, L., Alonso, S., Reveneau, N., Willery, E., Quatannens, B., Locht, C., Jacob-Dubuisson, F., 2003. Role of Adhesin Release for Mucosal Colonization by a Bacterial Pathogen. J. Exp. Med. 197, 735–742. doi:10.1084/jem.20021153
Cross, W.R., Eardley, I., Leese, H.J., Southgate, J., 2005. A biomimetic tissue from cultured normal human urothelial cells: analysis of physiological function. Am. J. Physiol. - Ren. Physiol. 289, F459–F468. doi:10.1152/ajprenal.00040.2005
da Silva Correia, J., Soldau, K., Christen, U., Tobias, P.S., Ulevitch, R.J., 2001. Lipopolysaccharide is in close proximity to each of the proteins in its membrane receptor complex. transfer from CD14 to TLR4 and MD-2. J. Biol. Chem. 276, 21129–21135. doi:10.1074/jbc.M009164200
Datsenko, K.A., Wanner, B.L., 2000. One-step inactivation of chromosomal genes in Escherichia coli K-12 using PCR products. Proc. Natl. Acad. Sci. U. S. A. 97, 6640–6645. doi:10.1073/pnas.120163297
Dhakal, B.K., Mulvey, M.A., 2012. The UPEC Pore Forming Toxin α-Hemolysin Triggers Proteolysis of Host Proteins to Disrupt Cell Adhesion, Inflammatory and Survival Pathways. Cell Host Microbe 11, 58–69. doi:10.1016/j.chom.2011.12.003
Donovan, G.T., Norton, J.P., Bower, J.M., Mulvey, M.A., 2013. Adenylate Cyclase and the Cyclic AMP Receptor Protein Modulate Stress Resistance and Virulence Capacity of Uropathogenic Escherichia coli. Infect. Immun. 81, 249–258. doi:10.1128/IAI.00796-12
Doyle, S.E., Vaidya, S.A., O'Connell, R., Dadgostar, H., Dempsey, P.W., Wu, T.-T., Rao, G., Sun, R., Haberland, M.E., Modlin, R.L., Cheng, G., 2002. IRF3 Mediates a TLR3/TLR4-Specific Antiviral Gene Program. Immunity 17, 251–263. doi:10.1016/S1074-7613(02)00390-4
Dua, H.S., Otri, A.M., Hopkinson, A., Mohammed, I., 2014. In vitro studies on the antimicrobial peptide human beta-defensin 9 (HBD9): signalling pathways and pathogen-related response (an American Ophthalmological Society thesis). Trans. Am. Ophthalmol. Soc. 112, 50–73.
Duguid, J.P., Clegg, S., Wilson, M.I., 1979. The Fimbrial and Non-Fimbrial Haemagglutinins of Escherichia Coli. J. Med. Microbiol. 12, 213–228. doi:10.1099/00222615-12-2-213
Dziarski, R., Gupta, D., 2006. The peptidoglycan recognition proteins (PGRPs). Genome Biol. 7, 232. doi:10.1186/gb-2006-7-8-232
Dziarski, R., Gupta, D., 2005. Staphylococcus aureus peptidoglycan is a toll-like receptor 2 activator: a reevaluation. Infect. Immun. 73, 5212–5216. doi:10.1128/IAI.73.8.5212-5216.2005
Dziarski, R., Tapping, R.I., Tobias, P.S., 1998. Binding of bacterial peptidoglycan to CD14. J. Biol. Chem. 273, 8680–8690.

Edwards, R.A., Puente, J.L., 1998. Fimbrial expression in enteric bacteria: a critical step in intestinal pathogenesis. Trends Microbiol. 6, 282–287.
Ejrnæs, K., Stegger, M., Reisner, A., Ferry, S., Monsen, T., Holm, S.E., Lundgren, B., Frimodt-Møller, N., 2011. Characteristics of Escherichia coli causing persistence or relapse of urinary tract infections: phylogenetic groups, virulence factors and biofilm formation. Virulence 2, 528–537. doi:10.4161/viru.2.6.18189
El-Achkar, T.M., Plotkin, Z., Marcic, B., Dagher, P.C., 2007. Sepsis induces an increase in thick ascending limb Cox-2 that is TLR4 dependent. AJP Ren. Physiol. 293, F1187–F1196. doi:10.1152/ajprenal.00217.2007
Fagarasan, S., Honjo, T., 2003. Intestinal IgA synthesis: regulation of front-line body defences. Nat. Rev. Immunol. 3, 63–72. doi:10.1038/nri982
Fayard, E., Tintignac, L.A., Baudry, A., Hemmings, B.A., 2005. Protein kinase B/Akt at a glance. J. Cell Sci. 118, 5675–5678. doi:10.1242/jcs.02724
Feng, Z., Jiang, B., Chandra, J., Ghannoum, M., Nelson, S., Weinberg, A., 2005. Human beta-defensins: differential activity against candidal species and regulation by Candida albicans. J. Dent. Res. 84, 445–450.
Fischer, H., Lutay, N., Ragnarsdóttir, B., Yadav, M., Jönsson, K., Urbano, A., Al Hadad, A., Rämisch, S., Storm, P., Dobrindt, U., Salvador, E., Karpman, D., Jodal, U., Svanborg, C., 2010. Pathogen Specific, IRF3-Dependent Signaling and Innate Resistance to Human Kidney Infection. PLoS Pathog. 6. doi:10.1371/journal.ppat.1001109
Fleming, A., 1922. On a Remarkable Bacteriolytic Element Found in Tissues and Secretions. Proc. R. Soc. Lond. B Biol. Sci. 93, 306–317. doi:10.1098/rspb.1922.0023
Foxman, B., 2010. The epidemiology of urinary tract infection. Nat. Rev. Urol. 7, 653–660. doi:10.1038/nrurol.2010.190
Foxman, B., 2002. Epidemiology of urinary tract infections: incidence, morbidity, and economic costs. Am. J. Med. 113 Suppl 1A, 5S–13S.
Franchi, L., Warner, N., Viani, K., Nuñez, G., 2009. Function of Nod-like Receptors in Microbial Recognition and Host Defense. Immunol. Rev. 227, 106–128. doi:10.1111/j.1600-065X.2008.00734.x
Frendéus, B., Godaly, G., Hang, L., Karpman, D., Lundstedt, A.C., Svanborg, C., 2000. Interleukin 8 receptor deficiency confers susceptibility to acute experimental pyelonephritis and may have a human counterpart. J. Exp. Med. 192, 881–890.
Frendéus, B., Wachtler, C., Hedlund, M., Fischer, H., Samuelsson, P., Svensson, M., Svanborg, C., 2001. Escherichia coli P fimbriae utilize the Toll-like receptor 4 pathway for cell activation. Mol. Microbiol. 40, 37–51. doi:10.1046/j.1365-2958.2001.02361.x
Frömter, E., Diamond, J., 1972. Route of Passive Ion Permeation in Epithelia. Nature 235, 9–13. doi:10.1038/10.1038/newbio235009a0
Ganz, T., 2003. Defensins: antimicrobial peptides of innate immunity. Nat. Rev. Immunol. 3, 710–720. doi:10.1038/nri1180
García, J.R., Krause, A., Schulz, S., Rodríguez-Jiménez, F.J., Klüver, E., Adermann, K., Forssmann, U., Frimpong-Boateng, A., Bals, R., Forssmann, W.G., 2001. Human beta-defensin 4: a novel inducible peptide with a specific salt-sensitive spectrum of antimicrobial activity. FASEB J. Off. Publ. Fed. Am. Soc. Exp. Biol. 15, 1819–1821.
Gazzinelli, R.T., Mendonça-Neto, R., Lilue, J., Howard, J., Sher, A., 2014. Innate resistance against Toxoplasma gondii: An evolutionary tale of mice, cats and men. Cell Host Microbe 15, 132–138. doi:10.1016/j.chom.2014.01.004

Gewirtz, A.T., Navas, T.A., Lyons, S., Godowski, P.J., Madara, J.L., 2001. Cutting edge: bacterial flagellin activates basolaterally expressed TLR5 to induce epithelial proinflammatory gene expression. J. Immunol. Baltim. Md 1950 167, 1882–1885.
Gewirtz, A.T., Simon, P.O., Schmitt, C.K., Taylor, L.J., Hagedorn, C.H., O'Brien, A.D., Neish, A.S., Madara, J.L., 2001. Salmonella typhimurium translocates flagellin across intestinal epithelia, inducing a proinflammatory response. J. Clin. Invest. 107, 99–109. doi:10.1172/JCI10501
Girardin, S.E., Boneca, I.G., Viala, J., Chamaillard, M., Labigne, A., Thomas, G., Philpott, D.J., Sansonetti, P.J., 2003a. Nod2 is a general sensor of peptidoglycan through muramyl dipeptide (MDP) detection. J. Biol. Chem. 278, 8869–8872. doi:10.1074/jbc.C200651200
Girardin, S.E., Travassos, L.H., Hervé, M., Blanot, D., Boneca, I.G., Philpott, D.J., Sansonetti, P.J., Mengin-Lecreulx, D., 2003b. Peptidoglycan molecular requirements allowing detection by Nod1 and Nod2. J. Biol. Chem. 278, 41702–41708. doi:10.1074/jbc.M307198200
Godaly, G., Otto, G., Burdick, M.D., Strieter, R.M., Svanborg, C., 2007. Fimbrial lectins influence the chemokine repertoire in the urinary tract mucosa. Kidney Int. 71, 778–786. doi:10.1038/sj.ki.5002076
Goetz, D.H., Holmes, M.A., Borregaard, N., Bluhm, M.E., Raymond, K.N., Strong, R.K., 2002. The neutrophil lipocalin NGAL is a bacteriostatic agent that interferes with siderophore-mediated iron acquisition. Mol. Cell 10, 1033–1043.
Goodrich, M.E., McGee, D.W., 1999. Preferential enhancement of B cell IgA secretion by intestinal epithelial cell-derived cytokines and interleukin-2. Immunol. Invest. 28, 67–75.
Guan, R., Brown, P.H., Swaminathan, C.P., Roychowdhury, A., Boons, G.-J., Mariuzza, R.A., 2006. Crystal structure of human peptidoglycan recognition protein Iα bound to a muramyl pentapeptide from Gram-positive bacteria. Protein Sci. 15, 1199–1206. doi:10.1110/ps.062077606
Guan, R., Wang, Q., Sundberg, E.J., Mariuzza, R.A., 2005. Crystal structure of human peptidoglycan recognition protein S (PGRP-S) at 1.70 A resolution. J. Mol. Biol. 347, 683–691. doi:10.1016/j.jmb.2005.01.070
Guo, H., Callaway, J.B., Ting, J.P.-Y., 2015. Inflammasomes: mechanism of action, role in disease, and therapeutics. Nat. Med. 21, 677–687. doi:10.1038/nm.3893
Gupta, K., Singh, S., van Hoek, M.L., 2015. Short, Synthetic Cationic Peptides Have Antibacterial Activity against Mycobacterium smegmatis by Forming Pores in Membrane and Synergizing with Antibiotics. Antibiot. Basel Switz. 4, 358–378. doi:10.3390/antibiotics4030358
Gupta, K., Trautner, B.W., 2013. Diagnosis and management of recurrent urinary tract infections in non-pregnant women. BMJ 346, f3140–f3140. doi:10.1136/bmj.f3140
Guyer, D.M., Henderson, I.R., Nataro, J.P., Mobley, H.L.T., 2000. Identification of Sat, an autotransporter toxin produced by uropathogenic Escherichia coli. Mol. Microbiol. 38, 53–66. doi:10.1046/j.1365-2958.2000.02110.x
Hancock, R.E.W., Rozek, A., 2002. Role of membranes in the activities of antimicrobial cationic peptides. FEMS Microbiol. Lett. 206, 143–149. doi:10.1111/j.1574-6968.2002.tb11000.x
Hannan, T.J., Totsika, M., Mansfield, K.J., Moore, K.H., Schembri, M.A., Hultgren, S.J., 2012. Host–pathogen checkpoints and population bottlenecks in persistent and intracellular uropathogenic Escherichia coli bladder infection. FEMS Microbiol. Rev. 36, 616–648. doi:10.1111/j.1574-6976.2012.00339.x
Hawn, T.R., Scholes, D., Li, S.S., Wang, H., Yang, Y., Roberts, P.L., Stapleton, A.E., Janer, M., Aderem, A., Stamm, W.E., Zhao, L.P., Hooton, T.M., 2009. Toll-Like Receptor

Polymorphisms and Susceptibility to Urinary Tract Infections in Adult Women. PLoS ONE 4. doi:10.1371/journal.pone.0005990
Hayashi, F., Smith, K.D., Ozinsky, A., Hawn, T.R., Yi, E.C., Goodlett, D.R., Eng, J.K., Akira, S., Underhill, D.M., Aderem, A., 2001. The innate immune response to bacterial flagellin is mediated by Toll-like receptor 5. Nature 410, 1099–1103. doi:10.1038/35074106
Haziot, A., Chen, S., Ferrero, E., Low, M.G., Silber, R., Goyert, S.M., 1988. The monocyte differentiation antigen, CD14, is anchored to the cell membrane by a phosphatidylinositol linkage. J. Immunol. 141, 547–552.
Hedlund, M., Frendéus, B., Wachtler, C., Hang, L., Fischer, H., Svanborg, C., 2001. Type 1 fimbriae deliver an LPS- and TLR4-dependent activation signal to CD14-negative cells. Mol. Microbiol. 39, 542–552. doi:10.1046/j.1365-2958.2001.02205.x
Hedlund, M., Svensson, M., Nilsson, A., Duan, R.D., Svanborg, C., 1996. Role of the ceramide-signaling pathway in cytokine responses to P-fimbriated Escherichia coli. J. Exp. Med. 183, 1037–1044.
Henderson, J.P., Crowley, J.R., Pinkner, J.S., Walker, J.N., Tsukayama, P., Stamm, W.E., Hooton, T.M., Hultgren, S.J., 2009. Quantitative Metabolomics Reveals an Epigenetic Blueprint for Iron Acquisition in Uropathogenic Escherichia coli. PLoS Pathog 5, e1000305. doi:10.1371/journal.ppat.1000305
Hicks, R.M., 1965. THE FINE STRUCTURE OF THE TRANSITIONAL EPITHELIUM OF RAT URETER. J. Cell Biol. 26, 25–48.
Hilt, E.E., McKinley, K., Pearce, M.M., Rosenfeld, A.B., Zilliox, M.J., Mueller, E.R., Brubaker, L., Gai, X., Wolfe, A.J., Schreckenberger, P.C., 2014. Urine Is Not Sterile: Use of Enhanced Urine Culture Techniques To Detect Resident Bacterial Flora in the Adult Female Bladder. J. Clin. Microbiol. 52, 871–876. doi:10.1128/JCM.02876-13
Hjelm, E., Forsum, U., Klareskog, L., 1982. Anti-Ia-reactive cells in the urinary tract of man, guinea-pig, rat and mouse. Scand. J. Immunol. 16, 531–538.
Hoffmann, E. de, Stroobant, V., 2013. Mass Spectrometry: Principles and Applications. John Wiley & Sons.
Hoover, D.M., Chertov, O., Lubkowski, J., 2001. The Structure of Human β-Defensin-1 NEW INSIGHTS INTO STRUCTURAL PROPERTIES OF β-DEFENSINS. J. Biol. Chem. 276, 39021–39026. doi:10.1074/jbc.M103830200
Hopkins, W.J., Hall, J.A., Conway, B.P., Uehling, D.T., 1995. Induction of urinary tract infection by intraurethral inoculation with Escherichia coli: refining the murine model. J. Infect. Dis. 171, 462–465.
Horrobin, D.F., 2003. Modern biomedical research: an internally self-consistent universe with little contact with medical reality? Nat. Rev. Drug Discov. 2, 151–154. doi:10.1038/nrd1012
Huang, H.W., 2000. Action of antimicrobial peptides: two-state model. Biochemistry (Mosc.) 39, 8347–8352.
Hughes, F.M., Hill, H.M., Wood, C.M., Edmondson, A.T., Dumas, A., Foo, W.-C., Oelsen, J.M., Rac, G., Purves, J.T., 2016a. The NLRP3 Inflammasome Mediates Inflammation Produced by Bladder Outlet Obstruction. J. Urol. 195, 1598–1605. doi:10.1016/j.juro.2015.12.068
Hughes, F.M., Kennis, J.G., Youssef, M.N., Lowe, D.W., Shaner, B.E., Purves, J.T., 2016b. The NACHT, LRR and PYD Domains-Containing Protein 3 (NLRP3) Inflammasome Mediates Inflammation and Voiding Dysfunction in a Lipopolysaccharide-Induced Rat Model of Cystitis. J. Clin. Cell. Immunol. 7. doi:10.4172/2155-9899.1000396

Hughes, F.M., Vivar, N.P., Kennis, J.G., Pratt-Thomas, J.D., Lowe, D.W., Shaner, B.E., Nietert, P.J., Spruill, L.S., Purves, J.T., 2014. Inflammasomes are important mediators of cyclophosphamide-induced bladder inflammation. Am. J. Physiol. Renal Physiol. 306, F299-308. doi:10.1152/ajprenal.00297.2013

Hull, R.A., Donovan, W.H., Del Terzo, M., Stewart, C., Rogers, M., Darouiche, R.O., 2002. Role of Type 1 Fimbria- and P Fimbria-Specific Adherence in Colonization of the Neurogenic Human Bladder by Escherichia coli. Infect. Immun. 70, 6481–6484. doi:10.1128/IAI.70.11.6481-6484.2002

Hung, C.-S., Dodson, K.W., Hultgren, S.J., 2009. A murine model of urinary tract infection. Nat. Protoc. 4, 1230–1243. doi:10.1038/nprot.2009.116

Hunter, C.A., Jones, S.A., 2015. IL-6 as a keystone cytokine in health and disease. Nat. Immunol. 16, 448–457. doi:10.1038/ni.3153

Hurst, R.E., 2003. A Deficit of Proteoglycans on the Bladder Uroepithelium in Interstitial Cystitis. Eur. Urol. Suppl., New Aspects in the Treatment of Interstitial Cystitis 2, 10–13. doi:10.1016/S1569-9056(03)00033-2

Ingersoll, M.A., Albert, M.L., 2013. From infection to immunotherapy: host immune responses to bacteria at the bladder mucosa. Mucosal Immunol. doi:10.1038/mi.2013.72

Inohara, N., Ogura, Y., Chen, F.F., Muto, A., Nuñez, G., 2001. Human Nod1 confers responsiveness to bacterial lipopolysaccharides. J. Biol. Chem. 276, 2551–2554. doi:10.1074/jbc.M009728200

Inohara, N., Ogura, Y., Fontalba, A., Gutierrez, O., Pons, F., Crespo, J., Fukase, K., Inamura, S., Kusumoto, S., Hashimoto, M., Foster, S.J., Moran, A.P., Fernandez-Luna, J.L., Nuñez, G., 2003. Host recognition of bacterial muramyl dipeptide mediated through NOD2. Implications for Crohn's disease. J. Biol. Chem. 278, 5509–5512. doi:10.1074/jbc.C200673200

Iwaki, D., Mitsuzawa, H., Murakami, S., Sano, H., Konishi, M., Akino, T., Kuroki, Y., 2002. The extracellular toll-like receptor 2 domain directly binds peptidoglycan derived from Staphylococcus aureus. J. Biol. Chem. 277, 24315–24320. doi:10.1074/jbc.M107057200

Jaillon, S., Moalli, F., Ragnarsdottir, B., Bonavita, E., Puthia, M., Riva, F., Barbati, E., Nebuloni, M., Cvetko Krajinovic, L., Markotic, A., Valentino, S., Doni, A., Tartari, S., Graziani, G., Montanelli, A., Delneste, Y., Svanborg, C., Garlanda, C., Mantovani, A., 2014. The humoral pattern recognition molecule PTX3 is a key component of innate immunity against urinary tract infection. Immunity 40, 621–632. doi:10.1016/j.immuni.2014.02.015

James, S., Gibbs, B.F., Toney, K., Bennett, H.P.J., 1994. Purification of Antimicrobial Peptides from an Extract of the Skin of Xenopus laevis Using Heparin-Affinity HPLC: Characterization by Ion-Spray Mass Spectrometry. Anal. Biochem. 217, 84–90. doi:10.1006/abio.1994.1086

James-Ellison, M.Y., Roberts, R., Verrier-Jones, K., Williams, J.D., Topley, N., 1997. Mucosal immunity in the urinary tract: changes in sIgA, FSC and total IgA with age and in urinary tract infection. Clin. Nephrol. 48, 69–78.

Jaskolla, T.W., Karas, M., 2011. Compelling Evidence for Lucky Survivor and Gas Phase Protonation: The Unified MALDI Analyte Protonation Mechanism. J. Am. Soc. Mass Spectrom. 22, 976–988. doi:10.1007/s13361-011-0093-0

Jia, H.P., Schutte, B.C., Schudy, A., Linzmeier, R., Guthmiller, J.M., Johnson, G.K., Tack, B.F., Mitros, J.P., Rosenthal, A., Ganz, T., McCray, P.B., 2001. Discovery of new human beta-defensins using a genomics-based approach. Gene 263, 211–218.

Johanson, I.-M., Plos, K., Marklund, B.-I., Svanborg, C., 1993. Pap, papG and prsG DNA sequences in Escherichia coli from the fecal flora and the urinary tract. Microb. Pathog. 15, 121–129. doi:10.1006/mpat.1993.1062

Johnson, J.R., 1998. papG Alleles among Escherichia coli Strains Causing Urosepsis: Associations with Other Bacterial Characteristics and Host Compromise. Infect. Immun. 66, 4568–4571.

Johnson, J.R., Weissman, S.J., Stell, A.L., Trintchina, E., Dykhuizen, D.E., Sokurenko, E.V., 2001. Clonal and Pathotypic Analysis of Archetypal Escherichia coli Cystitis Isolate NU14. J. Infect. Dis. 184, 1556–1565. doi:10.1086/323891

Joly, S., Maze, C., McCray, P.B., Guthmiller, J.M., 2004. Human beta-defensins 2 and 3 demonstrate strain-selective activity against oral microorganisms. J. Clin. Microbiol. 42, 1024–1029.

Jones, D.E., Bevins, C.L., 1993. Defensin-6 mRNA in human Paneth cells: implications for antimicrobial peptides in host defense of the human bowel. FEBS Lett. 315, 187–192.

Jones, D.E., Bevins, C.L., 1992. Paneth cells of the human small intestine express an antimicrobial peptide gene. J. Biol. Chem. 267, 23216–23225.

Jørgensen, M., Bergkvist, K.S.G., Welinder, K.G., 2006. Quantification of defensins by matrix-assisted laser desorption/ionization time-of-flight mass spectrometry. Anal. Biochem. 358, 295–297. doi:10.1016/j.ab.2006.08.029

Kaetzel, C.S., Robinson, J.K., Chintalacharuvu, K.R., Vaerman, J.P., Lamm, M.E., 1991. The polymeric immunoglobulin receptor (secretory component) mediates transport of immune complexes across epithelial cells: a local defense function for IgA. Proc. Natl. Acad. Sci. U. S. A. 88, 8796–8800.

Kannan, L., Liyanage, R., Lay, J., Packialakshmi, B., Anthony, N.B., Rath, N.C., 2013. Identification and structural characterization of avian beta-defensin 2 peptides from pheasant and quail. J. Proteomics Bioinform. 6, 31–37. doi:10.4172/jpb.1000258

Kannan, L., Liyanage, R., Lay, J.O., Jr, Rath, N.C., 2009. Evaluation of beta defensin 2 production by chicken heterophils using direct MALDI mass spectrometry. Mol. Immunol. 46, 3151–3156. doi:10.1016/j.molimm.2009.07.005

Karas, M., Hillenkamp, F., 1988. Laser desorption ionization of proteins with molecular masses exceeding 10,000 daltons. Anal. Chem. 60, 2299–2301. doi:10.1021/ac00171a028

Kashyap, D.R., Rompca, A., Gaballa, A., Helmann, J.D., Chan, J., Chang, C.J., Hozo, I., Gupta, D., Dziarski, R., 2014. Peptidoglycan Recognition Proteins Kill Bacteria by Inducing Oxidative, Thiol, and Metal Stress. PLoS Pathog. 10. doi:10.1371/journal.ppat.1004280

Kashyap, D.R., Wang, M., Liu, L.-H., Boons, G.-J., Gupta, D., Dziarski, R., 2011. Peptidoglycan Recognition Proteins kill bacteria by inducing suicide through protein-sensing two-component systems. Nat. Med. 17, 676–683. doi:10.1038/nm.2357

Kass, E.H., 2002. Asymptomatic infections of the urinary tract. 1956. J. Urol. 167, 1016-1019-1021.

Kawai, T., Akira, S., 2009. The roles of TLRs, RLRs and NLRs in pathogen recognition ARTICLE. Int. Immunol. 21, 317–337. doi:10.1093/intimm/dxp017

Kayagaki, N., Wong, M.T., Stowe, I.B., Ramani, S.R., Gonzalez, L.C., Akashi-Takamura, S., Miyake, K., Zhang, J., Lee, W.P., Muszyński, A., Forsberg, L.S., Carlson, R.W., Dixit, V.M., 2013. Noncanonical inflammasome activation by intracellular LPS independent of TLR4. Science 341, 1246–1249. doi:10.1126/science.1240248

Kelley, S.P., Courtneidge, H.R., Birch, R.E., Contreras-Sanz, A., Kelly, M.C., Durodie, J., Peppiatt-Wildman, C.M., Farmer, C.K., Delaney, M.P., Malone-Lee, J., Harber, M.A., Wildman, S.S., 2014. Urinary ATP and visualization of intracellular bacteria: a superior diagnostic marker for recurrent UTI in renal transplant recipients? SpringerPlus 3. doi:10.1186/2193-1801-3-200

Kiernan, 2008. Chapter 19: Immunohistochemistry, in: Histological and Histochemical Methods: Theory and Practice, 4th Edition. Cold Spring Harbor Laboratory Press, Bloxham UK.

Kirkham, N., Maciver, A.G., Anscombe, A.M., 1983. The secretory immunoglobulin system in urothelial neoplasia. Diagn. Histopathol. Publ. Assoc. Pathol. Soc. G. B. Irel. 6, 85–88.

Klumpp, D.J., Rycyk, M.T., Chen, M.C., Thumbikat, P., Sengupta, S., Schaeffer, A.J., 2006. Uropathogenic Escherichia coli Induces Extrinsic and Intrinsic Cascades To Initiate Urothelial Apoptosis. Infect. Immun. 74, 5106–5113. doi:10.1128/IAI.00376-06

Klumpp, D.J., Weiser, A.C., Sengupta, S., Forrestal, S.G., Batler, R.A., Schaeffer, A.J., 2001. Uropathogenic Escherichia coli Potentiates Type 1 Pilus-Induced Apoptosis by Suppressing NF-?B. Infect. Immun. 69, 6689–6695. doi:10.1128/IAI.69.11.6689-6695.2001

Koblansky, A.A., Jankovic, D., Oh, H., Hieny, S., Sungnak, W., Mathur, R., Hayden, M.S., Akira, S., Sher, A., Ghosh, S., 2013. Recognition of profilin by Toll-like receptor 12 is critical for host resistance to Toxoplasma gondii. Immunity 38, 119–130. doi:10.1016/j.immuni.2012.09.016

Koltsova, E.K., Ley, K., 2010. The Mysterious Ways of the Chemokine CXCL5. Immunity 33, 7–9. doi:10.1016/j.immuni.2010.07.012

Komai-Koma, M., Jones, L., Ogg, G.S., Xu, D., Liew, F.Y., 2004. TLR2 is expressed on activated T cells as a costimulatory receptor. Proc. Natl. Acad. Sci. U. S. A. 101, 3029–3034. doi:10.1073/pnas.0400171101

Kościuczuk, E.M., Lisowski, P., Jarczak, J., Strzałkowska, N., Jóźwik, A., Horbańczuk, J., Krzyżewski, J., Zwierzchowski, L., Bagnicka, E., 2012. Cathelicidins: family of antimicrobial peptides. A review. Mol. Biol. Rep. 39, 10957–10970. doi:10.1007/s11033-012-1997-x

Kreft, M.E., Sterle, M., Veranic, P., Jezernik, K., 2005. Urothelial injuries and the early wound healing response: tight junctions and urothelial cytodifferentiation. Histochem. Cell Biol. 123, 529–539. doi:10.1007/s00418-005-0770-9

Kummer, J.A., Broekhuizen, R., Everett, H., Agostini, L., Kuijk, L., Martinon, F., Bruggen, R. van, Tschopp, J., 2007. Inflammasome Components NALP 1 and 3 Show Distinct but Separate Expression Profiles in Human Tissues Suggesting a Site-specific Role in the Inflammatory Response. J. Histochem. Cytochem. 55, 443–452. doi:10.1369/jhc.6A7101.2006

Kunisawa, J., Gohda, M., Hashimoto, E., Ishikawa, I., Higuchi, M., Suzuki, Y., Goto, Y., Panea, C., Ivanov, I.I., Sumiya, R., Aayam, L., Wake, T., Tajiri, S., Kurashima, Y., Shikata, S., Akira, S., Takeda, K., Kiyono, H., 2013. Microbe-dependent CD11b+ IgA+ plasma cells mediate robust early-phase intestinal IgA responses in mice. Nat. Commun. 4, 1772. doi:10.1038/ncomms2718

Landy, M., Pillemer, L., 1956. INCREASED RESISTANCE TO INFECTION AND ACCOMPANYING ALTERATION IN PROPERDIN LEVELS FOLLOWING ADMINISTRATION OF BACTERIAL LIPOPOLYSACCHARIDES. J. Exp. Med. 104, 383–409.

Lane, M.C., Lockatell, V., Monterosso, G., Lamphier, D., Weinert, J., Hebel, J.R., Johnson, D.E., Mobley, H.L.T., 2005. Role of Motility in the Colonization of Uropathogenic

Escherichia coli in the Urinary Tract. Infect. Immun. 73, 7644–7656. doi:10.1128/IAI.73.11.7644-7656.2005
Lanne, B., Olsson, B.-M., Jovall, P.-, Öm, J., Linder, H., Marklund, B.-I., Bergström, J., Karlsson, K.-A., 1995. Glycoconjugate Receptors for P-fimbriated Escherichia coli in the Mouse AN ANIMAL MODEL OF URINARY TRACT INFECTION. J. Biol. Chem. 270, 9017–9025. doi:10.1074/jbc.270.15.9017
Laupland, K.B., Ross, T., Pitout, J.D.D., Church, D.L., Gregson, D.B., 2007. Community-onset Urinary Tract Infections: A Population-based Assessment. Infection 35, 150–153. doi:10.1007/s15010-007-6180-2
Lavelle, J.P., Meyers, S.A., Ruiz, W.G., Buffington, C.A., Zeidel, M.L., Apodaca, G., 2000. Urothelial pathophysiological changes in feline interstitial cystitis: a human model. Am. J. Physiol. Renal Physiol. 278, F540-553.
Lazzeri, M., 2006. The physiological function of the urothelium--more than a simple barrier. Urol. Int. 76, 289–295. doi:10.1159/000092049
Lehmann, J., Retz, M., Harder, J., Krams, M., Kellner, U., Hartmann, J., Hohgräwe, K., Raffenberg, U., Gerber, M., Loch, T., Weichert-Jacobsen, K., Stöckle, M., 2002. Expression of human beta-defensins 1 and 2 in kidneys with chronic bacterial infection. BMC Infect. Dis. 2, 20. doi:10.1186/1471-2334-2-20
Lehrer, R.I., Barton, A., Daher, K.A., Harwig, S.S., Ganz, T., Selsted, M.E., 1989. Interaction of human defensins with Escherichia coli. Mechanism of bactericidal activity. J. Clin. Invest. 84, 553–561. doi:10.1172/JCI114198
Lehrer, R.I., Ganz, T., 1999. Antimicrobial peptides in mammalian and insect host defence. Curr. Opin. Immunol. 11, 23–27. doi:10.1016/S0952-7915(99)80005-3
Lewis, D.A., White, P., Jacobson, S.K., Marchesi, J.R., Drake, M.J., 2013. The human urinary microbiome; bacterial DNA in voided urine of asymptomatic adults. Front. Cell. Infect. Microbiol. 3, 41. doi:10.3389/fcimb.2013.00041
Lewis, S.A., 2000. Everything you wanted to know about the bladder epithelium but were afraid to ask. Am. J. Physiol. Renal Physiol. 278, F867-874.
Li, H., Cui, X., Arnheim, N., 1990. Direct electrophoretic detection of the allelic state of single DNA molecules in human sperm by using the polymerase chain reaction. Proc. Natl. Acad. Sci. 87, 4580–4584. doi:10.1073/pnas.87.12.4580
Linzmeier, R., Ho, C.H., Hoang, B.V., Ganz, T., 1999. A 450-kb contig of defensin genes on human chromosome 8p23. Gene 233, 205–211. doi:10.1016/S0378-1119(99)00136-5
Liu, L., Wang, L., Jia, H.P., Zhao, C., Heng, H.H.Q., Schutte, B.C., McCray Jr., P.B., Ganz, T., 1998. Structure and mapping of the human β-defensin HBD-2 gene and its expression at sites of inflammation. Gene 222, 237–244. doi:10.1016/S0378-1119(98)00480-6
Liu, Y., Mémet, S., Saban, R., Kong, X., Aprikian, P., Sokurenko, E., Sun, T.-T., Wu, X.-R., 2015. Dual ligand/receptor interactions activate urothelial defenses against uropathogenic E. coli. Sci. Rep. 5, 16234. doi:10.1038/srep16234
Livak, K.J., Schmittgen, T.D., 2001. Analysis of relative gene expression data using real-time quantitative PCR and the 2(-Delta Delta C(T)) Method. Methods San Diego Calif 25, 402–408. doi:10.1006/meth.2001.1262
Lu, X., Wang, M., Qi, J., Wang, H., Li, X., Gupta, D., Dziarski, R., 2006. Peptidoglycan recognition proteins are a new class of human bactericidal proteins. J. Biol. Chem. 281, 5895–5907. doi:10.1074/jbc.M511631200
Lund, B., Lindberg, F., Marklund, B.I., Normark, S., 1987. The PapG protein is the alpha-D-galactopyranosyl-(1----4)-beta-D-galactopyranose-binding adhesin of uropathogenic Escherichia coli. Proc. Natl. Acad. Sci. U. S. A. 84, 5898–5902.

Lüthje, P., Lindén Hirschberg, A., Brauner, A., 2014. Estrogenic action on innate defense mechanisms in the urinary tract. Maturitas 77, 32–36. doi:10.1016/j.maturitas.2013.10.018
M D Säemann, T.W., 2005. Tamm-Horsfall protein: A multilayered defence molecule against urinary tract infection. Eur. J. Clin. Invest. 35, 227–35. doi:10.1111/j.1365-2362.2005.01483.x
Maeshima, N., Fernandez, R., 2013. Recognition of lipid A variants by the TLR4-MD-2 receptor complex. Front. Cell. Infect. Microbiol. 3, 3. doi:10.3389/fcimb.2013.00003
Mantis, N.J., Rol, N., Corthesy, B., 2011. Secretory IgA's Complex Roles in Immunity and Mucosal Homeostasis in the Gut. Mucosal Immunol. 4, 603–611. doi:10.1038/mi.2011.41
Marceau, N., 1990. Cell lineages and differentiation programs in epidermal, urothelial and hepatic tissues and their neoplasms. Lab. Investig. J. Tech. Methods Pathol. 63, 4–20.
Marklund, B.I., Tennent, J.M., Garcia, E., Hamers, A., Båga, M., Lindberg, F., Gaastra, W., Normark, S., 1992. Horizontal gene transfer of the Escherichia coli pap and prs pili operons as a mechanism for the development of tissue-specific adhesive properties. Mol. Microbiol. 6, 2225–2242.
Maroncle, N.M., Sivick, K.E., Brady, R., Stokes, F.-E., Mobley, H.L.T., 2006. Protease Activity, Secretion, Cell Entry, Cytotoxicity, and Cellular Targets of Secreted Autotransporter Toxin of Uropathogenic Escherichia coli. Infect. Immun. 74, 6124–6134. doi:10.1128/IAI.01086-06
Marrs, C.F., Zhang, L., Foxman, B., 2005. Escherichia coli mediated urinary tract infections: Are there distinct uropathogenic E. coli (UPEC) pathotypes? FEMS Microbiol. Lett. 252, 183–190. doi:10.1016/j.femsle.2005.08.028
Martinez, J.J., Mulvey, M.A., Schilling, J.D., Pinkner, J.S., Hultgren, S.J., 2000. Type 1 pilus-mediated bacterial invasion of bladder epithelial cells. EMBO J. 19, 2803–2812. doi:10.1093/emboj/19.12.2803
Martinon, F., Burns, K., Tschopp, J., 2002. The inflammasome: a molecular platform triggering activation of inflammatory caspases and processing of proIL-beta. Mol. Cell 10, 417–426.
Matsuzaki, K., 2009. Control of cell selectivity of antimicrobial peptides. Biochim. Biophys. Acta BBA - Biomembr., Amphibian Antimicrobial Peptides 1788, 1687–1692. doi:10.1016/j.bbamem.2008.09.013
Matsuzaki, K., Murase, O., Fujii, N., Miyajima, K., 1996. An antimicrobial peptide, magainin 2, induced rapid flip-flop of phospholipids coupled with pore formation and peptide translocation. Biochemistry (Mosc.) 35, 11361–11368. doi:10.1021/bi960016v
Medzhitov, R., Preston-Hurlburt, P., Janeway, C.A., 1997. A human homologue of the Drosophila Toll protein signals activation of adaptive immunity. Nature 388, 394–397. doi:10.1038/41131
Meyer, J.E., Harder, J., Sipos, B., Maune, S., Klöppel, G., Bartels, J., Schröder, J.-M., Gläser, R., 2008. Psoriasin (S100A7) is a principal antimicrobial peptide of the human tongue. Mucosal Immunol. 1, 239–243. doi:10.1038/mi.2008.3
Mi, H., Lazareva-Ulitsky, B., Loo, R., Kejariwal, A., Vandergriff, J., Rabkin, S., Guo, N., Muruganujan, A., Doremieux, O., Campbell, M.J., Kitano, H., Thomas, P.D., 2005. The PANTHER database of protein families, subfamilies, functions and pathways. Nucleic Acids Res. 33, D284–D288. doi:10.1093/nar/gki078

Mi, H., Muruganujan, A., Casagrande, J.T., Thomas, P.D., 2013. Large-scale gene function analysis with the PANTHER classification system. Nat. Protoc. 8, 1551–1566. doi:10.1038/nprot.2013.092

Miyazaki, J., Ba-Thein, W., Kumao, T., Obata Yasuoka, M., Akaza, H., Hayshi, H., 2002. Type 1, P and S fimbriae, and afimbrial adhesin I are not essential for uropathogenic Escherichia coli to adhere to and invade bladder epithelial cells. FEMS Immunol. Med. Microbiol. 33, 23–26.

Mogensen, T.H., 2009. Pathogen Recognition and Inflammatory Signaling in Innate Immune Defenses. Clin. Microbiol. Rev. 22, 240–273. doi:10.1128/CMR.00046-08

Moskowitz, S.M., Ernst, R.K., Miller, S.I., 2004. PmrAB, a Two-Component Regulatory System of Pseudomonas aeruginosa That Modulates Resistance to Cationic Antimicrobial Peptides and Addition of Aminoarabinose to Lipid A. J. Bacteriol. 186, 575–579. doi:10.1128/JB.186.2.575-579.2004

Müller, R., Marchetti-Deschmann, M., Elgass, H., Breiteneder, H., Kratzmeier, M., Allmaier, G., 2010. Molecular weight determination of high molecular mass (glyco)proteins using CGE-on-a-chip, planar SDS-PAGE and MALDI-TOF-MS. Electrophoresis 31, 3850–3862. doi:10.1002/elps.201000282

Mulvey, M.A., Schilling, J.D., Martinez, J.J., Hultgren, S.J., 2000. Bad bugs and beleaguered bladders: Interplay between uropathogenic Escherichia coli and innate host defenses. Proc. Natl. Acad. Sci. 97, 8829–8835. doi:10.1073/pnas.97.16.8829

Murphy, K.C., Campellone, K.G., 2003. Lambda Red-mediated recombinogenic engineering of enterohemorrhagic and enteropathogenic E. coli. BMC Mol. Biol. 4, 11. doi:10.1186/1471-2199-4-11

Murphy, K.C., Campellone, K.G., Poteete, A.R., 2000. PCR-mediated gene replacement in Escherichia coli. Gene 246, 321–330.

Nelson, D.E., Van Der Pol, B., Dong, Q., Revanna, K.V., Fan, B., Easwaran, S., Sodergren, E., Weinstock, G.M., Diao, L., Fortenberry, J.D., 2010. Characteristic Male Urine Microbiomes Associate with Asymptomatic Sexually Transmitted Infection. PLoS ONE 5, e14116. doi:10.1371/journal.pone.0014116

Nicolardi, S., Velstra, B., Mertens, B.J., Bonsing, B., Mesker, W.E., Tollenaar, R.A.E.M., Deelder, A.M., van der Burgt, Y.E.M., 2014. Ultrahigh resolution profiles lead to more detailed serum peptidome signatures of pancreatic cancer. Transl. Proteomics 2, 39–51. doi:10.1016/j.trprot.2013.12.003

Nicolle, L.E., 2014. Catheter associated urinary tract infections. Antimicrob. Resist. Infect. Control 3, 23. doi:10.1186/2047-2994-3-23

Nienhouse, V., Gao, X., Dong, Q., Nelson, D.E., Toh, E., McKinley, K., Schreckenberger, P., Shibata, N., Fok, C.S., Mueller, E.R., Brubaker, L., Wolfe, A.J., Radek, K.A., 2014. Interplay between Bladder Microbiota and Urinary Antimicrobial Peptides: Mechanisms for Human Urinary Tract Infection Risk and Symptom Severity. PLoS ONE 9, e114185. doi:10.1371/journal.pone.0114185

Old, D.C., Duguid, J.P., 1970. Selective Outgrowth of Fimbriate Bacteria in Static Liquid Medium. J. Bacteriol. 103, 447–456.

O'Neill, L.A.J., Golenbock, D., Bowie, A.G., 2013. The history of Toll-like receptors — redefining innate immunity. Nat. Rev. Immunol. 13. doi:10.1038/nri3446

Oppenheim, J.J., Biragyn, A., Kwak, L.W., Yang, D., 2003. Roles of antimicrobial peptides such as defensins in innate and adaptive immunity. Ann. Rheum. Dis. 62, ii17-ii21. doi:10.1136/ard.62.suppl_2.ii17

Oren, Z., Shai, Y., 1998. Mode of action of linear amphipathic alpha-helical antimicrobial peptides. Biopolymers 47, 451–463. doi:10.1002/(SICI)1097-0282(1998)47:6<451::AID-BIP4>3.0.CO;2-F

Ortega-Cava, C.F., Ishihara, S., Rumi, M.A.K., Aziz, M.M., Kazumori, H., Yuki, T., Mishima, Y., Moriyama, I., Kadota, C., Oshima, N., Amano, Y., Kadowaki, Y., Ishimura, N., Kinoshita, Y., 2006. Epithelial toll-like receptor 5 is constitutively localized in the mouse cecum and exhibits distinctive down-regulation during experimental colitis. Clin. Vaccine Immunol. CVI 13, 132–138. doi:10.1128/CVI.13.1.132-138.2006

Ouellette, A.J., Greco, R.M., James, M., Frederick, D., Naftilan, J., Fallon, J.T., 1989. Developmental regulation of cryptdin, a corticostatin/defensin precursor mRNA in mouse small intestinal crypt epithelium. J. Cell Biol. 108, 1687–1695.

Pak, J., Pu, Y., Zhang, Z.T., Hasty, D.L., Wu, X.R., 2001. Tamm-Horsfall protein binds to type 1 fimbriated Escherichia coli and prevents E. coli from binding to uroplakin Ia and Ib receptors. J. Biol. Chem. 276, 9924–9930. doi:10.1074/jbc.M008610200

Park, C.B., Kim, H.S., Kim, S.C., 1998. Mechanism of action of the antimicrobial peptide buforin II: buforin II kills microorganisms by penetrating the cell membrane and inhibiting cellular functions. Biochem. Biophys. Res. Commun. 244, 253–257. doi:10.1006/bbrc.1998.8159

Park, Y.S., 2012. Renal scar formation after urinary tract infection in children. Korean J. Pediatr. 55, 367–370. doi:10.3345/kjp.2012.55.10.367

Patole, P.S., Schubert, S., Hildinger, K., Khandoga, S., Khandoga, A., Segerer, S., Henger, A., Kretzler, M., Werner, M., Krombach, F., Schlöndorff, D., Anders, H.-J., 2005. Toll-like receptor-4: renal cells and bone marrow cells signal for neutrophil recruitment during pyelonephritis. Kidney Int. 68, 2582–2587. doi:10.1111/j.1523-1755.2005.00729.x

Pazgier, M., Hoover, D.M., Yang, D., Lu, W., Lubkowski, J., 2006. Human β-defensins. Cell. Mol. Life Sci. CMLS 63, 1294–1313. doi:10.1007/s00018-005-5540-2

Peters, H.P., Laarakkers, C.M., Pickkers, P., Masereeuw, R., Boerman, O.C., Eek, A., Cornelissen, E.A., Swinkels, D.W., Wetzels, J.F., 2013. Tubular reabsorption and local production of urine hepcidin-25. BMC Nephrol. 14, 70. doi:10.1186/1471-2369-14-70

Poltorak, A., He, X., Smirnova, I., Liu, M.-Y., Huffel, C.V., Du, X., Birdwell, D., Alejos, E., Silva, M., Galanos, C., Freudenberg, M., Ricciardi-Castagnoli, P., Layton, B., Beutler, B., 1998. Defective LPS Signaling in C3H/HeJ and C57BL/10ScCr Mice: Mutations in Tlr4 Gene. Science 282, 2085–2088. doi:10.1126/science.282.5396.2085

Proost, P., Wuyts, A., Conings, R., Lenaerts, J.P., Billiau, A., Opdenakker, G., Van Damme, J., 1993. Human and bovine granulocyte chemotactic protein-2: Complete amino acid sequence and functional characterization as chemokines. Biochemistry (Mosc.) 32, 10170–10177. doi:10.1021/bi00089a037

Rad, R., Brenner, L., Krug, A., Voland, P., Mages, J., Lang, R., Schwendy, S., Reindl, W., Dossumbekova, A., Ballhorn, W., Wagner, H., Schmid, R.M., Bauer, S., Prinz, C., 2007. Toll-Like Receptor–Dependent Activation of Antigen-Presenting Cells Affects Adaptive Immunity to Helicobacter pylori. Gastroenterology 133, 150–163.e3. doi:10.1053/j.gastro.2007.04.071

Riedasch, G., Heck, P., Rauterberg, E., Ritz, E., 1983. Does low urinary sIgA predispose to urinary tract infection? Kidney Int. 23, 759–763.

Robino, L., Scavone, P., Araujo, L., Algorta, G., Zunino, P., Pirez, M.C., Vignoli, R., 2014. Intracellular Bacteria in the Pathogenesis of Escherichia coli Urinary Tract Infection in Children. Clin. Infect. Dis. 59, e158–e164. doi:10.1093/cid/ciu634

Robino, L., Scavone, P., Araujo, L., Algorta, G., Zunino, P., Vignoli, R., 2013. Detection of intracellular bacterial communities in a child with Escherichia coli recurrent urinary tract infections. Pathog. Dis. 68, 78–81. doi:10.1111/2049-632X.12047

Rock, F.L., Hardiman, G., Timans, J.C., Kastelein, R.A., Bazan, J.F., 1998. A family of human receptors structurally related to Drosophila Toll. Proc. Natl. Acad. Sci. 95, 588–593.
Ronald, A., 2002. The etiology of urinary tract infection: traditional and emerging pathogens. Am. J. Med. 113, 14–19. doi:10.1016/S0002-9343(02)01055-0
Rouschop, K.M.A., Sylva, M., Teske, G.J.D., Hoedemaeker, I., Pals, S.T., Weening, J.J., Poll, T. van der, Florquin, S., 2006. Urothelial CD44 Facilitates Escherichia coli Infection of the Murine Urinary Tract. J. Immunol. 177, 7225–7232.
Royet, J., Dziarski, R., 2007. Peptidoglycan recognition proteins: pleiotropic sensors and effectors of antimicrobial defences. Nat. Rev. Microbiol. 5, 264–277. doi:10.1038/nrmicro1620
Russo, T.A., Stapleton, A., Wenderoth, S., Hooton, T.M., Stamm, W.E., 1995. Chromosomal restriction fragment length polymorphism analysis of Escherichia coli strains causing recurrent urinary tract infections in young women. J. Infect. Dis. 172, 440–445.
Sahl, H.-G., Pag, U., Bonness, S., Wagner, S., Antcheva, N., Tossi, A., 2005. Mammalian defensins: structures and mechanism of antibiotic activity. J. Leukoc. Biol. 77, 466–475. doi:10.1189/jlb.0804452
Sambuy, Y., De Angelis, I., Ranaldi, G., Scarino, M.L., Stammati, A., Zucco, F., 2005. The Caco-2 cell line as a model of the intestinal barrier: influence of cell and culture-related factors on Caco-2 cell functional characteristics. Cell Biol. Toxicol. 21, 1–26. doi:10.1007/s10565-005-0085-6
Samuelsson, P., Hang, L., Wullt, B., Irjala, H., Svanborg, C., 2004. Toll-Like Receptor 4 Expression and Cytokine Responses in the Human Urinary Tract Mucosa. Infect. Immun. 72, 3179–3186. doi:10.1128/IAI.72.6.3179-3186.2004
Sarma, J.V., Ward, P.A., 2011. The complement system. Cell Tissue Res. 343, 227–235. doi:10.1007/s00441-010-1034-0
Schilling, J.D., Martin, S.M., Hung, C.S., Lorenz, R.G., Hultgren, S.J., 2003a. Toll-like receptor 4 on stromal and hematopoietic cells mediates innate resistance to uropathogenic Escherichia coli. Proc. Natl. Acad. Sci. 100, 4203–4208. doi:10.1073/pnas.0736473100
Schilling, J.D., Martin, S.M., Hunstad, D.A., Patel, K.P., Mulvey, M.A., Justice, S.S., Lorenz, R.G., Hultgren, S.J., 2003b. CD14- and Toll-Like Receptor-Dependent Activation of Bladder Epithelial Cells by Lipopolysaccharide and Type 1 Piliated Escherichia coli. Infect. Immun. 71, 1470–1480. doi:10.1128/IAI.71.3.1470-1480.2003
Schilling, J.D., Mulvey, M.A., Vincent, C.D., Lorenz, R.G., Hultgren, S.J., 2001. Bacterial Invasion Augments Epithelial Cytokine Responses to Escherichia coli Through a Lipopolysaccharide-Dependent Mechanism. J. Immunol. 166, 1148–1155.
Schutte, B.C., Mitros, J.P., Bartlett, J.A., Walters, J.D., Jia, H.P., Welsh, M.J., Casavant, T.L., McCray, P.B., 2002. Discovery of five conserved beta -defensin gene clusters using a computational search strategy. Proc. Natl. Acad. Sci. U. S. A. 99, 2129–2133. doi:10.1073/pnas.042692699
Schwan, W.R., 2011. Regulation of fim genes in uropathogenic Escherichia coli. World J. Clin. Infect. Dis. 1, 17–25. doi:10.5495/wjcid.v1.i1.17
Scottish Intercollegiate Guidelines Network, 2012. Management of suspected bacterial urinary tract infection in adults (No. SIGN88). Healthcare Improvement Scotland.
Scriven, S.D., Booth, C., Thomas, D.F.M., Trejdosiewicz, L.K., Southgate, J., 1997. Reconstitution of Human Urothelium From Monolayer Cultures. J. Urol. 158, 1147–1152. doi:10.1016/S0022-5347(01)64407-0

Selsted, M.E., Harwig, S.S., Ganz, T., Schilling, J.W., Lehrer, R.I., 1985. Primary structures of three human neutrophil defensins. J. Clin. Invest. 76, 1436–1439. doi:10.1172/JCI112121

Shabir, S., Southgate, J., 2008. Calcium signalling in wound-responsive normal human urothelial cell monolayers. Cell Calcium 44, 453–464. doi:10.1016/j.ceca.2008.02.008

Shahin, R.D., Engberg, I., Hagberg, L., Svanborg Edén, C., 1987. Neutrophil recruitment and bacterial clearance correlated with LPS responsiveness in local gram-negative infection. J. Immunol. Baltim. Md 1950 138, 3475–3480.

Shai, Y., 2002. Mode of action of membrane active antimicrobial peptides. Pept. Sci. 66, 236–248. doi:10.1002/bip.10260

Shimizu, T., Yokota, S., Takahashi, S., Kunishima, Y., Takeyama, K., Masumori, N., Takahashi, A., Matsukawa, M., Itoh, N., Tsukamoto, T., Fujii, N., 2004. Membrane-anchored CD14 is important for induction of interleukin-8 by lipopolysaccharide and peptidoglycan in uroepithelial cells. Clin. Diagn. Lab. Immunol. 11, 969–976. doi:10.1128/CDLI.11.5.969-976.2004

Sirigu, P., Perra, M.T., Turno, F., Usai, E., 1995. Immunohistochemical demonstration of secretory IgA in human urothelium. Histol. Histopathol. 10, 645–650.

Smet, K.D., Contreras, R., 2005. Human Antimicrobial Peptides: Defensins, Cathelicidins and Histatins. Biotechnol. Lett. 27, 1337–1347. doi:10.1007/s10529-005-0936-5

Smith, N.J., Hinley, J., Varley, C.L., Eardley, I., Trejdosiewicz, L.K., Southgate, J., 2015. The human urothelial tight junction: claudin 3 and the ZO-1α(+) switch. Bladder 2, e9. doi:10.14440/bladder.2015.33

Smith, N.J., Varley, C.L., Eardley, I., Feather, S., Trejdosiewicz, L.K., Southgate, J., 2011. Toll-Like Receptor Responses of Normal Human Urothelial Cells to Bacterial Flagellin and Lipopolysaccharide. J. Urol. 186, 1084–1092. doi:10.1016/j.juro.2011.04.112

Söderhäll, M., Normark, S., Ishikawa, K., Karlsson, K., Teneberg, S., Winberg, J., Möllby, R., 1997. Induction of protective immunity after escherichia coli bladder infection in primates. Dependence of the globoside-specific P-fimbrial tip adhesin and its cognate receptor. J. Clin. Invest. 100, 364–372. doi:10.1172/JCI119542

Song, J., Abraham, S.N., 2008. TLR Mediated Immune Responses in the Urinary Tract. Curr. Opin. Microbiol. 11, 66–73. doi:10.1016/j.mib.2007.12.001

Song, J., Bishop, B.L., Li, G., Duncan, M.J., Abraham, S.N., 2007. TLR4-initiated and cAMP-mediated abrogation of bacterial invasion of the bladder. Cell Host Microbe 1, 287–298. doi:10.1016/j.chom.2007.05.007

Southgate, J., Hutton, K.A., Thomas, D.F., Trejdosiewicz, L.K., 1994. Normal human urothelial cells in vitro: proliferation and induction of stratification. Lab. Investig. J. Tech. Methods Pathol. 71, 583–594.

Spencer, J.D., Hains, D.S., Porter, E., Bevins, C.L., DiRosario, J., Becknell, B., Wang, H., Schwaderer, A.L., 2012. Human alpha defensin 5 expression in the human kidney and urinary tract. PloS One 7, e31712. doi:10.1371/journal.pone.0031712

Spencer, J.D., Schwaderer, A.L., Wang, H., Bartz, J., Kline, J., Eichler, T., DeSouza, K.R., Sims-Lucas, S., Baker, P., Hains, D.S., 2013. Ribonuclease 7, an antimicrobial peptide upregulated during infection, contributes to microbial defense of the human urinary tract. Kidney Int. 83, 615–625. doi:10.1038/ki.2012.410

Stapleton, A.E., Stroud, M.R., Hakomori, S.I., Stamm, W.E., 1998. The globoseries glycosphingolipid sialosyl galactosyl globoside is found in urinary tract tissues and is a preferred binding receptor In vitro for uropathogenic Escherichia coli expressing pap-encoded adhesins. Infect. Immun. 66, 3856–3861.

Storici, P., Tossi, A., Lenarčič, B., Romeo, D., 1996. Purification and Structural Characterization of Bovine Cathelicidins, Precursors of Antimicrobial Peptides. Eur. J. Biochem. 238, 769–776. doi:10.1111/j.1432-1033.1996.0769w.x

Stothers, L., 2002. A randomized trial to evaluate effectiveness and cost effectiveness of naturopathic cranberry products as prophylaxis against urinary tract infection in women. Can. J. Urol. 9, 1558–1562.

Strupat, K., Kampmeier, J., Horneffer, V., 1997. Investigations of 2,5-DHB and succinic acid as matrices for UV and IR MALDI. Part II: Crystallographic and mass spectrometric analysis. Int. J. Mass Spectrom. Ion Process., Matrix-Assisted Laser Desorption Ionization Mass Spectrometry 169, 43–50. doi:10.1016/S0168-1176(97)00225-5

Stuler, k, Meyer, M., 2004. MALDI: more than peptide mass fingerprints. Curr. Opin. Mol. Ther. 6, 239–248.

Subramanian, H., Gupta, K., Lee, D., Bayir, A.K., Ahn, H., Ali, H., 2013. β-defensins activate human mast cells via Mas-related Gene-X2 (MrgX2). J. Immunol. Baltim. Md 1950 191, 345–352. doi:10.4049/jimmunol.1300023

Sutmuller, R.P.M., den Brok, M.H.M.G.M., Kramer, M., Bennink, E.J., Toonen, L.W.J., Kullberg, B.-J., Joosten, L.A., Akira, S., Netea, M.G., Adema, G.J., 2006. Toll-like receptor 2 controls expansion and function of regulatory T cells. J. Clin. Invest. 116, 485–494. doi:10.1172/JCI25439

Svanborg-Edén, C., Svennerholm, A.M., 1978. Secretory immunoglobulin A and G antibodies prevent adhesion of Escherichia coli to human urinary tract epithelial cells. Infect. Immun. 22, 790–797.

Svensson, M., Lindstedt, R., Radin, N.S., Svanborg, C., 1994. Epithelial glucosphingolipid expression as a determinant of bacterial adherence and cytokine production. Infect. Immun. 62, 4404–4410.

Szájli, E., Fehér, T., Medzihradszky, K.F., 2008. Investigating the Quantitative Nature of MALDI-TOF MS. Mol. Cell. Proteomics 7, 2410–2418. doi:10.1074/mcp.M800108-MCP200

Takemura, H., Kaku, M., Kohno, S., Hirakata, Y., Tanaka, H., Yoshida, R., Tomono, K., Koga, H., Wada, A., Hirayama, T., Kamihira, S., 1996. Evaluation of susceptibility of gram-positive and -negative bacteria to human defensins by using radial diffusion assay. Antimicrob. Agents Chemother. 40, 2280–2284.

Takeshima, K., Chikushi, A., Lee, K.-K., Yonehara, S., Matsuzaki, K., 2003. Translocation of analogues of the antimicrobial peptides magainin and buforin across human cell membranes. J. Biol. Chem. 278, 1310–1315. doi:10.1074/jbc.M208762200

Thumbikat, P., Berry, R.E., Zhou, G., Billips, B.K., Yaggie, R.E., Zaichuk, T., Sun, T.-T., Schaeffer, A.J., Klumpp, D.J., 2009. Bacteria-Induced Uroplakin Signaling Mediates Bladder Response to Infection. PLoS Pathog 5, e1000415. doi:10.1371/journal.ppat.1000415

Tibayrenc, M., Ayala, F.J., 2012. Reproductive clonality of pathogens: A perspective on pathogenic viruses, bacteria, fungi, and parasitic protozoa. Proc. Natl. Acad. Sci. U. S. A. 109, E3305–E3313. doi:10.1073/pnas.1212452109

Torres, A.M., Kuchel, P.W., 2004. The β-defensin-fold family of polypeptides. Toxicon 44, 581–588. doi:10.1016/j.toxicon.2004.07.011

Uhlén, M., Björling, E., Agaton, C., Szigyarto, C.A.-K., Amini, B., Andersen, E., Andersson, A.-C., Angelidou, P., Asplund, A., Asplund, C., Berglund, L., Bergström, K., Brumer, H., Cerjan, D., Ekström, M., Elobeid, A., Eriksson, C., Fagerberg, L., Falk, R., Fall, J., Forsberg, M., Björklund, M.G., Gumbel, K., Halimi, A., Hallin, I., Hamsten, C., Hansson, M., Hedhammar, M., Hercules, G., Kampf, C., Larsson, K., Lindskog, M., Lodewyckx, W., Lund, J., Lundeberg, J., Magnusson,

K., Malm, E., Nilsson, P., Ödling, J., Oksvold, P., Olsson, I., Öster, E., Ottosson, J., Paavilainen, L., Persson, A., Rimini, R., Rockberg, J., Runeson, M., Sivertsson, Å., Sköllermo, A., Steen, J., Stenvall, M., Sterky, F., Strömberg, S., Sundberg, M., Tegel, H., Tourle, S., Wahlund, E., Waldén, A., Wan, J., Wernérus, H., Westberg, J., Wester, K., Wrethagen, U., Xu, L.L., Hober, S., Pontén, F., 2005. A Human Protein Atlas for Normal and Cancer Tissues Based on Antibody Proteomics. Mol. Cell. Proteomics 4, 1920–1932. doi:10.1074/mcp.M500279-MCP200

Uniprot Consortium, T.U., 2015. UniProt: a hub for protein information. Nucleic Acids Res. 43, D204–D212. doi:10.1093/nar/gku989

Vaidyanathan, S., McDicken, I.W., Soni, B.M., Singh, G., Sett, P., Husin, N.M., 2000. Secretory immunoglobulin A in the vesical urothelium of patients with neuropathic bladder--an immunohistochemical study. Spinal Cord 38, 378–381.

Valore, E.V., Park, C.H., Quayle, A.J., Wiles, K.R., McCray, P.B., Ganz, T., 1998. Human beta-defensin-1: an antimicrobial peptide of urogenital tissues. J. Clin. Invest. 101, 1633–1642.

Vanaja, S.K., Rathinam, V.A.K., Fitzgerald, K.A., 2015. Mechanisms of inflammasome activation: recent advances and novel insights. Trends Cell Biol. 25, 308–315. doi:10.1016/j.tcb.2014.12.009

Vandamme, D., Landuyt, B., Luyten, W., Schoofs, L., 2012. A comprehensive summary of LL-37, the factotum human cathelicidin peptide. Cell. Immunol. 280, 22–35. doi:10.1016/j.cellimm.2012.11.009

Varley, C.L., Bacon, E.J., Holder, J.C., Southgate, J., 2008. FOXA1 and IRF-1 intermediary transcriptional regulators of PPARγ-induced urothelial cytodifferentiation. Cell Death Differ. 16, 103–114. doi:10.1038/cdd.2008.116

Varley, C.L., Garthwaite, M.A.E., Cross, W., Hinley, J., Trejdosiewicz, L.K., Southgate, J., 2006. PPARgamma-regulated tight junction development during human urothelial cytodifferentiation. J. Cell. Physiol. 208, 407–417. doi:10.1002/jcp.20676

Varley, C.L., Southgate, J., 2008. Effects of PPAR agonists on proliferation and differentiation in human urothelium. Exp. Toxicol. Pathol. Off. J. Ges. Für Toxikol. Pathol. 60, 435–441. doi:10.1016/j.etp.2008.04.009

Varsano, S., Kaminsky, M., Kaiser, M., Rashkovsky, L., 2000. Generation of complement C3 and expression of cell membrane complement inhibitory proteins by human bronchial epithelium cell line. Thorax 55, 364–369. doi:10.1136/thorax.55.5.364

Vasileiou, I., Katsargyris, A., Theocharis, S., Giaginis, C., 2013. Current clinical status on the preventive effects of cranberry consumption against urinary tract infections. Nutr. Res. 33, 595–607. doi:10.1016/j.nutres.2013.05.018

Wang, G., Li, X., Wang, Z., 2009. APD2: the updated antimicrobial peptide database and its application in peptide design. Nucleic Acids Res. 37, D933-937. doi:10.1093/nar/gkn823

Wang, M., Liu, L.-H., Wang, S., Li, X., Lu, X., Gupta, D., Dziarski, R., 2007. Human peptidoglycan recognition proteins require zinc to kill both gram-positive and gram-negative bacteria and are synergistic with antibacterial peptides. J. Immunol. Baltim. Md 1950 178, 3116–3125.

Wang, R., Ahmed, J., Wang, G., Hassan, I., Strulovici-Barel, Y., Salit, J., Mezey, J., Crystal, R.G., 2012. Airway Epithelial Expression of Toll-like Receptor 5 is Down-regulated in Healthy Smokers and Smokers with Chronic Obstructive Pulmonary Disease. J. Immunol. Baltim. Md 1950 189, 2217–2225. doi:10.4049/jimmunol.1101895

Wehkamp, J., Koslowski, M., Wang, G., Stange, E.F., 2008. Barrier dysfunction due to distinct defensin deficiencies in small intestinal and colonic Crohn's disease. Mucosal Immunol. 1, S67–S74. doi:10.1038/mi.2008.48

Welch, R.A., Burland, V., Plunkett, G., Redford, P., Roesch, P., Rasko, D., Buckles, E.L., Liou, S.-R., Boutin, A., Hackett, J., Stroud, D., Mayhew, G.F., Rose, D.J., Zhou, S., Schwartz, D.C., Perna, N.T., Mobley, H.L.T., Donnenberg, M.S., Blattner, F.R., 2002. Extensive mosaic structure revealed by the complete genome sequence of uropathogenic Escherichia coli. Proc. Natl. Acad. Sci. 99, 17020–17024. doi:10.1073/pnas.252529799

Wiles, T.J., Dhakal, B.K., Eto, D.S., Mulvey, M.A., 2008a. Inactivation of host Akt/protein kinase B signaling by bacterial pore-forming toxins. Mol. Biol. Cell 19, 1427–1438. doi:10.1091/mbc.E07-07-0638

Wiles, T.J., Kulesus, R.R., Mulvey, M.A., 2008b. Origins and Virulence Mechanisms of Uropathogenic Escherichia coli. Exp. Mol. Pathol. 85, 11–19. doi:10.1016/j.yexmp.2008.03.007

Wright, K.J., Seed, P.C., Hultgren, S.J., 2005. Uropathogenic Escherichia coli Flagella Aid in Efficient Urinary Tract Colonization. Infect. Immun. 73, 7657–7668. doi:10.1128/IAI.73.11.7657-7668.2005

Wu, X.-R., Kong, X.-P., Pellicer, A., Kreibich, G., Sun, T.-T., 2009. Uroplakins in urothelial biology, function, and disease. Kidney Int. 75, 1153–1165. doi:10.1038/ki.2009.73

Wu, X.R., Sun, T.T., Medina, J.J., 1996. In vitro binding of type 1-fimbriated Escherichia coli to uroplakins Ia and Ib: relation to urinary tract infections. Proc. Natl. Acad. Sci. U. S. A. 93, 9630–9635.

Wullt, B., Bergsten, G., Connell, H., Röllano, P., Gebratsedik, N., Hang, L., Svanborg, C., 2001. P-fimbriae trigger mucosal responses to Escherichia coli in the human urinary tract. Cell. Microbiol. 3, 255–264. doi:10.1046/j.1462-5822.2001.00111.x

Wullt, B., Bergsten, G., Connell, H., Röllano, P., Gebretsadik, N., Hull, R., Svanborg, C., 2000. P fimbriae enhance the early establishment of Escherichia coli in the human urinary tract. Mol. Microbiol. 38, 456–464.

Yamamoto, T., Endo, S., Yokota, T., Echeverria, P., 1991. Characteristics of adherence of enteroaggregative Escherichia coli to human and animal mucosa. Infect. Immun. 59, 3722–3739.

Yang, D., Chertov, O., Bykovskaia, S.N., Chen, Q., Buffo, M.J., Shogan, J., Anderson, M., Schröder, J.M., Wang, J.M., Howard, O.M.Z., Oppenheim, J.J., 1999. β-Defensins: Linking Innate and Adaptive Immunity Through Dendritic and T Cell CCR6. Science 286, 525–528. doi:10.1126/science.286.5439.525

Yang, X., Hu, Y., Xu, S., Hu, Y., Meng, H., Guo, C., Liu, Y., Liu, J., Yu, Z., Wang, H., 2013. Identification of multiple antimicrobial peptides from the skin of fine-spined frog, Hylarana spinulosa (Ranidae). Biochimie, Special section : The Mesenchymal Stem Cell secretome in Regenerative Medicine 95, 2429–2436. doi:10.1016/j.biochi.2013.09.002

Yoon, S., Kurnasov, O., Natarajan, V., Hong, M., Gudkov, A.V., Osterman, A.L., Wilson, I.A., 2012. Structural basis of TLR5-flagellin recognition and signaling. Science 335, 859–864. doi:10.1126/science.1215584

Young, K.D., 2011. Peptidoglycan, in: John Wiley & Sons, Ltd (Ed.), eLS. John Wiley & Sons, Ltd, Chichester, UK.

Yu, W., Hill, W.G., 2011. Defining protein expression in the urothelium: a problem of more than transitional interest. Am. J. Physiol. - Ren. Physiol. 301, F932–F942. doi:10.1152/ajprenal.00334.2011

Zanetti, M., Gennaro, R., Romeo, D., 1995. Cathelicidins: a novel protein family with a common proregion and a variable C-terminal antimicrobial domain. FEBS Lett. 374, 1–5. doi:10.1016/0014-5793(95)01050-O

Zarember, K.A., Godowski, P.J., 2002. Tissue Expression of Human Toll-Like Receptors and Differential Regulation of Toll-Like Receptor mRNAs in Leukocytes in

Response to Microbes, Their Products, and Cytokines. J. Immunol. 168, 554–561. doi:10.4049/jimmunol.168.2.554
Zhang, C., Zhang, H., Lichfield, D., Yeung, K., 2010. CHCA or DHB? Systematic Comparison of the Two Most Commonly Used Matrices for Peptide Mass Fingerprint Analysis with MALDI-MS. Spectroscopy.
Zhang, D., Zhang, G., Hayden, M.S., Greenblatt, M.B., Bussey, C., Flavell, R.A., Ghosh, S., 2004. A Toll-like Receptor That Prevents Infection by Uropathogenic Bacteria. Science 303, 1522–1526. doi:10.1126/science.1094351
Zhang, L., Yu, W., He, T., Yu, J., Caffrey, R.E., Dalmasso, E.A., Fu, S., Pham, T., Mei, J., Ho, J.J., Zhang, W., Lopez, P., Ho, D.D., 2002. Contribution of Human α-Defensin 1, 2, and 3 to the Anti-HIV-1 Activity of CD8 Antiviral Factor. Science 298, 995–1000. doi:10.1126/science.1076185
Zhang, P.J., Wang, H., Wrona, E.L., Cheney, R.T., 1998. Effects of Tissue Fixatives on Antigen Preservation for Immunohistochemistiy: A Comparative Study of Microwave Antigen Retrieval on Lillie Fixative and Neutral Buffered Formalin. J. Histotechnol. 21, 101–106. doi:10.1179/his.1998.21.2.101
Zhou, G., Mo, W.-J., Sebbel, P., Min, G., Neubert, T.A., Glockshuber, R., Wu, X.-R., Sun, T.-T., Kong, X.-P., 2001. Uroplakin Ia is the urothelial receptor for uropathogenic Escherichia coli: evidence from in vitro FimH binding. J. Cell Sci. 114, 4095–4103.